

**STUDY ON BEHAVIOR OF BURIED PIPELINES
SUBJECTED TO EARTHQUAKE FAULT MOVEMENT BY
ANALYTICAL, NUMERICAL AND EXPERIMENTAL
APPROACHES**

2020

FARZAD TALEBI

Abstract

Onshore pipeline networks (e.g. oil, gas, water, sewer, chemical transmission lines) are spread worldwide even in hazardous (e.g. high seismic risk) zones to provide human societies vital needs. Damage and even rupture of buried pipelines during earthquakes have caused severe health, economic and environmental issues. Most of the exposed damage to buried pipelines was observed owing to permanent ground deformation (PGD), even though a very limited extent of pipelines is damaged by wave propagation. The influence of a pipeline's lifecycle on human life is vital because it provides crucial services to human societies, such as energy and water distribution. Additionally, environmental hazards that can result from the leakage of ecologically dangerous materials (e.g., chemicals, natural gas, fuel, or liquid waste) cannot be ignored. Thus, it is evident that the construction of buried pipelines subjected to fault displacement in earthquake-risk zones and mainly fault intersections is a major engineering task because PGD can cause severe pipeline damage.

In this study, we investigated the problem of buried pipelines at faults crossing from a comprehensive point of view, including earthquake site investigation, analytical stability analysis, numerical FE based analysis, and full-scale experimental studies.

Despite substantial advances made by previous studies in the development of analytical stability analysis methods for a buried pipeline with regard to fault-crossing problems, axial soil-pipe interaction and axial forces owing to geometrical nonlinearity have not been appropriately applied in analytical methodologies even in linear ranges. The development of a comprehensive analytical method that incorporates exact nonlinear axial and transverse soil-pipe interaction terms within a united governing equation is therefore urgently required.

For establishment of an improved comprehensive analytical solution for this problem, it is needed to first evaluate the performance of buried pipelines at faults crossing and extract the effective variables and terms on the soil-pipe interaction and pipeline forces. And after all, check the experimental results for improving the design guideline for HDPE buried pipelines.

In this regard, firstly, damage to the lifeline systems during the 2017 Sarpole-Zahab earthquake investigated. A large range of damages to the pipeline system is observed, and it had a significant impact on the recovery of the cities and villages after the earthquake. In which in some cities, they had water outage up to two weeks because of the contamination of the water resources due to pipeline network damage.

Secondly, changes in the behavior of the buried pipelines due to the axial soil-pipe interaction at strike-slip fault investigated by FEM, and effective terms on axial force and axial soil-pipe interactions besides some new boundary conditions are detected for future analytical studies in the elastic range. Moreover, the effect of steel pipe material nonlinearity on buried pipeline performance evaluated against the large dislocated strike-slip fault movements.

Thirdly, based on previous steps, for the problem of buried pipeline subjected to strike-slip fault movements, we introduced a novel linear governing equation and its corresponding solution. The introduced governing equation includes the linear axial soil-pipe interaction,

linear frictional axial force terms, and axial forces made by geometrical nonlinearity effects within it. We also verified our novel linear analytical method's results versus identical verified FEM models. New analytical methodology substantially increased the accuracy and application range of the analytical solution for linear analysis.

Fourthly, a new comprehensive governing equation including elastic perfectly plastic longitudinal soil-pipe interaction, elastoplastic lateral soil-pipe interaction, and improved geometrical nonlinearity effects within it, and its corresponding solution also is introduced. The mentioned methodology includes the effects of the buried pipeline sliding within the soil, the plasticity of the lateral soil springs, and geometrical nonlinearity effects. Introduced methodology significantly has improved the past studies and has extended the application area of the analytical solutions even in large deformation cases.

Fifthly, a comparative study is conducted between the 3D solid and shell nonlinear FEM modeling approach and 3D nonlinear beam-spring modeling approach and their application ranges, for the problem of buried pipelines at strike-slip faults crossing. Additionally, the performance and damage criteria are evaluated through 3D nonlinear FEM analysis. All the analyses have nonlinear soil material, nonlinear pipe material, nonlinear interface, and geometrical nonlinearity effects. The results of both modeling approaches are in the same range. however, there exist some discrepancies. We found that the design guidelines should have some detailed recommendations for each modeling approach.

Finally, to evaluate the performance of the HDPE pipelines buried in loose and dense sands subjected to strike-slip faults movement, we conducted two full-scale experiments for buried HDPE pipelines subjected to a 90° strike-slip fault movement. Based on full-scale experiments results, two 3D nonlinear FEM models are calibrated to evaluate soil-pipe interaction forces beside the HDPE pipeline performance more detailly at strike-slip fault crossing. Moreover, the influence of important variables on the buried HDPE pipeline at 90° strike-slip is studied to improve the seismic design guidelines of buried HDPE pipelines. we found small diameter HDPE pipelines have a good resistance against the strike-slip earthquake fault movement.

Acknowledgement

I would like to express my sincerest gratitude to my supervisor, Professor Junji Kiyono, for granting me the opportunity to carry out my studies in his laboratory (Laboratory of Earthquake and Lifeline Engineering, Kyoto University) and I am so grateful for his kind and continuous support throughout my doctoral course. I have been delighted with his perfect guidance and precious advice regarding all the aspects of my academic life and scientific research. It was a great pleasure for me to conduct my Ph.D. studies under the kind and insightful supervision of him, and indeed his perfect character and immense knowledge have been always inspiring me.

The sincere appreciations are also extended to Professor Yoshikazu Takahashi, Structural Engineering Structural Dynamics Laboratory and Associate Professor Akio Furukawa, Earthquake and Lifeline Engineering Laboratory for their kind advice, review, and comments for the final stage of this Doctoral thesis preparation.

This dissertation is conducted under the Ph.D. course of Human Security Engineering (HSE) program, which is promoted and sponsored by the MEXT scholarship funded by the Ministry of Education, Culture, Sports, Science, and Technology of Japan, in Graduate School of Engineering, Kyoto University. I would like to express my sincere appreciation to the HSE program and the MEXT scholarship for their financial supports during my Ph.D. course.

I would like to express my sincere thanks to Dr. Gentaro Nishikawa and POLITEC association for their help and financial supports in conducting my experimental study.

I also would like to express my sincere acknowledgments to Associate Professor Akio Furukawa for her kind supports in providing requirements throughout my studies and research in the Laboratory of Earthquake and Lifeline Engineering. Besides, I would like to extend my sincerest appreciation to my former master course supervisor Prof. Abdolhossein Fallahi in Azarbaijan Shahid Madani University, Iran, for his kind and insightful supports. I would also like to extend my sincere gratitude to Ms. Yoshimi Yoshida for her kind and invaluable assistance, someone whose help cannot be overestimated.

Finally, my gratitude goes to my dearest parents, all of my family members, and loved ones for their kind and continuous support and encouragement. Their companionship has been always inspiring to me.

Table of Contents

1. Introduction.....	1
1.1. General problem.....	2
1.2. Background.....	2
1.3. Research objective	5
1.4. Organization of the thesis	7
1.5. Damages to the lifeline system owing to the earthquake.....	8
1.5.1. 2017 Sarpole-Zahab earthquake.....	9
1.5.2. Damage to lifelines and infrastructures at Sarpole-Zahab earthquake.....	10
References.....	14
2. Literature review	19
2.1. General remarks	20
2.2. Surface faulting.....	20
2.3. Modelling of buried steel pipeline subjected to strike slip faulting	21
2.3.1. Analytical studies.....	21
2.3.2. Finite element method studies.....	28
2.4. Experimental studies.....	33
References.....	36
3. Effect of axial soil-pipe interaction and pipe material nonlinearity effect on behavior buried pipeline at strike-slip fault crossing.....	41
3.1. General remarks	42
3.2. Background.....	42
3.3. Importance of axial soil-pipe interaction on pipeline crossing a strike-slip fault	43
3.3.1. Performance of buried pipelines during previous earthquakes	44
3.3.2. Analytical solution.....	44
3.3.3. FEM results and verification.....	46
3.4. Effect of steel pipe material nonlinearity on performance of buried pipelines at strike-slip faults crossing	60
3.4.1. FEM models definition	60
3.4.2. Analysis cases	62
3.4.3. Analysis results	65
3.5. Conclusions.....	66
References.....	69

Nomenclature.....	71
4. Introduction of governing equation for buried pipelines at strike-slip faults crossing including the linear axial force terms	73
4.1. General remarks.....	74
4.2. Background.....	74
4.3. Evaluation of axial force of pipeline.....	76
4.3.1. Frictional axial soil-pipe interaction	77
4.3.2. Axial force owing to geometrical nonlinearity at the pipeline high curvature zone	80
4.4. Pipeline model	81
4.4.1. Existing governing equation	81
4.4.2. Solution algorithm.....	81
4.5. Numerical modeling and verification of the analytical method.....	87
4.5.1. Finite element pipeline model.....	87
4.5.2. Comparison of proposed methodology versus finite element solutions under various loading conditions.	89
4.6. Conclusions.....	94
References.....	96
5. Introduction of nonlinear governing equation and corresponding semi-analytical solution for buried pipelines at strike-slip faults crossing	99
5.1. General remarks	100
5.2. Background.....	100
5.3. Evaluation of axial force of pipeline.....	102
5.3.1. Frictional axial soil-pipe interaction	103
5.3.2. Axial force owing to geometrical nonlinearity (membrane force).....	107
5.4. Transverse soil-pipe interaction nonlinearity.....	108
5.5. Pipeline model	109
5.5.1. Solution algorithm.....	109
5.6. Finite element model description and verification.....	113
5.6.1. Verification of the finite element model	115
5.7. Validation of proposed analytical methodology versus FEM.....	116
5.8. Conclusions.....	122
References.....	124
Nomenclature.....	127
6. Evaluation of FEM modeling approaches and buried pipeline’s performance at fault crossing	

.....	129
6.1. General remarks	130
6.2. Background	130
6.3. Axial and transverse soil springs	131
6.3.1. 3D FEM analyses results.....	131
6.4. Modeling of buried pipeline at strike-slip fault crossing	134
6.5. Results and discussion	137
6.6. Conclusions.....	140
References.....	142
7. Full-scale experiments on buried HDPE pipelines subjected to strike-slip Faults movements	145
7.1. General remarks	146
7.2. Background.....	146
7.3. Split-box size estimation.....	147
7.3.1. FEM analyses for split-box size estimation	147
7.4. Experimental study	150
7.4.1. Experimental setup.....	150
7.4.2. Experiment material.....	152
7.4.3. Instrumentation	155
7.4.4. Experiment model	156
7.5. Experiment results	157
7.5.1. Deformation results.....	157
7.5.2. Strain results.....	160
7.5.3. Local buckling and ovalization	164
7.6. 3D nonlinear FEM simulations	165
7.6.1. Calibration of soil-pipe interaction	166
7.6.2. 3D nonlinear FE models versus full-scale experiments for HDPE pipelines at fault crossing	168
7.7. Conclusions.....	181
References.....	184
8. Concluding Remarks	189
8.1. General remarks and summary	190
8.1.1. Damage evaluation during 2017 Sarpole-Zahab earthquake	190

8.1.2. Finite element-based study.....	190
8.1.3. Analytical studies.....	191
8.1.4. Full-scale experimental study	192
8.2. Summary of the results	192
8.2.1. 2017 Sarpole-Zahab earthquake site investigation conclusions.....	192
8.2.2. Finite element-based study's conclusions.....	192
8.2.3. Analytical study's conclusions.....	194
8.2.4. Full-scale experimental study's conclusions.....	196
8.3. Future studies	197
References.....	198

Table of Figures

Fig. 1.1. (a) Locations of the recording stations together with the obtained maximum PGA values of two horizontal components; (b) and (c) acceleration time series for Sarpole-Zahab and Nosood stations, respectively; (d) and (e) obtained absolute spectral acceleration for Sarpole-Zahab and Nosood stations, respectively [13].	9
Fig. 1.2. (a) Damage to the retaining walls beside the bridge of Sarpole-Zahab City, (b) Damage to little stone and concrete bridge at a Village road nearby Sarpole-Zahab [13].	10
Fig. 1.3. Damage to Ban-Zardeg village road due to severe rock-fall.	11
Fig. 1.4. Damage to village road nearby Sarpole-Zahab (the road has rehabilitated temporarily).	11
Fig. 1.5. Collapse of transmission tower duo to rock fall on the mountains nearby the Sarpole-Zahab city.	12
Fig. 1.6. (a) Damage to Palane-Olya village main water polyethylene pipeline due to a long land slide (repaired), (b) big deformation in main water polyethylene pipeline of Gurchi-Bashi village.	12
Fig. 1.7. Damage to the Gurchi-Bashi village vessel and Pipeline due to settlement and landslide in some parts.	13
Fig. 1.8. Damage to joint of the gas pipeline at the entrance to the houses at Sarpole-Zahab city.	13
Fig. 2.1. Fault movement classification: (a) normal, (b) strike-slip, (c) reverse [17].	20
Fig. 2.2. Schematic representation of the Newmark-Hall model for buried pipeline crossing a strike-slip fault [19].	21
Fig. 2.3. Schematic diagram of the pipe deformed shape assumed by Kennedy et al. [20].	22
Fig. 2.4. Schematic representation of the Wang and Yeh. [22] model for pipeline crossing a strike-slip fault.	23
Fig. 2.5. Schematic representation of the Karamitros et al. (2007) [23] model for pipeline crossing a strike-slip fault.	24
Fig. 2.6. Schematic representation of the Trifonov and Cherniy (2010) [24] model for pipeline crossing a strike-slip fault.	25
Fig. 2.7. Schematic representation of the Trifonov and Cherniy (2010) [24] model for axial force in problem of buried pipeline at strike-slip fault crossing.	26
Fig. 2.8. valid axial force responses shape for a steel buried pipeline at strike-slip fault crossing (chapter 3).	26
Fig. 2.9. Schematic representation of the Karamitros et al. (2011) [25] model for pipeline crossing a normal fault.	27
Fig. 2.10. Schematic representation of the Trifonov and Cherniy (2012) [26] model for pipeline crossing a strike-slip fault.	28
Fig. 2.11. Schematic representation of shell FEM models for a pipe crossing the fault according Liu et al. study [35]: (a) hybrid shell-beam model, (b) shell model with equivalent boundary.	29

Fig. 2.12. Geometry of proposed FEM model for buried pipeline by Joshi et al. [36]	30
Fig. 2.13. Finite element model of buried steel pipeline at strike-slip fault crossing made by created Vazouras et al. [37].	30
Fig. 2.14. Sketch of finite element model of Liu et al. [38].	31
Fig. 2.15. Local buckling under reverse fault displacement [38].	31
Fig. 2.16. Created model by Demirci et al. [39]: (a) cross-section of three-dimensional (3D) soil continuum model, (b) side view of the 3D FE model showing displacements of foot wall and hanging wall, (c) displacement profile of the pipeline, (d) longitudinal pipe strains in the dashed red zone.	32
Fig. 2.17. Centrifuge model of Abdoun et al. [47] experiment: (a) moist sand back fill and (b) dry sand backfill.	33
Fig. 2.18. Sketch of the split-box test basin of Rofooei et al. experiment model [52]: (a) front view, (b) side view before and (c) after a fault offset of 0.60 m, (d) photograph of the experimental results.	33
Fig. 2.19. Experiment model proposed by Demirci et al. [39]: (a) 1-g physical model of buried pipeline subjected to reverse fault, (b) working principle of 1-g scaled model, (c) observed shear bands after application of displacement in both horizontal and vertical planes.	34
Fig. 3.1. Buried pipeline analysis model at strike-slip fault crossing: (a) definition of x and y-axes and fault displacement of δx , δy , and δ ; (b) pipeline-fault-intersection angle in plane φ	43
Fig. 3.2. Damaged steel pipeline after (a) 1999 Kocaeli earthquake [22], (b) 1999 Chi-Chi earthquake in Taiwan [23], (c) 2017 Iran-Iraq earthquake in Sarpole-Zahab city (drinking water contamination) [24].	44
Fig. 3.3. Coordinate system and partitioning of pipeline for analytical solution.	45
Fig. 3.4. Schematic soil spring diagram of buried pipeline at strike-slip fault crossing implemented in FEM model.	46
Fig. 3.5. FEM analysis result versus analytical solution results for problem of buried pipeline subjected to strike-slip fault ($\varphi = 90^\circ$): (a) w_y diagram for soft soil cases, (b) w_y diagram hard soil cases, (c) M diagram for soft soil cases; (d) M diagram for hard soil cases; (e) N diagram for soft soil cases, (f) N diagram for hard soil cases.	48
Fig. 3.6. Experimental results of pipeline crossing strike-slip fault with angle of 90° : (a) buried in soft soil, (b) buried in hard soil [21].	50
Fig. 3.7. Bending moment responses obtained by FE pipeline models for cases 15 and 16. ...	50
Fig. 3.8. Transverse displacement (w_y) response counters of pipeline resulting from two-dimensional dislocation of strike-slip fault at 90° angle in soft soil, as obtained by FEM analysis.	51
Fig. 3.9. Pipeline crossing strike-slip fault analysis displacement field responses: (a) w_y for soft soil cases, (b) w_y for hard soil cases, (c) w_x for soft soil cases, (d) w_x for hard soil cases, (e) w_{xs} for cases buried either in soft and hard soil with existence of axial soil springs.	52
Fig. 3.10. (a) Schematic representation of L_c and L_{conv} at left side of pipe-fault intersection point O, (b) Force subcomponents of pipeline in curved zone.	54

Fig. 3.11. Pipeline at strike-slip fault crossing analysis force and stress field responses: (a) N for soft soil cases, (b) N for hard soil cases, (c) N_s for soft soil with existence of axial soil springs, (d) N_s for hard soil with existence of axial soil springs, (e) V for soft soil cases, (f) V for hard soil cases, (g) M for soft soil cases, (h) M for hard soil cases.	55
Fig. 3.12. Maximum/minimum stress of pipeline section crossing strike-slip fault on point (I) path: (a) soft soil cases, (b) hard soil cases.	59
Fig. 3.13. (a) Illustration of deformed buried steel pipeline crossing strike-slip fault and the coordinate system. (b) pipeline section, A and B Paths [1].	61
Fig. 3.14. Schematic bilinear force-displacement curves of soil-pipe interaction springs [1].	62
Fig. 3.15. Schematic model of pipeline and soil springs modeled by FEM [1].	62
Fig. 3.16. Transverse displacement response of pipeline [1].	63
Fig. 3.17. Axial force response of pipeline [1].	63
Fig. 3.18. Bending moment response of pipeline [1].	63
Fig. 3.19. Shear force response of pipeline [1].	64
Fig. 3.20. Maximum stress response of pipeline on A Path [1].	64
Fig. 3.21. Maximum longitudinal strain response of pipeline on A Path [1].	64
Fig. 4.1. Buried pipeline subjected to a strike-slip fault with faulting angle of (ψ) [1].	77
Fig. 4.2. Buried pipeline subjected to the strike-slip fault with $\psi = 0^\circ$ [1].	78
Fig. 4.3. The axial soil spring displacement results of the analytical Eq. (4.7) versus FEM analysis for cases A – E [1].	79
Fig. 4.4. The axial force of pipeline results of the analytical Eq. (4.9) versus FEM analysis: (a) cases A – C and (b) cases D – E [1].	79
Fig. 4.5. L_{conv} length of the pipeline based on deflection w_{yx} [1].	80
Fig. 4.6. Coordinate system and pipeline partitioning for the analytical solution [1].	82
Fig. 4.7. Deformed pipeline element subjected to strike-slip fault movement [1].	82
Fig. 4.8. Soil-pipe interaction springs adjustment [1].	88
Fig. 4.9. Part of the finite element model and attached soil-pipe interaction springs [1].	88
Fig. 4.10. Transverse deflection response of a buried pipeline subjected to strike-slip fault movement (analytical versus FEM results) [1].	89
Fig. 4.11. Axial force response of a buried pipeline subjected to strike-slip fault movement (analytical versus FEM results) [1].	90
Fig. 4.12. Bending moment response of buried pipeline subjected to strike-slip fault movement (analytical versus FEM results) [1].	91
Fig. 4.13. Shear force response of buried pipeline subjected to strike-slip fault movement (analytical versus FEM results) [1].	92
Fig. 4.14. Maximum stress (springline stress) response of buried pipeline subjected to strike-slip fault movement (analytical versus FEM results) [1].	93
Fig. 5.1. Buried pipeline subjected to a strike-slip fault with faulting angle of (ψ). (a) 3D view [21]. (b) pipe section.	103
Fig. 5.2. Buried pipeline subjected to a strike-slip fault with $\psi = 0^\circ$: (a) 3D section view, (b) vertical section view.	104
Fig. 5.3. Axial soil-pipe interaction's (axial soil spring) force-displacement curve.	104

Fig. 5.4. Free body diagram of the slid segment of the pipeline.	105
Fig. 5.5. Transverse elastoplastic soil pipe-interaction curve.....	109
Fig. 5.6. Coordinate system and pipeline partitioning for the analytical solution.....	110
Fig. 5.7. Deformed pipeline element subjected to strike-slip fault movement.....	110
Fig. 5.8. Force-displacement curves of the soil-pipe interaction springs.	114
Fig. 5.9. Soil-pipe interaction spring adjustment.....	114
Fig. 5.10. Part of the finite element model and attached soil-pipe interaction springs.	115
Fig. 5.11. Response of a buried pipeline at a 0° strike-slip fault crossing, FEM (dashed curves) versus closed-form solution (solid curves). Analysis cases with fault movements of 0.5D, 1D, 2D, 4D, and 6D are shown in black, blue, red, green, and magenta, respectively: (a) Axial displacement distribution of the pipeline. (b) Axial force distribution of the pipeline.	115
Fig. 5.12. Transverse deflection response of a buried pipeline subjected to strike-slip fault movement (analytical versus FEM results) for $\delta = 0.5D-6D$ and $\psi = 90^\circ-45^\circ$. Curve and color representations are the same as in Fig. 5.11	117
Fig. 5.13. Axial force distribution of buried pipeline subjected to strike-slip fault movement (analytical versus FEM results) for $\delta = 0.5D-6D$ and $\psi = 90^\circ-45^\circ$. Curve and color representations are the same as in Fig. 5.11	118
Fig. 5.14. Bending moment distribution of buried pipeline subjected to strike-slip fault movement (analytical versus FEM results) for $\delta = 0.5D-6D$ and $\psi = 90^\circ-45^\circ$. Curve and color representations are the same as in Fig. 5.11	119
Fig. 5.15. Shear force response of buried pipeline subjected to strike-slip fault movement (analytical versus FEM results) for $\delta = 0.5D-6D$ and $\psi = 90^\circ-45^\circ$. Curve and color representations are the same as in Fig. 5.11	120
Fig. 5.16. Maximum stress distribution (on springlines) of buried pipeline at a strike-slip fault crossing (analytical versus FEM results) for $\delta = 0.5D-6D$ and $\psi = 90^\circ-45^\circ$. Curve and color representations are the same as in Fig. 5.11	121
Fig. 5.17. Maximum stress distribution (on crown/invert) of buried pipeline at a strike-slip fault crossing (analytical versus FEM results) for $\delta = 0.5D-6D$ and $\psi = 90^\circ-45^\circ$. Curve and color representations are the same as in Fig. 5.11	122
Fig. 6.1. Axial pull-out test model of buried pipeline (displacement contours) [1].	132
Fig. 6.2. stress-strain relationship at the pipe-soil interface for friction coefficients of 0.2, 0.3 and 0.4: (a) this study, (b) Vazouras et al. (2015) [12].	132
Fig. 6.3. Axial soil pipe interaction force-displacement relationship at the pipe-soil interface for friction coefficients of 0.2, 0.3 and 0.4 [1].	132
Fig. 6.4. Transverse sliding test model of buried pipeline (displacement contours) [1].	133
Fig. 6.5. Transverse soil-pipe interactions force displacement relationship for friction coefficients of 0.2, 0.3 and 0.4 [1].	133
Fig. 6.6. Ramberg-Osgood steel model.	135
Fig. 6.7. 3D-soild model for buried steel pipeline subjected to 60° strike-slip fault movement. Points A and B are springlines of the pipe.	135
Fig. 6.8. A part of beam model for buried steel pipeline subjected to 60° strike-slip fault	

movement with length of 60 m [1].	136
Fig. 6.9. Equivalent nonlinear soil springs for beam model [1].	136
Fig. 6.10. Transverse displacement of pipeline 3D-solid model versus Beam model at strike-slip fault crossing on neutral axis of pipe section [1].	137
Fig. 6.11. Mises stress and buckling status of buried pipeline at 60° strike-slip fault crossing with 0.17D, 0.5D, 1D, 2D, 3D and 4D fault movements [1].	138
Fig. 6.12. Maximum longitudinal stresses of buried pipeline subjected to 60° strike-slip fault 0.17D to 1D movement, 3D-solid model versus Beam model: (a) Left springline (b) Right springline [1].	139
Fig. 6.13. Maximum longitudinal stresses of buried pipeline subjected to 60° strike-slip fault 2D to 4D movement, 3D-solid model versus Beam model: (a) Left springline (b) Right springline [1].	139
Fig. 6.14. Maximum longitudinal strain of buried pipeline subjected to 60° strike-slip fault 0.17D to 1D movement, 3D-solid model versus Beam model: (a) Left springline (b) Right springline [1].	139
Fig. 6.15. Maximum longitudinal strain of buried pipeline subjected to 60° strike-slip fault 2D to 4D movement, 3D-solid model versus Beam model: (a) Left springline (b) Right springline [1].	140
Fig. 7.1. Soil-pipe interaction springs adjustment.	148
Fig. 7.2. Part of the finite element model and attached soil-pipe interaction springs [30].	149
Fig. 7.3. L_{conv} length of the pipeline based on deflection w_x [30].	149
Fig. 7.4. Test box schematic partitions	150
Fig. 7.5. The split-box test basin for 90° strike-slip faulting: (a) sketch before faulting, (b) sketch after 10D faulting, (c) photograph of the experiment split-box.	151
Fig. 7.6. Loose and dense sand grain size distribution.	152
Fig. 7.7. Triaxial shear test (CD) photograph.	153
Fig. 7.8. Triaxial shear consolidated drained test results: (a) Loose sand ($D_r = 75\%$), (b) Dense sand ($D_r = 95\%$).	153
Fig. 7.9. Lateral load test (LLT) inside the split-box, before faulting.	154
Fig. 7.10. HDPE pipe material stress-strain curve extracted from tensile/compression tests.	155
Fig. 7.11. Buried pipeline subjected to a strike-slip fault with faulting angle of (ψ). (a) Schematically 3D view [30]. (b) Pipe section.	155
Fig. 7.12. Setup of the sensors.	156
Fig. 7.13. Faultline and soil surface gridlines in experiment, fine and coarse grids size are 0.1 m and 0.2 m, respectively.	157
Fig. 7.14. Surface deformation at $10D = 0.63\text{ m}$ strike-slip fault movement: (a) case 1 (loose soil), (b) case 2 (dense soil).	158
Fig. 7.15. HDPE pipe deformation at $10D = 0.63\text{ m}$ strike-slip fault movement: (a) case 1 (loose sand), (b) case 2 (dense sand).	158
Fig. 7.16. HDPE pipelines deflection at $10D = 0.63\text{ m}$ fault movement: (a) Loose sand case (b) Dense sand case.	159

Fig. 7.17. Residual deformation of the pipeline after faulting experiments.....	160
Fig. 7.18. longitudinal strain on springlines of the HDPE pipeline buried in loose sand (test 1) at 2D–10D fault movements: (a) Right side, (b) Left side.....	161
Fig. 7.19. Longitudinal strain on springlines of the HDPE pipeline buried in dense sand (test 2) at 2D–10D fault movements: (a) Right side, (b) Left side.	161
Fig. 7.20. Peak longitudinal strain growth on pipe springlines: (a) loose sand case (test 1) at ± 30 cm from fault plane, (b) Dense sand case (test 2) at ± 10 cm from fault plane.	162
Fig. 7.21. Strain distribution of the HDPE pipeline buried in loose sand (test 1) at 2D–10D fault movements: (a) Axial strains, (b) Maximum bending strains.	163
Fig. 7.22. Strain distribution of the HDPE pipeline buried in dense sand (test 2) at 2D–10D fault movements: (a) Axial strains, (b) Maximum bending strains.	163
Fig. 7.23. Push-in experiment for 63 mm HDPE pipeline buried in dense sand (95% compacted sand) by Nishikawa 2017 [42].....	165
Fig. 7.24. 3D FEM model geometry and meshing of push-in test.....	166
Fig. 7.25. Shear stress–displacement curvature of the soil-pipe interaction interface for our FE model in comparison with full-scale push-in test of Nishikawa et al. [42]..	167
Fig. 7.26. FE-based maximum principal strain distribution of push-in test at 1.5 cm push..	167
Fig. 7.27. 3D FE model for buried HDPE pipeline subjected to 90° strike-slip fault movement, Left and Right points are springlines of the pipe section.	168
Fig. 7.28. Vertical deformation distribution at 10D movement of 90° strike-slip fault: (a) test 1, (b) test 2.....	169
Fig. 7.29. Longitudinal strain distribution of HDPE pipeline buried in loose sand subjected to 90° strike-slip fault with 2D to 10D movement for FEM versus experiment (test 1): (a,b) Left springline, (c,d) Right springline.	170
Fig. 7.30. Longitudinal strain distribution of HDPE pipeline buried in dense sand subjected to 90° strike-slip fault with 2D to 10D movement for FEM versus experiment (test 2): (a,b) Left springline, (c,d) Right springline.	171
Fig. 7.31. Maximum principal stress distribution of HDPE pipeline buried in loose sand at 90° strike-slip fault crossing (test 1) for 2D, 4D, 6D, 8D and 10D fault movements (unit: Pa).	172
Fig. 7.32. Maximum principal stress distribution of HDPE pipeline buried in dense sand at 90° strike-slip fault crossing (test 2) for 2D, 4D, 6D, 8D and 10D fault movements (unit: Pa).	173
Fig. 7.33. Maximum principal stress distribution of HDPE pipeline buried in Dense sand at 90° strike-slip fault crossing with 10D fault movements: (a) Loose sand case, (b) Dense sand case.	174
Fig. 7.34. Critical ovalized pipe cross-section at 10D movement: (a) test 1 (loose sand), (b) test 2 (dense sand).	175
Fig. 7.35. Pressure distributions on buried HDPE pipe perimeter under gravity load (unit: kPa), (a) Test 1, (b) Test 2.....	176
Fig. 7.36. Sketch of the assumptions and soil pressure distribution in integrating lateral soil-pipe interaction force calculation [45].....	177

Fig. 7.37. Pressure distributions on HDPE pipe perimeter buried in loose sand during faulting (test 1) (unit: kPa).....	178
Fig. 7.38. Pressure distributions on HDPE pipe perimeter buried in dense sand during faulting (test 2) (unit: kPa).....	179
Fig. 7.39. Lateral soil-pipe interaction force at different strike-slip fault movements for: (a) test 1 (loose sand), (b) test 2 (dense sand).	180
Fig. 7.40. Longitudinal bearing soil force on corner of HDPE joint of HDPE pipes.....	181

Tables List

Table 1.1. Details of moment tensor solution [47].....	10
Table 3.1. Soil-pipe interaction springs properties	47
Table 3.2. FEM-base and analytical model cases	47
Table 3.3. Distance between maximum bending moments of pipeline in experiment and analysis.	49
Table 3.4. API5L-X65 steel properties [1].....	61
Table 3.5. Parameters of Ramberg-Osgood stress-strain for steel API5L-X65 [1].	61
Table 3.6. Soil springs bilinear properties implemented in FEM analysis (Soil-1) [1].	61
Table 3.7. FE-based analysis cases [1].....	62
Table 4.1. Analysis cases scenarios [1].....	79
Table 4.2. Soil-pipe interaction properties [1].	87
Table 5.1. Soil-pipe interaction properties.	113
Table 6.1. API5L-X65 steel material of pipeline [1].	134
Table 6.2. Parameters of Ramberg-Osgood stress-strain for steel API5L-X65 [1].	134
Table 7.1. Estimated nonlinear soil-pipe interaction springs properties [33].	148
Table 7.2. The FEM analysis cases detail and the FEM analysis results.	149
Table 7.3. Split-box estimated.....	150
Table 7.4. Loose and dense properties based on aggregate test, triaxial CD testes and LLT.	154
Table 7.5. Details of the experiment cases.....	157

Chapter I:

Introduction

1.1. General problem

Pipeline systems have played a significant role in human history and industrial development. Pipeline networks such as oil and gas transmission lines and water and sewer lines provide the vital needs of human societies and have been constructed worldwide. Those pipeline systems basically convey food, water, fuel, energy, information, and other materials necessary for human existence. Therefore, pipelines have been constructed even in high seismic risk zones such as fault zones, which are prone to permanent ground displacements owing to fault rupture, sloping ground failure, or transient ground displacements caused by seismic waves [1].

Damage and even rupture of buried pipelines during earthquakes have caused severe health and environmental issues [2–13]. Earthquakes pose the largest risk for widespread structural damage. In the case of buried pipelines, most damage arises owing to permanent ground deformation (PGD) such as fault dislocations, liquefaction, and landslides, even though a very limited extent of pipelines is damaged by wave propagation [14, 15]. PGD has been reported to cause extensive damage and even ruptures of buried pipelines during historical earthquakes [2-13]. The influence of a pipeline's lifecycle on human life is vital because it provides crucial services to human societies, such as energy and water distribution. Additionally, environmental hazards that can result from the leakage of ecologically dangerous materials (e.g., chemicals, natural gas, fuel, or liquid waste) cannot be ignored. Thus, it is evident that the construction of buried pipelines subjected to fault displacement in earthquake-risk zones and mainly fault intersections is a key problem in engineering design [1, 16].

For having reliable resistance design of such pipelines, analysis methods of the buried pipelines are being developed in the last 50 years. In this regard, the problem of the buried pipeline at fault crossing is a major engineering task because PGD can cause severe pipeline damage [1, 15, 16].

1.2. Background

Recent developments in computing and finite element method (FEM) offer applicable solutions to the problem of buried pipelines at fault crossings [17]. Nowadays, FEM has been used for the verification and refinement of analytical methods, evaluation of factors influencing pipe response under different types of PGD, and assessment of pipeline performance criteria (e.g., local buckling, ovalization, tensile rupture) [18-30]. Vazouras et al. [28] modeled a hybrid (shell + spring) pipeline buried in solid soil by adding an analytically-extracted nonlinear pipe and soil-pipe interaction springs to the model at further distances from the fault line, which shortened the size required by the FEM model with the same accuracy. Criteria have been established regarding the buckling of a buried pipeline-crossing fault. Liu et al. [31] modeled pipeline response to reverse faulting using the FE commercial code ABAQUS. In their study, the pipe was modeled as shell elements and soil-pipe interaction was modeled as non-linear soil springs. The effects of yield strength and strain hardening parameters have been investigated for the buckling effect. A review of the FE models in the literature indicates that

various types of models including beam, shell, hybrid (beam+shell), new hybrid (spring+shell) are utilized to simulate the pipeline in the problem of the buried pipeline at crossing with active fault. There is a need to compare the different FEM modelling approaches including different element for pipe and soil to evaluate their advantages and limitations. Moreover, there is a need to evaluate and improve the design criteria by validated nonlinear FEM analyses.

Although FEM is a powerful engineering tool for stability analysis, its results are not valid unless they are not verified by experiments or analytical approaches. Experimental studies have also investigated the effect of faults on buried pipelines. Palmer et al. [32] described a large-scale testing facility at Cornell University and its working principles. O'Rourke and Bonneau [33] then performed large-scale tests to evaluate the effects of ground rupture on high-density polyethylene (HDPE) pipelines and the performance of steel gas pipelines distributed with 90° elbows. Lin et al. [34] performed small-scale tests to analyze the performance of buried pipelines under strike-slip faults. The centrifuge-based approach was first proposed by O'Rourke et al. [34, 35] to model ground faulting effects on buried pipelines and several centrifuge tests have been performed to investigate the response of buried HDPE pipeline subjected to faulting displacement [36-39]. Recently, Demirci et al. [30] investigated the behavior of continuous buried pipeline subjected to reverse fault motion using a new experimental centrifuge model of pipelines that cross reverse faults in addition to three-dimensional finite element (3D FE) analysis. Although several experimental studies have been done on the problem of buried pipeline at fault crossing, still there exist a need for more full-scale experiments on buried pipelines to develop the seismic design guidelines about the buried HDPE pipelines.

Simulation of the buried pipeline and surrounding soil respectively by shell elements and solid elements for a 3D FEM-based analysis is the most detailed approach for modeling the pipeline at fault crossing problem. which can produce the most realistic performance of buried pipeline including the local buckling, ovalization, and tensile damages. Because of the modeling complexity, this method mostly is used for research purposes which in this study we call it 3D-solid modeling approach. It is common to use the beam element for modeling of pipe and spring elements for modeling of soil-pipe interactions for design and even research purposes which is simpler than the 3D-solid modeling approach and in this study, we call it beam modeling approach. Both over mentioned FEM models include the geometrical nonlinearity effects and material nonlinearity effects.

Recent developments in computing and finite element method (FEM) offer applicable solutions to the problem of buried pipelines at fault crossings [17]. FEM has been extensively used for a range of applications including evaluation of factors that influence pipe response under different PGD types, verification and refinement of analytical methods, and pipeline performance assessment with respect to performance criteria (e.g. local buckling, ovalization, tensile rupture) [18–31]. However, FEM-based analysis for the reproduction of valid results is needed to be verified by experiments or analytical methods. A review of the FE models in the literature indicates that various types of models including beam, shell, hybrid (beam+shell),

new hybrid (spring+shell) are utilized to simulate the pipeline in the problem of the buried pipeline at crossing with active fault. Aside from numerical studies, several recent experimental studies have also addressed the problem of buried pipelines at active fault crossings [31–39].

The first analytical attempt in this area was based on a simplified analytical model by Newmark and Hall [40] that has been further extended [41,42]. However, these papers ignored the bending stiffness of the pipeline at the high-curvature zone, which results in an overestimation of the bending strain while increasing the axial forces and strains. The study of Kennedy et al. [41] was extended to strike-slip fault crossings with a simple development of pipeline bending stiffness by Wang and Yeh [43] who modeled transverse soil yielding conditions and partitioned the pipeline into four segments (two on both sides of the crossing fault, called the high-curvature zone) and two others further from the fault line and beside the high-curvature zone. The partitioning of the pipeline into four segments assumes that the soil yields over the entire high-curvature zone. However, in real cases, the yield of transverse soil springs across and beyond the high-curvature segments depends on the soil properties and fault movement amplitude. Moreover, the pipeline partitioning assumption causes each segment to be solved as a separate problem even with different equations, which increases the solution complexity and decreases the accuracy of the obtained results. Karamitros et al. [18] developed an analytical method for strike-slip faults that partitioned the pipeline into four segments for analysis based on beam-on-elastic-foundation and elastic beam theories, and the effects of axial forces and the steel pipe material's non-linearity was calculated externally and separately. Karamitros et al. [18] solved some limitations of previous methods but some shortcomings remain, as summarized here. (1) The same assumptions and issues faced by Wang and Yeh regarding the pipeline partitioning into four segments for the nonlinearity of transverse soil-pipe interaction. (2) The axial force terms and axial soil-pipe interaction are not implemented inside the governing equation and its effect is calculated in an indirect, external, and simplified manner. It is evident that a lack of axial forces within the governing equation has important consequences on the overall pipeline results (e.g. deflection, bending moment, shear force, stress, strain). (3) The effects of steel pipe material nonlinearity is applied by updating the Young's modulus of the steel inside the governing equation. A pipeline during fault movement can yield in specific areas, however, they use the same updated Young's modulus for all of the pipeline elongation even in sections that do not yield. In real cases, the Young's modulus changes only in the yielded sections and may differ in different sections depending on their yield ratio. (4) The calculation of bending strain is unclear. Trifonov and Cherniy [19] extended the Karamitros et al. [18] model to normal fault crossings, removed the symmetry conditions about the intersection point, and contributed transverse displacements for estimating a pipeline's axial elongation. The axial force was included in the governing differential equations only at the high-curvature zone, and geometrically induced second-order effects were taken into account. Although the study by Trifonov and Cherniy [19] presents progress for semi-analytical pipeline models, some shortcomings also remain. (1) The axial force and geometrical nonlinearity in the governing differential equation is only conducted in the two high-curvature

segments, and axial forces are assumed to be zero in the two further segments. In real cases, the axial force exists not only at the high-curvature zone but also along the pipeline elongation, which exponentially attenuates several hundred meters beyond the fault line. This assumption can drastically affect all of the pipeline results (e.g. deflection, stress, strain distributions). (2) The axial force term and geometrical nonlinearity within the governing equation at the high-curvature zone is implemented as a constant and calculated externally from another approximate solution for the entire pipeline at the high-curvature segment. In reality, the axial force of the pipeline is from friction and geometrical nonlinearity effects and is not constant, even in yielded soil. It undergoes a maximum at the crossing point with the fault line and, in most cases, does not attenuate even up to hundreds of meters beyond the fault line along either side of the pipeline. (3) The model includes shortcoming nos. 1, 2, and 3 from Karamitros et al. [18] regarding the partitioning of the pipeline into four segments and steel pipe material nonlinearity problems. These simplification assumptions introduce errors to the obtained results. Additionally, the developed solution by Trifonov et al. entails a complex system of equations, which can only be solved using optimization techniques among experts. In 2011, Karamitros et al. [20] extended their previous study to normal-slip fault crossings, which was not as complicated as that of Trifonov and Cherniy [19]. However, this solution had the same shortcomings as the results obtained in Karamitros et al. [18]. In 2012, Trifonov and Cherniy [21] presented an analytical model for the stress-strain analysis of buried steel pipelines that cross active faults by considering the effects of operational loads (internal pressure and temperature variation) on the basis of plane strain plasticity theory. However, this study had the same shortcomings as those of Trifonov and Cherniy [19] with regards to the governing differential equation of the buried pipeline.

1.3. Research objective

Despite substantial advances made by previous studies in the development of analytical solutions for a pipeline with regard to fault-crossing problems, axial soil-pipe interaction and axial forces owing to geometrical nonlinearity have not been appropriately applied in analytical solutions even in linear ranges. The abovementioned approximations are performed because the exact term of the axial soil-pipe interaction in the related differential equations has not thus far been considered. The main term that explains the effect of the crossing angle between the pipeline and fault in analytical analysis is the axial soil-pipe interaction. Therefore, implementation of an improper axial soil-pipe interaction term affects the buried pipeline's performance, especially in oblique fault crossings. Accordingly, there exists a need for developing a comprehensive analytical solution that incorporates the exact axial soil-pipe interaction term. Moreover, the nonlinearity of soil-pipe interaction has not yet been introduced within the governing equation. In previous studies, the transverse soil-pipe interaction nonlinearity was assumed by partitioning the pipeline into four segments, which does not reproduce real pipeline behavior and presents several issues. Moreover, none of the previous studies designed the axial soil-pipe interaction nonlinearity to include pipeline sliding and its

effects on the geometrical nonlinearity terms inside the analytical solutions. An inappropriate definition of soil-pipe interaction in the analytical solutions can lead to an unrealistic and uneconomical design and even disaster during future earthquakes. The development of a comprehensive analytical solution that incorporates exact nonlinear axial and transverse soil-pipe interaction terms within a united governing equation is therefore urgently required.

For establishment of an improved comprehensive analytical solution for this problem, it is needed to firstly evaluate the performance of buried pipeline at faults crossing and extract the effective variables and terms on the soil-pipe interaction and pipeline forces. And after all, check the experimental results for improving the design guideline for HDPE buried pipelines. According to what overmentioned, the objectives of present research are listed as follows:

- Investigation of the damage to the lifeline system during the 2017 Sarpole-Zahab Earthquake: A field investigation has been done by joint team of JSCE between 24th and 28th of December 2017. And the findings obtained through the quick survey. During the survey, we studied the damage to the lifeline system (e.g. pipelines) and the constructions and the results are reported.
- Identification of effective terms on axial soil-pipe interaction in problem of buried pipelines performance at strike-slip faults crossing: Effect of axial soil-pipe interaction and axial force of pipeline on pipeline performance by FEM analysis is investigated, to derive effective parameters on axial soil-pipe interaction spring term for developing in future analytical studies in elastic range. For verification of the FEM-based analysis an existing analytical solution, based on beam on elastic foundation theory is implemented for the case of buried pipeline at 90° strike-slip fault crossing. Additionally, FEM-based models result for 90° fault cases are compared by Hasegawa and Kiyono [44] experiment result.
- Steel pipe material nonlinearity effect on the force-displacement analysis of buried pipelines subjected to PGD: FEM-based analyses are conducted to evaluate the steel pipeline material's nonlinearity effect on the buried pipeline performance in crossing with the large dislocated strike-slip fault. Besides for deeper understanding of the steel pipeline material nonlinearity effect, some cases with elastic and some cases with plastic pipe materials by applying nonlinear soil-pipe interaction with various faulting angles are studied.
- Introduction of the axial force terms to governing equation for buried pipeline subjected to strike-slip fault movements: The axial soil-pipe interaction terms and axial forces terms of pipeline are extracted by a linear closed-form solution. Removed most of the previous simplification assumptions and introduced a new linear governing equation that includes axial force, axial soil-pipe interaction, and geometrical nonlinearity effects within the governing equation, which substantially increased the accuracy of the analytical solution for linear analysis. However, axial and transverse soil-pipe interaction nonlinearity were not considered within the governing equation.
- Introduction of nonlinear governing equation and corresponding semi-analytical solution

for buried pipelines at strike-slip faults crossing: We derived the analytical terms of nonlinear axial soil-pipe interaction, the frictional axial force and the axial force made by geometrical nonlinearity effects of the pipeline under large deformation including the sliding phenomenon effects of the buried pipeline within soil. And, we developed a united comprehensive governing equation for the entire pipeline elongation based on the beam-on-elastoplastic-foundation case and introduced the elastoplastic transverse soil pipe-interaction springs within the comprehensive nonlinear governing differential equation. Finally, we improved the solution procedure for the nonlinear governing equation and the analytical solution results are thoroughly validated using verified FEM models (consisting of geometrical nonlinearity and soil-pipe interaction nonlinearity with elastic pipe material). Introduced methodology significantly improved the past studies and extended the application area of the analytical solutions even in large deformation cases.

- Evaluation of nonlinear 3D FEM modeling approaches and damage criterions: To evaluate the applicatin range of the FEM modeling approaches and damage criterions of buried pipeline at strike-slip fault crossing, Firstly, the performance of buried pipeline at strike-slip fault crossing by nonlinear 3D-solid FEM and nonlinear beam modeling approaches is investigated. And secondly, pipe damage criterions (e.g. tensile rupture, local bucking, and cross-section distortion ovalization) are investigated.
- Damage evaluation of buried HDPE pipeline at strike slip fault crossing by Full-scale experimental study and calibration of 3D FE models: After introducing the analytical solution and FEM based studies about the problem of buried pipeline at fault crossing. For enrichment the achievements 2 full-scale experiments are conducted. Experiments are designated for evaluation of the SEKISUI CHEMICAL CO.'s HDPE pipes performance subjected to the strike-slip fault movements. Experiments are done for 2 cases of loose and dense sands and its results are compared with 3D FEM analyses results. Herein influence of important variables on the buried HDPE pipeline at 90° strike-slip are studied to improve the seismic design guidelines of buried HDPE pipelines.

1.4. Organization of the thesis

The results of this study are presented in eight chapters as follows:

In chapter I, an introduction about the problem and an abstract review of past studies and their shortcomings is expressed. In second part of this section objectives and achievements of this study is abstractly introduced. Finally, damage to the lifeline systems during historical earthquake [2–12] and more recently 2017 Sarpole-Zahab Earthquake [13] (our field survey) are reported.

In chapter II, a review is conducted on the literature corresponding to FEM-based, experimental and analytical solution methods employed for study of the buried pipeline subjected to the earthquake faults movement.

In chapter III, changes on behavior of the buried pipeline due to the changes in axial soil-

pipe interaction at strike-slip fault is investigated by FEM, and effective terms on axial force and axial soil-pipe interactions boundary conditions are detected for future analytical studies in elastic range. Moreover, effect of steel pipe material nonlinearity on buried pipeline performance evaluated against the large dislocated strike-slip fault movements.

In chapter IV, we introduced a novel linear governing equation and its corresponding solution for problem of buried pipeline subjected to strike-slip fault movements. Introduced governing equation includes the linear axial soil-pipe interaction, linear frictional axial force terms and axial forces made by geometrical nonlinearity effects within it. Firstly, the linear axial soil-pipe interaction terms, axial forces terms, and axial forces made by geometrical nonlinearity are derived through closed-form solutions. Secondly, derived the new linear governing equation of buried pipeline at strike-slip fault crossing and introduced the corresponding solution procedure. Thirdly, verified the FEM models. Finally, verified results of the new governing equation versus identical verified FEM models. New analytical methodology substantially increased the accuracy of the analytical solution for linear analysis.

In chapter V, a new comprehensive governing equation including elastic perfectly plastic axial soil-pipe interaction and elastoplastic transverse soil-pipe and corresponding solution method, is introduced. Mentioned methodology includes the effects the buried pipeline sliding within the soil, plasticity of the transverse soil and geometrical nonlinearity effects. Introduced methodology significantly improved the past studies and extended the application area of the analytical solutions even in large deformation cases.

In chapter VI, a comparative study is conducted between the 3D solid and shell nonlinear FEM modeling approach and 3D nonlinear beam-spring modeling approaches and their application ranges, for the problem of buried pipelines at strike-slip faults crossing. Additionally, the performance and damage criteria are evaluated through 3D nonlinear FEM analysis. All the analyses have the nonlinear soil material, nonlinear pipe material, the nonlinear interface properties, and geometrical nonlinearity effects.

In chapter VIII, two full-scale experiments are carried out for buried HDPE pipeline at strike slip fault crossing. Experiments are designated for performance evaluation of the SEKISUI CHEMICAL CO's HDPE pipes subjected to the strike-slip fault movements. Experiments are done for 2 cases of loose and dense sands and its results are compared with 3D FEM analyses results. Moreover, influence of important variables on the buried HDPE pipeline at 90° strike-slip are studied to improve the seismic design guidelines of buried HDPE pipelines.

In chapter VIII, the results of the study are summarized and concluding remarks are presented. Prospective advancements of research efforts are presented in terms of future works.

1.5. Damages to the lifeline system owing to the earthquake

The crucial importance of lifeline systems during the earthquake were first emphasized in the in San Francisco earthquake and ensuing fires in 1906 [45]. This earthquake disaster caused failure of several lifelines, including: breakage of gas distribution and service lines, damage to fire stations, breaks to the water distribution system resulting in total loss of water for fire-

fighting purposes. Following 1906, several earthquakes continued to illustrate the importance of lifelines in earthquakes. The 1971 San Fernando Earthquake, illustrated more effects of earthquake on lifelines; there were damage to electrical substations, hundreds of breaks in the water distribution system, loss of telephone service due to this damage, near-collapse of a major dam, numerous breaks in the gas distribution system, collapse of major freeway overcrossings, damage to emergency facilities, including collapse and major loss of life at a hospital, and major damage or partial collapse at several other hospitals[6].

Lifeline earthquake engineering is a relatively new field. It recognized formally in the 1970's with the establishment in the United States of ASCE's Technical Council on Lifeline Earthquake Engineering [46].

1.5.1. 2017 Sarpole-Zahab earthquake

On November 12, 2017, at 21:48 local time (18:18 UTC) a destructive earthquake occurred near the town of Sarpole-Zahab in Kermanshah Province, Western Iran. The earthquake had the moment magnitude of 7.4 as reported by Iranian Seismological Center (IRSC) and Global Centroid Moment Tensor Catalog (GCMT) or 7.3 as reported by United States Geological Survey (USGS) [13]. Seismic characteristics of Sarpole-Zahab earthquake is illustrated in **Fig. 1.1** and **Table 1.1**.

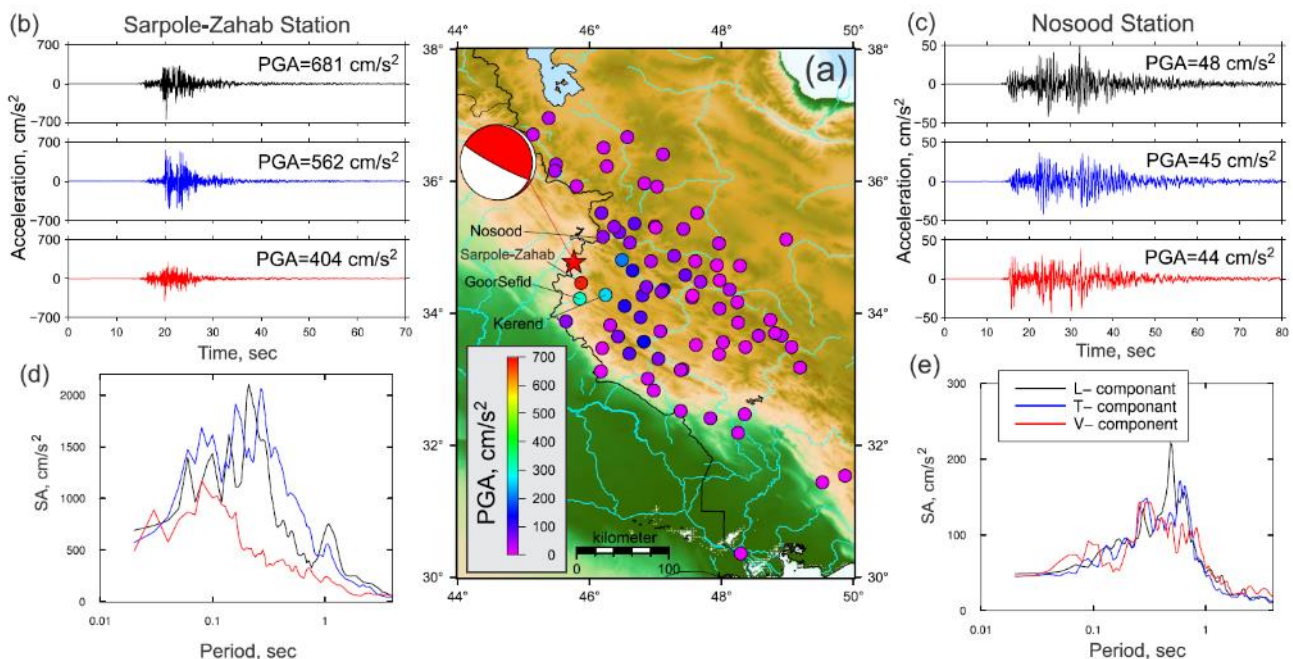



Fig. 1.1. (a) Locations of the recording stations together with the obtained maximum PGA values of two horizontal components; (b) and (c) acceleration time series for Sarpole-Zahab and Nosood stations, respectively; (d) and (e) obtained absolute spectral acceleration for Sarpole-Zahab and Nosood stations, respectively [13].

Table 1.1. Details of moment tensor solution [47].

Centroid; Lat: 34.77° N, Lon: 45.76° E, Depth: 8 km, Time relative to the origin time (Sec): +5.96	
Mw: 7.4, Moment (N.m): 1.366e+20, DC%: 93.4, CLVD%: 6.6, Variance Reduction: 0.51	
Nodal Planes; strike: 4°, dip: 10°, rake: 157°	
strike: 116°, dip: 86°, rake: 81°	
P-axis; azimuth: 215°, plunge: 41° - T-axis; azimuth: 17°, plunge: 48°	
Moment Tensor (N.m); Mrr: 0.201, Mtt: 0.035, Mpp: -0.236, Mrt: 1.209, Mrp: -0.572, Mtp: 0.174, Exponent :20	

Regarding the event location IRSC seems to have the best estimation since they have used stations near the epicenter. **Table 1.1** shows the details of moment tensor solution of IRSC4). They report the latitude of 34.77° and longitude of 45.76° and depth of 18 km for the main event. One important foreshock has been reported by IRSC which has occurred at 17:35 UTC (less than an hour before the main shock) with magnitude of 4.4. As of 11 January 2018, there have been 598 aftershocks in magnitude range of 2.5 to 5.4 according to IRSC bulletin4). Seismographs and seismological data are illustrated in **Fig. 1.1** [13].

1.5.2. Damage to lifelines and infrastructures at Sarpole-Zahab earthquake

(1) Damage to bridges and roads

In general, the significant structural damage was not observed in main bridges, the deck bridges that are very common for low span bridges were all safe and ready for use. However, in some cases, there were cracks and even collapse in some parts of stone retaining walls beside the structure of the bridge, like the Sarpole-Zahab main road bridge. The expansion joints have become active during the ground motion. And all of the spans of the bridges adjacent to the joints have experienced some minor or moderate movements. Damages and big cracks were detected on the stone walls of some little bridges (**Fig. 1.2**) in the village roads; one was in the road of Taze-Kand Village to Sarpole-Zahab city. There were apparent cracks both sides of the



Fig. 1.2. (a) Damage to the retaining walls beside the bridge of Sarpole-Zahab City, (b) damage to little stone and concrete bridge at a Village road nearby Sarpole-Zahab [13].



Fig. 1.3. Damage to Ban-Zardeg village road due to severe rock-fall.



Fig. 1.4. Damage to village road nearby Sarpole-Zahab (the road has rehabilitated temporarily).

bridge in the joint locations in the asphalt [13].

On the roads of damage area due to the settlement, landslide and rock fall (**Fig. 1.3**), some damages were observed on the roads, but it was only in some parts only. On the roads of the Sarpole-Zahab to some Villages nearby it, there was observed some of that mentioned damages (**Fig. 1.4**). One of the severe damages on the roads was in Ban-Zardeg Village road that was because of severe rock fall that can be seen in the figures. And most of the mentioned damages have been repaired during the first week after the earthquake [13].

(2) Damage to electricity network

After earthquake 3 cities of Sarpole-Zahab, Qasr-e Shirin and Tazehabad and the villages in their territory had 100% power outage. The cities of Pave, Gilan-e Gharb and Kermanshah and territory villages had 30-60% power outage, totally around 480 villages had a power outage after the main earthquake. In big cities from some hours to at most 48 hours the power was restored and in Villages with-in less than 4 days power was restored [48]. In transmission network, different levels of damage have been happened from light to severe. The main observed cases: tilting and collapse of Utility poles in cities due to buildings or walls falling



Fig. 1.5. Collapse of transmission tower due to rock fall on the mountains nearby the Sarpole-Zahab city.

on them, falling of 63kV transformer in Sarpole-Zahab city, even one collapse of Transmission tower (**Fig. 1.5**) due to rock fall on the mountains nearby the Sarpole-Zahab city. Damages to the electrical power network were estimated about 36 million Dollars by Power ministry [49,13].

(3) Damage to water supply network

Rural water and Wastewater Company of Kermanshah Province established that 13 cities of Kermanshah Province were damaged, and because of Contamination in 7 cities mainly Sarpole-Zahab, Qasr-e Shirin and Gilan-e Gharb water was cut for 2 weeks. More than 500 cases on the main water pipelines and more than 300 cases on main wastewater pipelines were damaged [50]. Damages to the water supply network were estimated about 72 million Dollars by Power ministry [49]. These damages were observed even in large polyethylene pipelines (**Fig. 1.6**) with the diameter of 600mm. In some Villages due to landslide and settlement in main water pipelines (**Fig. 1.7**), severe damages and failures were observed, it is needed to say that the pipelines were repaired before our observation; one was the Gurchi-Bashi Village's main water pipeline and the water vessel [13].



(a)



(b)

Fig. 1.6. (a) Damage to Palane-Olya village main water polyethylene pipeline due to a long land slide (repaired), (b) big deformation in main water polyethylene pipeline of Gurchi-Bashi village.



Fig. 1.7. Damage to the Gurchi-Bashi village vessel and Pipeline due to settlement and landslide in some parts.

(4) Damage to the gas network

National Iran Gas Company established that in general, there was no damage in main Gas pipelines. However, there was some damage to joints of the gas pipelines at the entrance to the houses (**Fig. 1.8**). And because of this after the main earthquake, the gas was cut off for one day [4]. One of this kind damages were observed at Ahmadabad town in Sarpole-Zahab due to the falling of walls on the gas pipe joints [13].



Fig. 1.8. Damage to joint of the gas pipeline at the entrance to the houses at Sarpole-Zahab city.

References

- [1] O'Rourke, M. J., Liu, X. [1999] "Response of buried pipelines subject to earthquake effects," Monograph Series, Multidisciplinary Center for Earthquake Engineering Research (MCEER).
- [2] O'Rourke, T. D., Lane, P. A. [1989] "Liquefaction hazards and their effects on buried pipelines," Technical report NCEER-89-0007, National Center for Earthquake Engineering Research, Buffalo, NY, USA.
- [3] O'Rourke, T. D., Palmer, M.C. [1996] "Earthquake performance of gas transmission pipelines," *Earthquake Spectra* 20(3), 493–527.
- [4] Earthquake Engineering Research Institute [1999] "Kocaeli, Turkey Earthquake of August 17," EERI Special Earthquake Report.
- [5] Uzarski, J., Arnold, C. [2001] "Chi-Chi, Taiwan, earthquake of September 21, 1999 reconnaissance Report," *Earthquake Spectra* 17 (Suppl. A).
- [6] Jennings, P. C., [1971] "Engineering features of the San Fernando earthquake February 9, 1971," California Institute of Technology Report, EERL, 71–02.
- [7] MaCaffrey, M. A., O'Rourke, T. D. [1983] "Buried pipeline response to reverse faulting during the 1971 San Fernando Earthquake," *ASME, PVP* 77, 151–9.
- [8] Desmond, T. P., Power, M. S., Taylor, C. L., Lau, R. W. [1995] "Behavior of large-diameter pipeline at fault crossings," *ASCE, TCLEE* (6), 296–303.
- [9] Nakata, T., Hasuda, K. [1995] "Active fault I 1995 Hyogoken Nanbu earthquake," *Kagaku* 65, 127–42. (in Japanese)
- [10] Shih, B. J., Chang C. H. [2006] "Damage Survey of Water Supply Systems and Fragility Curve of PVC Water Pipelines in the Chi–Chi Taiwan Earthquake," *Natural Hazards* 37, 71–85. <https://doi.org/10.1007/s11069-005-4657-9>
- [11] Kazama, M., Noda, T. [2012] "Damage statistics (Summary of the 2011 off the Pacific Coast of Tohoku Earthquake damage)," *Journal of Soils and Foundations* 52(5), 780–792.
- [12] Wham, B. P, Dashti, S., Franke, K., Kayen, R., Oettle, N. K. [2017] "Water supply damage caused by the 2016 Kumamoto Earthquake," *Journal of Lowland Technology International* 19(3), 165-174.
- [13] Miyajima, M., Fallahi, A., Ikemoto, T., Samaei, M., Karimzadeh, S., Setiawan, H., Talebi, F., Karashi J. [2018] "Site Investigation of the Sarpole-Zahab Earthquake, Mw 7.3 in SW Iran of November 12, 2017" *JSCE J. Disaster FactSheets* 2018, FS2018-E-0002. Available online: http://committees.jsce.or.jp/disaster/system/files/FS2018-E0002_0.pdf
- [14] Ariman, T., Muleski, G. E. [1981] "A review of the response of buried pipelines under seismic excitations." *Earthquake Engineering and Structural Dynamics* 9, 133–51.

- [15] Liang, J., Sun, S. [2000] “Site effects on seismic behavior of pipelines: a review,” *ASME Journal of Pressure Vessel Technology* 122(4), 469–75.
- [16] Manolis, G. D., Beskos, D. E. [1997] “Underground and lifeline structures,” in *Computer analysis and design of earthquake resistant structures: a handbook*, ed. Beskos, D. E and Anagnostopoulos, S.A. (CMP, Southampton, United Kingdom), 775–837.
- [17] American Lifelines Alliance—ASCE. *Guidelines for the Design of Buried Steel Pipe*” July 2001 (with addenda through February 2005).
- [18] Karamitros, D., Bouckovalas, G., Kouretzis, G. [2007] “Stress analysis of buried steel pipelines at strike-slip fault crossings,” *Soil Dynamics and Earthquake Engineering* 27, 200–11.
- [19] Trifonov, O. V., Cherniy, V. P. [2010] “A semi-analytical approach to a nonlinear stress–strain analysis of buried steel pipelines crossing active faults,” *Soil Dynamics and Earthquake Engineering* 30(11), 1298–308.
- [20] Karamitros, D. K., Bouckovalas, G. D., Kouretzis G. P., Gkesouli V. [2011] “An analytical method for strength verification of buried steel pipelines at normal fault crossings,” *Soil Dynamics and Earthquake Engineering* (13), 1452-1464.
- [21] Trifonov, O. V., Cherniy V. P. (2012). “Elastoplastic stress-strain analysis of buried steel pipelines subjected to fault displacements with account for service loads,” *Soil Dyn Earthq Eng* 33,54–62.
- [22] Lim, M. L., Kim, M. K., Kim, T. W., Jang, J. W. (2001). “The behavior analysis of buried pipeline considering longitudinal permanent ground deformation,” In *pipeline 2001: advances in pipelines engineering & construction* (San Diego, California), vol. 3, 107. ASCE. [https://doi.org/10.1061/40574\(2001\)3](https://doi.org/10.1061/40574(2001)3)
- [23] O’Rourke, M. J., Vikram, G., Abdoun, T. (2003). “Centrifuge modeling of buried pipelines,” In: *Proceedings of the Sixth U.S. conference and workshop on lifeline earthquake engineering*, August 10–13, 2003, Long Beach, CA. pp. 757–768.
- [24] Sakanoue, T., Yoshizaki, K. (2004). “A study on earthquake-resistant design for buried pipeline using lightweight backfill,” In: *Proceedings of the 13th world conference on earthquake engineering*, Vancouver, B.C., Canada, August 1-6, Paper No.2389.
- [25] Takada, S., Hassani, N., Fukuda, K. (2001). “A new proposal for simplified design of buried steel pipes crossing active faults,” *Earthq Eng Struct Dyn* ;30:1243–57.
- [26] Vazouras, P., Karamanos, S. A., Dakoulas, P. (2010). “Finite element analysis of buried steel pipelines under strike-slip fault displacement,” *Soil Dyn Earthq Eng* ;30:1361–76.
- [27] Vazouras, P., Karamanos, S. A., Dakoulas, P. (2012). “Mechanical behavior of buried steel pipes crossing active strike-slip fault,” *S, Soil Dyn Earthq Eng*;41:164–80.
- [28] Vazouras, P., Dakoulas, P., Karamanos, S. A. (2015). “Pipe–soil interaction and pipeline

- performance under strike–slip fault movements,” *Soil Dyn Earthq Eng* ;72:48–65.
- [29] Zhang, L., Zhao, X., Yan, X., Yang, X. (2016). “A new finite element model of buried steel pipelines crossing strike-slip faults considering equivalent boundary springs,” *Eng Struct*;123:30–44.
- [30] Demirci, H. E., Bhattacharya, S., Karamitros, D., Alexander, N. (2018) “Experimental and numerical modelling of buried pipelines crossing reverse faults,” *Soil Dyn Earthq Eng* ;114:198–214.
- [31] Liu, X., Zhang, H., Li, M., Xia, M., Zheng, W., Wu, K., Han, Y. (2016). “Effects of steel properties on the local buckling response of high strength pipelines subjected to reverse faulting,” *J Nat Gas Sci Eng* ;33:378–87.
- [32] Palmer, M. C., O’Rourke, T. D., Stewart, H. E., O’Rourke, M. J., Symans, M. (2006). “Large displacement soil-structure interaction test facility for lifelines” In: *Proceedings of the 8th US national conference commemorating the 1906 San Fransisco earthquake*, EERI, San Fransisco.
- [33] O’Rourke, T. D., Bonneau, A. (2007). “Lifeline performance under extreme loading during earthquakes,” In: Pitilakis KD, editor. *Earthquake Geotechnical Engineering*. Dordrecht, Netherlands: Springer; 407–32.
- [34] Lin, T. J., Liu, G. Y., Chung, L. L., Chou, C.H., Huang, C. W. (2012). “Verification of Numerical Modeling in Buried Pipelines under Large Fault Movements by Small-Scale Experiments,” In: *Proceedings of the 15WCEE*, 2012, 9, 6685–6693.
- [35] O’Rourke, M. J., Gadicherla, V., Abdoun, T. (2005). “Centrifuge modeling of PGD response of buried pipe,” *Earthq Eng Eng Vib* ;4:69–73.
- [36] Ha, D., Abdoun, T. H., O’Rourke, M. J., Symans, M. D., O’Rourke, T.D., Palmer, M. C., Stewart, H. E. (2008). “Buried high-density polyethylene pipelines subjected to normal and strike–slip faulting — a centrifuge investigation,” *Can Geot J* ;45: 1733–1742.
- [37] Ha, D., Abdoun, T. H., O’Rourke, M. J., Symans, M. D., O’Rourke, T. D., Palmer, M. C., Stewart, H. E. (2008). “Centrifuge modelling of earthquake effects on buried high-density polyethylene (HDPE) pipelines crossing fault zones,” *ASCE J Geotech Geoenviron Eng* ;134(10):1501–15.
- [38] Abdoun T. H., Ha, D., O’Rourke, M.J., Symans MD, O’Rourke TD, Palmer MC, Stewart HE. (2009). “Factors influencing the behavior of buried pipelines subjected to earthquake faulting” *Soil Dyn Earthq Eng* ;29:415–27.
- [39] Xie, X., Symans, M. D., O’Rourke, M. J., Abdoun, T. H., O’Rourke, T. D., Palmer, M. C., Stewart, H. E. (2011). “Numerical 47odelling of buried HDPE pipelines subjected to strike-slip faulting” *J Earthq Eng* ;15(8):1273–96.
- [40] Newmark, N. M., Hall, W. J. [1975] “Pipeline design to resist large fault displacement,”

Proc. of the U.S. national conference on earthquake engineering, University of Michigan, Ann Arbor, Michigan, 416–25.

- [41] Kennedy, R. P., Chow, A. M., Williamson, R. A. [1977] “Fault movement effects on buried oil pipeline,” ASCE Transportation Engineering Journal 103(5), 617–33.
- [42] Kennedy, R. P., Kincaid, R. H. [1983] “Fault crossing design for buried gas oil pipelines” ASME, PVP conference 77, 1–9.
- [43] Wang, L. R. L., Yeh, Y. A. [1983] “A refined seismic analysis and design of buried pipeline for fault movement,” Earthquake Engineering and Structural Dynamics 13(1), 75–96.
- [44] Hasegawa, N., Kiyono, J. (2016). “Study of the plastic hinge position buried steel pipeline on fault displacement” JSCE Journal of Earthquake Engineering, (35), 161-166. (in Japanese)
- [45] ATC-25, (1991). Seismic Vulnerability and Impact of Disruption of Lifelines in the Conterminous U.S. Earthquake Hazard Reduction Series 58, Federal Emergency Management Agency, FEMA 224.
- [46] Duke, C.M., and Matthiesen, R.B. (1973). Earthquakes, lifelines and ASCE. Civil Engineering, ASCE, 65-67.
- [47] Iranian Seismological Center, <http://irsc.ut.ac.ir> [Accessed 28 Feb. 2018].
- [48] Report of the November 12th 2017 sarpol-zahab Kermanshah province earthquake, International Institute of Earthquake Engineering and Seismology, 5th edition, Vol. 3, Iran, December 2017. (In Persian)
- [49] Kermanshah Earthquake’s damaged 107 million Dollars to infrastructures, Fars News website, Iran, January 12th 2018. (In Persian)
<http://www.farsnews.com/13960923001215>
- [50] “260 milliard Tomans damage to water and wastewater Installations”, Iranian Students News Agency (ISNA), Iran, January 11th 2018. (In Persian)
<https://www.isna.ir/news/96092312832>
- [51] National Iran gas company’s activities at west part of country explained, PetroEnergy Information Network, Iran, November 15th 2018. (In Persian)
<http://www.shana.ir/fa/newsagency/279720>

Chapter II:
Literature review

2.1. General remarks

Pipeline systems have played a significant role in human history and industrial development. Pipeline networks such as oil and gas transmission lines and water and sewer lines provide the vital needs of human societies and have been constructed worldwide even in high seismic risk zones [1]. Earthquakes pose the largest risk for widespread structural damage. In the case of buried pipelines, most damage arises owing to permanent ground deformation (PDG) such as fault dislocations, liquefaction, and landslides, even though very few pipelines themselves are damaged by wave propagations [2, 3]. PDG has been reported to cause extensive damage and even ruptures of buried pipelines during historical earthquakes [4-7] such as the 1971 San Fernando earthquake [8-10], 1995 Kobe earthquake [11], 1999 Kocaeli earthquake [6], 1999 Chi-Chi earthquake [12], 2011 Tohoku earthquake [13], 2016 Kumamoto earthquake [14], and more recently, the 2017 Sarpole-Zahab earthquake [15]. The influence of a pipeline's lifecycle on human life is vital because it provides crucial services to human societies, such as energy and water distribution. Additionally, environmental hazards that can result from the leakage of ecologically dangerous materials (e.g., chemicals, natural gas, fuel, or liquid waste) cannot be ignored. Thus, it is evident that the construction of buried pipelines subjected to fault displacement in earthquake-risk zones and mainly fault intersections is a key problem in engineering design [1, 16].

2.2. Surface faulting

Faulting comprise of seismic induced permanent ground deformation (PDG) associated with the relative displacement of parts of the earth's crust. Faults are classified based on the motion direction to three types as illustrated in **Fig. 2.1**. If the normal or reverse fault occurs in combination with the strike-slip fault it is termed oblique fault.

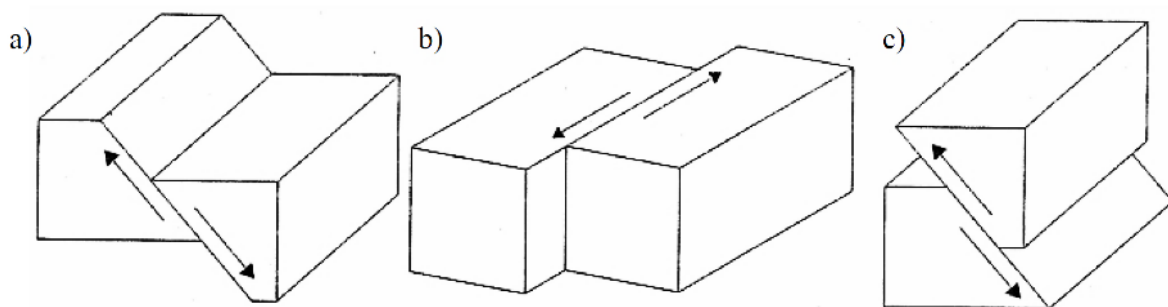


Fig. 2.1. Fault movement classification: (a) normal, (b) strike-slip, (c) reverse [17].

The fault displacement amplitude depends on the fault type, earthquake magnitude, focal depth and geology. In absence of accurate data of the expected fault displacement, the relationships introduced by Wells and Coppersmith [18] can be useful:

$$\log \delta_{fs} = -6.32 + 0.90M, \quad \text{strike - slip fault movement} \quad (2.1)$$

$$\log \delta_{fn} = -4.45 + 0.63M, \quad \text{normal fault movement} \quad (2.2)$$

$$\log \delta_{fr} = -0.74 + 0.08M, \quad \text{reverse fault movement} \quad (2.3)$$

$$\log \delta_{fb} = -4.80 + 0.69M, \quad \text{blind fault movement (i. e. poorly known fault)} \quad (2.4)$$

where δ_{fs} , δ_{fn} , δ_{fr} and δ_{fb} respectively are the average fault displacements of the strike-slip, normal and reverse, and blind fault respectively expressed in meters, whereas M is the moment magnitude of the earthquake. Based on Wells and Coppersmith [18], the observed fault displacement is in range 0.05 to 8.0 m for strike slip faults, 0.08 to 2.1 m for normal faults and 0.06 to 1.5 m for reverse faults.

2.3. Modelling of buried steel pipeline subjected to strike slip faulting

2.3.1. Analytical studies

Since the 1970s, this problem has been addressed in a range of numerical, experimental, and analytical studies. starting from the pioneering work of Newmark and Hall in 1975 [19] that formally analyzed the fault crossing problem in connection with the design of the TransAlaskan Pipeline. Their simplified model consists in a straight buried pipeline subjected to a strike-slip fault movement with β faulting angle, which is schematically illustrated in **Fig 2.2**. The pipeline is assumed fixed in the ground at the two anchor points located at a distance L_a from the fault trace where it is able to deform axially due to the imposed fault movement.

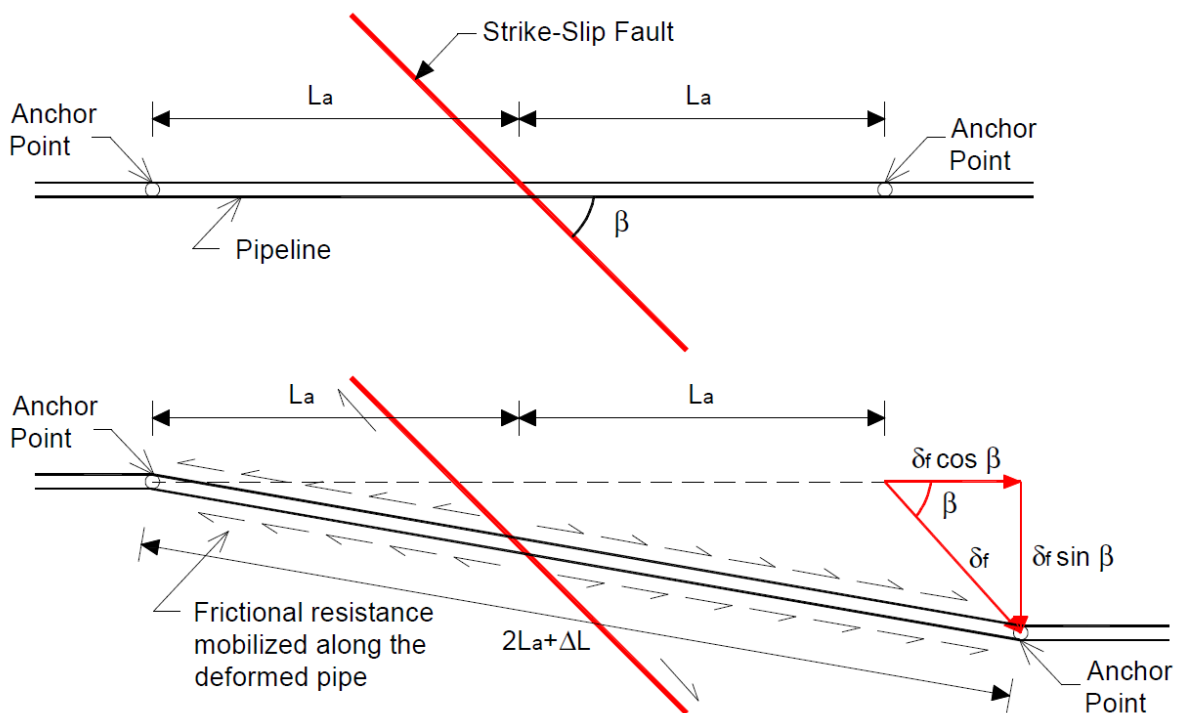


Fig. 2.2. Schematic representation of the Newmark-Hall model for buried pipeline crossing a strike-slip fault [19].

The pipe is considered as a cable by neglecting its bending stiffness and only the axial soil-pipeline interaction is taken into account. Then, the elongation of the pipe ΔL is calculated as the geometrical change in length of the pipeline between the two anchor points as a result of the fault displacement δ_f , while its average strain ε was evaluated as the ratio of the pipeline elongation ΔL and its initial length between the two anchorage points ($2L_a$). The pipe elongation ΔL is calculated by a simplified cable assumption based on the two anchorage lengths ($2L_a$) and the axial component of the fault movement which is shown in **Fig. 2.2**:

$$\delta_f^2 + (2L_a)^2 + 2\delta_f \cos\beta = (2L_a + \Delta L)^2 \quad (2.5)$$

dividing both sides of the Eq. (2.5) by $8L_a$ and neglecting the ΔL^2 , the average strain in the pipe ε , in function of the fault displacement δ_f and inclination angle β is obtained as follows:

$$\varepsilon = \frac{\Delta L}{2L_a} \cong \frac{\delta_f}{2L_a} \cos\beta + \frac{\delta_f^2}{8L_a^2} \quad (2.6)$$

According to the Newmark and Hall approach, pipeline failure is assumed to occur when the average tensile strain value of 4% is exceeded. Newmark and Hall ignored the bending stiffness of the pipeline at the high-curvature zone, which results in an overestimation of the bending strain while increasing the axial forces and strains. They assumed, the transverse component of soil has small effect for local flexural strains, if the anchoring points are sufficiently away from the fault crossing.

The Newmark and Hall [19] approach, was extended by Kennedy et al. [20] at 1977 through proposing an analytical method which accounts the lateral soil interaction. In this method, the assumed deformed profile of the pipe is shown in **Fig. 2.3**. As a simplification, it was assumed that the pipe deforms with constant curvature between an anchoring point and the fault intersection. Beyond the anchoring points, the pipe is assumed straight. And consequently, the

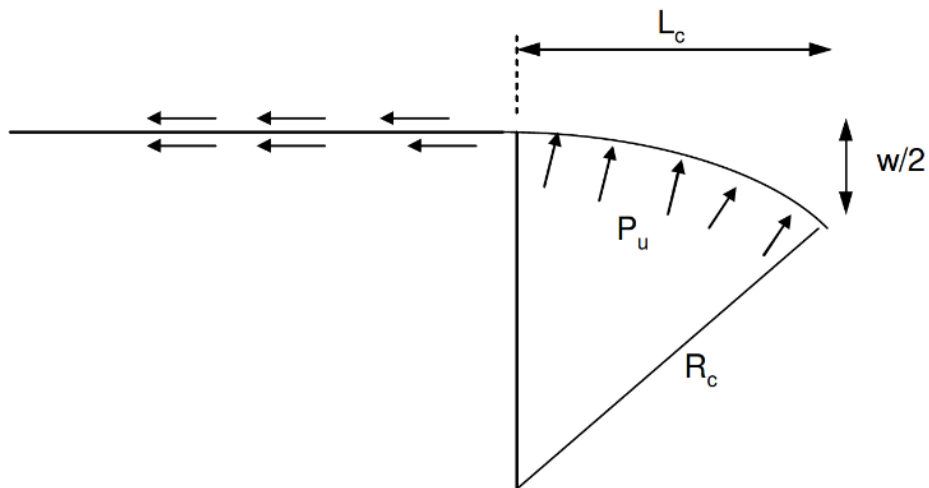


Fig. 2.3. Schematic diagram of the pipe deformed shape assumed by Kennedy et al. [20].

bending strain of the pipe is derived as:

$$\varepsilon_b = \frac{D}{2R_c} \quad (2.7)$$

Where R_c is the constant curvature assumed for the pipe segment between anchor point and fault movement. This assumption of constant curvature is required to determine the axial force in the pipe segment. It is assumed that the axial tensile force is essentially independent of the curvature if the bending is less than 80% of the axial strain. However, in reality, the pipe curvature is likely to change gradually as moving away from the faultline; as such the pipe sections away from the abrupt ground displacement will resemble a beam on an elastic foundation. Furthermore, they assumed that the pipeline section yields in the high-curvature zone, which means that the bending stiffness of the pipeline is ignored. This assumption does not represent the real pipeline performance and overestimates the bending strain while increasing the axial forces and strains. In this method, The models proposed by Kennedy et al. [20] and Newmark and Hall [19] are referenced in ASCE 1984 [21] guidelines for strike-slip and normal fault movements.

The study of Kennedy et al. [20] was extended to strike-slip fault crossings with a simple development of pipeline bending stiffness by Wang and Yeh [22]. they attempted to incorporate the bending stiffness of the pipe segment closest to the faultline. They assumed; the bending stiffness of the pipe cannot be ignored unless the pipe undergoes very large deformations. In this method, buried pipeline is partitioned into four segments, two on both sides of the crossing fault, called the high-curvature zone (segments AB and BC) and two others further from the fault line and beside the high-curvature zone (segments AA' and CC') as illustrated in Fig. 2.4.

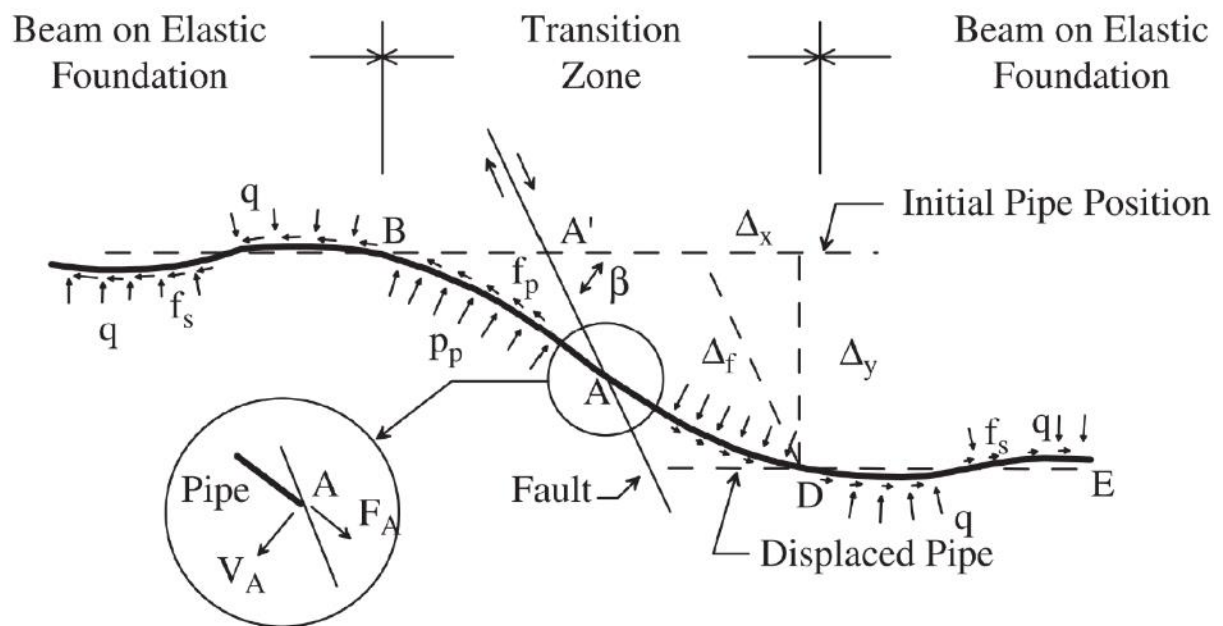


Fig. 2.4. Schematic representation of the Wang and Yeh. [22] model for pipeline crossing a strike-slip fault.

The outside segments (AA' and CC') are modeled based on the beams on elastic foundation theory (Eq. (2.8)), while the pipe sections in high-curvature zone (AB and BC) are assumed to be behaving as a cable with constant curvature. Neglect of the pipeline bending stiffness in high curvature segments causes the reduction in bending moment resulting from the increased axial force. However, when considering the force equilibrium of these pipe segments, the end bending moment and shear forces transmitted further segments are considered. Additionally, partitioning of the pipeline into four segments assumes that the soil yields in the two high-curvature zones. However, the soil yielding starting point can differ from soil to soil and may yield away or closer from the high curvature zone and this assumption is not realistic. The pipeline partitioning assumption causes each segment to be solved as a separate problem even with different equations, which increases the solution complexity and decreases the accuracy of the obtained results.

$$EI \frac{d^4 w}{dx^4} + k_t w = 0 \quad (2.8)$$

Karamitros et al. [23] developed Wang and Yeh [22] analytical method through adding the pipe's bending stiffness at the high curvature zone for strike-slip faults. They also partitioned the pipeline into four segments, two further segments (AA' and CC') where analyzed based on beam-on-elastic-foundation with governing equation of Eq. (2.8) and two high curvature segments (AB and BC) assumed as a beam and solved based on the elastic beam theories (see **Fig. 2.5**). Additionally, the effects of axial forces and the steel pipe material's non-linearity was calculated externally and separately. Karamitros et al. [23] solved some limitations of previous methods but some shortcomings remain, as summarized here. (1) The same assumptions and issues faced by Wang and Yeh regarding the pipeline partitioning into four segments for the nonlinearity of transverse soil-pipe interaction. (2) The axial force terms and

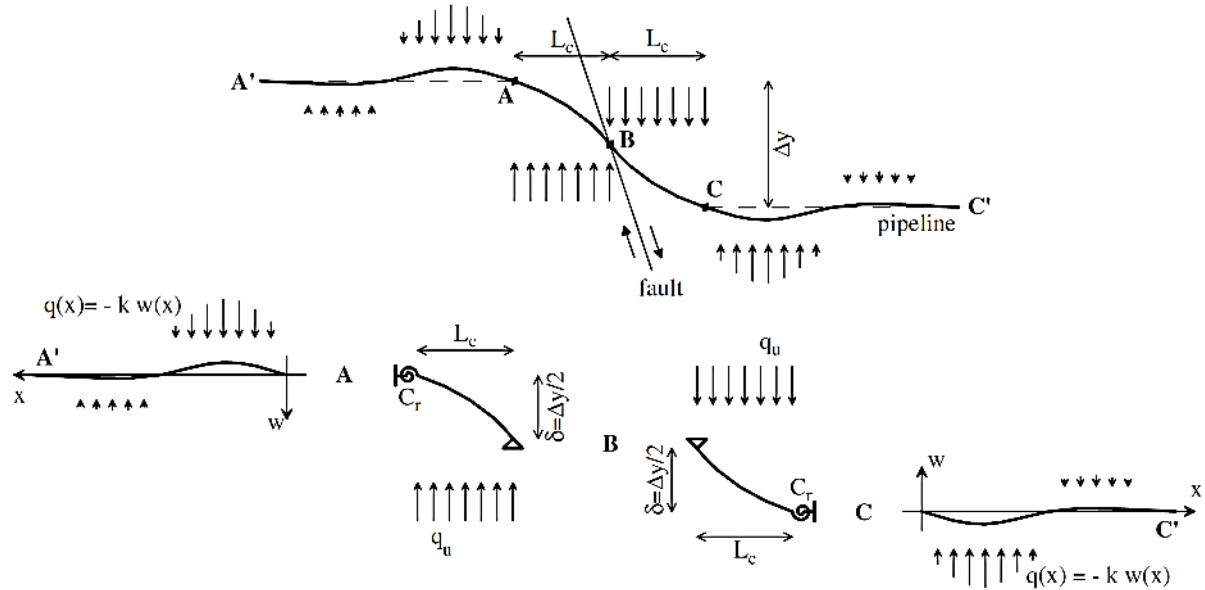


Fig. 2.5. Schematic representation of the Karamitros et al. (2007) [23] model for pipeline crossing a strike-slip fault.

axial soil-pipe interaction are not implemented inside the governing equation and its effect is calculated in an indirect, external, and simplified manner. It is evident that a lack of axial forces within the governing equation has important consequences on the overall pipeline results (e.g. deflection, bending moment, shear force, stress, strain). (3) The effects of steel pipe material nonlinearity is applied by updating the Young's modulus of the steel inside the governing equation. A pipeline during fault movement can yield in specific areas, however, they use the same updated Young's modulus for all of the pipeline elongation even in sections that do not yield. In real cases, the Young's modulus changes only in the yielded sections and may differ in different sections depending on their yield ratio. (4) The calculation of bending strain is unclear.

Trifonov and Cherniy [24] extended the Karamitros et al. [23] model to strike-slip and normal fault crossings, removed the symmetry conditions about the intersection point, and contributed transverse displacements for estimating a pipeline's axial elongation. The axial force was included in the governing differential equations only at the high-curvature zone, and geometrically induced second-order effects were taken into account. They also followed the Wang and Yeh [22] assumption and partitioned the pipeline to four segments, two further segments (AA' and CC') where analyzed based on beam-on-elastic-foundation with governing equation of Eq. (2.8) and two high curvature segments (AB and BC) analyzed based on Eq. (2.9) by adding axial forces to the beam on elastic foundation equation.

$$EI \frac{d^4 w}{dx^4} - F \frac{d^2 w}{dx^2} = q \quad (2.9)$$

where E is the elastic Young's modulus of the pipeline, w_y is the transverse deflection, I is moment of inertia of the pipeline, k_t is the transverse soil springs constant, q is soil transverse reaction at high curvature zone, and F is the axial force at high curvature zone. Based on their definitions F , is a constant force along the pipeline for all the high curvature zone segments,

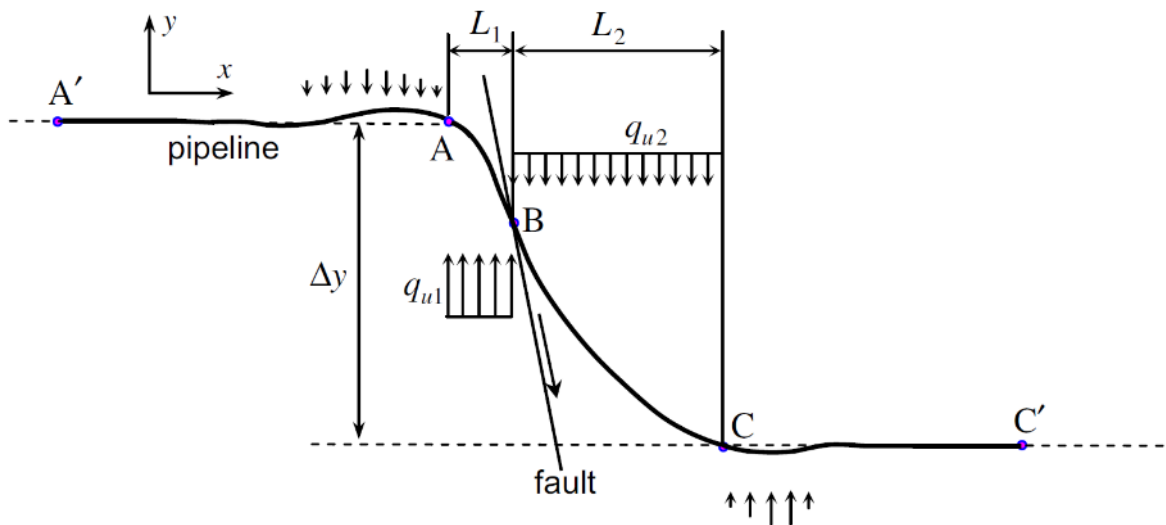


Fig. 2.6. Schematic representation of the Trifonov and Cherniy (2010) [24] model for pipeline crossing a strike-slip fault.

which is calculated externally through a simplified equation and input inside the Eq. (2.9) and q is also constant soil reaction force at all the high curvature zone segments. And further segments based on Eq. (2.8) does not have any axial forces effect.

For better understanding in **Fig. 2.7** and **Fig. 2.8**, schematically axial force of pipeline for Trifonov and Cherniy [24] is compared versus a verified FEM model (real axial force distribution in pipeline). As illustrated in **Fig. 2.8**, not only the axial force is not constant at high curvature zones, but also axial force exists with a large magnitude inside the further segments up to very long distances. In their study, two Eq. (2.8) and Eq. (29) have been connected through a complex optimization method which is not only cumbersome but also decreases the results accuracy.

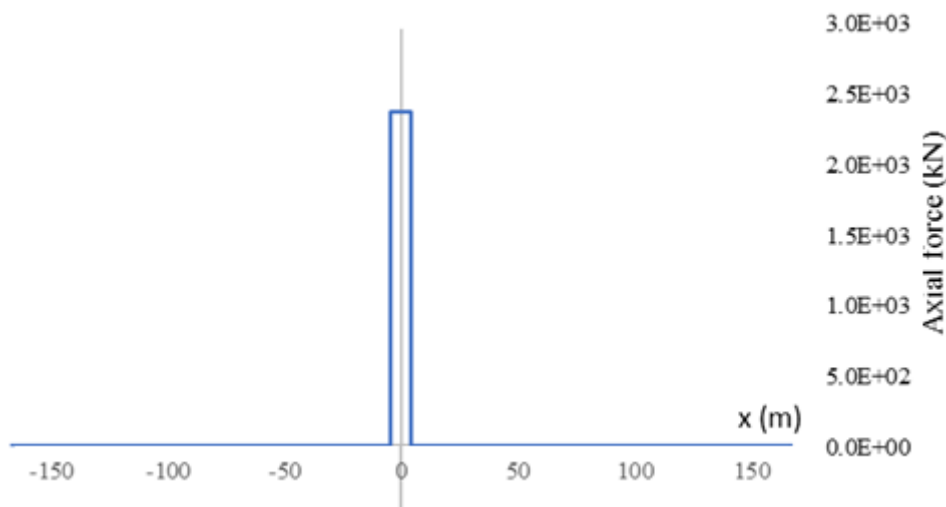


Fig. 2.7. Schematic representation of the Trifonov and Cherniy (2010) [24] model for axial force in problem of buried pipeline at strike-slip fault crossing.

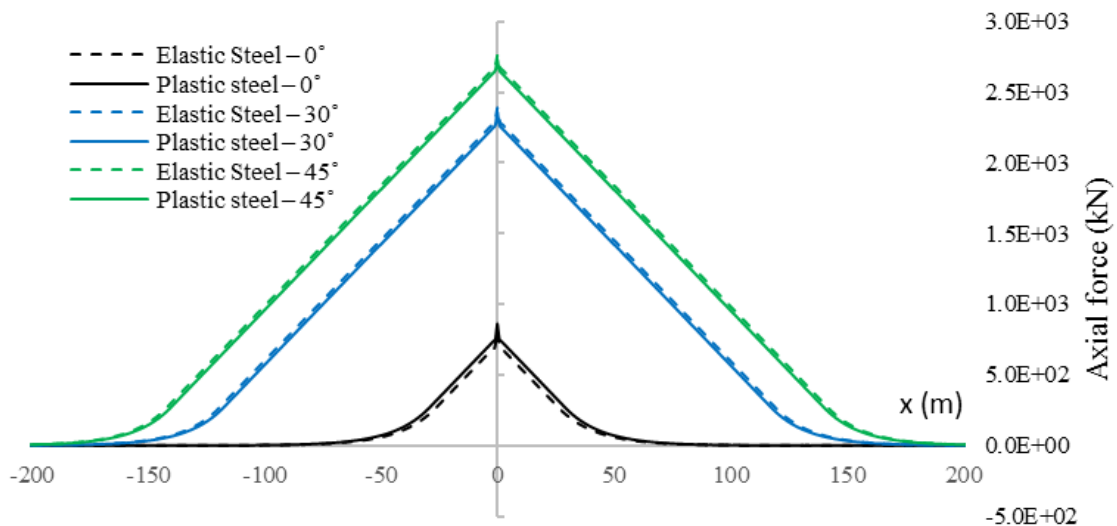


Fig. 2.8. valid axial force responses shape for a steel buried pipeline at strike-slip fault crossing (chapter 3).

Although the study by Trifonov and Cherniy [19] presents progress for semi-analytical pipeline models, some shortcomings also remain. (1) The axial force and geometrical

nonlinearity in the governing differential equation is only conducted in the two high-curvature segments, and axial forces are assumed to be zero in the two further segments (**Fig. 2.7**). In real cases, the axial force exists not only at the high-curvature zone but also along the pipeline elongation, which exponentially attenuates several hundred meters beyond the fault line. This assumption can drastically affect all of the pipeline results (e.g. deflection, stress, strain distributions). (2) The axial force term and geometrical nonlinearity within the governing equation at the high-curvature zone is implemented as a constant and calculated externally from another approximate solution for the entire pipeline at the high-curvature segment. In reality, the axial force of the pipeline is from friction and geometrical nonlinearity effects and is not constant, even in yielded soil. It undergoes a maximum at the crossing point with the fault line and, in most cases, does not attenuate even up to hundreds of meters beyond the fault line along either side of the pipeline. (3) The model includes shortcoming nos. 1, 2, and 3 from Karamitros et al. [18] regarding the partitioning of the pipeline into four segments and steel pipe material nonlinearity problems. These simplification assumptions introduce errors to the obtained results. Additionally, the developed solution by Trifonov et al. entails a complex system of equations, which can only be solved using optimization techniques among experts.

In 2011, Karamitros et al. [25] extended their previous study [23] 2007 model to normal fault crossings and removed the symmetry conditions about the intersection point (see **Fig. 2.9**). However, this study had the same shortcomings as the results obtained in Karamitros et al. [23].

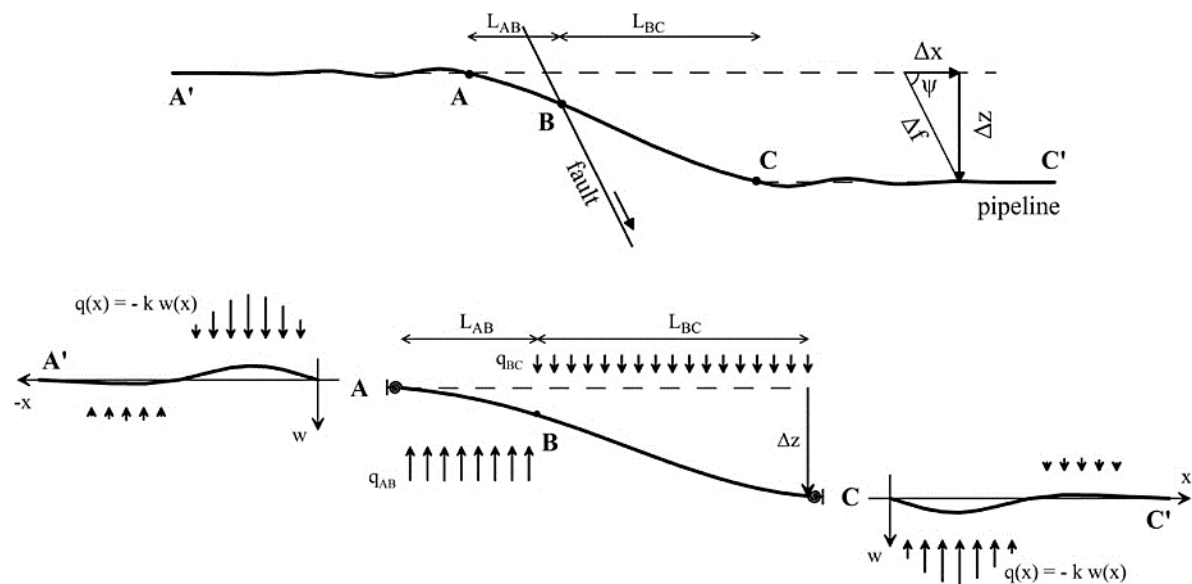


Fig. 2.9. Schematic representation of the Karamitros et al. (2011) [25] model for pipeline crossing a normal fault.

In 2012, Trifonov and Cherniy [26] presented an analytical model for the stress-strain analysis of buried steel pipelines that cross active faults by considering the effects of operational loads (internal pressure and temperature variation) on the basis of plane strain plasticity theory. They used the same partitioning assumption and Eq. (2.8) and Eq. (2.9) as their governing equations (see **Fig. 2.10**). And their study had the same shortcomings as those

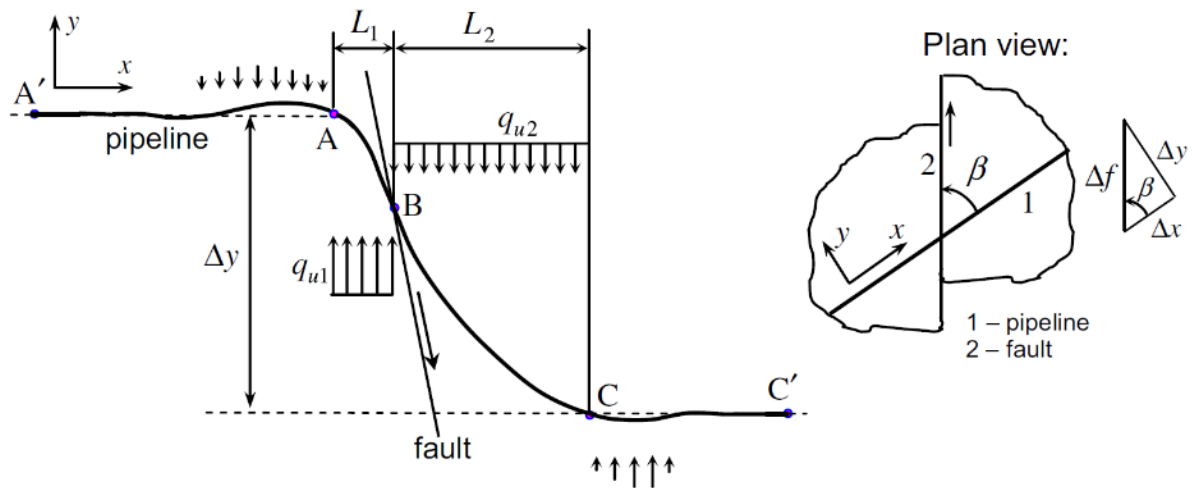


Fig. 2.10. Schematic representation of the Trifonov and Cherniy (2012) [26] model for pipeline crossing a strike-slip fault.

of Trifonov and Cherniy [24] with regards to the governing differential equation of the buried pipeline. Although, they employed the von Mises yield surface in their external calculations to include the pipe material nonlinearity, but because the effects of steel pipe material nonlinearity are applied by updating the Young's modulus of the steel inside the governing equation. It updates same Young's modulus for all of the pipeline elongation even in sections that do not yield. In real cases, the Young's modulus changes only in the yielded sections and may differ in different sections depending on their yield ratio.

2.3.2. Finite element method studies

Nowadays, by improvement of processors and finite element method (FEM), FEM-based analysis is applicable solutions for the problem of the buried pipeline crossing active fault. FEM has been recently used for verification of analytical solutions and evaluation of the buried pipeline performance for assessment of criteria such as local buckling, ovalization and tensile damages [23-32]. There exist several FEM-based pieces of research, with different modeling approaches.

In 2001, Takada et al. [33] employed a beam-shell hybrid model to develop a new simplified method for evaluating the bending angle and critical axial strain in the pipeline at fault crossings. In their model, the central segment of the pipeline within 30m at both sides of the fault, was modelled with shell elements, whereas the remaining part was modelled as a beam, allowing to reduce the computational costs and avoid the error associated with the enforced boundaries at the ends of the shell segment. In 2004, Liu et al. [34,35] analyzed a buried pipeline subjected to fault movement by modelling the pipe segment around the fault zone with shell elements and the surrounding soil with springs in the three orthogonal directions connected at each node of the shell pipeline. In further distances from faultline, the observed pipeline behaviour was elastic and the relative soil-pipe displacement in the transverse direction

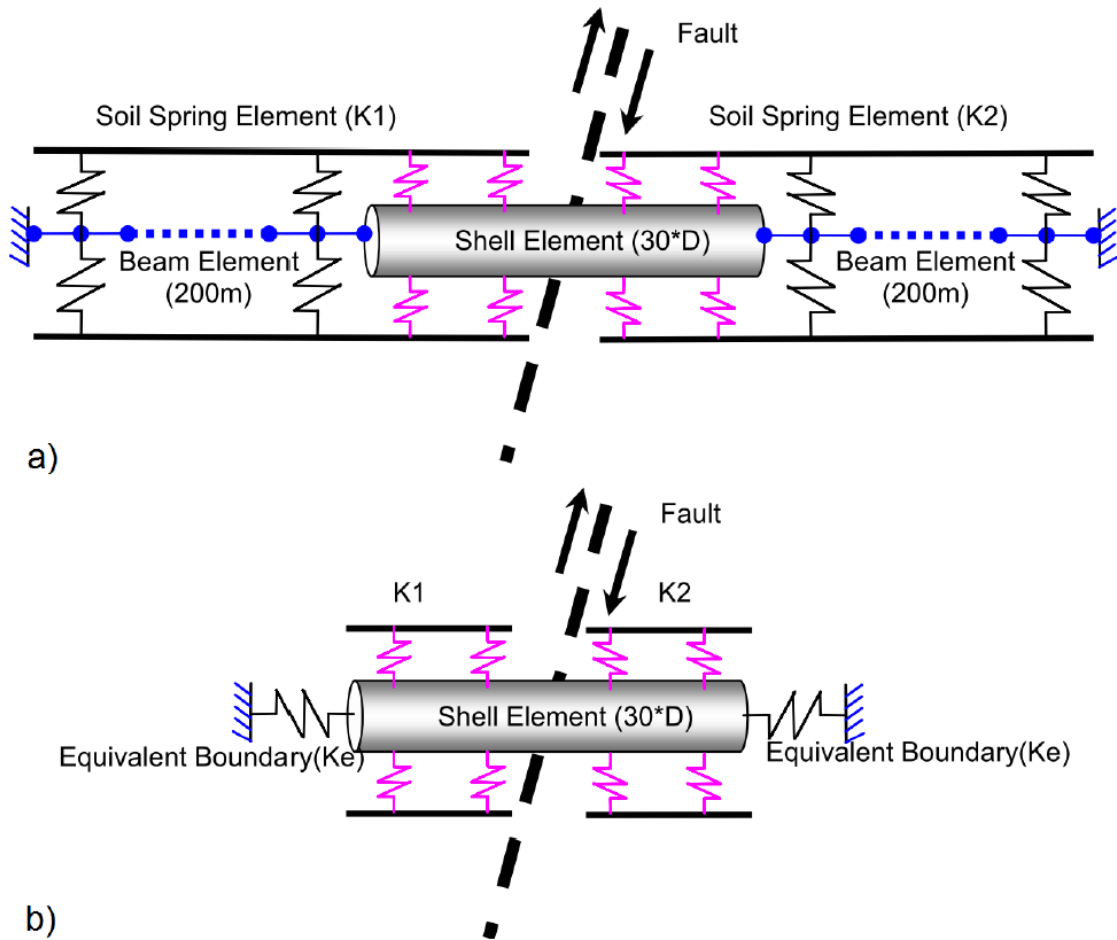


Fig. 2.11. Schematic representation of shell FEM models for a pipe crossing the fault according Liu et al. study [35]: **(a)** hybrid shell-beam model, **(b)** shell model with equivalent boundary.

was negligible so that the pipeline resulted only loaded axially by the soil friction. Differently from other previous methods, they evaluated analytically the force-displacement relationship of the soil-pipe system away from the fault, which was subsequently applied in terms of a nonlinear axial spring at the two ends of the shell model, as schematically illustrated in **Fig. 2.11**.

The proposed shell-spring model with the equivalent boundary was employed by the authors to assess the seismic performance of two water steel pipelines with large diameters damaged at fault crossing during the Kocaeli and Chi-Chi Earthquake.

In 2011, Joshi et al. [36] analyzed the response of buried pipelines subjected to reverse fault motion by developing a simple finite element model using 3-D beam elements as shown in **Fig. 2.12**. Soil surrounding the pipeline was modeled using nonlinear springs which support the pipeline at discrete points. features incorporated in the model were pipe-material nonlinearity, nonlinear Winkler spring model of the soil, geometric nonlinearity associated with large deformations, and post-buckling behaviour of pipeline (in case of beam buckling).

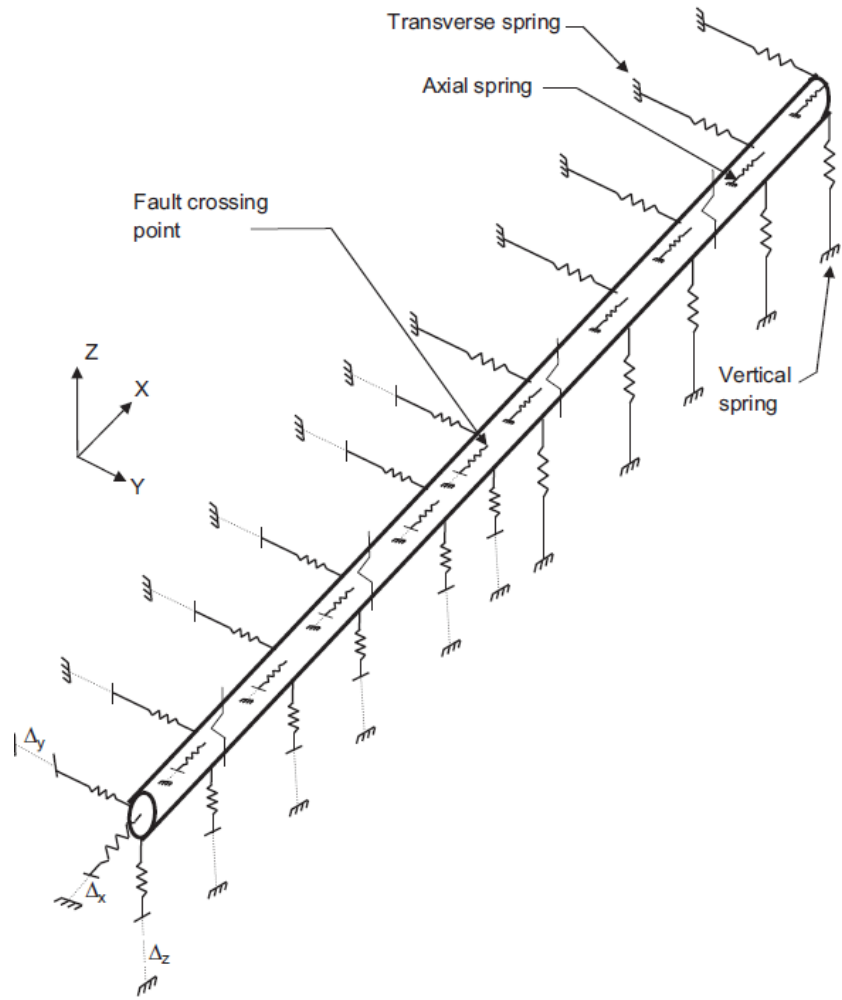


Fig. 2.12. Geometry of proposed FEM model for buried pipeline by Joshi et al. [36]

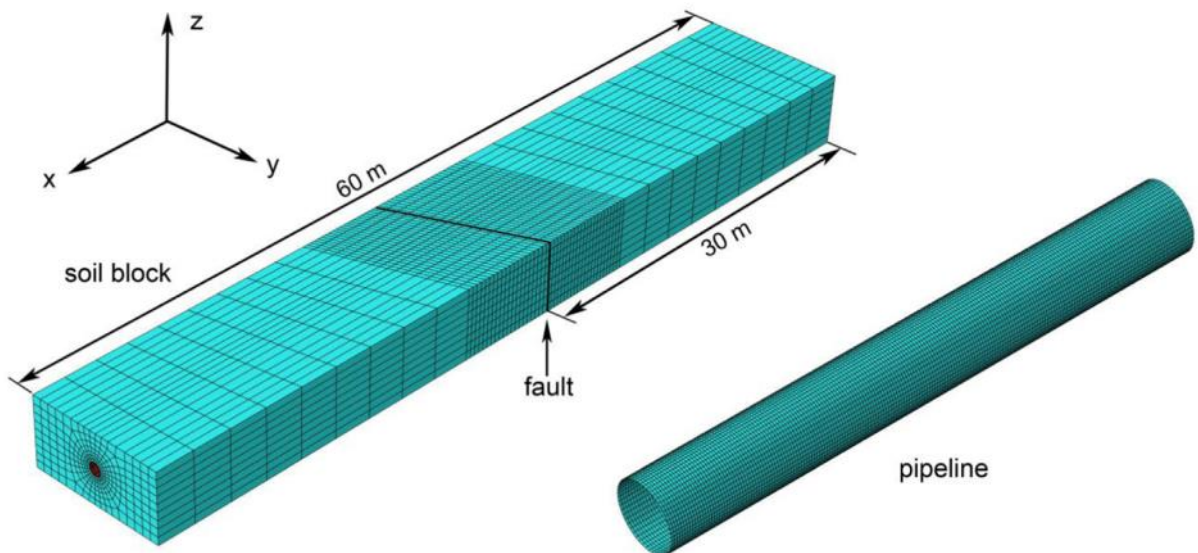


Fig. 2.13. Finite element model of buried steel pipeline at strike-slip fault crossing made by created Vazouras et al. [37].

In 2015, Vazouras et al. [37] modeled a hybrid (shell and solid elements beside equivalent

springs) pipeline buried in solid soil, by adding the analytically extracted equivalent axial springs of soil and pipeline, they shortened the size of needed FEM model with the same accuracy of the full FEM model (see **Fig. 2.13**). they investigated the pipeline performance under strike-slip fault movement, refining the numerical methodology presented in the previous publications by substituting the fixed boundaries at the pipeline ends with an equivalent nonlinear spring. The latter accounted for a finite or infinite length of the pipeline beyond the shell model and was obtained analytically, considering the elastic deformation of the system as well as the development of sliding once the shear strength was reached at the pipe-soil interface.

In 2016, Liu et al. [38] modeled buried pipeline at reverse fault crossing using FE commercial code ABAQUS which pipe was modeled as shell elements and soil-pipe interaction was modeled as non-linear soil springs. They modeled pipe as shell elements and soil-pipe interaction was modeled as non-linear soil springs. besides, they had an investigation on buckling of buried pipeline influenced by yield strength and strain hardening parameters (see **Figs. 2.14** and **2.15**).

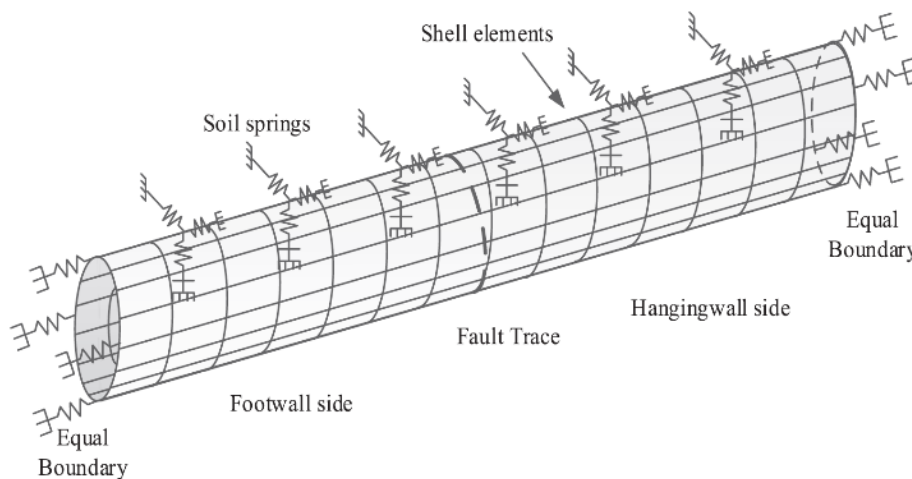


Fig. 2.14. Sketch of finite element model of Liu et al. [38].

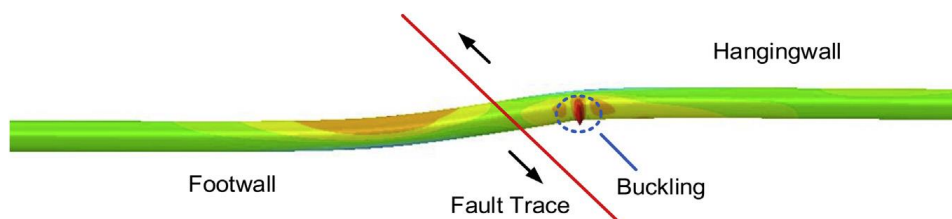


Fig. 2.15. Local buckling under reverse fault displacement [38].

In 2018, Demirci et al. [39] studied the behavior of a continuous buried pipeline subjected to reverse fault motion by a new experimental centrifuge modeling of pipeline crossing reverse fault. Which used 3D FEM analyses besides for more details (see **Fig. 2.16**). A review of the FEM-based researches in the literature shows that for modeling of pipe various modeling approaches including beam, shell, hybrid (beam+shell), new hybrid (spring+shell) and soil continuum-shell model are used to evaluate pipeline performance against earthquake fault

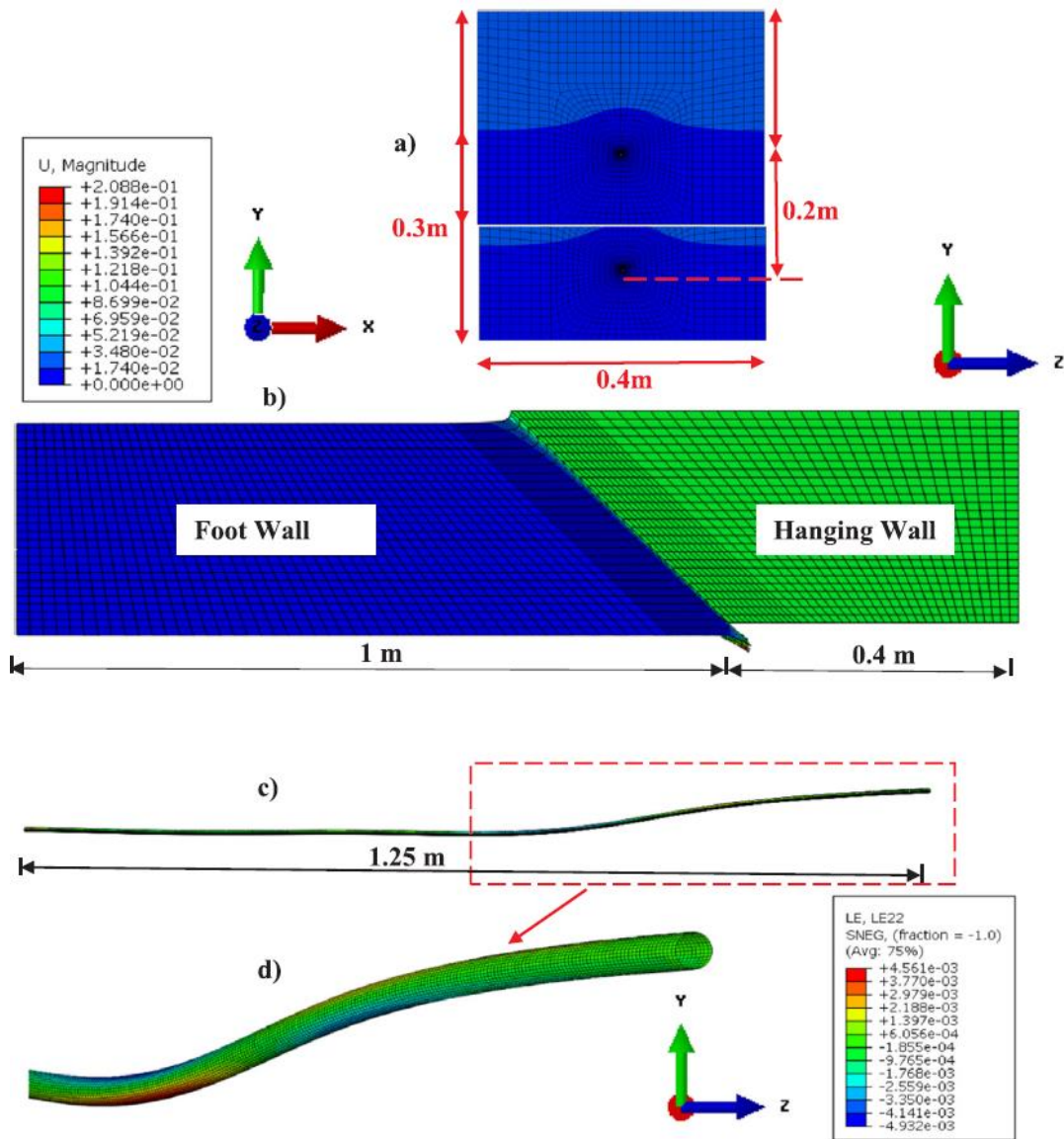


Fig. 2.16. Created model by Demirci et al. [39]: (a) cross-section of three-dimensional (3D) soil continuum model, (b) side view of the 3D FE model showing displacements of foot wall and hanging wall, (c) displacement profile of the pipeline, (d) longitudinal pipe strains in the dashed red zone.

movement.

Simulation of the buried pipeline and surrounding soil respectively by shell elements and solid elements for a 3D FEM-based analysis is the most detailed approach for modeling the pipeline at fault crossing problem. which can produce the most realistic performance of buried pipeline including the local buckling, ovalization, and tensile damages. Because of the modeling complexity, this method mostly is used for research purposes which in this study we call it 3D-solid modeling approach. It is common to use the beam element for modeling of pipe and spring elements for modeling of soil-pipe interactions for design and even research purposes which is simpler than the 3D-solid modeling approach and in this study, we call it beam modeling approach. Both over mentioned FEM models include the geometrical nonlinearity effects and material nonlinearity effects.

2.4. Experimental studies

In 2003, Yoshizaki et al. [40] using a large split-box at Cornell University did an experimental study on the effects of PGD caused by pure strike-slip fault movement on buried steel pipelines with elbows, and calibrated FE models for further studies. Palmer et al. [41] described a large-scale testing facility at Cornell University and its working principles.

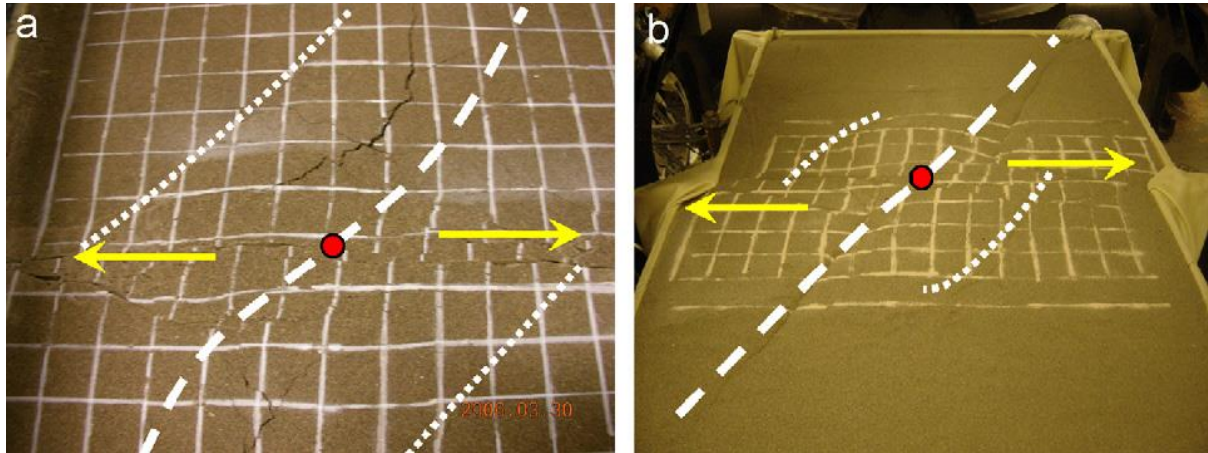


Fig. 2.17. Centrifuge model of Abdoun et al. [47] experiment: (a) moist sand back fill and (b) dry sand backfill.

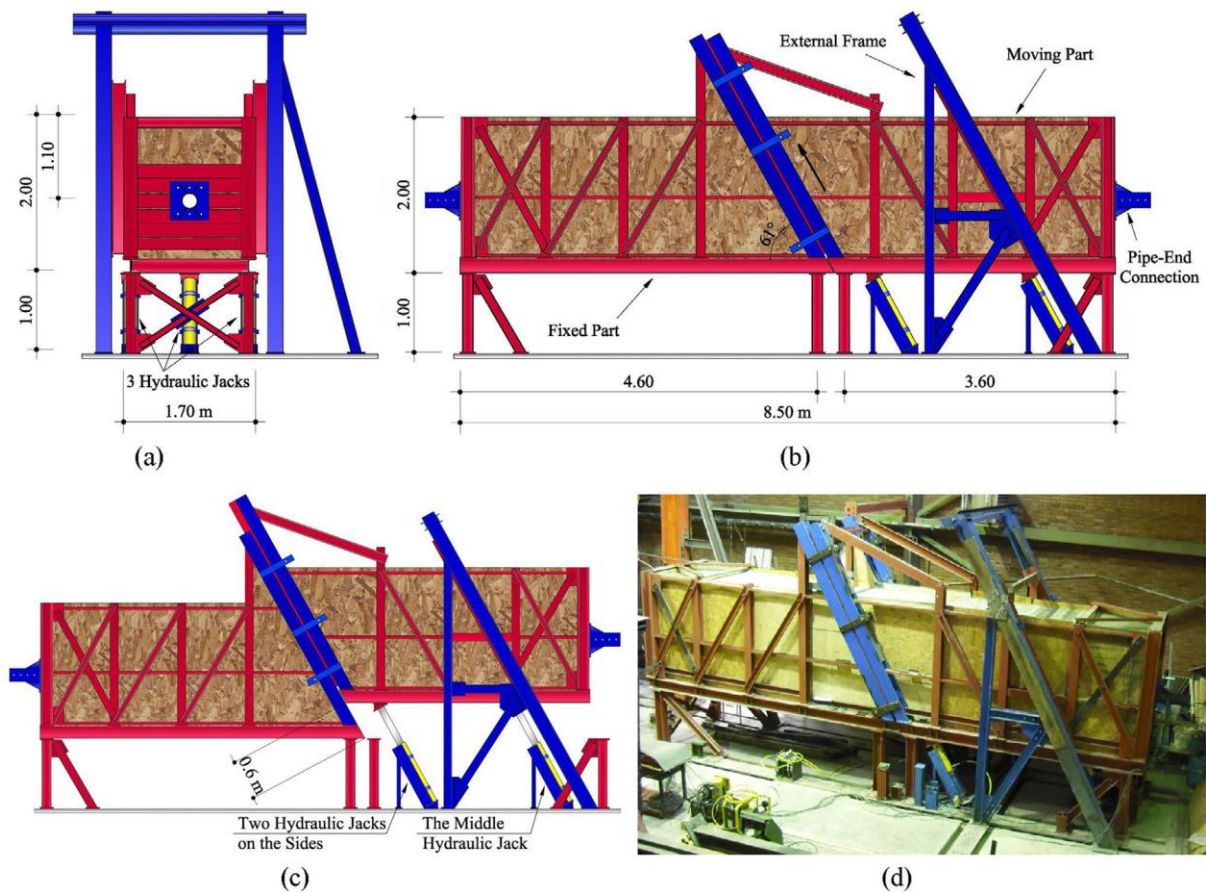


Fig. 2.18. Sketch of the split-box test basin of Rofooei et al. experiment model [52]: (a) front view, (b) side view before and (c) after a fault offset of 0.60 m, (d) photograph of the experimental results.

O'Rourke and Bonneau [42] then carried out large-scale tests to evaluate the effects of 60° strike-slip fault movement on high-density polyethylene (HDPE) pipelines and performance evaluation of steel gas pipelines with 90° elbows. Lin et al. [43] performed small-scale tests to analyze the performance of buried pipelines under strike-slip faults. The centrifuge-based approach was first proposed by O'Rourke et al. [43, 44] to model ground faulting effects on buried pipelines and several centrifuge tests have been performed to investigate the response of buried HDPE pipeline subjected to faulting movements [45-50]. Abdoun et al. [47],

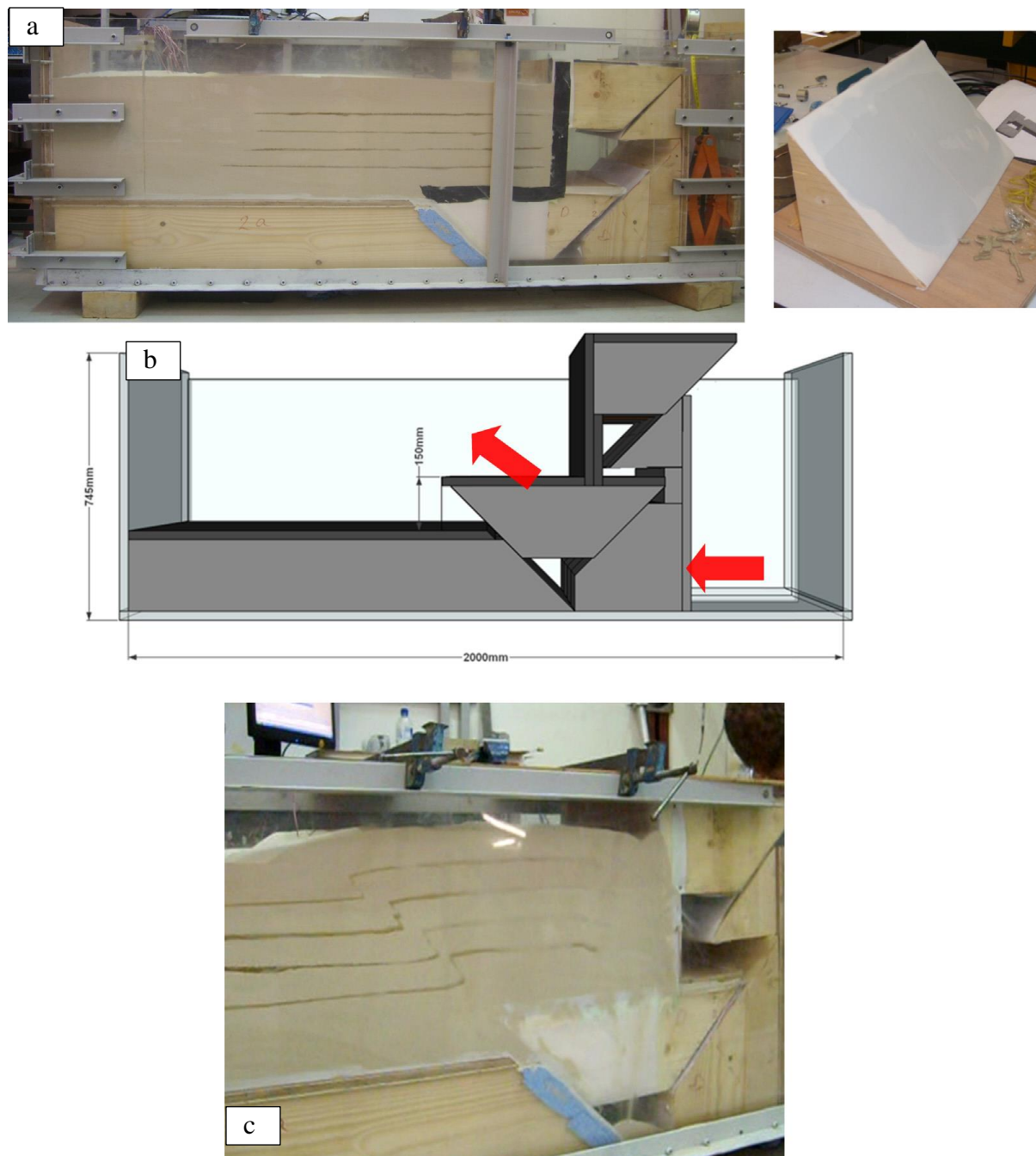


Fig. 2.19. Experiment model proposed by Demirci et al. [39]. (a) 1-g physical model of buried pipeline subjected to reverse fault, (b) working principle of 1-g scaled model, (c) observed shear bands after application of displacement in both horizontal and vertical planes.

presented results of five pairs of centrifuge tests designed to investigate the influence of various factors on the behavior of HDPE pipelines subjected to strike-slip faulting. They considered parameters of the soil moisture content, fault offset rate, relative burial depth (H/D), and pipe diameter in their experimental study (see **Fig. 2.17**).

Several studies [45–50] have done by centrifuge test to study the effect of various parameters on the performance of HDPE pipelines at earthquake fault crossing. They were accomplished at Rensselaer Polytechnic Institute (RPI) accompanied by several large-scale experiments at NEES facility at Cornell University on buried HDPE pipes. More detailed explanations about experiments are available in the NEESR-SG final report [51]. Rofooei et al. [52] performed a full-scale experiment on a steel pipe under reverse faulting of 0.6 m with a dip angle of 61° and calibrated a three-dimensional FE model using the experimental results (see **Fig. 2.18**). Recently, Demirci et al. [39] studied the behavior of a continuous buried pipeline subjected to reverse fault motion and proposed experimental centrifuge model for reverse faults in addition to a calibrated three-dimensional FE model (see **Fig. 2.19**).

Several experimental studies have been carried out on the behavior of buried pipelines subjected to strike-slip fault movements. However, more experimental research is needed to investigate the performance of buried HDPE pipelines and their complex soil–pipe interaction at strike-slip fault crossing. There is a need to investigate the performance of the HDPE pipeline buried in special soil types subjected to earthquake fault movements to improve seismic design guidelines of the HDPE pipelines and validate the FE models that are usually created for parametric studies and predicting the buried pipeline performance under seismically-induced PGD.

References

- [1] O'Rourke, M. J., Liu, X. [1999] "Response of buried pipelines subject to earthquake effects," Monograph Series, Multidisciplinary Center for Earthquake Engineering Research (MCEER).
- [2] Ariman, T., Muleski, G. E. [1981] "A review of the response of buried pipelines under seismic excitations." *Earthquake Engineering and Structural Dynamics* 9, 133–51.
- [3] Liang, J., Sun, S. [2000] "Site effects on seismic behavior of pipelines: a review," *ASME Journal of Pressure Vessel Technology* 122(4), 469–75.
- [4] O'Rourke, T. D., Lane, P. A. [1989] "Liquefaction hazards and their effects on buried pipelines," Technical report NCEER-89-0007, National Center for Earthquake Engineering Research, Buffalo, NY, USA.
- [5] O'Rourke, T. D., Palmer, M.C. [1996] "Earthquake performance of gas transmission pipelines," *Earthquake Spectra* 20(3), 493–527.
- [6] Earthquake Engineering Research Institute [1999] "Kocaeli, Turkey Earthquake of August 17," EERI Special Earthquake Report.
- [7] Uzarski, J., Arnold, C. [2001] "Chi-Chi, Taiwan, earthquake of September 21, 1999 reconnaissance Report," *Earthquake Spectra* 17 (Suppl. A).
- [8] Jennings, P. C. [1971] "Engineering features of the San Fernando earthquake February 9, 1971," California Institute of Technology Report, EERL, 71–02.
- [9] MaCaffrey, M. A., O'Rourke, T. D. [1983] "Buried pipeline response to reverse faulting during the 1971 San Fernando Earthquake," *ASME, PVP* 77, 151–9.
- [10] Desmond, T. P., Power, M. S., Taylor, C. L., Lau, R. W. [1995] "Behavior of large-diameter pipeline at fault crossings," *ASCE, TCLEE* (6), 296–303.
- [11] Nakata, T., Hasuda, K. [1995] "Active fault I 1995 Hyogoken Nanbu earthquake," *Kagaku* 65, 127–42 (in Japanese).
- [12] Shih, B. J., CHang C. H. [2006] "Damage Survey of Water Supply Systems and Fragility Curve of PVC Water Pipelines in the Chi-Chi Taiwan Earthquake," *Natural Hazards* 37, 71–85. <https://doi.org/10.1007/s11069-005-4657-9>
- [13] Kazama, M., Noda, T. [2012] "Damage statistics (Summary of the 2011 off the Pacific Coast of Tohoku Earthquake damage)," *Soils and Foundations* 52(5), 780–792.
- [14] Wham, B. P, Dashti, S., Franke, K., Kayen, R., Oettle, N. K. [2017] "Water supply damage caused by the 2016 Kumamoto Earthquake," *Lowland Technology International* 19(3), 165-174.
- [15] Miyajima, M., Fallahi, A., Ikemoto, T., Samaei, M., Karimzadeh, S., Setiawan, H., Talebi,

- F., Karashi J. [2018] “Site Investigation of the Sarpole-Zahab Earthquake, Mw 7.3 in SW Iran of November 12, 2017,” JSCE Journal of Disaster FactSheets.
- [16] Manolis, G. D., Beskos, D. E. [1997] “Underground and lifeline structures,” in Computer analysis and design of earthquake resistant structures: a handbook, ed. Beskos, D. E and Anagnostopoulos, S.A. (CMP, Southampton, United Kingdom), 775–837.
- [17] Calvi G.M., Nascimbene R., 2011, Progettare i Gusci, IUSS Press (in Italian).
- [18] Wells D. L., Coppersmith K. J., 1994, New Empirical Relationships among Magnitude, Rupture Length, Rupture Width, Rupture Area, and Surface Displacement. Bulletin of the Seismological Society of America, Vol. 84, N. 4.
- [19] Newmark, N. M., Hall, W. J. [1975] “Pipeline design to resist large fault displacement,” Proc. of the U.S. national conference on earthquake engineering, University of Michigan, Ann Arbor, Michigan, 416–25.
- [20] Kennedy, R. P., Chow, A. M., Williamson, R. A. [1977] “Fault movement effects on buried oil pipeline,” ASCE Transportation Engineering Journal 103(5), 617–33.
- [21] ASCE Technical Council on Lifeline Earthquake Engineering. [1984]. “Differential ground movement effects on buried pipelines,” Guidelines for the Seismic Design of Oil and Gas Pipeline Systems.
- [22] Wang, L. R. L., Yeh, Y. A. [1985] “A refined seismic analysis and design of buried pipeline for fault movement,” Earthquake Engineering and Structural Dynamics 13(1), 75–96.
- [23] Karamitros, D., Bouckovalas, G., Kouretzis, G. [2007] “Stress analysis of buried steel pipelines at strike-slip fault crossings,” Soil Dynamics and Earthquake Engineering 27, 200–11.
- [24] Trifonov, O. V., Cherniy, V. P. [2010] “A semi-analytical approach to a nonlinear stress–strain analysis of buried steel pipelines crossing active faults,” Soil Dynamics and Earthquake Engineering 30(11), 1298–308.
- [25] Karamitros, D. K., Bouckovalas, G. D., Kouretzis G. P., Gkesouli V. [2011] “An analytical method for strength verification of buried steel pipelines at normal fault crossings,” Soil Dynamics and Earthquake Engineering (13), 1452-1464.
- [26] Trifonov, O. V., Cherniy V. P. (2012). “Elastoplastic stress-strain analysis of buried steel pipelines subjected to fault displacements with account for service loads,” Soil Dyn Earthq Eng 33,54–62.
- [27] Lim, M. L., Kim, M. K., Kim, T. W., Jang, J. W. (2001). “The behavior analysis of buried pipeline considering longitudinal permanent ground deformation,” In pipeline 2001: advances in pipelines engineering & construction (San Diego, California), vol. 3, 107. ASCE. [https://doi.org/10.1061/40574\(2001\)3](https://doi.org/10.1061/40574(2001)3)

- [28] O'Rourke, M. J., Vikram, G., Abdoun, T. (2003). "Centrifuge modeling of buried pipelines," In: Proceedings of the Sixth U.S. conference and workshop on lifeline earthquake engineering, August 10–13, 2003, Long Beach, CA. pp. 757–768.
- [29] Sakanoue, T., Yoshizaki, K. (2004). "A study on earthquake-resistant design for buried pipeline using lightweight backfill," In: Proceedings of the 13th world conference on earthquake engineering, Vancouver, B.C., Canada, August 1-6, Paper No.2389.
- [30] Vazouras, P., Karamanos, S. A., Dakoulas, P. (2010). "Finite element analysis of buried steel pipelines under strike-slip fault displacement," *Soil Dyn Earthq Eng* ;30:1361–76.
- [31] Vazouras, P., Karamanos, S. A., Dakoulas, P. (2012). "Mechanical behavior of buried steel pipes crossing active strike-slip fault," *S, Soil Dyn Earthq Eng*;41:164–80.
- [32] Zhang, L., Zhao, X., Yan, X., Yang, X. (2016). "A new finite element model of buried steel pipelines crossing strike-slip faults considering equivalent boundary springs," *Eng Struct*;123:30–44.
- [33] Takada, S., Hassani, N., Fukuda, K. (2001). "A new proposal for simplified design of buried steel pipes crossing active faults," *Earthq Eng Struct Dyn* ;30:1243–57.
- [34] Liu. Aw., Hu. Yx., Zhao. Fx., Li. Xj., Takada. S., Zhao. L. (2004) "An equivalent-boundary method for the shell analysis of buried pipelines under fault movement" *Acta Seismologica Sinica*, Vol. 17, pp. 150-156.
- [35] Liu. Aw., Takada. S., Hu. Y. (2004) "A Shell Model with an Equivalent Boundary for Buried Pipelines under the Fault Movement" 13th World Conference on Earthquake Engineering Vancouver, B.C., Canada.
- [36] Joshi, Sh., Prashant, A., Deb, A., S.K. Jain. (2011) "Analysis of buried pipelines subjected to reverse fault motion" *Soil Dyn Earthq Eng* ;31:930-940.
- [37] Vazouras, P., Dakoulas, P., Karamanos, S. A. (2015). "Pipe–soil interaction and pipeline performance under strike–slip fault movements," *Soil Dyn Earthq Eng* ;72:48–65.
- [38] Liu, X., Zhang, H., Li, M., Xia, M., Zheng, W., Wu, K., Han, Y. (2016). "Effects of steel properties on the local buckling response of high strength pipelines subjected to reverse faulting," *J Nat Gas Sci Eng* ;33:378–87.
- [39] Demirci, H. E., Bhattacharya, S., Karamitros, D., Alexander, N. (2018) "Experimental and numerical modelling of buried pipelines crossing reverse faults," *Soil Dyn Earthq Eng* ;114:198–214.
- [40] Yoshizaki K, O'Rourke TD, Hamada M. Large scale experiments of buried steel pipelines with elbows subjected to permanent ground deformation. *J Struct Mech Earthq Eng* 2003;20(1):1s–11s.
- [41] Palmer, M. C., O'Rourke, T. D., Stewart, H. E., O'Rourke, M. J., Symans, M. (2006) "Large displacement soil-structure interaction test facility for lifelines" In: Proceedings of

the 8th US national conference commemorating the 1906 San Fransisco earthquake, EERI, San Fransisco.

- [42] O'Rourke, T. D., Bonneau, A. (2007) "Lifeline performance under extreme loading during earthquakes," In: Pitilakis KD, editor. *Earthquake Geotechnical Engineering*. Dordrecht, Netherlands: Springer; 407–32.
- [43] Lin, T. J., Liu, G. Y., Chung, L. L., Chou, C.H., Huang, C. W. (2012) "Verification of Numerical Modeling in Buried Pipelines under Large Fault Movements by Small-Scale Experiments," In: *Proceedings of the 15WCEE*, 9, 6685–6693.
- [44] O'Rourke, M. J., Gadicherla, V., Abdoun, T. (2005) "Centrifuge modeling of PGD response of buried pipe," *Earthq Eng Eng Vib* ;4:69–73.
- [45] Ha, D., Abdoun, T. H., O'Rourke, M. J., Symans, M. D., O'Rourke, T. D., Palmer, M. C., Stewart, H. E. (2008) "Buried high-density polyethylene pipelines subjected to normal and strike-slip faulting — a centrifuge investigation," *Can Geot J* ;45: 1733–1742.
- [46] Ha, D., Abdoun, T. H., O'Rourke, M. J., Symans, M. D., O'Rourke, T. D., Palmer, M. C., Stewart, H. E. (2008) "Centrifuge modeling of earthquake effects on buried high-density polyethylene (HDPE) pipelines crossing fault zones," *ASCE J Geotech Geoenviron Eng* ;134(10):1501–15.
- [47] Abdoun T. H., Ha, D., O'Rourke, M. J., Symans M. D., O'Rourke T. D., Palmer M.C., Stewart HE. (2009) "Factors influencing the behavior of buried pipelines subjected to earthquake faulting" *Soil Dyn Earthq Eng* ;29:415–27.
- [48] Xie, X., Symans, M. D., O'Rourke, M. J., Abdoun, T. H., O'Rourke, T. D., Palmer, M. C., Stewart, H. E. (2011) "Numerical modelling of buried HDPE pipelines subjected to strike-slip faulting" *J Earthq Eng* ;15(8):1273–96.
- [49] Ha, D., Abdoun, T. H., O'Rourke M. J., Symans. M. D., O'Rourke. T. D., Palmer. M. C., Stewart, H.E. (2010) "Earthquake faulting effects on buried pipelines – case history and centrifuge study". *J Earthq Eng* ;14(5):646–69.
- [50] Xie, X., Symans, M. D., O'Rourke, M. J., Abdoun, T. H., O'Rourke, T. D., Palmer M. C., Stewart H. E. (2013) "Numerical modeling of buried HDPE pipelines subjected to normal faulting: a case study". *Earthq Spectra* ;29(2):609–32.
- [51] NEESR-SG Final Report (2008) Prepared by Cornell University, Rensselaer Polytechnic Institute and Sciencenter Discovery Center; 47 p.
- [52] Jalali H. H., Rofooei F. R., Attari, N. K. A., Samadian, M. (2016) "Experimental and finite element study of the reverse faulting effects on buried continuous steel gas pipelines" *Soil Dyn Earthq Eng*;86:1–14.

Chapter III:

**Effect of axial soil-pipe interaction
and pipe material nonlinearity
effect on behavior buried pipeline at
strike-slip fault crossing**

3.1. General remarks

Performance of buried steel pipeline at strike-slip fault crossing is investigated using FEM analysis. In this chapter has two major subsections. First one is, evaluation of the axial soil-pipe interaction and axial force of the buried pipeline at strike-slip fault crossing. In this subsection, the simulations included various faulting angles and soil stiffness values, with contribution of the existence variable of the axial soil-pipe interaction springs. The FEM results are verified using a simple existing analytical approach in conjunction with experiment result. Since in previous researches axial soil-pipe interaction has been roughly simplified [1–8] there was a demand on derivation of soil-pipe interaction terms for analytical solution methods even in elastic range, beside evaluation of the importance of axial force of pipeline and axial soil-pipe interaction on this problem. First subsection has concentrated on effect of axial soil-pipe interaction and axial force of pipeline on pipeline performance to derive effective parameters on axial soil-pipe interaction spring terms and new boundary conditions for developing in future analytical studies in elastic range. In second subsection, performance of buried pipelines crossing strike-slip fault with nonlinear pipe material and nonlinear soil-pipe interaction is investigated by FEM-based simulations. Wherein mainly focused on the evaluation of steel pipeline nonlinearity effects on pipeline performance. Additionally, FEM-based cases were created by applying various faulting angles to investigate deeply the steel pipeline material nonlinearity effect on different cases by comparing plastic steel pipeline material cases with elastic ones [1].

3.2. Background

As mentioned in literature review, there has been already done several great studies with great outcome in pipeline crossing earthquake fault topic by analytical [2–9] and numerical [10–20] approaches. Despite the substantial advances made by previous studies in developing analytical solutions for a buried pipeline at fault crossing problems, the effect of the axial soil-pipe interaction terms has only been approximated through iterative procedures by employing initial assumptions with regard to the strain/stress states of pipeline section. The abovementioned approximations are performed because the exact term of the axial soil-pipe interaction in the governing differential equations has not been considered properly thus far (not only in nonlinear range but also even in elastic range). Therefore, there exists a need for developing a comprehensive analytical solution by incorporating the exact axial soil-pipe interaction term in the governing differential equation. However, the buried pipeline at fault crossing problem is a nonlinear problem but for fulfilling of this need, as first step in derivation of the axial soil-pipe interaction, this study is adopted in elastic range (non-sliding). The elastic range was preferred to avoid the interference of non-linear effects on identifying the relationships between the affected parameters and the axial soil-pipe interaction. Besides, in most of researches, mainly they have focused on the transverse soil-pipe interaction, and axial soil-pipe interaction has been roughly simplified. by these simplifications, importance and

sensitivity of the axial soil-pipe soil interaction and effect of it on pipeline performance has been underestimated. Additionally, to investigate the steel pipe material nonlinearity effect on the buried pipeline performance at strike-slip fault crossing, in the second subsection of this chapter, an FEM-based investigation is conducted by taking the nonlinear soil-pipe interaction and the steel pipeline material nonlinearity into account. The main aim of second subsection is evaluation of the steel pipeline material nonlinearity effect on the buried pipeline performance in crossing with the large dislocated strike-slip fault. Besides for deeper understanding of the steel pipeline material nonlinearity effect, the problem by applying nonlinear soil-pipe interaction with various faulting angles are also investigated [1].

3.3. Importance of axial soil-pipe interaction on pipeline crossing a strike-slip fault

In this subsection, an FEM based approach is implemented (1) to evaluate the importance of the axial soil-pipe interaction in the buried pipeline at fault crossing problems; And (2) to derive the effective variables and their relationship on the variation of the axial soil-pipe interaction term and axial force of soil and pipeline in the pipeline crossing fault problem. For verification of the FEM-based analysis an analytical solution, based on beam on elastic foundation theory is implemented. Additionally, FEM-based model of the pipeline crossing the 90° strike-slip fault verified by Hasegawa and Kiyono [21] experiment result. (**Fig. 3.1**). By verification of the FEM-based analysis results by analytical and experiment, the FEM-based model was employed to accurately reproduce various pipe crossing fault scenarios. This study was conducted to identify the effective parameters and new boundary conditions for developing the axial soil-pipe interaction to utilized for future analytical researches to the pipeline crossing fault problem.

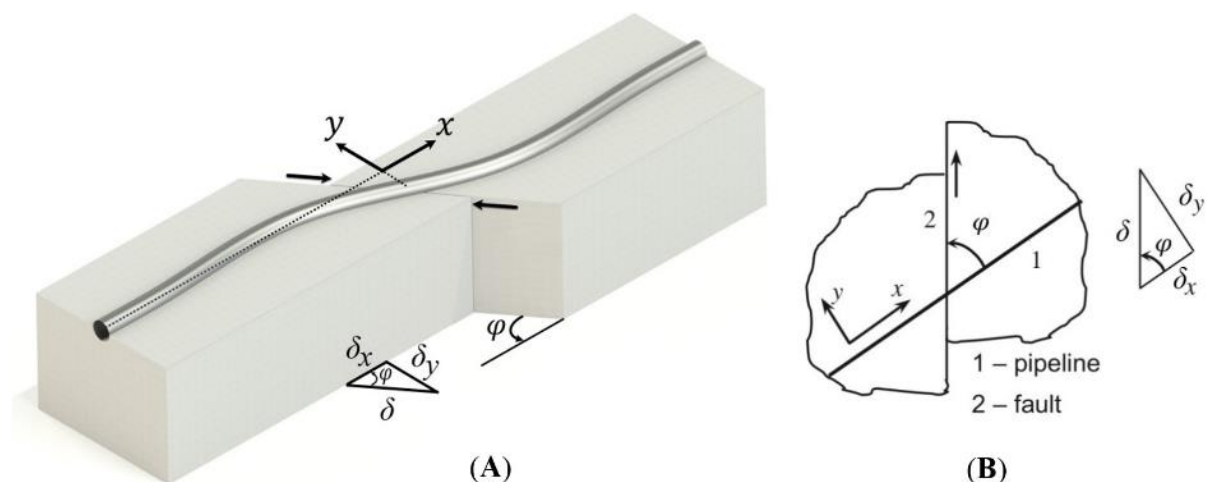


Fig. 3.1. Buried pipeline analysis model at strike-slip fault crossing: (a) definition of x and y-axes and fault displacement of δ_x , δ_y , and δ ; (b) pipeline-fault-intersection angle in plane φ .

3.3.1. Performance of buried pipelines during previous earthquakes

Owing to earthquakes, severe damages have been observed in buried steel pipelines subjected to active fault displacements, even with very large sizes. For example, a steel water transmission pipeline was damaged owing to the fault crossing near Arefiye, Turkey, during the Kocaeli earthquake in 1999 (**Fig. 3.2a**) [22]; a large size steel pipeline with diameter of 2 m and thickness of 1.9 cm was severely damaged owing to fault crossings during the 1999 Chi-Chi earthquake in Taiwan (**Fig. 3.2b**) [23]. In the 2017 Iran-Iraq earthquake, more than 500 cases of damages were reported for the main water pipelines, while more than 300 cases were reported for the main wastewater pipelines. These damages caused the contamination of the Sarpole-Zahab water resources for more than one week (**Fig. 3.2c**) [24]. These pieces of evidence demonstrate that the damage to the pipelines caused by the fault crossings did not only result in high economical loss, but also led to environmental problems in the damaged area. Therefore, the behavior of the pipeline at the fault crossings is an important engineering problem, and the resulting damage must be controlled through appropriate design based on knowledge about the responses of the pipe at crossing zones with faults.

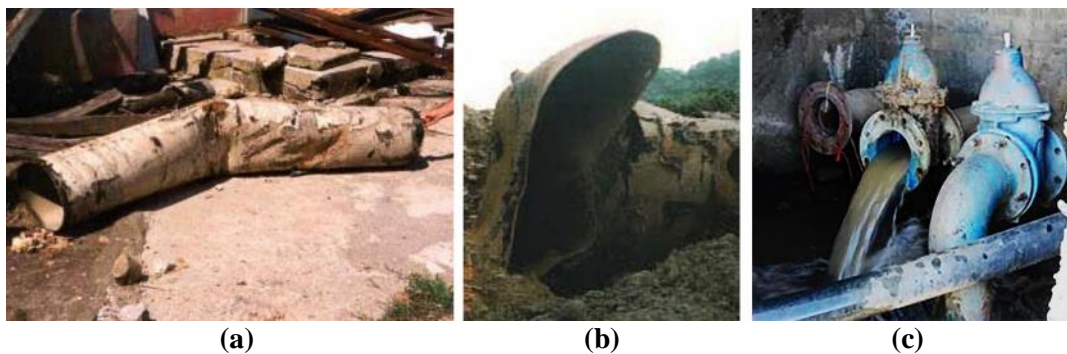


Fig. 3.2. Damaged steel pipeline after: (a) 1999 Kocaeli earthquake [22], (b) 1999 Chi-Chi earthquake in Taiwan [23], (c) 2017 Iran-Iraq earthquake in Sarpole-Zahab city (drinking water contamination) [24].

3.3.2. Analytical solution

In this part, an existing elastic analytical solution based on the beam-on-elastic-foundation theory for a steel pipeline subjected to a strike-slip fault displacement was used. Based section 3.3.3.2.1, 3.3.3.3.3 and 3.3.3.3.6 for the cases of buried pipeline crossings with a 90° strike-slip fault displacement, the effects of the axial soil-pipe interaction and axial force responses were negligible. Since this simple analytical solution doesn't consider the axial forces and axial soil-pipe interactions, therefore, the analytical solution was implemented only for a 90° fault displacement with regard to the two scenarios of pipeline buried in hard and soft soil.

Subsequently, in this analytical solution, the lack of the axial soil-pipe interaction in the results was negligible, and the solution in elastic range has very good accuracy for pipeline crossings with a 90° strike-slip fault.

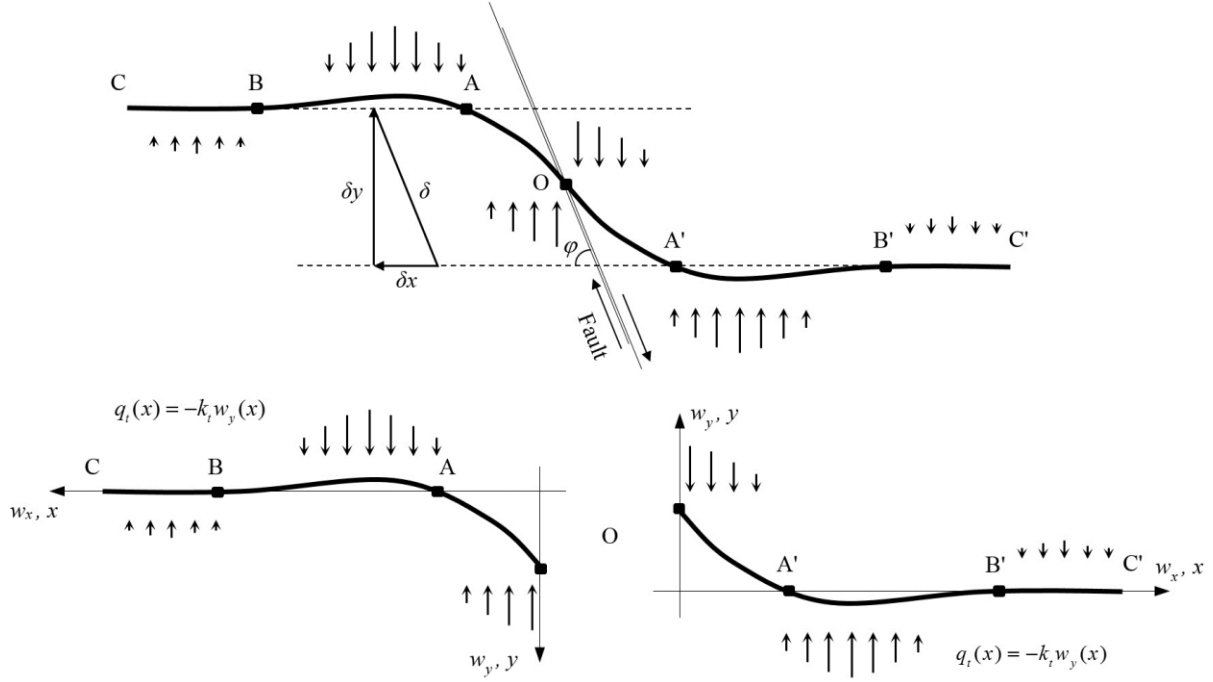


Fig. 3.3. Coordinate system and partitioning of pipeline for analytical solution.

In the problem of pipeline crossing strike-slip fault, the pipeline responses were symmetric. Based on **Fig. 3.3**, the problem was solved for the left segment of the fault and the results were extended to the right segment. In the elastic range, the differential equilibrium equation for the pipeline crossing the strike-slip with an angle of 90° is expressed as follows:

$$-EI \frac{d^4 w_y}{dx^4} - k_t w_y = 0 \quad (3.1)$$

By imposing the boundary conditions of $w = 0$ for $x \rightarrow -\infty$ and $w_y = \delta/2$ for $x = 0$ and $M = 0$ for $x = 0$, Eq. (3.1) yields the following expression:

$$w_y(x) = \frac{\delta_y}{2} e^{\beta x} \cos \beta x \quad (3.2)$$

Where w_y is the transverse displacement of the fault.

$$\beta = \sqrt[4]{\frac{k_t}{4EI}} \quad (3.3)$$

Additionally, from the bending moment obtained by applying the beam theory, the maximum bending location and maximum bending moment of the pipeline are expressed as follows:

$$M(x) = \delta_y EI \beta^2 e^{\beta x} \sin \beta x \quad (3.4)$$

$$x_{M \max} = -\frac{\pi}{4\beta} \quad (3.5)$$

$$M_{max} = -\frac{\sqrt{2}}{2} \delta_y EI \beta^2 e^{-\frac{\pi}{4}} \quad (3.6)$$

The shear force is expressed as follows:

$$V(x) = \delta_y EI \beta^3 e^{\beta x} (\sin \beta x + \cos \beta x) \quad (3.7)$$

Here, w_y is the transverse displacement of the pipeline; E is the pipeline steel's Young's modulus, I is the moment of inertia of the pipeline cross section, and k_t is the elastic constant of the transverse soil springs.

3.3.3. FEM results and verification

3.3.3.1. Clarification of pipeline model

To evaluate the pipeline response at strike-slip fault crossings, a number of representative numerical analyses were conducted using the FEM in the commercial code of ABAQUS [25]. Based on the Hasegawa and Kiyono [21] experiment, a 4" steel pipeline with 1 km length buried in 0.6m sand with an external diameter of 0.1143 m and thickness of 0.0023 m (without internal pressure) was simulated. Transverse soil spring constants in Table 2 are determined based on the lateral load test LLT experiment results of the (Hasegawa and Kiyono 2016) experiments and axial spring constants are extended based on the seismic design guideline for high-pressure gas pipeline of Japan gas association [26]. To improve the FEM results accuracy, meshing and elements size are selected based on the mesh size sensitivity analyses results. The elements in both sides of the fault symmetrically discretized gradually from 0.0125m to 1m in further distances from faultline. The pipeline was made of API5L-X65 steel material with an elastic Young's modulus of 200 GPa. For pipe elements the B21 elements, for rigid bodies RB2D2 elements and CONN2D2 element for soil spring elements are applied. The soil-pipe spring parameters listed in **Table 3.1** were considered in the transverse, vertical and axial directions in the elastic range as **Fig. 3.4**.

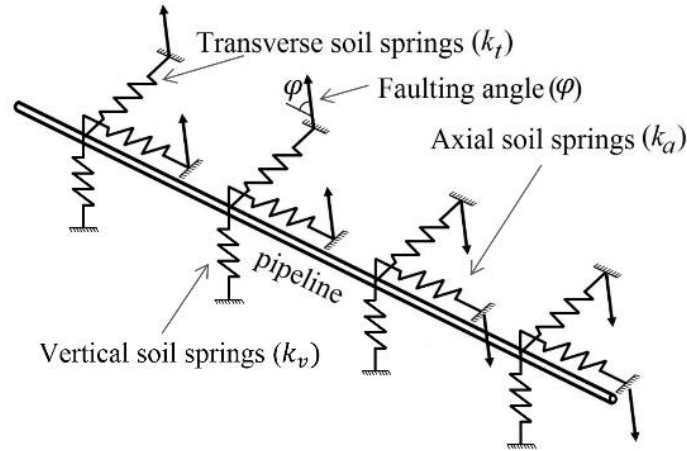


Fig. 3.4. Schematic soil spring diagram of buried pipeline at strike-slip fault crossing implemented in FEM model.

The fault displacement components are applied to the ends of the soil spring elements and

Table 3.1. Soil-pipe interaction springs properties

Soil name	k_t (MN/m ³)	k_a (MN/m ³)	k_v (MN/m ³)	G (MN/m ²)	V_s (m/s)	Soil type (<i>NEHRP</i>)
Soft T.	1.8	-	3.2	0.78	21	E*
Hard T.	180	-	320	75	190	D**
Soft T. A.	1.8	0.9	3.2	0.78	21	E
Hard T. A.	180	90	320	75	190	D

* E (soft soil) (Building Seismic Safety Council, 2003)

** D (stiff soil) (Building Seismic Safety Council, 2003)

Table 3.2. FEM-base and analytical model cases

No.	Case Name	Solver	Soil type (<i>NEHRP</i>)	Soil type	ϕ
1	Anal-Soft T. soil-90°	Analytical	E	Soft T.	90°
2	Anal-Hard T. soil-90°	Analytical	D	Hard T.	90°
3	FEM-Soft T. soil-90°	FEM	E	Soft T.	90°
4	FEM-Hard T. soil-90°	FEM	D	Hard T.	90°
5	FEM-Soft T. A. soil-90°	FEM	E	Soft T. A.	90°
6	FEM-Hard T. A. soil-90°	FEM	D	Hard T. A.	90°
7	FEM-Soft T. soil-60°	FEM	E	Soft T.	60°
8	FEM-Hard T. soil-60°	FEM	D	Hard T.	60°
9	FEM-Soft T. A. soil-60°	FEM	E	Soft T. A.	60°
10	FEM-Hard T. A. soil-60°	FEM	D	Hard T. A.	60°
11	FEM-Soft T. soil-45°	FEM	E	Soft T.	45°
12	FEM-Hard T. soil-45°	FEM	D	Hard T.	45°
13	FEM-Soft T. A. soil-45°	FEM	E	Soft T. A.	45°
14	FEM-Hard T. A. soil-45°	FEM	D	Hard T. A.	45°
15	FEM-Experiment-Soft soil	FEM	E	Soft T. A.	90°
16	FEM-Experiment-Hard soil	FEM	D	Hard T. A.	90°

the pipeline is free to move on axial direction in both sides. To evaluate the response of the buried pipeline crossing the strike-slip fault, two analytical and 14 FEM-based analysis cases were investigated by analysing of the various faulting angles, soil stiffness, and axial soil-pipe interaction existence variables listed in **Table 3.2**. In the FEM and analytical method, a transverse fault dislocation of 0.2 m with three different faulting angles, respectively, was specified for the pipeline (**Fig. 3.1** and **Fig. 3.8**). The hard soil has a spring constant (k) that was 100 times stiffer than soft soil. Hence, based on Eq. 9, it can be said that in the hard soil shear wave velocity is 10 times faster than the soft soil. It is mentionable that the Eq. 9 is expressed based on Eq.8.

$$V_s = \sqrt{\frac{G}{\rho}} \quad (3.8)$$

$$\frac{V_{s(i)}}{V_{s(j)}} = \sqrt{\frac{k_{(i)}}{k_{(j)}}} \quad (3.9)$$

3.3.3.2. Verification of FEM model

To ensure the FEM-based simulation results, the FEM model results were evaluated versus analytical approach and experiment.

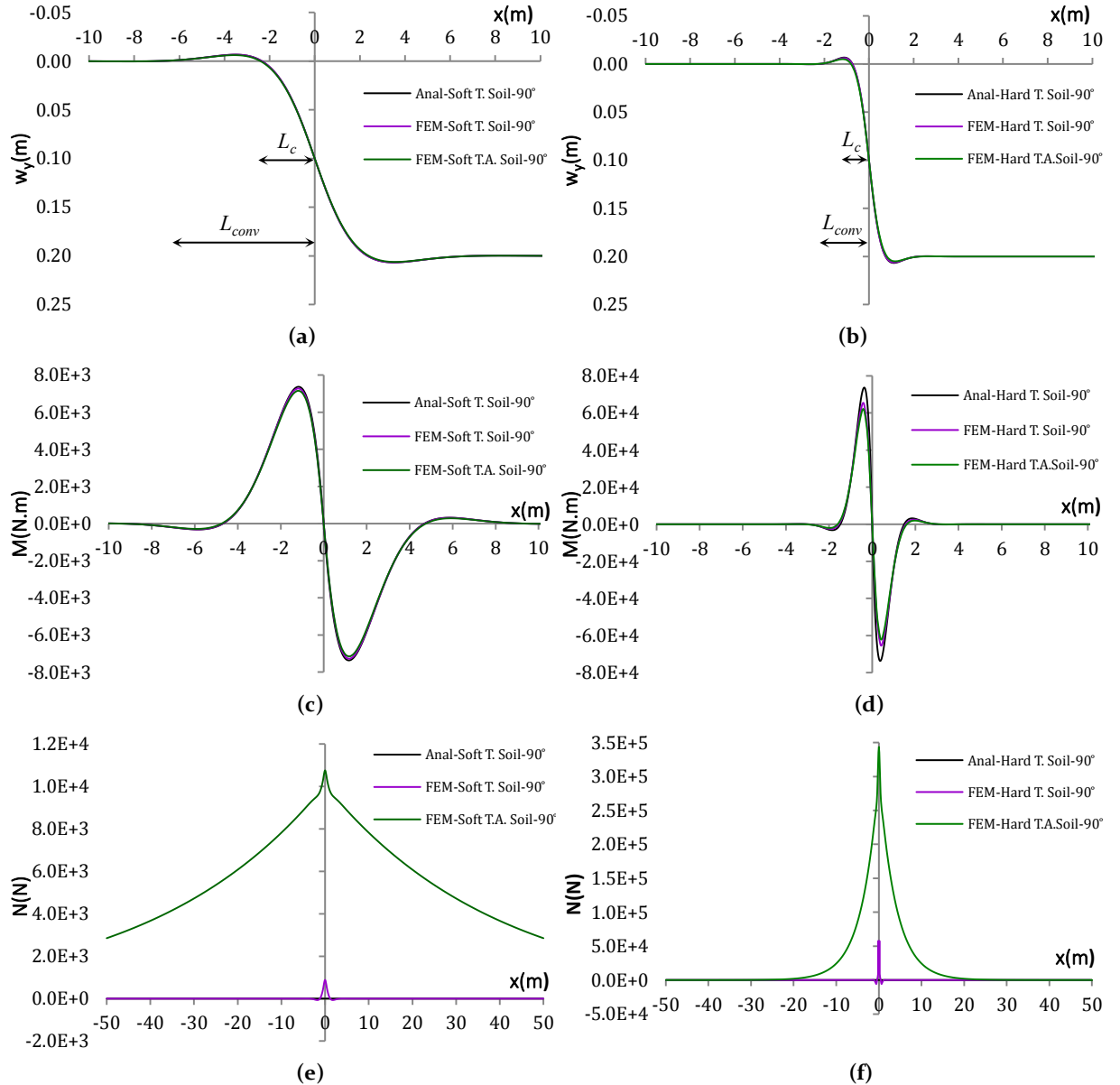


Fig. 3.5. FEM analysis result versus analytical solution results for problem of buried pipeline subjected to strike-slip fault ($\varphi = 90^\circ$): (a) w_y diagram for soft soil cases, (b) w_y diagram hard soil cases, (c) M diagram for soft soil cases, (d) M diagram for hard soil cases, (e) N diagram for soft soil cases, (f) N diagram for hard soil cases.

(A). Verification of FEM model by analytical solution

Overmentioned analytical method in section 3.3.2 was implemented to verify the results of the FEM based simulation for the problem of buried pipeline subjected to 90° strike-slip fault displacement. Cases 1, 3, and 5 for the pipelines buried in soft soil, and cases 2, 4, and 6 for the pipelines buried in hard soil were considered to verify the FEM models with regard to the analytical solution, as follows.

Cases 1 and 3, are buried in soft soil, and cases 2 and 4, are buried in hard soil which have no axial soil-pipe interactions and are the same models with different solution methods (analytical vs FEM). As shown in **Figs. 3.5a,b**, the displacement and moment results obtained by the FEM analysis of cases 3 and 4 were verified using the analytical solution results for cases 1 and 2. Additionally, in the FEM-based models, the distance between the two maximum moment points in the pipeline was verified by the results obtained by the analytical solution.

The displacement field results obtained by the FEM and analytical solution were almost same. Additionally, the bending moment diagrams cases buried in soft soil were almost same, and there only existed a slight difference (less than 3%) for the magnitude of the maximum bending moment in the case of the hard soil, for the reason explained in Section 3.3.3.3.5. As shown in **Fig. 3.5c**, the axial force response for the cases without axial soil-pipe interaction was negligible. The axial force resulting from the cases included the axial soil-pipe interaction in the FEM models (cases 5 and 6) was not zero. However, based on the stress responses (**Fig. 3.12**) discussed in Section 3.3.3.3.6, the axial forces of pipelines buried in hard or soft soil for case with 90° faulting angle (cases 5 and 6) were negligible in comparison with the bending moment effect on the stresses of the pipeline section. Therefore, generally, it can be said that the axial soil-pipe interaction was negligible for the buried pipeline crossing the strike-slip faults and did not affect the results. As shown in **Figs. 3.5a-c**, the pipeline responses obtained by the FEM were in good agreement with the analytical solution results.

(B). Validation of FEM model by experimental results

Based on Hasegawa and Kiyono experiments at 2016 [21], cases 15 and 16 were developed by FE models with the same boundary conditions of the experiment at the end points, and considering a pipeline with a length of 5 m crossing a strike-slip fault with a faulting angle of 90°, and an axial and transverse soil-pipe interaction.

Table 3.3. Distance between maximum bending moments of pipeline in experiment and analysis.

Type	Distance (m)	
	Soft soil	Hard soil
Experiment [21] (Hasegawa and Kiyono, 2016)	1.900	0.780
FEM (cases 15 and 16)	1.990	0.788

Hasegawa and Kiyono's experimental study was focused on the distance between two local buckling locations. Buckling occurs owing to compression stresses, which are maximum at the

maximum bending moment in the pipeline. Therefore, the buckled points in the pipeline have the maximum bending moment. Since the local buckling locations are the same with maximum bending moment's locations, here for verification purposes, we have compared the distance between the two local bucklings of the experiment with the distance between the maximum bending moment locations of our FEM analysis (cases 15 and 16). The distances between two maximum bending moment locations in the soft and hard soil experiments (**Fig. 3.6**) were compared with the results obtained by the FE models (**Fig. 3.7**) for cases 15 and 16, as presented in **Table 3.3**. It can be seen that the FE models were in good agreement by the experimental and analytical results.



Fig. 3.6. Experimental results of pipeline crossing strike-slip fault with angle of 90°: (a) buried in soft soil, (b) buried in hard soil [21].

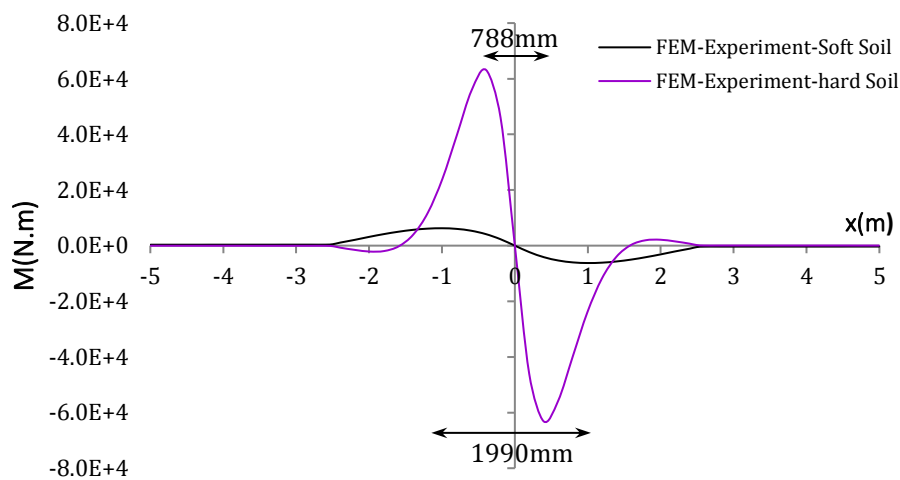


Fig. 3.7. Bending moment responses obtained by FE pipeline models for cases 15 and 16.

3.3.3.3. FEM analysis results

After verification of FEM model of the buried pipeline subjected to the active strike-slip fault displacement, 12 FEM cases by implementing changing variables for the axial soil-pipe interaction existence, soil stiffness (k), and faulting angle (ϕ) were analyzed. These analyses were conducted to evaluate the effect of the changing variables on the responses of the buried pipeline. In Figures bellow, cases with transverse and without axial soil-pipe interaction springs are shown with dashed lines and the cases with transverse and axial soil-pipe interaction springs shown in solid lines. The analytical solution results are in black colour, cases buried in soft soil are in the green colour range and cases buried in hard soil are in blue colour range. The lightest

green/blue colour line is for case of $\varphi = 45^\circ$, the medium green/blue colour line is for case of $\varphi = 60^\circ$ and the darkest green/blue colour line is for case of $\varphi = 90^\circ$.

(A). Transverse displacement (w_y)

In the analytical solution, all of the pipeline responses were calculated based on deflection (w_y). Therefore, the transverse displacement response of the pipeline is very important. In other words, the accuracy of this output can strongly affect the accuracy of the other pipeline responses (**Fig. 3.8**). The transverse displacement response obtained by the FEM analysis was verified with the analytical solution. Based on the transverse displacements of the pipeline in the soft and hard soil cases (**Figs. 3.9a,b**), the curved zone of the pipeline resulting from the soil stiffness of the hard soil was much shorter in comparison with that of the soft soil. The curved zone was approximately 4.5 m for the hard soil and approximately 14.2 m for the soft soil. In the evaluation of the pipeline's transverse displacement responses, the FEM cases in the same soil type without axial soil-pipe interaction springs exhibited exactly same w_y response, even with different faulting angles φ . This means that there existed a strong relationship between the axial soil-pipe interaction and the faulting angle φ , because the faulting angle effect was completely removed by removing the axial soil-pipe interaction effect. Additionally, it was observed that, in crossings with a strike-slip fault of $\varphi=90^\circ$, the pipeline responses were almost independent of the axial soil-pipe interaction springs effect (**Fig. 3.9e**).

Many analytical solutions determined L_c as the soil yielding zone at the curved zone of the pipeline. In fact, L_c is the distance between the pipe-fault intersection point and the first point with zero deflection on pipeline (**Fig. 3.5a** and **Fig. 3.9a**).

L_c is the first point after fault line which deflection reaches zero. Based on Eq. (2) while $x = L_c$ and $w = 0$:

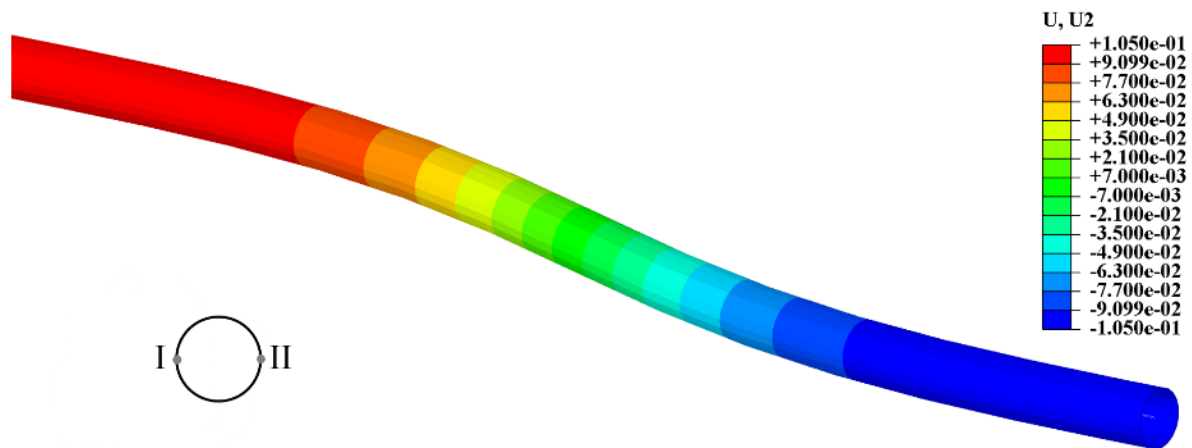


Fig. 3.8. Transverse displacement (w_y) response counters of pipeline resulting from two-dimensional dislocation of strike-slip fault at 90° angle in soft soil, as obtained by FEM analysis.

$$L_c \approx \frac{\pi^4}{2} \sqrt{\frac{4EI}{k}} \tag{3.10}$$

It was found that L_c had a reverse relationship with the faulting angle (φ) and soil stiffness (k). With regard to **Fig. 3.9a**, L_c changes by having the axial soil-pipe interaction. In various very well-known analytical solution methods (e.g., Karamitros et al., Trifonov et al.), the L_c parameter was calculated without considering the perfect axial soil-pipe interaction. Therefore,

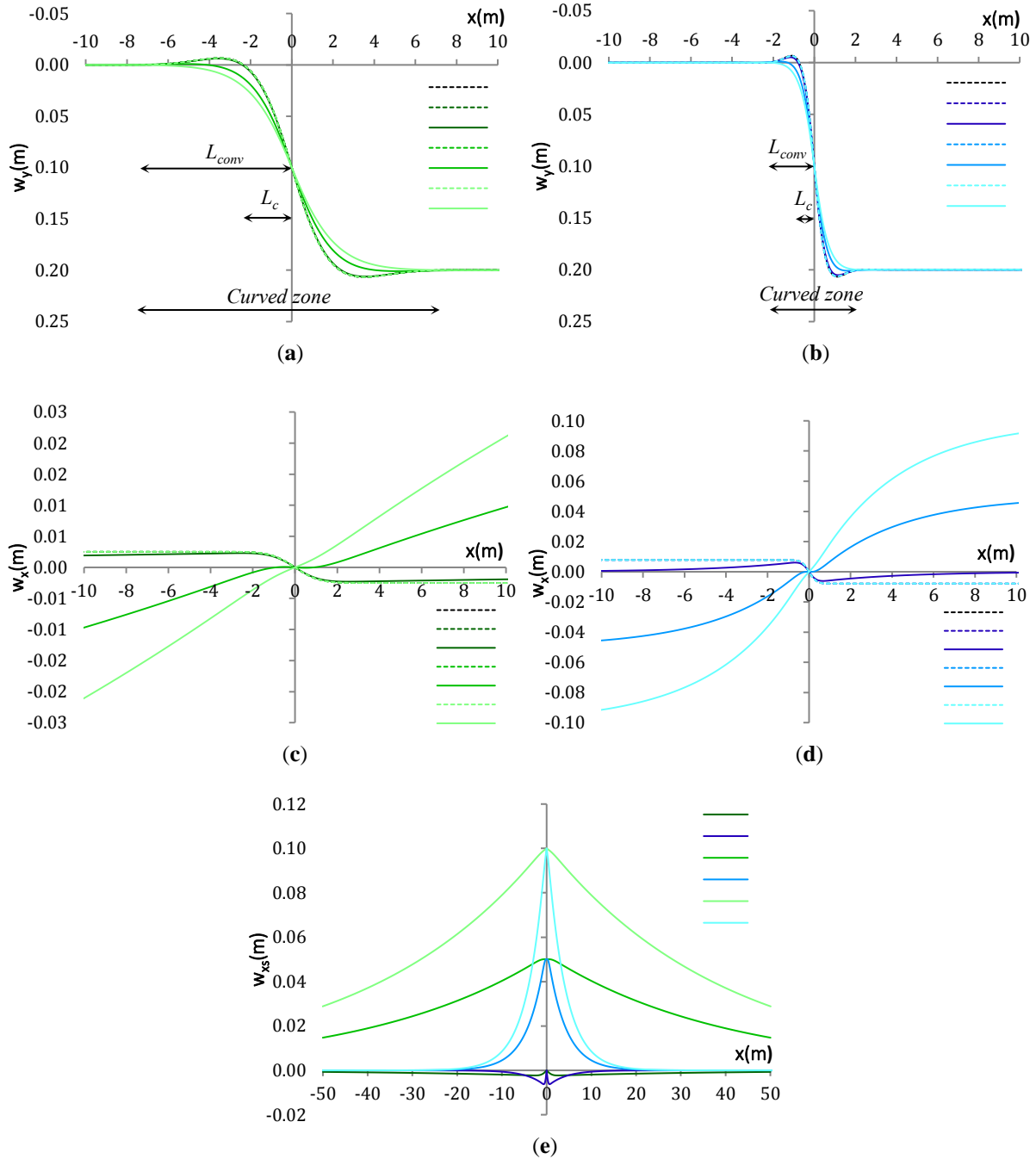


Fig. 3.9. Pipeline crossing strike-slip fault analysis displacement field responses: **(a)** w_y for soft soil cases, **(b)** w_y for hard soil cases, **(c)** w_x for soft soil cases, **(d)** w_x for hard soil cases, **(e)** w_{xs} for cases buried either in soft and hard soil with existence of axial soil springs.

the analytical solution will not have good accuracy in the pipeline response. It is important to mention that the analytical calculation of L_c without the axial soil-pipe effect is acceptable only for case of $\varphi=90^\circ$.

By evaluating the displacement results, it has been discovered that all cases with the same soil type converged to point B at a specific point (**Fig. 3.10a**). The distance between the pipe-fault intersection point and point B is defined as L_{conv} . Moreover, it was determined that parameter L_{conv} is almost independent of the axial soil-pipe interaction and faulting angle, although it is related with k_t as Eq. (3.11).

$$L_{conv} \approx \frac{3\pi}{2} \sqrt[4]{\frac{4EI}{k_t}} \quad (3.11)$$

Additionally, by gradually decreasing the faulting angle φ in the cases with axial soil springs, L_c approached L_{conv} ; subsequently, the angle $L_c = L_{conv}$. This phenomenon is attributed to the enormous increase of the axial tensile forces in the pipeline, around the faulting point, as shown in **Fig. 3.11a,b**. This axial force stretched the pipeline at the curved zone and prevented the change of the concavity direction. Consequently, the inflection points in the pipeline did not appear at the sides of the fault. Therefore, in the scenarios with axial soil-pipe interaction, L_c increased and became equal to L_{conv} . Additionally, in the case of $\varphi = 90^\circ$, it was observed that the pipeline responses at strike-slip fault crossings were independent of the axial soil-pipe interaction springs existence.

(B). Axial displacement (w_x)

As it can be seen in **Fig. 3.9c,d**, for all cases with the same soil stiffness and without axial soil-pipe interaction springs, the same reverse axial displacement was observed in the pipeline's curved zone. At the pipe-fault intersection point, this displacement was zero and gradually increased up to L_{conv} , while the reverse axial displacement increased. After point B, this displacement was constant up to infinity. By increasing the soil stiffness, the tendency of the pipeline to reverse the displacement at the curved zone of the pipe slightly increased. Moreover, with the 100-fold increase of the soil stiffness, only a 3-fold increase was observed for the reverse axial displacement, while the amplitude of this reverse displacement for the pipeline buried in the soft soil was 0.003 m, and that of the pipeline buried in the hard soil was 0.008 m.

Regarding **Fig. 3.10b**, in the curved zone of the pipeline that resulted from a large deflection, the axial force (q_{ta}) and transverse force (q_{tt}) appeared in the pipeline as components of the transverse soil-spring reaction force (q_t). Moreover, q_{tx} and q_{ty} were components of q_t and can be calculated as follows:

$$q_t(x) = k_t w_y(x) \quad (3.12)$$

$$q_{ta}(x) = q_t(x) \sin\theta(x) \quad (3.13)$$

$$q_{tt}(x) = q_t(x) \cos\theta(x) \quad (3.14)$$

$$q_{tx}(x) = \frac{q_t(x) \sin 2\theta(x)}{2} \quad (3.15)$$

$$q_{ty}(x) = q_t(x)\cos^2\theta(x) \quad (3.16)$$

The main reason for the reverse axial displacement of pipeline is the membrane forces which has been appeared because of the high deflection of the pipeline at the curved zone. The membrane forces have been appeared due to the stretching of the pipeline at the high curvature zone which makes membrane strain on the pipeline section at curved zone as shown in Eq. 17.

$$\varepsilon_m = \sqrt{1 + \left(\frac{\partial y}{\partial x}\right)^2} - 1 \quad (3.17)$$

Based on the Eq. 17, the membrane force of pipeline which is the main cause of the reverse axial displacement of the pipeline is derivable as Eq. 18.

$$N_m(x) = \frac{EA}{|L_{conv} - x|} \int_{L_{conv}-x}^{\infty} \varepsilon_m dx \quad (3.18)$$

The reverse axial displacement rate of the pipeline at the fault intersection point, was maximum, and gradually decreased up to point B (in L_{conv}), and was thereafter equal to zero until infinity. The reverse axial displacement was constant until the end. However, when an axial displacement for the fault and an axial soil-pipe interaction existed, this reverse axial displacement decreased in the curved zone resulting from the summation with the fault axial displacement, and gradually approached half of the axial displacement of Fault ($\delta_x/2$) after the curved zone (Point B).

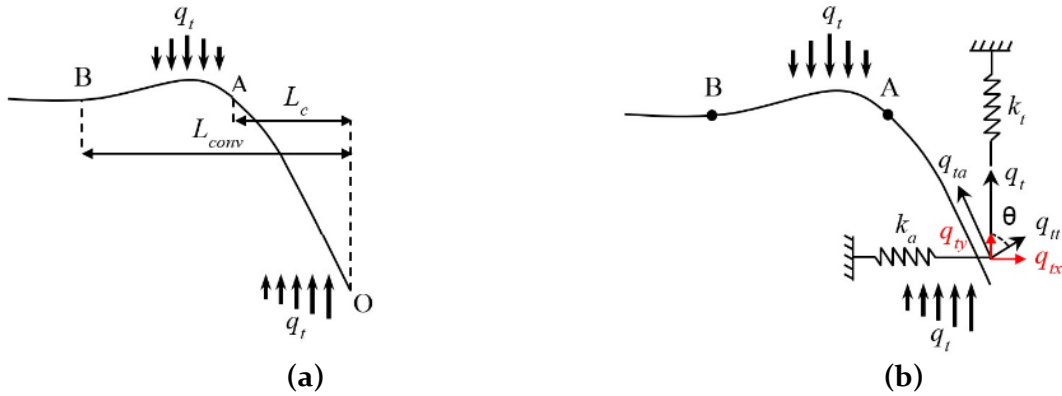


Fig. 3.10. (a) Schematic representation of L_c and L_{conv} at left side of pipe-fault intersection point O, (b) Force subcomponents of pipeline in curved zone.

(C). Axial force (N)

The axial force response of the pipeline is very effective in the pipeline's maximum tensile and compression stresses. Its combination with the bending moment, increase the probability of the pipeline buckling or yielding. With regard to **Fig. 3.11a-d**, it can be observed that the axial force of the pipeline and axial soil springs are related with the soil stiffness and faulting angle φ , and changes with the changing of these parameters. Additionally, the axial force responses of the pipeline were exactly equal to each other in the cases without axial soil-pipe interaction springs, and much lower than in cases with axial soil-pipe interaction springs.

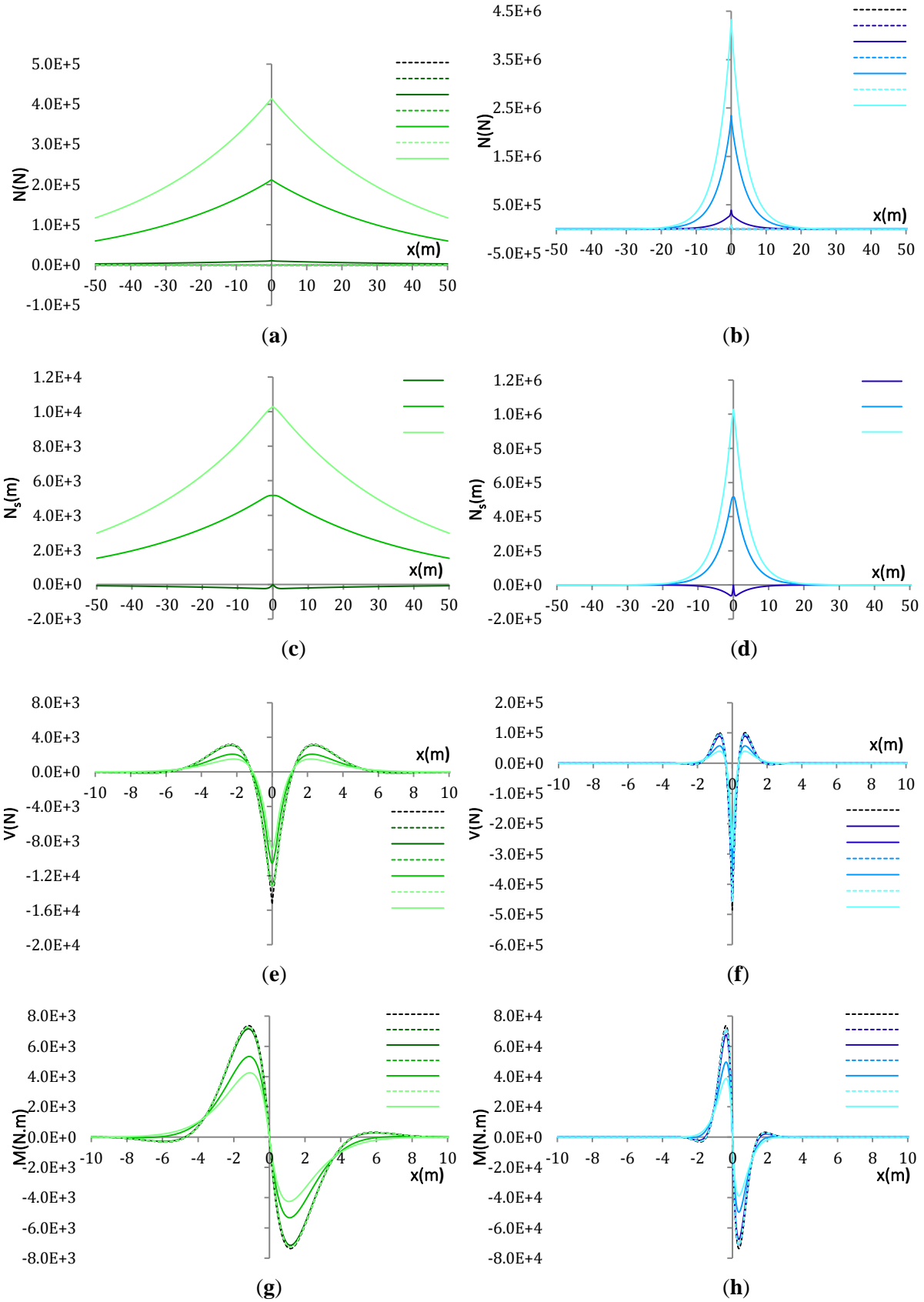


Fig. 3.11. Pipeline at strike-slip fault crossing analysis force and stress field responses: **(a)** N for soft soil cases, **(b)** N for hard soil cases; **(c)** N_s for soft soil with existence of axial soil springs, **(d)** N_s for hard soil with existence of axial soil springs, **(e)** V for soft soil cases; **(f)** V for hard soil cases, **(g)** M for soft soil cases, **(h)** M for hard soil cases.

Moreover, it was found that there exists a strong relationship between axial force of the axial soil-pipe interaction spring and buried pipeline. Note that all of these axial forces are tensile forces.

In the cases with axial soil-pipe interaction, the faulting angle was very effective in the axial force of the pipeline. The case with a 90° faulting angle had the least axial force, and with the decrease of the faulting angle from 90° up to 45°, the axial force increased substantially. In the soft soil cases, a 20-fold and 39-fold increase in the axial forces of the buried pipeline was observed with the decrease of the faulting angle (ϕ) from 90° to 60° and from 90° to 45°, respectively. In the hard soil cases, a 6-fold and 11-fold increase was observed in the axial forces of the buried pipeline with the decrease of the faulting angle (ϕ) from 90° to 60° and from 90° to 45°, respectively. Moreover, with regard to the axial force response, it was observed that the pipelines buried in soft soil were very sensitive to the faulting angle in comparison with the pipelines buried in hard soil. However, the axial force responses of the pipelines buried in hard soil were also highly affected by the faulting angle. By increasing the soil stiffness, a high rate of increase was observed in the axial force response of the buried pipeline. In other words, the axial force of the pipeline buried in hard soil had much higher axial forces in comparison with the pipeline buried in soft soil. By increasing the soil stiffness 100-fold, the axial force of the buried pipeline relatively increased from 32-fold to 10-fold in the cases of faults with angles of 90° to 45°, which is considered as a very substantial increase.

The cases of faults with angles of 90° to 45°, which is considered as a very substantial increase. Because the axial forces were slight in cases with a 90° faulting angle, it can be said that the axial forces were not sufficiently effective on pipeline crossings 90° strike-slip fault displacements. Additionally, it was observed that the axial force of the buried pipeline in the hard soil cases attenuated within much shorter distances in comparison with the soft soil cases (e.g., the axial force became zero after 20 m from the fault in the hard soil and after 150 m from the fault in the soft soil).

In all cases, the maximum axial force of the buried pipeline was observed at the point of intersection of pipeline with the fault, which means that $\partial N/\partial x$ was zero at point $x = 0$.

$$\left. \frac{\partial N}{\partial x} \right|_{x=0} = 0 \quad (3.19)$$

As shown in **Fig. 3.11a-d**, in the cases without axial soil-pipe interaction, by comparing the axial force responses of FEM cases 3 and 4 with the analytical cases 1 and 2 in the soft and hard soil, it was found that an axial force appeared in the curved zone of the pipeline in the FEM cases. The effect of this axial force can even be seen in cases with axial soil-pipe interaction. In all cases with same soil in the curved zone, an additional equal increase in the axial force response of the buried pipelines was observed. This increase in the axial force at the curved zone resulted from the appearance of membrane force at the large deflected zone of the pipeline which amount of it is calculable by Eq. 18.

The maximum amount of this membrane force (H_m) was 0.88 kN in the case of the soft soil

and 5.74 kN in the case of the hard soil. In the cases wherein the pipeline was buried in hard soil, the deflection was higher and based on Eq. 17 made higher ε_m and consequently, based on Eq. 18 made higher membrane force in the curved zone of the pipeline, which was 6.5 times larger than that of the soft soil.

(D). Shear force response (V)

With regard to **Fig. 3.11e,f**, there existed three extrema in the shear diagram of the pipeline crossing the strike-slip fault. As mentioned previously, the absolute extrema (maximum shear force of pipeline) existed at the intersection point of the pipeline and fault, and the axial force was also maximum at that point. Therefore, the high shear force also amplified the stresses at the critical point of the pipeline.

By comparing the shear force results obtained by the FEM analysis in the cases with and without axial soil-pipe interaction springs, it was found that the shear force diagram was same for all cases without axial soil-pipe interaction springs, even with different faulting angles. Additionally, the shear force diagram was higher than that in all cases with axial soil-pipe interaction springs. Accordingly, the axial soil-pipe interaction exerted strong a diminishing effect on the shear force response of the buried pipeline at the strike-slip fault crossing.

In cases with axial soil-pipe interaction, the faulting angle was very effective in the shear force of the pipeline. The case with a 90° faulting angle was determined as the case with the highest shear force response. Additionally, it was found that the shear forces decreased with the decrease of the faulting angle from 90° up to 45°. In cases wherein the pipeline was buried in soft soil, a 20% and 32% decrease in the maximum shear force of the buried pipeline was observed with the decrease of the faulting angle (φ) from 90° to 60° and from 90° to 45°, respectively. Additionally, in the cases wherein the pipeline was buried in hard soil, a 22% and 37% decrease in the shear forces of the buried pipeline was observed with the decrease of the faulting angle (φ) from 90° to 60° and from 90° to 45°, respectively (**Fig. 3.11e,f**).

For all cases observed at the point of intersection with the fault, $\partial V/\partial x$ was zero at the point of $x=0$ and could be used as a boundary condition for the analytical solutions at $x=0$, as expressed by Eq. 20.

$$\left. \frac{\partial^4 w_y}{\partial x^4} \right|_{x=0} = 0 \quad (3.20)$$

By comparing the shear force response of pipeline between the soft and hard soil cases, approximately 32-fold increase was observed for the maximum shear force with the 100-fold increase of the soil stiffness. The axial soil-pipe interaction springs in the shear force responses of the buried pipeline crossing the strike-slip fault were very effective, except for the case with a 90° faulting angle. The soil stiffness and faulting angle were observed to be effective parameters in the shear force response of the buried pipeline.

(E). Bending moment (M)

The bending moment response of the buried pipeline crossing the fault is very important because it is the main cause for pipeline buckling, as has been reported with regard to historical pipeline damages.

With regard to **Fig. 3.5c,d**, in the bending moment response of the pipeline, the maximum bending moment of the FEM cases 3 and 4 slightly decreased in comparison with the exact same analytical results for cases 1 and 2 in the soft and hard soil. This decrease in the pipeline's maximum bending moment resulted from the moment caused by the membrane force in the curved zone. In comparison with the analytical solution, the decrease in the bending moment of the pipeline in the FEM was 1.2% for the pipeline buried in soft and hard soil. By comparing the bending moment results obtained by the FEM in the cases with and without axial soil-pipe interaction springs, it was observed that the same bending diagram was obtained in all cases without axial soil-pipe interaction springs, even when the faulting angles were different. Additionally, the bending moment diagram was higher than that obtained for the cases with axial soil-pipe interaction. Accordingly, the axial soil-pipe interaction has a diminishing effect on the bending moment response the buried pipeline crossing the strike-slip fault.

In both the soft and hard soil, the maximum bending moment of the buried pipeline crossing the strike-slip fault approximately decreased by 27% and 42% with the decrease of the faulting angle (φ) from 90° to 60° and from 90° to 45° , respectively (**Fig. 3.11g,h**). Additionally, in all cases with a different faulting angle, the maximum bending moment of the pipeline buried in hard soil was around 9 to 9.5 times higher than that of the pipeline buried in soft soil. This means that by increasing the buried pipeline soil stiffness 100-fold, the bending moment increased nine times. Consequently, there existed a strong and direct relationship between the bending moment response of the buried pipeline with a faulting angle (φ) and soil stiffness (k). Finally, the axial soil-pipe interaction was found to be very effective in the bending moment response of the buried pipeline crossing the strike-slip fault, except for the cases with normal strike-slip faults ($\varphi=90^\circ$).

(F). Stress field (σ)

A good estimation of the stress field in the critical zones of the pipeline is very important to ensure an optimized and safe design. If the design maximum tensile and compression stresses are overestimated, the design will not be economic for a long pipeline route. Additionally, if the maximum stress is underestimated, this may cause a disaster during future earthquakes. **Fig. 3.12** shows the stress path of point (I) (check **Fig. 3.8** for point I) on the pipeline which is the maximum stress of pipeline (tensile) at the positive side of x axis and is minimum at the negative part of the x-axis, additionally the positive stresses are for illustration of tensile stresses and the negative stress are showing the compression stresses.

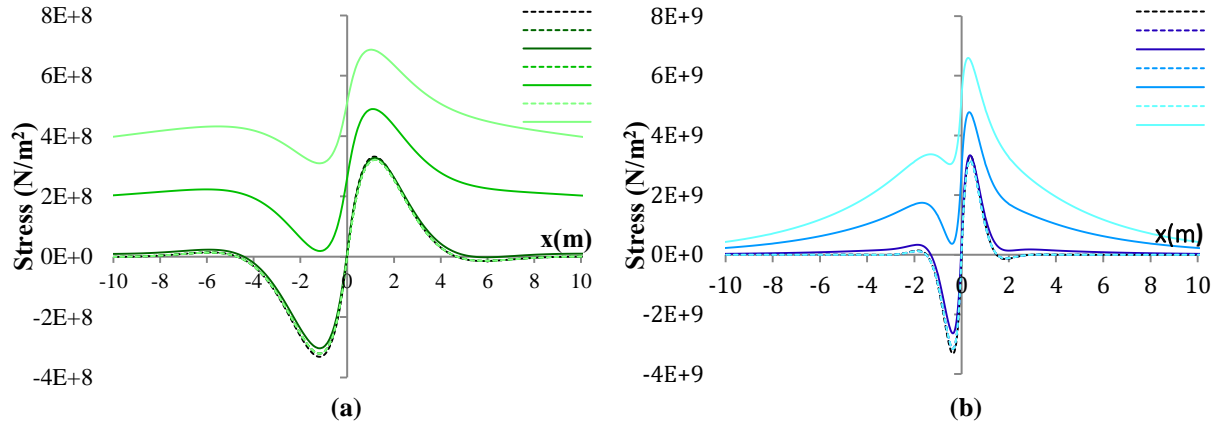


Fig. 3.12. Maximum/minimum stress of pipeline section crossing strike-slip fault on point (I) path: (a) soft soil cases, (b) hard soil cases.

By comparing the stress results obtained by the FEM analysis of cases with and without axial soil-pipe interaction springs, it was found that all cases without axial soil-pipe interaction springs had exactly the same stress diagram, even when the faulting angles were different. Additionally, the maximum stress diagram was lower than that in the cases with axial soil-pipe interaction springs. Therefore, the axial soil-pipe interaction was very effective in the stress field response of the buried pipeline crossing the strike-slip fault. Additionally, existence of the axial soil-pipe interaction exerted an increasing effect on the stress field response of pipeline by adding the effect of the axial forces in the pipeline section.

In the cases with axial soil-pipe interaction, the faulting angle changes had substantial effect in the maximum and minimum stresses of the pipeline. The cases with a 45° faulting angle had the highest maximum tensile stress, owing to the combination of a high axial force and bending moment. Additionally, the cases with a 90° faulting angle had the highest compression stress in the pipeline, owing to the high bending moment and very low tensile axial force in the curved zone of the pipeline. As can be seen in **Fig. 3.12**, in the cases with faulting angles of 60° and 45° resulting from the high axial tensile force in the pipeline, owing to the axial component of the fault displacement, compression stress did not exist in the pipeline section. Consequently, the probability of the pipeline buckling did not exist in the curved zone. However, in the cases with a 90° faulting angle, there was approximately no axial stress and the bending stress had the highest efficiency. Therefore, the maximum compression stress was equal to the tensile stresses. Consequently, the pipeline was highly vulnerable to buckling damage in the cases wherein the pipeline crossing was normal to the strike-slip fault.

Because the bending moment at the intersection point of the pipeline and fault ($x = 0$) was zero, the stress at the intersection point had to be equal to the maximum axial stress. At the intersection point (point B) in the cases wherein the pipeline was buried in soft soil, a 20-fold and 39-fold increase in the maximum stress of the buried pipeline was observed with the decrease of the faulting angle (φ) from 90° to 60° and from 90° to 45° , respectively. Moreover, in the cases wherein the pipeline was buried in hard soil, a 6-fold and 11-fold increase in the stress of the buried pipeline was observed at point ($x = 0$) with the decrease of the faulting

angle (φ) from 90° to 60° and from 90° to 45° , respectively. This increase in the maximum stress of the pipeline at the intersection point with the strike-slip fault was exactly equal to the increase of the pipeline's maximum axial forces. Therefore, this validates the previous statement of the maximum pipeline stress at the intersection point with the strike-slip fault ($x=0$) being exactly equal to the maximum axial stress of the pipeline.

In the cases wherein the pipeline was buried in either soft or hard soil, the maximum tensile stress of the pipeline increased by 49% and 200% with the decrease of the faulting angle (φ) from 90° to 60° and from 90° to 45° , respectively. Additionally, in all cases with axial soil-pipe interaction and with any faulting angle, the maximum tensile stress of the pipeline was 9.5 times higher in the cases wherein the pipeline was buried in hard soil, in comparison with the cases wherein the pipeline was buried in soft soil. In other words, there existed an approximate relationship between the maximum stress of the pipeline and the square root of the soil stiffness ratio and shear wave velocity in same cases with different soils.

3.4. Effect of steel pipe material nonlinearity on performance of buried pipelines at strike-slip faults crossing

In this subsection, a FEM-based investigation is conducted to study on the performance of buried pipeline crossing strike-slip fault by taking the nonlinear soil-pipe interaction and the nonlinearity of the steel pipeline material into account. The FEM-Based models are created with and without pipe material nonlinearity for cases with faulting angles of 90° , 60° and 45° .

The main aim of this subsection is to evaluate the steel pipeline material's nonlinearity effect on the buried pipeline performance in crossing with the large dislocated strike-slip fault. Besides, for a deeper understanding of the steel pipeline material's nonlinearity effect, the nonlinear soil-pipe interaction with various faulting angles are also included in FEM models.

3.4.1. FEM models definition

To evaluation of the pipeline performance at strike-slip fault crossing illustrated in **Fig. 3.13**, a number of representative numerical analyses were conducted by the Finite Element method, using the Abaqus commercial code [25]. For creating the FE-based models an API5L-X65 steel material (**Table 3.4**) for 4 inches pipeline, with an outside diameter of 0.1143m and thickness of 0.0023m and with conducting of introduced soil-pipe interaction springs in **Table 3.6** and **Fig. 3.14-15** are implemented. The plasticity of the steel material in the FEM model is defined based on the Ramberg-Osgood method for API5L-X65 steel material which is presented in **Table 3.5**. For gaining high accurate results, in this FEM-based analysis, a total length of 1km is simulated. After doing mesh sensitivity analysis with critical soil materials (extremely hard and soft soils) for representing accurate FEM results, the Mesh sizes are determined to be as follows. The pipeline in both sides of the fault symmetrically discretized gradually from 1.25 cm fine meshes up to bigger sizes of 1m after 300 meters further from the fault line.

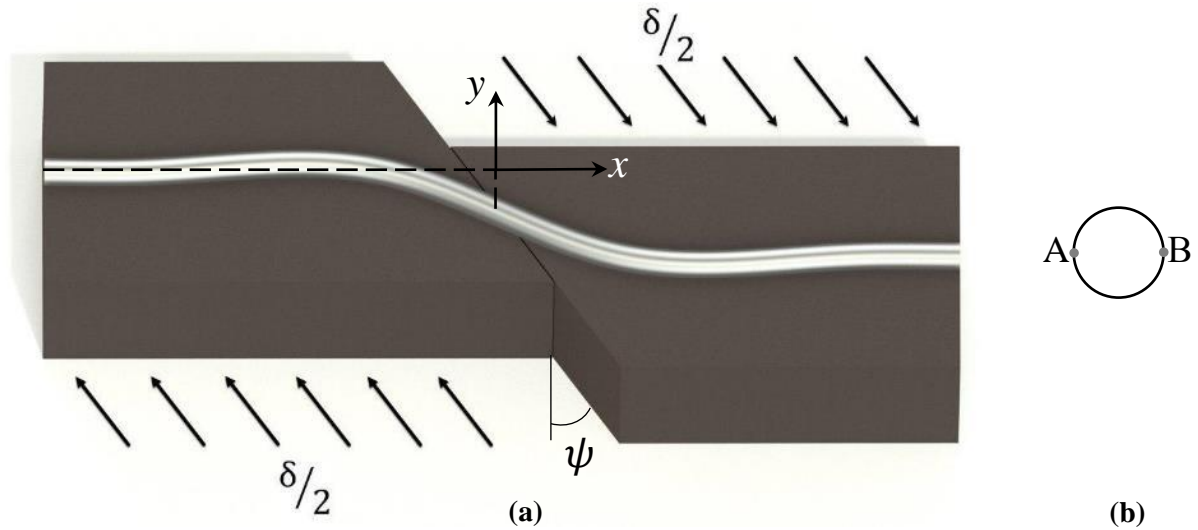


Fig. 3.13. (a) Illustration of deformed buried steel pipeline crossing strike-slip fault and the coordinate system. (b) pipeline section, A and B Paths [1].

Table 3.4. API5L-X65 steel properties [1].

Elastic Young modulus (E)	210 GPa
Poisson's ratio (ν)	0.3
Yielding stress (σ_y)	490 MPa
Yielding strain (ϵ_y)	0.00233
Failure stress (σ_u)	531 MPa
Failure strain (ϵ_u)	0.04

Table 3.5. Parameters of Ramberg-Osgood stress-strain for steel API5L-X65 [1].

Initial Young's modulus (E)	210 GPa
Yielding stress	490 MPa
a	38.31
r	31.51

Table 3.6. Soil springs bilinear properties implemented in FEM analysis (Soil-1) [1].

	Yielding force (f) (kN/m)	Yielding displacement (δ) (mm)
Transverse-horizontal springs (t)	60.58	26.0
Axial springs (frictional) (a)	1.71	2.5
Vertical springs (upward) (v1)	2.20	2.0
Vertical springs (downward) (v2)	259.08	200.0

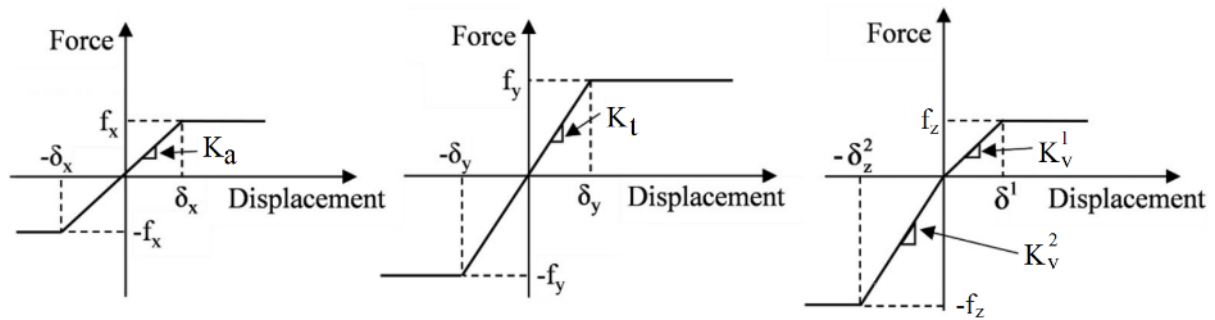


Fig. 3.14. Schematic bilinear force-displacement curves of soil-pipe interaction springs [1].

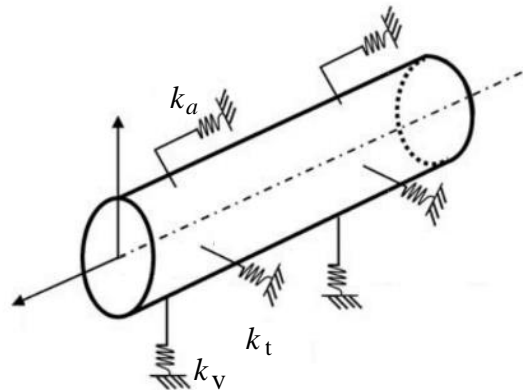


Fig. 3.15. Schematic model of pipeline and soil springs modeled by FEM [1].

3.4.2. Analysis cases

The problem of pipeline crossing strike-slip fault, in large deformations of fault is a highly nonlinear problem which these nonlinearities are related to the soil-pipe interaction nonlinearities and the pipe material nonlinearities.

Table 3.7. FE-based analysis cases [1].

Case No.	Case name	Soil springs	Steel pipe material	Fault dip. δ (m)	ψ
1	Elastic Steel – 0°	Soil-1 (Nonlinear)	API5L-X65 steel (Elastic)	3D*	0°
2	Plastic Steel – 0°	Soil-1 (Nonlinear)	API5L-X65 steel (Ramberg-Osgood)	3D	0°
3	Elastic Steel – 30°	Soil-1 (Nonlinear)	API5L-X65 steel (Elastic)	3D	30°
4	Plastic Steel – 30°	Soil-1 (Nonlinear)	API5L-X65 steel (Ramberg-Osgood)	3D	30°
5	Elastic Steel – 45°	Soil-1 (Nonlinear)	API5L-X65 steel (Elastic)	3D	45°
6	Plastic Steel – 45°	Soil-1 (Nonlinear)	API5L-X65 steel (Ramberg-Osgood)	3D	45°

* D: pipe diameter

For investigating the steel pipe material nonlinearity effect on the pipeline responses in the problem of buried pipeline crossing strike-slip fault, the FEM base models for each case is created in two cases with elastic and plastic material of steel pipeline. For achieving a deeper

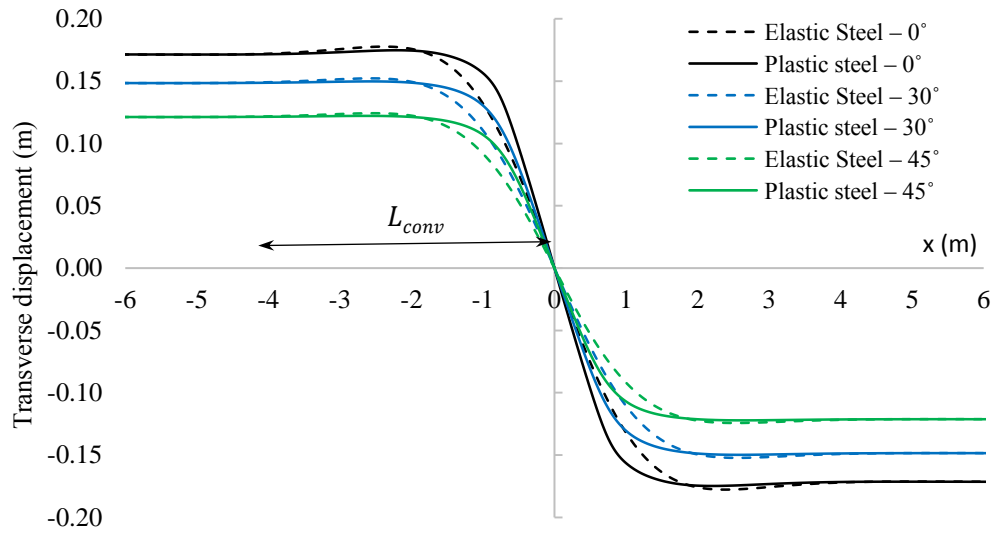


Fig. 3.16. Transverse displacement response of pipeline [1].

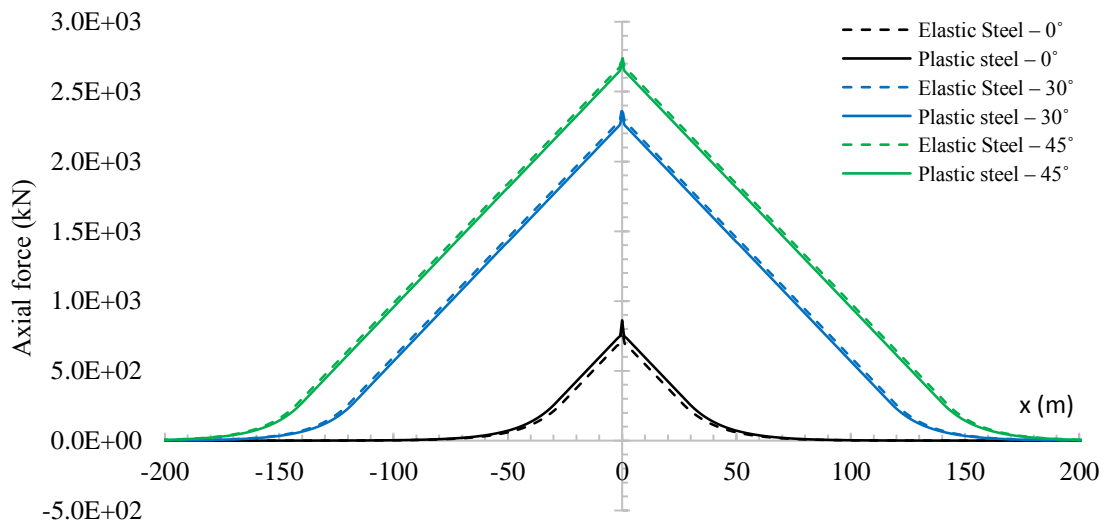


Fig. 3.17. Axial force response of pipeline [1].

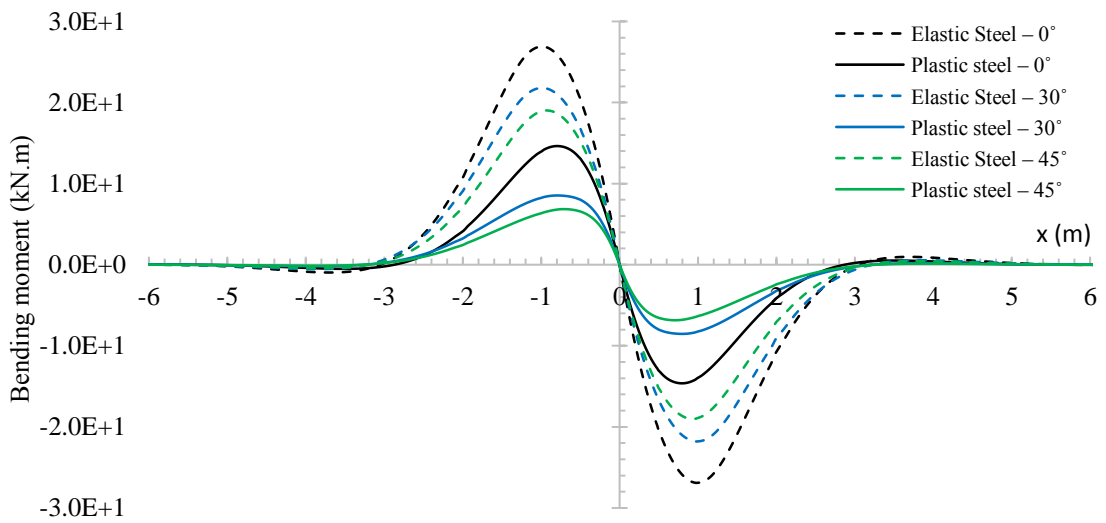


Fig. 3.18. Bending moment response of pipeline [1].

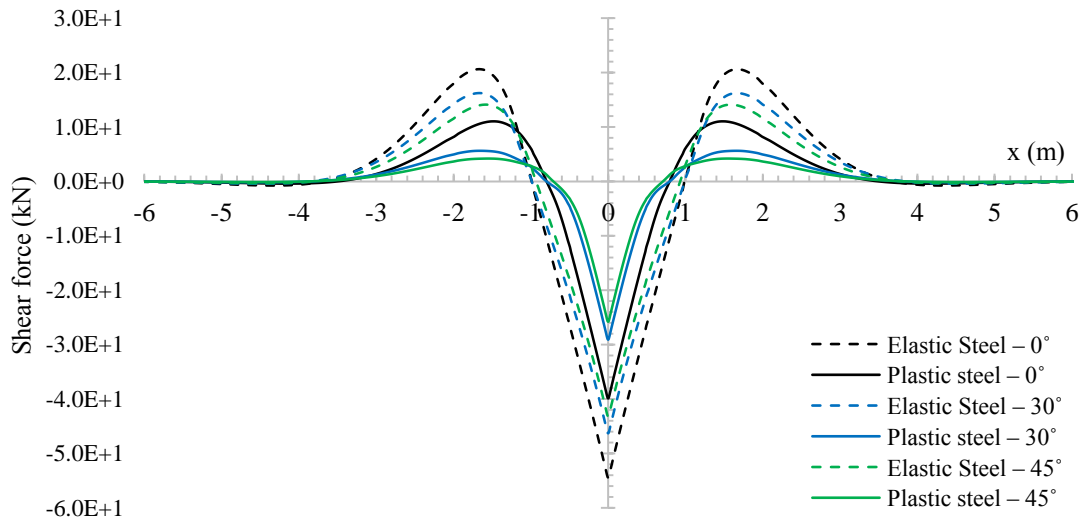


Fig. 3.19. Shear force response of pipeline [1].

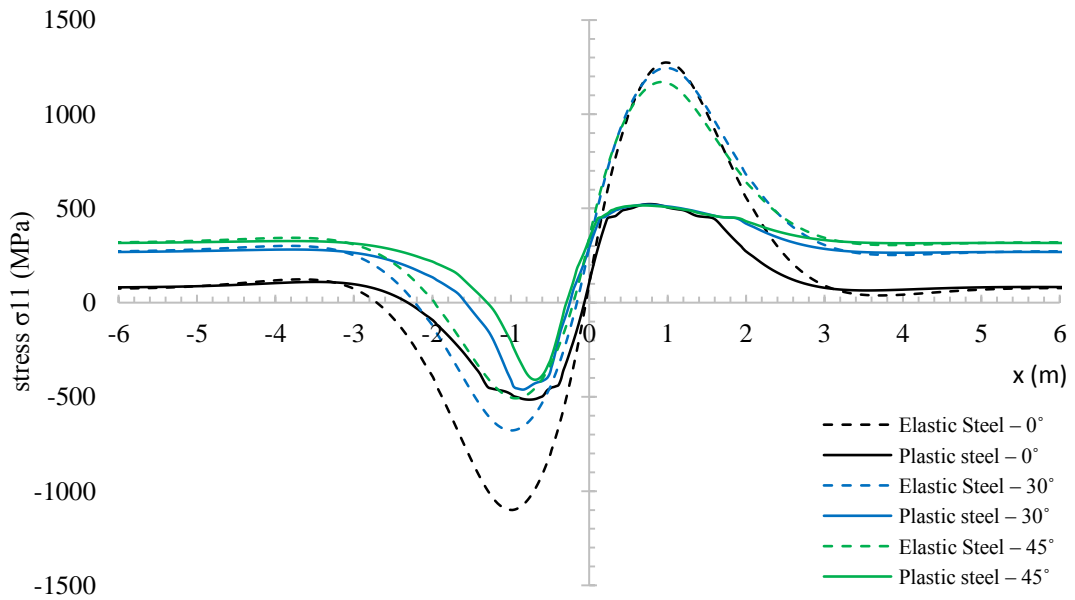


Fig. 3.20. Maximum stress response of pipeline on A Path [1].

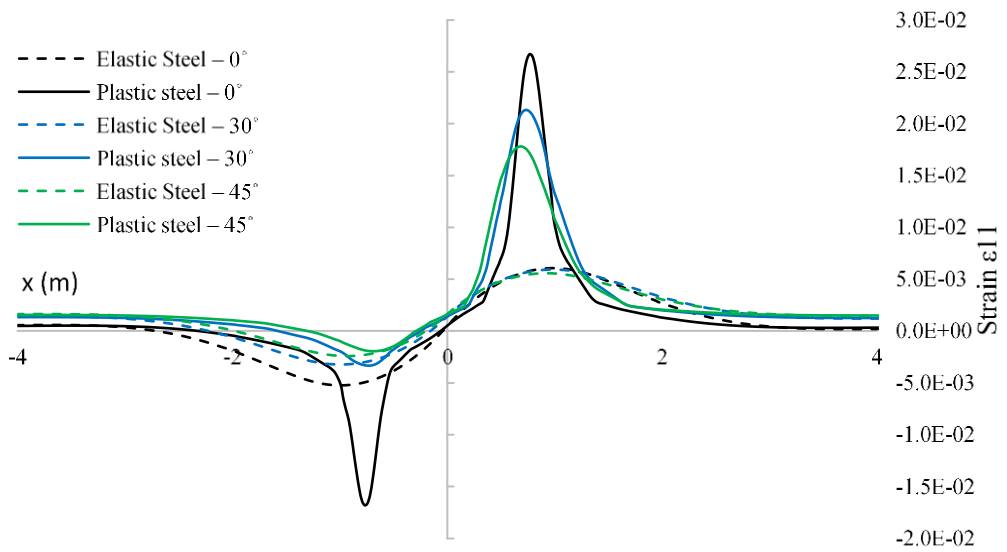


Fig. 3.21. Maximum longitudinal strain response of pipeline on A Path [1].

understanding of the effect of pipe material nonlinearity in this problem, models of the FEM based analysis in three angles of 0° , 30° and 45° are created as introduced in **Table 3.7**.

3.4.3. Analysis results

In this research, 6 FEM-based analysis for the problem of the buried pipeline crossing strike-slip fault with nonlinear soil-pipe interaction is simulated to investigate the effect of the steel pipeline material nonlinearity in large displacements and different faulting angles of the pipeline crossing strike-slip fault. The pipeline responses for transverse displacement, Axial forces, shear forces, bending moment and the maximum stress are presented in **Fig. 3.16** to **Fig. 3.20** as below.

As it is observable in **Fig. 3.16**, the curved zone length (L_{conv}) in the cases with plastic steel pipeline material are shorter than the cases with elastic pipe material. It seems by yielding of the pipeline the bending stiffness of pipeline decreases and pipeline deflects easier and causes shorter curved zone on the plastic pipelines.

Axial force response by increasing of the faulting angle (ψ) increases drastically (**Fig. 3.17**) and evidently, oblique fault and pipeline crossing cause higher axial forces in the pipeline cross-section. Moreover, difference of the axial force response of pipeline in the cases with plastic pipeline material in comparison with the cases with elastic pipeline material was negligible.

Indeed, increasing in faulting angle (ψ) causes highly decreasing in the bending moment response of pipeline and in other words the oblique strike-slip fault and pipeline crossing causes lower bending moments in the pipeline cross-section (**Fig. 3.18**). Besides, cases with plastic steel pipeline material (case 2, 4 and 6) proposed much lower pipeline bending moment response. In other words, yielding of the pipeline at the curved zone in the cases with plastic steel pipeline material (case 2, 4 and 6) decreased the bending stiffness of pipeline which results in lower pipeline bending moment response.

Similar to the bending moment response of pipeline, it has been found that by increasing of faulting angle (ψ) the shear force response of pipeline diminishes and besides, cases with plastic pipeline materials also experienced much lower shear forces (**Fig. 3.19**)

From **Fig. 3.20** it has been observed that the higher transverse fault displacement (δ_y) causes higher maximum tensile stresses. Besides, higher faulting angle (ψ) makes higher axial tensile stress in the pipeline and lower maximum compression stresses in pipeline cross-section. The cases with plastic pipeline material (case 2, 4 and 6) in comparison with the cases with elastic pipeline material (case 1, 3 and 5), experienced lower maximum tensile and compression stresses. Moreover, these lower maximum stresses appeared because of yielding of pipeline in cases (case 2, 4 and 6) due to large dislocation of the strike-slip fault which was 3 times bigger than the pipeline diameter.

Evidently, the plasticity of pipeline material and it's accurately modeling has a great effect on the pipeline responses of the problem of pipeline crossing strike-slip fault. Which needs to be more considered in analytical solution methods for this problem.

3.5. Conclusions

The force-displacement fields of a buried pipeline at a strike-slip fault crossing were investigated by FEM based simulations which were verified by an existing simple analytical solution and experiment result. Moreover, the mechanical behavior of the pipeline was evaluated under several scenarios with various faulting angles, different soil stiffnesses, with and without axial soil-pipe interaction springs, and with and without steel pipe material plasticity including nonlinear soil-pipe interactions to derive the effective parameters in the axial soil-pipe interaction, pipe material nonlinearity and buried pipeline performance at strike slip fault crossing for use in future analytical studies. The most important conclusions drawn from this study are as follow:

- 1) There exists a direct and strong relationship between the axial soil-pipe interaction, faulting angle (φ), and fault dislocation amplitude (δ). In other words, the axial soil-pipe interaction is strongly related with the axial fault dislocation amplitude (δ_x).
- 2) Changes in axial soil-pipe interaction of the buried pipeline crossing the strike-slip fault has substantial effect on the pipeline's force-displacement and stress field responses. The axial soil-pipe interaction exerted a decreasing effect on the shear force, bending moment, and compression stress responses and a radically increasing effect on the axial force and tensile stress responses of the buried pipeline. Because the axial soil-pipe interaction is very effective in the analytical solutions results, the implementation of an appropriate axial soil-pipe interaction in the analytical solutions is very important.
- 3) The effect of the axial soil-pipe interaction on the buried pipeline crossing the strike-slip faults was negligible and had approximately no effect on the pipeline responses subjected to the 90° strike-slip fault displacements.
- 4) The adequate axial soil-pipe interaction term has high complexity and a comprehensive analytical method is lacking. Based on conclusion 3, to ensure the simplicity and accuracy of the results, it is recommended to use the existing analytical solution as a validation method for the verification of the FE model only in the case of a buried pipeline crossing a 90° strike-slip fault in the elastic range. Moreover, the solution can be extend to other cases.
- 5) L_c has a direct relationship with φ and a reverse relationship with k_t . Additionally, there exists a relationship between φ and the axial soil-pipe interaction. Therefore, in the analytical solutions for calculating L_c , it is important to consider the axial soil-pipe interaction. However, in previous analytical studies, this important point was not adequately considered.
- 6) L_{conv} is almost independent of the axial soil-pipe interaction and φ . It has an inverse relationship with k_t and direct relationship with EI . Therefore, it is strongly recommended to use L_{conv} instead of L_c in the analytical calculations.
- 7) Owing to the inadequate number of boundary conditions in the analytical solutions to the problem of the pipeline crossing the fault, the use of optimization methods is required to

solve the problem. In this study, some new boundary conditions for the analytical solution was discovered and is expressed as follows:

$$a) w_y(x)|_{x=L_{conv}} = 0$$

$$b) V(x)|_{x=L_{conv}} = 0$$

$$c) w_x(x)|_{x=L_{conv}} = 0$$

$$d) \frac{dN}{dx}|_{x=0} = 0$$

$$e) \frac{dV}{dx}|_{x=0} = \frac{d^4y}{dx^4}|_{x=0} = 0$$

- 8) Owing to the appearance of the membrane force and the large deformation of the pipeline in the curved zone, a slight reverse axial displacement was observed in the curved zone. This displacement was zero at the intersection point and its rate was maximum at the intersection point of the fault and pipeline. Additionally, its rate gradually approached zero up to the point $x=L_{conv}$. Moreover, by increasing the soil stiffness, the tendency of the pipeline to reverse the displacement in the curved zone of the pipe slightly increased.
- 9) By decreasing the Faulting angle φ and increasing the soil stiffness, the axial forces of the pipeline substantially increased. Moreover, there existed a strong relationship between the axial force of the pipeline and the axial soil-pipe interaction, whereas in the cases without axial soil-pipe interaction, the axial force was approximately equal to zero.
- 10) The soil stiffness (k) was a very effective parameter in the buried pipeline force-displacement responses. It was observed that the axial forces, bending moment, shear force, and stress responses and axial reverse displacement of the buried pipeline had a direct relationship, and that l_{conv} had a reverse relationship with the soil stiffness (k).
- 11) Based on the FEM analysis for same scenarios with different soils and Eq. 9, approximately there is a strong relationship between the ratio of soils shear wave velocity and the ratio of stress, bending moment and axial force responses of the buried pipeline crossing the strike-slip fault as below. (which this ratio in this study was 10).

$$\frac{\sigma_{max(i)}}{\sigma_{max(j)}} \approx \frac{M_{max(i)}}{M_{max(j)}} \approx \frac{N(i)}{N(j)} \approx \sqrt{\frac{k(i)}{k(j)}} \approx \frac{V_{s(i)}}{V_{s(j)}} \quad (3.21)$$

By changing the soil stiffness, the changes of the axial force, shear force response, bending moment response, and stress field responses of the buried pipeline crossing the strike-slip fault were approximately equal to the changes of the shear wave velocity in the soils (10-fold in this study).

- 12) By having the analysis responses of a pipeline buried in an specific soil subjected to strike-slip fault displacement, the response of the pipeline buried in other soil conditions could be

approximately estimated by Eq. 21.

13) In the case with a 90° faulting angle, the bending moment response was predominantly in the stress field, while in the cases with smaller angles of φ (Oblique), the axial tensile force response gradually became the predominant response in the stress field of the buried pipeline. Therefore, in the case of a pipeline crossing a 90° strike-slip fault, buckling phenomena were the predominant damage case in the pipeline. Additionally, by decreasing the faulting angle (e.g., 60° and 45°), the predominant damage case is the tensile yielding of the pipeline.

Based on the nonlinear FEM analysis for the problem of pipeline crossing strike-slip fault, with the investigation of pipeline material nonlinearity beside faulting angle effect in 6 cases, it has been found that [1]:

- 14) Increasing of faulting angle (ψ) has a significant decreasing effect on the bending moment, shear force and maximum compression stress responses of the pipeline. however, it has a drastically increasing effect on the axial force and axial stress responses of the pipeline.
- 15) Cases with higher faulting angle had experienced larger yielded zone on the tensile part of the pipeline cross section.
- 16) Yielding of the pipeline has a decreasing effect on the bending stiffness of the pipeline and it causes the shortening of curved zone length (L_{conv}) of the pipeline.
- 17) Yielding of pipeline in some parts doesn't have a remarkable effect on the axial force and axial stress responses of the pipeline, However, it has a very significant effect on the bending moment, shear force and bending stress response of the pipeline.

Because the axial soil-pipe interaction was effective in all responses of the buried pipeline crossing the strike-slip fault, it is very important to implement an adequate axial soil-pipe interaction term in the analytical solutions. Otherwise, the design might become uneconomical and disaster may occur during future earthquakes as a result of overestimating or underestimating the design parameters. This study mainly, investigated to identify the effective parameters for the development of axial soil-pipe interaction terms, axial force terms of pipeline and derivation of new boundary conditions for future extension of analytical studies for this problem. Additionally, a verification case for FEM analysis in elastic range is identified.

References

- [1] Talebi, F. Kiyono, J. “Steel pipeline nonlinearity effect on the force-displacement analysis of buried pipelines crossing strike-slip fault” International Conference in Commemoration of 20th Anniversary of the 1999 Chi-Chi Earthquake, Taipei, Taiwan, Sep 2019;
- [2] Karamitros, D., Bouckovalas, G., Kouretzis, G. [2007] “Stress analysis of buried steel pipelines at strike-slip fault crossings,” *Soil Dynamics and Earthquake Engineering* 27, 200–11.
- [3] Trifonov, O. V., Cherniy, V. P. [2010] “A semi-analytical approach to a nonlinear stress–strain analysis of buried steel pipelines crossing active faults,” *Soil Dynamics and Earthquake Engineering* 30(11), 1298–308.
- [4] Karamitros, D. K., Bouckovalas, G. D., Kouretzis G. P., Gkesouli V. [2011] “An analytical method for strength verification of buried steel pipelines at normal fault crossings,” *Soil Dynamics and Earthquake Engineering* (13), 1452-1464.
- [5] Trifonov, O. V., Cherniy V. P. (2012). “Elastoplastic stress-strain analysis of buried steel pipelines subjected to fault displacements with account for service loads,” *Soil Dyn Earthq Eng* 33,54–62.
- [6] Newmark, N. M., Hall, W. J. [1975] “Pipeline design to resist large fault displacement,” *Proc. of the U.S. national conference on earthquake engineering*, University of Michigan, Ann Arbor, Michigan, 416–25.
- [7] Kennedy, R. P., Chow, A. M., Williamson, R. A. [1977] “Fault movement effects on buried oil pipeline,” *ASCE Transportation Engineering Journal* 103(5), 617–33.
- [8] Kennedy, R. P., Kincaid, R. H. [1983] “Fault crossing design for buried gas oil pipelines” *ASME, PVP conference* 77, 1–9.
- [9] Wang, L. R. L., Yeh, Y. A. [1983] “A refined seismic analysis and design of buried pipeline for fault movement,” *Earthquake Engineering and Structural Dynamics* 13(1), 75–96.
- [10] American Lifelines Alliance—ASCE. *Guidelines for the Design of Buried Steel Pipe*” July 2001 (with addenda through February 2005).
- [11] Lim, M. L., Kim, M. K., Kim, T. W., Jang, J. W. (2001). “The behavior analysis of buried pipeline considering longitudinal permanent ground deformation,” In *pipeline 2001: advances in pipelines engineering & construction* (San Diego, California), vol. 3, 107. ASCE. [https://doi.org/10.1061/40574\(2001\)3](https://doi.org/10.1061/40574(2001)3)
- [12] O’Rourke, M. J., Vikram, G., Abdoun, T. (2003). “Centrifuge modeling of buried pipelines,” In: *Proceedings of the Sixth U.S. conference and workshop on lifeline earthquake engineering*, August 10–13, 2003, Long Beach, CA. pp. 757–768.
- [13] Sakanoue, T., Yoshizaki, K. (2004). “A study on earthquake-resistant design for buried

- pipeline using lightweight backfill,” In: Proceedings of the 13th world conference on earthquake engineering, Vancouver, B.C., Canada, August 1-6, Paper No.2389.
- [14] Takada, S., Hassani, N., Fukuda, K. (2001). “A new proposal for simplified design of buried steel pipes crossing active faults,” *Earthq Eng Struct Dyn* ;30:1243–57.
- [15] Vazouras, P., Karamanos, S. A., Dakoulas, P. (2010). “Finite element analysis of buried steel pipelines under strike-slip fault displacement,” *Soil Dyn Earthq Eng* ;30:1361–76.
- [16] Vazouras, P., Karamanos, S. A., Dakoulas, P. (2012). “Mechanical behavior of buried steel pipes crossing active strike-slip fault,” *S, Soil Dyn Earthq Eng*;41:164–80.
- [17] Vazouras, P., Dakoulas, P., Karamanos, S. A. (2015). “Pipe–soil interaction and pipeline performance under strike–slip fault movements,” *Soil Dyn Earthq Eng* ;72:48–65.
- [18] Zhang, L., Zhao, X., Yan, X., Yang, X. (2016). “A new finite element model of buried steel pipelines crossing strike-slip faults considering equivalent boundary springs,” *Eng Struct*;123:30–44.
- [19] Demirci, H. E., Bhattacharya, S., Karamitros, D., Alexander, N. (2018) “Experimental and 22Eng ;114:198–214.
- [20] Liu, X., Zhang, H., Li, M., Xia, M., Zheng, W., Wu, K., Han, Y. (2016). “Effects of steel properties on the local buckling response of high strength pipelines subjected to reverse faulting,” *J Nat Gas Sci Eng* ;33:378–87.
- [21] Hasegawa, N., Kiyono, J. (2016). “Study of the plastic hinge position buried steel pipeline on fault displacement” *JSCE Journal of Earthquake Engineering*, (35), 161-166. (in Japanese)
- [22] Earthquake Engineering Research Institute [1999] “Kocaeli, Turkey Earthquake of August 17,” *EERI Special Earthquake Report*.
- [23] Uzarski, J., Arnold, C. [2001] “Chi-Chi, Taiwan, earthquake of September 21, 1999 reconnaissance Report,” *Earthquake Spectra* 17 (Suppl. A).
- [24] Miyajima, M., Fallahi, A., Ikemoto, T., Samaei, M., Karimzadeh, S., Setiawan, H., Talebi, F., Karashi J. [2018] “Site Investigation of the Sarpole-Zahab Earthquake, Mw 7.3 in SW Iran of November 12, 2017” *JSCE J. Disaster FactSheets 2018*, FS2018-E-0002. Available online: http://committees.jsce.or.jp/disaster/system/files/FS2018-E0002_0.pdf
- [25] ABAQUS/CAE 2017. Dassault Systems Simulia Corp, documentation of 2017 release.
- [26] Japan Gas Association. [2013] “Seismic Design Guideline for High-Pressure Gas Pipeline” JGA, specified, 206-13 (in Japanese)

Nomenclature

E	Young's modulus of steel pipeline	V	Shear force of pipeline
G	Shear Modulus of soil	V_s	Shear wave velocity in soil
I	Moment of inertia of pipeline cross-section	w_x	Axial displacement of pipeline
k	Elastic constant of soil springs	w_{xs}	Axial displacement of axial soil springs
k_a	Elastic constant of axial soil springs	w_y	Transverse displacement of pipeline
k_t	Elastic constant of transverse soil springs	x	Position along pipeline's longitudinal axis
L_c	Curved length of pipeline	$x_{M_{max}}$	Maximum bending moment position on x-axis
L_{conv}	Converged length of pipeline	y	Position along pipeline's transverse axis
M	Bending moment of pipeline	β	Coefficient defined in Eq. (3)
N	Axial force	ρ	Soil density
N_m	Membrane force of pipeline	δ	Fault dislocation
N_s	Axial force of axial soil springs	δ_x	Projection of fault displacement on x-axis
q_t	Spring force of transverse soil	δ_y	Projection of fault displacement on y-axis
q_{ta}	Spring force component of transverse soil along pipeline axis	φ	Faulting angle
q_{tt}	Spring force component of transverse soil along pipeline transverse	θ	Angle between q_{tt} and x-axis
q_{tx}	Vector projection of on x-axis	ε_m	Membrane strain

Chapter IV:

**Introduction of governing equation
for buried pipelines at strike-slip
faults crossing including the linear
axial force terms**

4.1. General remarks

In past studies, several simplification assumptions exist in analytical methodologies and the axial force effect is calculated through external formulations and applied as a constant value to parts of the partitioned governing equations. However, applicability range of them is limited and can lead to significant errors with increasing solution complexity. In this chapter, we establish an improved governing equation to analyze buried pipeline as a linear material subjected to active strike-slip faults. This approach includes geometrical nonlinearity effects and exact axial force terms of the pipeline inside governing equation, and requires no additional external calculations, which significantly increases application range and accuracy even in the case of large deformation. The proposed methodology is verified against finite element-based results with various faulting angles and displacement ranges. Results of the analytical methods are in good agreement with numerical results in both qualitative and quantitative aspects even for cases with large fault movements [1].

4.2. Background

Nowadays, FEM-based analysis offers applicable solutions to the problem of pipelines that cross faults [2]. Recently FEM has been used for the verification and refinement of analytical methods, evaluation of factors influencing pipe response under different types of PGD, and assessment of pipeline performance criteria (e.g., local buckling, ovalization, tensile rupture) [3-15].

Since the 1970s, this problem has been addressed in a range of numerical, experimental, and analytical studies. Newmark and Hall [16] evaluated a simplified analytical pipeline model for pipelines crossing faults that includes the behavior of the cable for small displacement, which only had a friction effect on the pipeline. Kennedy et al. [17] proposed the most known method for evaluating a pipeline crossing both strike-slip and normal faults and extended the Newmark and Hall work by adding a longitudinal soil-pipe interaction term to the transverse soil-pipe interaction, which was consequently incorporated into the ASCE guidelines for the seismic design of pipelines. They assumed that the pipeline section yields in the high-curvature zone, which means that the bending stiffness of the pipeline is ignored. This assumption does not represent the real pipeline performance and overestimates the bending strain while increasing the axial forces and strains [3]. Kennedy and Kincaid [19] proposed non-uniform friction between the pipe and surrounding soil. The first study of Kennedy et al. was extended to strike-slip fault crossings with a simple developing of pipeline bending stiffness by Wang and Yeh [20]. Wang and Yeh partitioned the pipeline into four segments: two on both sides of the crossing fault (called the high-curvature zone) and the other two further from the fault and beside the high-curvature zone. Using this approach, they tried to solve one of the limitations in the study by Kennedy et al. but ignored the inappropriate contribution of axial forces on the pipeline bending stiffness [3]. Additionally, partitioning of the pipeline into four segments assumes that the soil yields in the two high-curvature zones. However, the soil yielding

startingpoint can differ from soil to soil and may yield away or closer from the high curvature zone and this assumption is not realistic. Karamitros et al. [3] developed a method for strike-slip faults, wherein the pipeline is partitioned into four segments that are analyzed on the basis of the beam-on-elastic-foundation and elastic beam theories. After the analytical solution, the axial soil-pipe interaction was determined in addition to the steel pipe material's non-linearity using a bilinear stress-strain relationship. Karamitros et al. solved various limitations that existed in previous methods, but some shortcomings still existed. In particular, the calculation of bending strain was unclear, axial soil-pipe interaction was not implemented in the governing beam-on-elastic-foundation differential equation, and its effect was calculated in an indirect and simplified manner. Moreover, it contained the same assumptions and issues faced by Wang and Yeh regarding the pipeline partitioning into four segments.

Trifonov and Cherniy [4] extended the Karamitros et al. model to normal fault crossings, removed the symmetry conditions about the intersection point, and contributed transverse displacements for estimating a pipeline's axial elongation. The axial force was directly included in the governing differential equations, and geometrically induced second-order effects were consistently taken into account. Although the study by Trifonov and Cherniy presented substantial progress in semi-analytical pipeline models, we must first state some shortcomings. First, the axial force in the governing differential equation is only conducted in the two high curvature zones and is not extended for the two further zones. The axial force term in the governing equation at the high-curvature zone is implemented as a constant number calculated indirectly from another approximate solution for the entire pipeline. In reality, the axial force of the pipeline, even in yielded soil, is not constant; it undergoes a maximum at the crossing point with the fault line and in most cases, does not attenuate even up to hundreds of meters further than the fault line along either side of the pipeline. However, this simplification assumption can evidently introduce errors to the obtained results and also follows the same assumptions as Wang and Yeh with regards to partitioning the pipeline into four segments. Additionally, the developed solution by Trifonov and Cherniy entails a very complex system of equations, which can only be solved using optimization techniques. Karamitros et al. [5] extended their previous study to normal slip fault crossings and their method was not as complicated as that of Trifonov and Cherniy, However, this solution had the same shortcomings as results obtained in previous study of Karamitros et al. [3]. At 2012 Trifonov and Cherniy [6] presented an analytical model for stress-strain analysis of buried steel pipelines that cross active faults by taking into consideration the effect of operational loads such as internal pressure and temperature variation on the basis of plane strain plasticity theory. However, this study had the same shortcomings with the governing differential equation of the buried pipeline as the previous study of Trifonov and Cherniy [4].

All previous studies were unable to expose an analytical approach with a governing equation including an appropriate axial soil-pipe interaction term for the problem of buried pipeline subjected to fault movement.

Despite substantial advances made by previous studies in the development of analytical

solutions for a pipeline with regard to fault-crossing problems, axial soil-pipe interaction and axial forces owing to geometrical nonlinearity have not been appropriately applied in analytical solutions. As mentioned in literature review section, abovementioned approximations are performed because the exact term of the axial soil-pipe interaction in the related differential equations has not thus far been considered. The main term that explains the effect of the crossing angle between the pipeline and fault in analytical analysis is the axial soil-pipe interaction. Therefore, implementation of an improper axial soil-pipe interaction term affects the buried pipeline's performance, especially in oblique fault crossings. Accordingly, there exists a need for developing a comprehensive analytical solution that incorporates the exact axial soil-pipe interaction term.

In this study, we first conducted a closed-form solution for the problem of the buried pipeline at 0° strike-slip fault crossing (only with axial fault movement), to obtain the axial soil-pipe interaction terms and pipe's frictional axial force term. Secondly, verified FEM-based model versus closed-form analytical solution for the identical case of the buried pipeline at 0° strike-slip fault crossing. Thirdly, the axial force made by the geometrical nonlinearity effect is derived. Fourthly, at a new analytical approach with exact terms of the axial soil-pipe interaction, including effects of geometrical nonlinearity under large deformation, is applied inside the governing differential equation of a pipeline crossing a strike-slip fault in the linear range. Finally, verified FEM model extended to various faulting angles and the analytical solution results are thoroughly validated using the verified FEM models (consisting of geometrical nonlinearity effects) of a buried pipeline crossing a strike-slip fault with different fault angles and dislocation amplitudes [1].

4.3. Evaluation of axial force of pipeline

Because discovery and implementation of the axial force term of the pipeline into the governing differential equation was complex, previous studies do not include this term in the governing equation [3–4], [16–20] and it is approximated to be constant by some complex optimization methods [4,6]. However, in reality, the pipeline axial force is not constant throughout, reaches a maximum at the fault crossing, and attenuates exponentially with distance from the fault.

In this study, we assume that the axial force of the pipeline is made of two parts: an axial force caused by frictional axial soil-pipe interaction and a second part caused by geometrical nonlinearity effects owing to large deflections at the pipeline high curvature zone. Because of the differential equation procedure for having the axial soil-pipe interaction and pipeline axial force, a horizontal projection of the latter on the x-axis (H) must be derived according to:

$$H = H_s + H_m \quad (4.1)$$

Where H_s is horizontal projection of frictional axial force and H_m is horizontal projection of the pipeline membrane force. According to prior research [21,22] and several analyses, there is a strong relationship between the pipeline axial force and k_α and δ_x and axial stiffness of

pipeline (EA). Here k_a is, axial soil springs constant, δ_x and δ_y are horizontal and transverse components of the fault displacement (δ), respectively (**Fig. 4.1**).

$$\delta_x = \delta \cdot \cos\psi \quad (4.2)$$

$$\delta_y = \delta \cdot \sin\psi \quad (4.3)$$

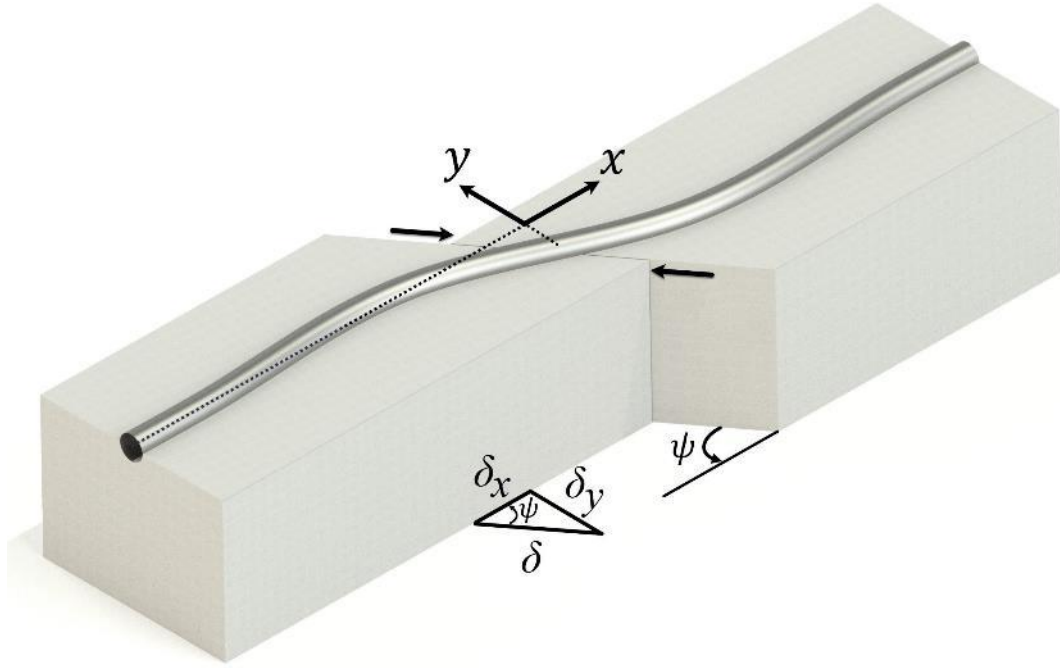


Fig. 4.1. Buried pipeline subjected to a strike-slip fault with faulting angle of (ψ) [1].

4.3.1. Frictional axial soil-pipe interaction

The axial soil-pipe interaction term has a large effect on the results of the pipeline-crossing-fault problem, which effects of the faulting angle (ψ) and pipeline axial forces are acquired by this term inside the governing equation. Since the transverse component of fault movement approximately does not affect frictional axial soil-pipe interaction [21]. To evaluate the axial frictional soil-pipe interaction, a model of buried pipeline subjected to a 0° strike-slip fault (i.e., only axial displacement) is modeled analytically for the left side of fault line (front segment of pipeline in **Fig. 4.2**) as shown in **Fig. 4.2**. For this segment with no sliding behavior, governing differential equation is derived as Eq. (4.4):

$$\frac{d^2 w_x}{dx^2} - \lambda^2 w_x = 0 \quad (4.4)$$

Where w_x is pipeline displacement on x axis and λ is:

$$\lambda = \sqrt{\frac{k_a}{EA}} \quad (4.5)$$

By implementation of the boundary conditions of $w_x = \delta_x$ at $x = 0$ and $w_x = 0$ at $x \rightarrow \infty$

and, Eq. (4.4) yields the following expression.

$$w_x = \delta_x e^{-\lambda x} \quad (4.6)$$

Since axial soil springs are connected to the pipeline at each point, it can be express:

$$d_s = w_x = \delta_x e^{-\lambda x} \quad (4.7)$$

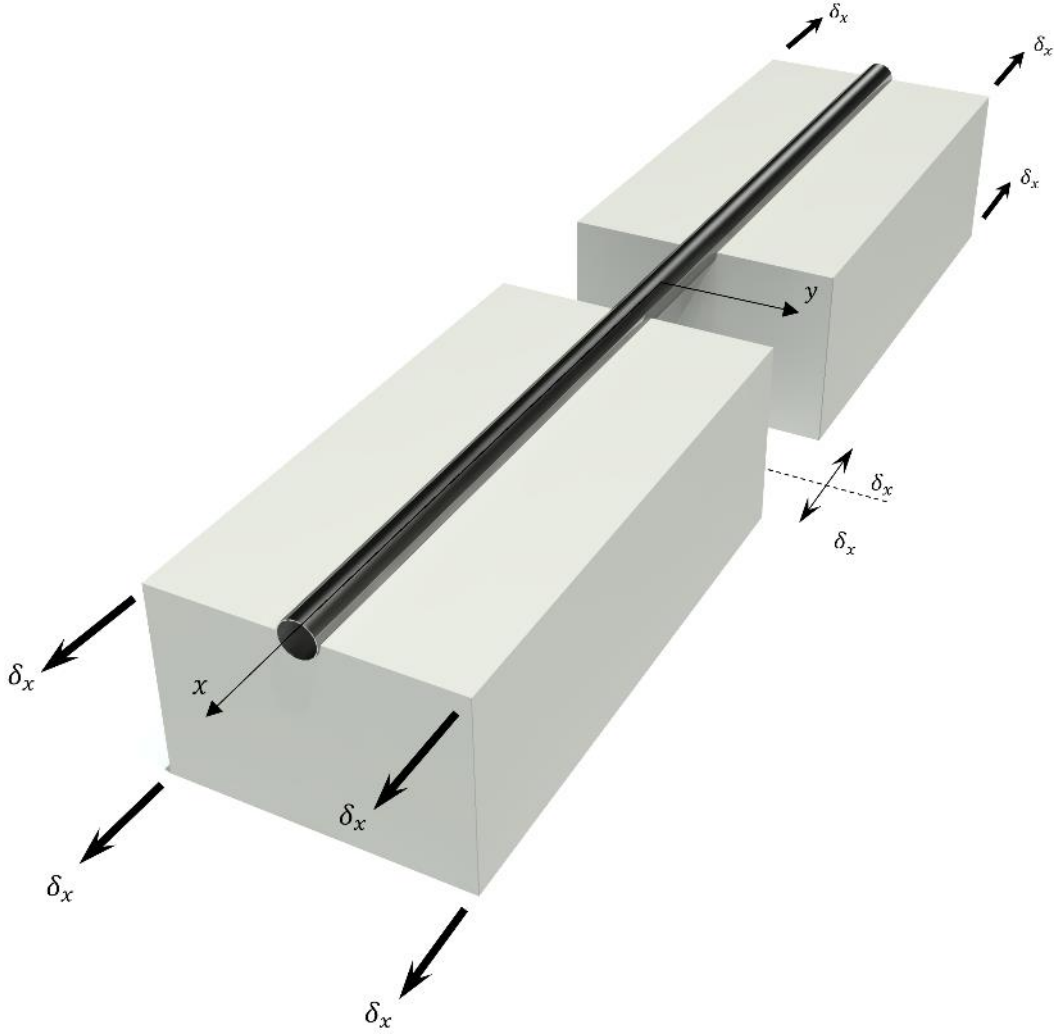


Fig. 4.2. Buried pipeline subjected to the strike-slip fault with $\psi = 0^\circ$ [1].

Where d_s is axial soil spring displacement. From Eq. (4.7), soil springs axial force (h_s) is extracted:

$$h_s(x) = k_a \delta_x e^{-\lambda x} \quad (4.8)$$

Based on Eq. (4.8) from integration of the forces, pipe frictional axial force is derived as:

$$H_s(x) = \frac{k_a \delta_x}{\lambda} e^{-\lambda x} \quad (4.9)$$

A FE-based evaluation with a faulting angle of 0° (i.e., only axial displacement) as **Fig. 4.2** with verification purpose is modeled for the cases presented in **Table 4.1**. And results are

compared with analytical results of Eq. (4.7) and (4.9). FE-based analysis implemented by Abaqus 2017 [23]. For modeling of steel pipeline, a B32 Timoshenko beam element, for modeling of soil springs, connector CONN3D2 elements are utilized. Moreover, a rigid beam as the boundary condition input point is then made of the RB3D2 rigid-beam element. Because of the symmetry of the problem, the analysis outputs are presented for only one side of the faultline. In **Table 4.1**, A is pipeline section area, E is the elastic Young's modulus of the steel pipeline, D is pipe external diameter, t is pipe thickness and EA , k_a and δ_x are mentioned

Table 4.1. Analysis cases scenarios [1].

Case name	δ_x (m)	k_a (N/m)	E (Gpa)	D (m)	t (m)	A (m ²)	EA (GN)
Case A	0.1	102870	200	0.1143	0.0023	8.093e-3	1.162e8
Case B	0.2	102870	200	0.1143	0.0023	8.093e-3	1.162e8
Case C	0.1	102870	400	0.1143	0.0023	8.093e-3	3.237e8
Case D	0.1	10287000	200	0.1143	0.0023	8.093e-3	1.162e8
Case E	0.1	1028700	200	0.1143	0.0023	8.093e-3	1.162e8

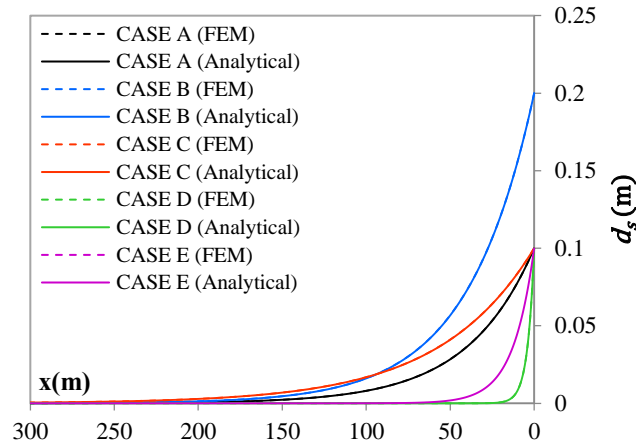


Fig. 4.3. The axial soil spring displacement results of the analytical Eq. (4.7) versus FEM analysis for cases A – E [1].

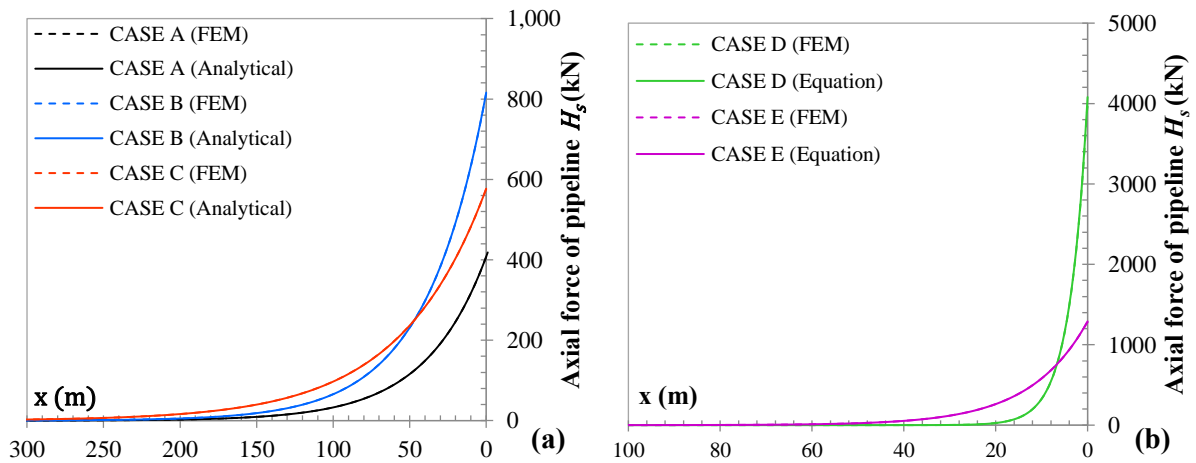


Fig. 4.4. The axial force of pipeline results of the analytical Eq. (4.9) versus FEM analysis: (a) cases A – C and (b) cases D – E [1].

above. According to **Fig. 4.3** and **Fig. 4.4**, results present that FEM-based results and analytical results are in very good agreement for soil springs displacement and axial force of pipeline which the error is almost zero. And the FEM-based model of the buried pipeline at 0° strike-slip crossing is verified versus the analytical solution.

4.3.2. Axial force owing to geometrical nonlinearity at the pipeline high curvature zone

A tensile axial force appears in the pipeline high curvature zone owing to elongation of the pipeline generated by extensive deformation. The axial strain of the pipeline owing to large deflection (membrane strain) at point x is:

$$\varepsilon_m(x) = \frac{1}{|L_{conv} - x|} \int_x^{L_{conv}} \left(\sqrt{1 + \left(\frac{\partial w_y}{\partial x} \right)^2} - 1 \right) dx \quad (4.10)$$

Where w_y is deflection in y direction of the pipeline.

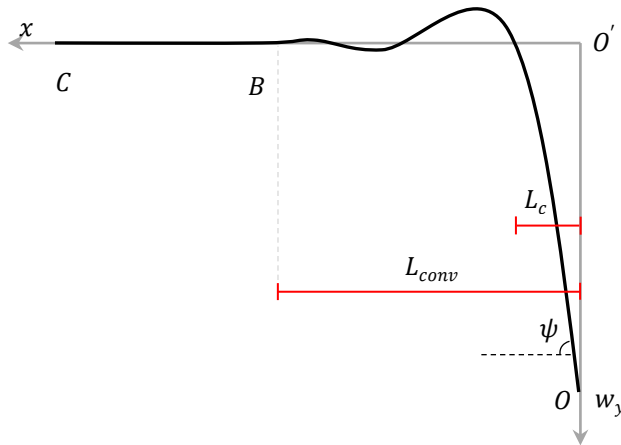


Fig. 4.5. L_{conv} length of the pipeline based on deflection $w_y(x)$ [1].

In **Fig. 4.5**, L_{conv} is the length of the pipeline between the fault line (point O) and point B where the deflection of the pipeline is almost attenuated according to the acquired $w_y(x)$. Following Eq. (4.10), horizontal projection of the pipeline membrane force on the x-axis is derived as:

$$H_m(x) = \frac{EA \cdot \cos\varphi}{|L_{conv} - x|} \int_x^{L_{conv}} \left(\sqrt{1 + \varphi^2} - 1 \right) dx \quad (4.11)$$

Where φ is rotation of pipeline:

$$\varphi(x) = \frac{\partial w_y}{\partial x} \quad (4.12)$$

According to Eq. (4.1) and with H_s and H_m , the projection of the total pipeline axial force

onto the x-axis is derived as:

$$H(x) = \frac{k_a \delta_x}{\lambda} e^{-\lambda x} + \frac{EA}{|L_{conv} - x|} \int_x^{L_{conv}} (\sqrt{1 + \varphi^2} - 1) dx \cdot \cos\varphi \quad (4.13)$$

4.4. Pipeline model

4.4.1. Existing governing equation

Regarding explanations in section 4.2, Trifonov and Cherniy [4], partitioned the pipeline to 4 segments: 2 segments near the fault trace (high curvature zones) and 2 further segments. And governing equation for 2 segments at high curvature zones was as Eq. (4.14) and the governing equation for further segments from fault was as Eq. (4.15).

$$EI \frac{d^4 w_y}{dx^4} - F \frac{d^2 w_y}{dx^2} = q \quad (4.14)$$

$$EI \frac{d^4 w_y}{dx^4} + k_t w_y = 0 \quad (4.15)$$

where E is the elastic Young's modulus of the pipeline, w_y is the transverse deflection, I is moment of inertia of the pipeline, k_t is the transverse soil springs constant, q is soil transverse reaction at high curvature zone, and F is the axial force at high curvature zone. Based on their definitions F , is a constant force along the pipeline for all the high curvature zone segments, which is calculated externally through a simplified equation and input inside the Eq. (4.14) and q is also constant soil reaction force at all the high curvature zone segments. And further segments based on Eq. (4.15) does not have any axial forces effect. Wherein not only the axial force is not constant at high curvature zones, but also axial force exists with a large magnitude inside the further segments up to very long distances. In their study, two Eq. (4.14) and Eq. (4.15) have been connected through a complex optimization method. As it has been mentioned in background section has shortcomings.

4.4.2. Solution algorithm

In this study, the proposed methodology solves the problem of a buried pipeline crossing a strike-slip fault with any angle in a linear range of axial and transverse soil-pipe interaction. In the proposed analytical method, the axial and transverse soil-pipe interactions were properly implemented in the governing equation of a buried pipeline subjected to fault movement.

As observed in **Fig. 4.6**, there is symmetry in the problem of a pipeline subjected to strike-slip fault movement. For simplicity, only the left side of the fault-line (segment OC) is evaluated in the analytical model and the results can be extended to the right side. Computation of a buried pipeline subjected to strike-slip faulting problem is presented in five steps:

4.4.2.1. Step-1

On the basis of the illustrated differential element (**Fig. 4.7**) and coordinate system for segment OC (**Fig. 4.6**):

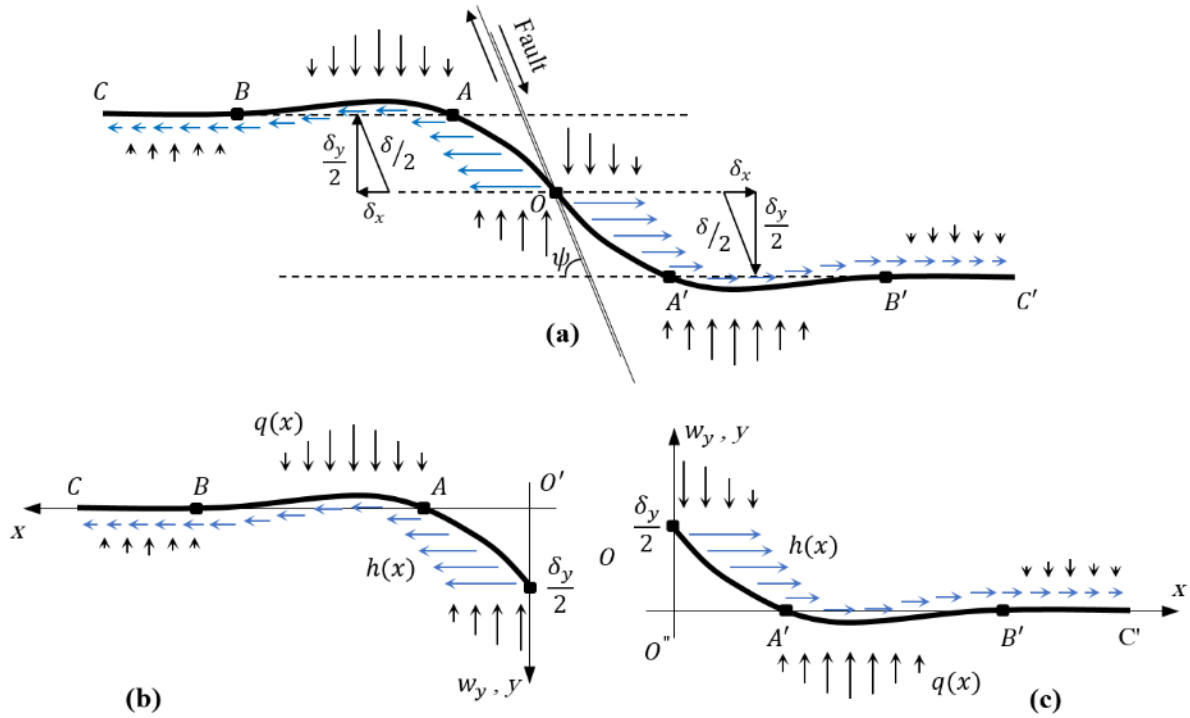


Fig. 4.6. Coordinate system and pipeline partitioning for the analytical solution [1].

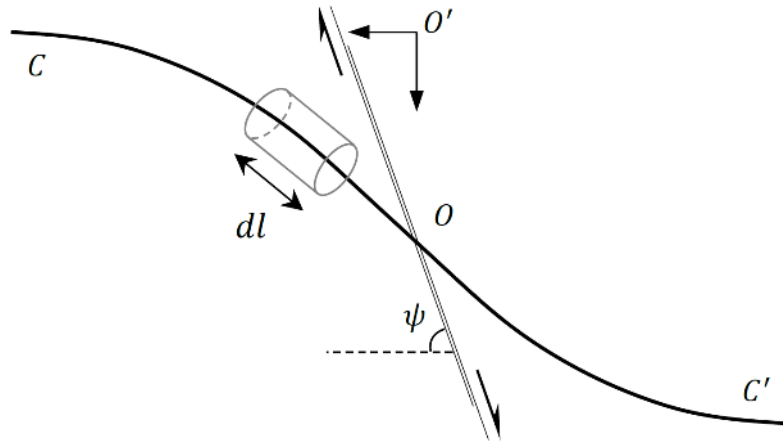


Fig. 4.7. Deformed pipeline element subjected to strike-slip fault movement [1].

$$dx = dl \cdot \cos \varphi \quad (4.16)$$

$$dw_y = dl \cdot \sin \varphi \quad (4.17)$$

Where, differential dx and dw_y are the projection of dl onto the x and y axis (**Fig. 4.7**). The transverse soil spring reaction is:

$$q(x) = k_t w_y(x) \quad (4.18)$$

Bending moment of pipeline is:

$$M(x) = -EI \frac{\partial^2 w_y}{\partial x^2} \quad (4.19)$$

From free body equilibrium of forces in y direction:

$$\frac{dQ}{dx} = \frac{k_t w_y(x)}{\cos \varphi} \quad (4.20)$$

Where Q is the vertical projection of transverse force of pipeline onto the x-axis.

Free body equilibrium of moment yields:

$$\frac{dM}{dx} \approx H(x) \frac{dw_y}{dx} + Q(x) \quad (4.21)$$

Based on Eq. (4.19) and Eq. (4.21), $Q(x)$ is:

$$Q(x) = -EI \frac{\partial^3 w_y}{\partial x^3} - H(x) \frac{dw_y}{dx} \quad (4.22)$$

By taking a derivative from both sides of Eq. (4.21), results Eq. (4.23)

$$\frac{\partial^2 M}{\partial x^2} = -\frac{\partial H}{\partial x} \cdot \frac{dw_y}{dx} - H \frac{\partial^2 w_y}{\partial x^2} + \frac{dQ}{dx} \quad (4.23)$$

Based on Eq. (4.13) it can be drive:

$$\begin{aligned} \frac{dH}{dx} = & k_a \delta_x e^{-\lambda x} + \left(-EA \left(\frac{\partial^2 w_y}{\partial x^2} \right) \sin \varphi + \frac{EA \cdot \cos \varphi}{L_c - x} \right) \int_x^{L_{conv}} \left(\sqrt{1 + \varphi^2} - 1 \right) dx \\ & + \frac{EA \cdot \cos \varphi}{L_c - x} \cdot \left(\sqrt{1 + \varphi^2} - 1 \right) \end{aligned} \quad (4.24)$$

By substituting of Eq. (4.24), Eq. (4.20), Eq. (4.13) inside Eq. (4.23), the governing differential equilibrium equation for OC segment is derived:

$$\begin{aligned} EI \frac{\partial^4 w_y}{\partial x^4} - \left[\frac{k_a \delta_x}{\lambda} e^{-\lambda x} + \frac{EA \cdot \cos \varphi}{|L_{conv} - x|} \int_x^{L_{conv}} \left(\sqrt{1 + \varphi^2} - 1 \right) dx \right] \frac{\partial^2 w_y}{\partial x^2} \\ + \left[k_a \delta_x e^{-\lambda x} + \left(\frac{EA \cdot \cos \varphi}{L_{conv} - x} - EA \cdot \sin \varphi \cdot \frac{\partial^2 w_y}{\partial x^2} \right) \int_x^{L_{conv}} \left(\sqrt{1 + \varphi^2} - 1 \right) dx \right. \\ \left. + \frac{EA \cdot \cos \varphi}{L_{conv} - x} \left(\sqrt{1 + \varphi^2} - 1 \right) \right] \frac{dw_y}{dx} + \frac{k_t w_y}{\cos \varphi} = 0 \end{aligned} \quad (4.25)$$

where λ is as Eq. (4.5), x is distance from point O along the pipeline axis, E is the elastic Young's modulus of the pipeline steel, w_y is the transverse deflection, I is moment of inertia of the pipeline cross-section, k_t is the transverse soil springs constant, k_a is the axial soil springs constant, and δ_x is the fault horizontal displacement in one direction (**Fig. 4.6**).

Following previous studies, the boundary conditions at $x = 0$ are $w_y \rightarrow \delta_y/2$,

$\partial^2 w_y / \partial x^2 \rightarrow 0$, and at $x \rightarrow \infty$, they are $w_y \rightarrow 0$, $\partial w_y / \partial x \rightarrow 0$.

In comparison with governing equations of previous study (Eq. (4.14) and Eq. (4.15)), in this study governing equation is extended majorly and Eq. (4.25) is derived as the main governing differential equilibrium equation for the problem of a buried pipeline subjected to strike-slip faulting. Which has integrated all the segments in one united segment and includes axial force and geometrical nonlinearity effects inside the governing equation.

Eq. (4.25) is a boundary value problem (BVP) with a nonlinear 4th order ordinary differential equation (ODE).

The governing differential Eq. (4.25) becomes cumbersome since the lower bond of the integral term is not constant, making its mathematical solution essentially impossible. This is because the membrane force effect, which is included the integral terms, and the additional input of L_{conv} , are both unknown in this step. As reported previously, L_{conv} is approximately insensitive to faulting angle and is therefore calculatable without considering the membrane force effect of the pipeline.

To solve Eq. (4.25), the integral terms must be solved. An iterative approach is therefore designated to gradually solve this integral term until convergence.

The $w_y(x)$ matrix for cases without membrane forces is obtained by removing the membrane force terms from the governing equation (integral terms=0) and solving it. The integral terms and L_{conv} are then calculatable from $w_y(x)$ of the governing equation for the case without the membrane force effect. The integral term of membrane force of pipeline is:

$$P_i(x) = \int_x^{L_{conv}} (\sqrt{1 + \varphi^2} - 1) dx \quad (4.26)$$

where $P_i(x)$ is the integral term in Eq. (4.25) which is related to the membrane forces of pipeline, i is the solution step number. Because solving of Eq. (4.25) with exact integral terms of $P_i(x)$ is cumbersome. To solve the Eq. (4.25), an approximated mathematic function (Eq. (4.27)) is substituted integral term (Eq. (4.26)). And the value of Eq. (4.26) in each step is calculated from previous solution step. After solving several cases, it has been found that $P_i(x)$ can be approximated with an exponential function:

$$P_i(x) \approx A_{3i} e^{-\lambda x} \quad (4.27)$$

where A_{3i} is equal to $P_i(x)$ at the pipeline-fault crossing point ($x = 0$):

$$A_{3i} \approx P_i(0) \quad (4.28)$$

Substituting the integral term with the exponential function of Eq. (4.27) into the governing Eq. (4.25), the main governing differential equilibrium equation of the pipeline-fault crossing is approximated as:

$$\begin{aligned}
EI \frac{\partial^4 w_y}{\partial x^4} - \left[\frac{k_a \delta_x}{\lambda} e^{-\lambda x} + \frac{EA \cdot \cos \varphi}{|L_{conv} - x|} A_{31} e^{-\lambda x} \right] \frac{\partial^2 w_y}{\partial x^2} \\
+ \left[k_a \delta_x e^{-\lambda x} + \left(\frac{EA \cdot \cos \varphi}{L_{conv} - x} - EA \cdot \sin \varphi \cdot \frac{\partial^2 w_y}{\partial x^2} \right) A_{31} e^{-\lambda x} \right. \\
\left. + \frac{EA \cdot \cos \varphi}{L_{conv} - x} \left(\sqrt{1 + \varphi^2} - 1 \right) \right] \frac{dw_y}{dx} + \frac{k_t w_y}{\cos \varphi} = 0
\end{aligned} \tag{4.29}$$

Consequently, Eq. (4.29) as a boundary value problem with nonlinear higher-order ordinary differential equation is numerically solvable. The boundary conditions for Eq. (4.29) are the same as in Eq. (4.25). By following this procedure, $w_y(x)$ is obtainable by solving Eq. (4.29).

The closed-form solution of this complex governing equation is cumbersome and after some attempts, it has found that there is no analytical solution. The differential equation of Eq. (4.29) is therefore solved numerically by the collocation method and Simpson's method [24–26].

Based on numerous analyses we found that L_{conv} is practically the same for different faulting angles (different axial forces owing to different axial fault movements). Since the membrane force is an axial force inside the pipeline, therefore, the L_{conv} is calculatable without considering membrane force effects.

Since in step-1, A_{31} and L_{conv} are still unknown variables and L_{conv} is calculatable without having the membrane force effect on the pipeline. We therefore assume $A_{30} = 0$ and $L_{conv} = 100000$ as the initial condition of the solution.

Upon numerical solution of Eq. (4.29), $w_y(x)$ is acquired for step-1 in addition to A_{31} and L_{conv} .

4.4.2.2. Step-2

By substituting A_{31} and L_{conv} obtained in step-1 inside the governing Eq. (4.29) and solving it, the $w_y(x)$ is achieved for the case of having a membrane force effect and consequently geometrical nonlinearity owing to large deformation in the governing equation. A_{32} is thus calculated from Eq. (4.28) on the basis of the $w_y(x)$ acquired in step-2.

4.4.2.3. Step-3

Since, in step-2, the A_{32} is calculated on the basis of the pipeline curvature obtained in step-1, which has no membrane force effect. For accurate reproduction of $w_y(x)$ of a buried pipeline it is needed to calculate the A_{33} . Therefore, calculated A_{32} in step-2 has been substituted in Eq. (4.29). Consequently, by solving Eq. (4.29) with A_{32} , the $w_y(x)$ and A_{33} are achieved with higher accuracy.

4.4.2.4. Step-4

To ensure sufficient accuracy of the calculated $w_y(x)$, Eq. (4.29) must be repeatedly resolved with new A_{33} calculated from the $w_y(x)$ obtained in step-3. The final $w_y(x)$ and A_{34}

are evaluated by solving Eq. (4.29). A_{34} from step-4 and A_{33} from step-3 must be compared; if the results are similar, the procedure can be stopped and the $w_y(x)$ of step-4 is determined as the final $w_y(x)$. However, in cases where A_{34} in step-4 is different from the previous step, this procedure must be continued until A_{3i} is nearly the same as A_{3i-1} . Indeed, in all calculated cases, A_{3i} converged and the final $w_y(x)$ is obtained.

In most cases, the solution up to step-4 is sufficient and an additional step is rarely necessary. The entire solution procedure is typically solved in less than 10 minutes using a computer with i7 4.2GHz CPU and 32 GB memory.

4.4.2.5. Step-5

After acquiring the final $w_y(x)$, the remaining pipeline responses can be extracted on the basis of the pipeline's deflection response. Using Eqs. (4.13) and (4.27), the horizontal force of the pipeline (H) on the x-axis is derived as:

$$H(x) = \frac{k_a \delta_x}{\lambda} e^{-\lambda x} + \frac{EA}{|L_{conv} - x|} A_{3i} e^{-\lambda x} \quad (4.30)$$

where A_{3i} is calculated in the last step on the basis of vertical projection of the transverse force of the pipeline section at Eq. (4.22) and utilizing of Eq. (4.28) and Eq. (4.30). the pipeline axial force is:

$$N(x) = \left[\frac{k_a \delta_x}{\lambda} e^{-\lambda x} + \frac{EA}{|L_{conv} - x|} A_{3i} e^{-\lambda x} \right] \cos \varphi(x) - \left[EI \frac{\partial^3 w_y}{\partial x^3} + H(x) \cdot \varphi(x) \right] \sin \varphi(x) \quad (4.31)$$

In the same manner, the shear force of the pipeline is:

$$V(x) = \left[\frac{k_a \delta_x}{\lambda} e^{-\lambda x} + \frac{EA}{|L_{conv} - x|} A_{3i} e^{-\lambda x} \right] \sin \varphi(x) - \left[EI \frac{\partial^3 w_y}{\partial x^3} + H(x) \cdot \varphi(x) \right] \cos \varphi(x) \quad (4.32)$$

And the pipeline bending moment is as Eq. (4.19). By obtaining all responses of the pipeline, the maximum and minimum (maximum tensile/compression) elastic stress and strain of the pipeline cross-section are respectively:

$$\begin{aligned} \sigma_{max/min}(x) &= \sigma_a(x) \pm \sigma_b(x) \\ &= \frac{N(x)}{A} \pm \frac{M(x) \cdot (r - t/2)}{I} \end{aligned} \quad (4.33)$$

$$\varepsilon_{max/min}(x) = \varepsilon_a(x) \pm \varepsilon_b(x) = \frac{N(x)}{EA} \pm \frac{M(x) \cdot (r - t/2)}{EI} \quad (4.34)$$

Where, σ_a and ε_a are axial stress and strain of the pipeline. And σ_b and ε_b are the maximum

bending stress and strain of the pipeline at the sprongline point.

4.4.2.6. The complete solution algorithm

In summary, computation of a buried pipeline subjected to strike-slip faulting is presented as follows.

1. Solve the governing differential equilibrium equation (Eq. (4.29)) without the membrane force effect on the basis of initial assumptions to calculate A_{31} and L_{conv} .
2. Input the calculated integral term (A_{31}) and acquired L_{conv} from step-1 and solve governing differential Eq. (4.29) to calculate A_{32} .
3. Substitute A_{32} in the governing differential equation and resolve by having the membrane force effect to calculate A_{33} .
4. Repeat step-3 and check the A_{3i} convergence to acquire the final $w_y(x)$.
5. Calculate pipeline responses.

4.5. Numerical modeling and verification of the analytical method

The developed analytical method is verified through comparison of its results with those obtained from FE-based analysis. For the analysis cases, we consider a 16" steel pipeline with an external diameter of 0.4064 m and thickness of 0.0071 m without internal pressure and a total length of 3000 m. The pipeline material is SS400 steel with an elastic Young's modulus of 200 GPa and Poisson's ratio of 0.3. Properties of the soil-pipe interaction springs (**Table 4.2**) are calculated on the basis of seismic design guidelines for a high-pressure gas pipeline in Japan [27]. The pipeline is assumed to be buried under 1.8 m of medium-density sand with an internal frictional angle of 40° and unit weight of 1800 kg/m³.

Table 4.2. Soil-pipe interaction properties [1].

	k (kN/m)
Axial direction (k_a)	2438.4
Transverse horizontal direction (k_t)	5660.8
Vertical upward direction (k_{v_1})	2753.4
Vertical downward (k_{v_2})	4787.4

4.5.1. Finite element pipeline model

Verified FEM-based model of the buried pipeline at 0° strike-slip fault crossing at section 4.3 is extended to various angles of strike-slip movements in this subsection. In this subsection, FEM-based analyses are created to validate the proposed analytical method. And FEM-based analyses are implemented in Abaqus 2017 [23]. We used a B32 Timoshenko beam element on the basis of shear flexible beam theory, which can provide useful results for transverse shear

deformation and large axial strain. The soil-pipe interaction spring elements are modeled by connector CONN3D2 elements oriented in three orthogonal directions (**Fig. 4.8**). A rigid beam as the boundary condition input point is then made of the RB3D2 rigid-beam element. The element size after doing sensitivity analysis has been determined. The pipeline is gradually discretized from fine at the fault zone to slightly bigger mesh sizes at further distances (from a length of 0.0125 to 1 m) symmetric to the fault line. A segment of the finite-element model is illustrated in **Fig. 4.9**. Beam elements (pipe) through connector elements (soil springs in 3 directions) are connected to the rigid elements. The boundary conditions related to the fault movements are applied to rigid elements and soil spring transmitted the fault movement effects on the pipeline; Which is the same with the real situation.

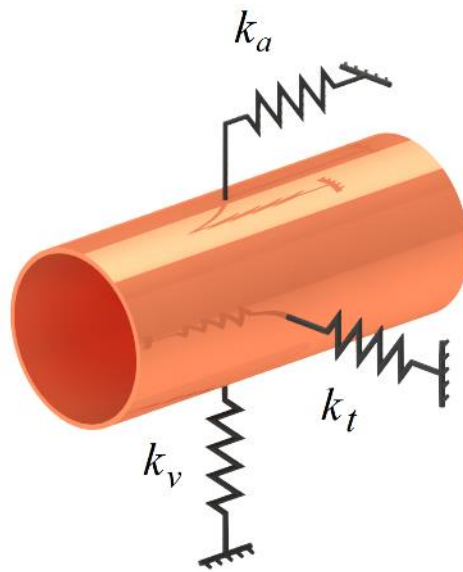


Fig. 4.8. Soil-pipe interaction springs adjustment [1].

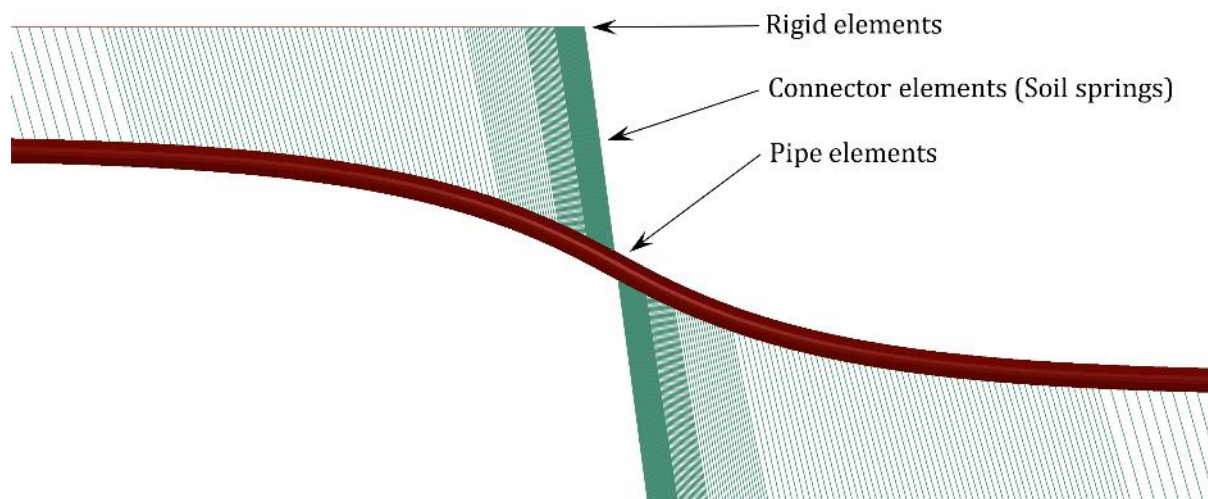


Fig. 4.9. Part of the finite element model and attached soil-pipe interaction springs [1].

As the problem of buried pipeline subjected to the fault movement is a large deformation problem, for having the geometric nonlinearity effects in the simulations, the Nlgeom option in Abaqus has been implemented. The fault displacement components are set as the boundary

conditions of the analysis scenarios and are specified to the rigid elements at each step.

4.5.2. Comparison of proposed methodology versus finite element solutions under various loading conditions.

Figs. 4.10–4.14 illustrate the deflection, axial force, bending moment, shear force, and maximal stress responses of the buried pipeline subjected to strike-slip fault movement from FEM analysis results versus the proposed analytical solution results. The analytical results are plotted as solid lines and the FEM results are plotted as dashed lines. For a comprehensive evaluation of the proposed method, analyses are implemented for fault movement from 1D to 6D of the pipeline, where D is the pipeline external diameter, and faulting angle of 90° to 45°. Cases with fault movement of 4D and 6D are proposed to evaluate the analytical method results in very large deformation situations. Each figure is shown in four rows and four columns where the first to fourth rows illustrate results for cases in which δ is equal to 1D, 2D, 4D, and 6D, respectively, and the first to fourth columns shows cases with faulting angles of 90°, 75°, 60°, and 45°, respectively. Owing to the symmetry of the problem, all responses in **Figs. 4.10–4.14**

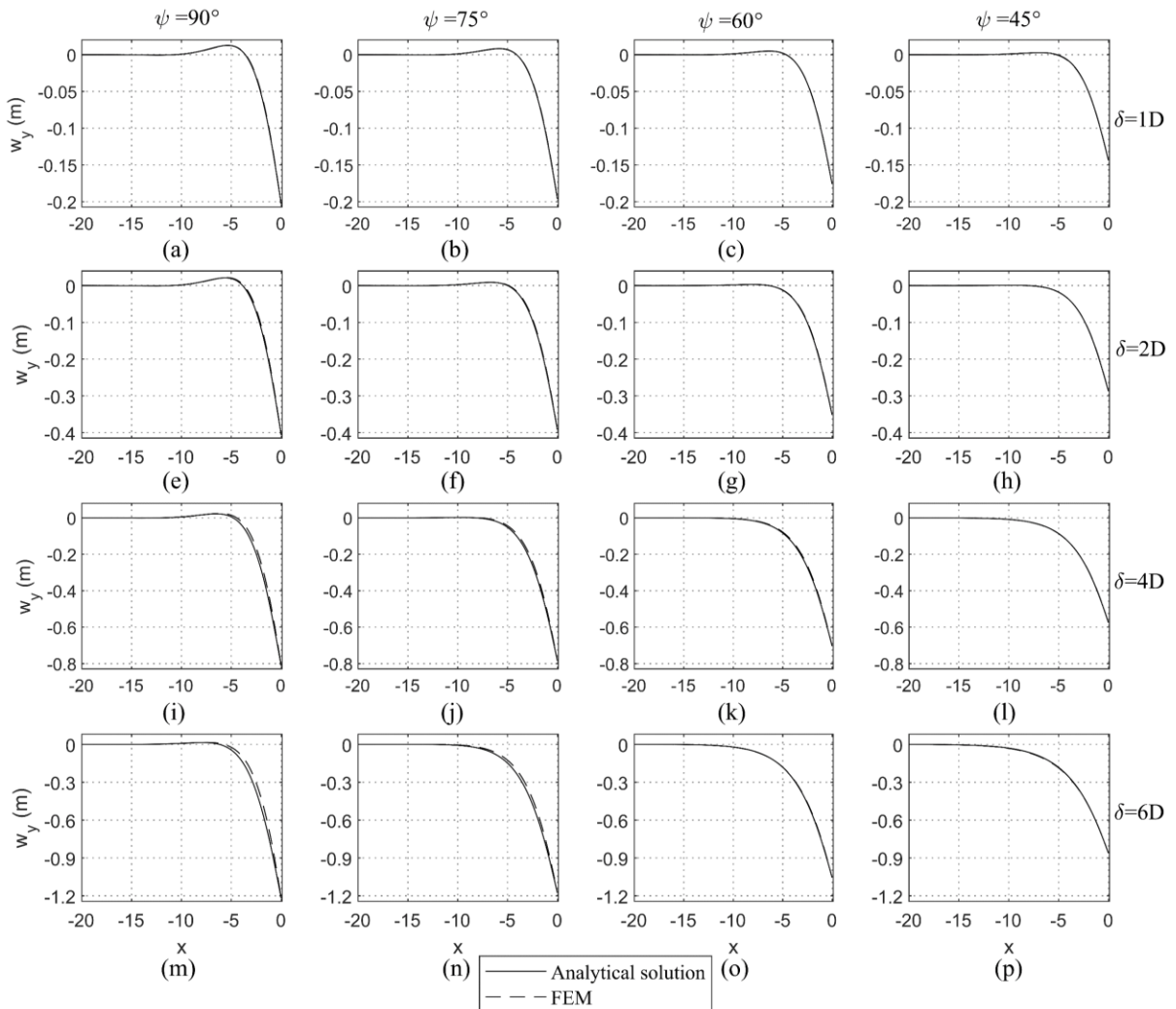


Fig. 4.10. Transverse deflection response of a buried pipeline subjected to strike-slip fault movement (analytical versus FEM results) [1].

are provided only for the left side of the fault line and the coordinate system is based on **Fig. 4.6b**.

The deflection responses for the proposed analytical method in **Fig. 4.10** are in excellent agreement with the FE-based analysis. The analytical deflection results for all the cases up to 2D fault movement are meticulously covered by the FEM-based analysis results. The deflection response in the case of large deformation ($\delta = 4D$ and $6D$) and faulting angles of 60° and 45° are exactly same for the analytical and FEM-based results. Owing to the large geometrical nonlinearity of the problem, the largest discrepancy between the analytical solution and FEM-based analysis is observed in **Fig. 4.10m** for the case of $\delta = 6D$ and $\psi = 90^\circ$. However, the difference is not substantial.

Based on **Fig. 4.10**, the previously reported parameter L_{conv} is nearly constant for all analyses and is almost independent of δ and ψ . L_{conv} changes in the case of pipeline or soil stiffness change. In cases of higher ψ and lower δ , the pipelines tend to have higher reverse deflection.

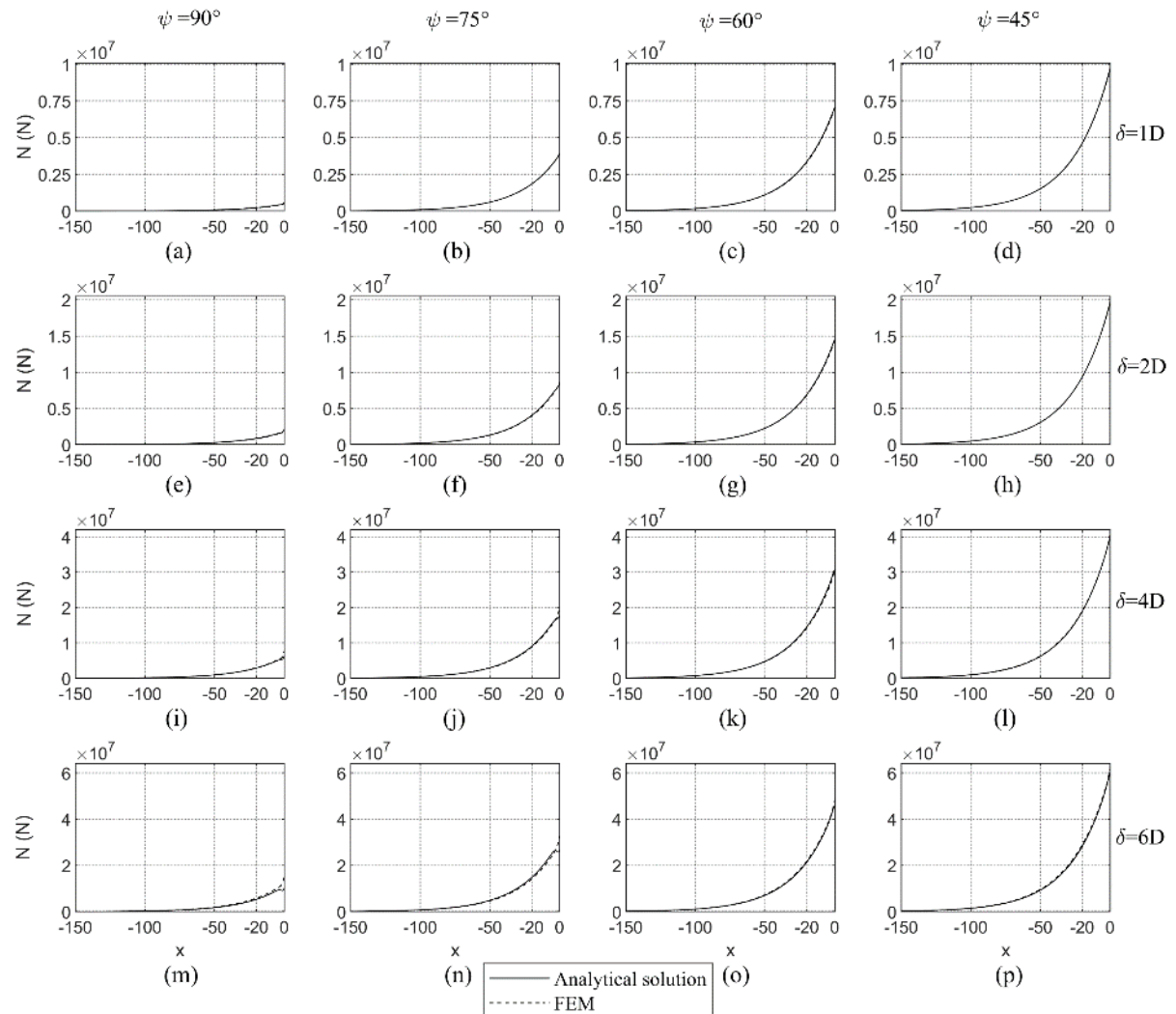


Fig. 4.11. Axial force response of a buried pipeline subjected to strike-slip fault movement (analytical versus FEM results) [1].

The axial force response in the cases with fault displacements up to 2D and any faulting angles, in cases with 4D, and 6D in cases with 60° and 45° faulting angles, the analytical solution results are in excellent agreement with the FEM-based analysis results. One observed difference occurs at the fault intersection point (**Figs. 4.11i, j, m, and n**) in which the difference between analytical and FEM results is 10%, 10%, 24%, and 19%, respectively. However, in the rest of the cases, this difference is less than 3%. It has been found that, the axial force response of the buried pipeline (**Fig. 4.11**) determined from the analytical methodology is very consistent with the FE-based analysis results. The results show that the axial force increases with decreasing faulting angle and increasing fault movement and the highest axial force occurs in the case of a pipeline with 6D fault movement and a 45° faulting angle (**Fig. 4.11p**). Moreover, a relationship is observed between N and δ . Wherein by increasing fault movement (δ) in each fault angle from 1D to 6D, the axial force response of pipeline increases by a factor of six.

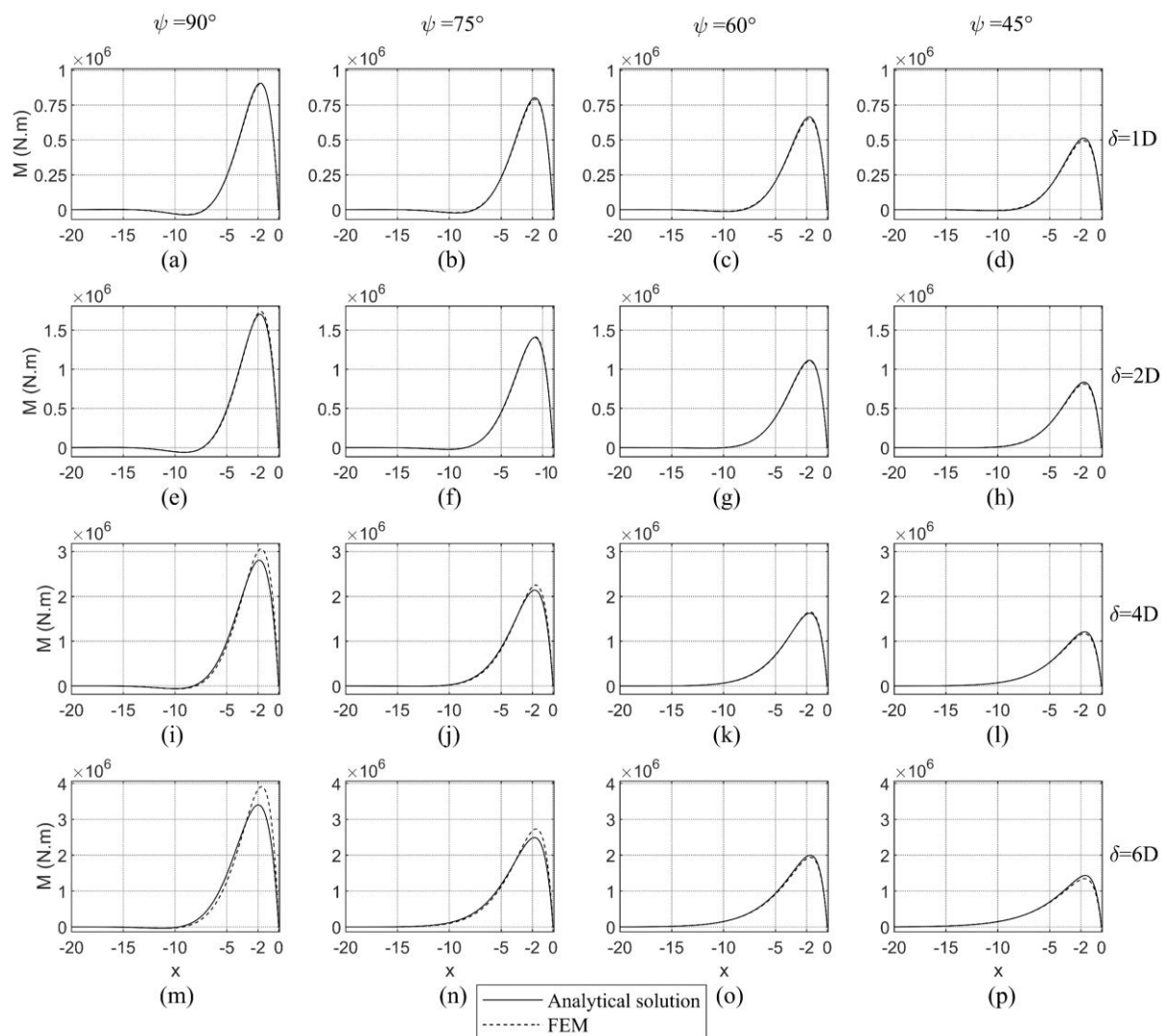


Fig. 4.12. Bending moment response of buried pipeline subjected to strike-slip fault movement (analytical versus FEM results) [1].

The bending moment response obtained from the analytical methodology is also highly

verified by the FE results, especially in cases with fault displacement up to 2D with any faulting angles and in cases with 4D and 6D fault movement with 60° and 45° faulting angles. Only in the case of 6D fault movement and a 90° faulting angle does the difference of maximum bending moment obtained between the two methods exceed 9%, reaching 16%.

Increased faulting angle and fault movement are associated with a substantial increase in pipeline bending moment. The case of 6D fault movement and a 90° faulting angle produces the highest bending moment (**Fig. 4.12m**).

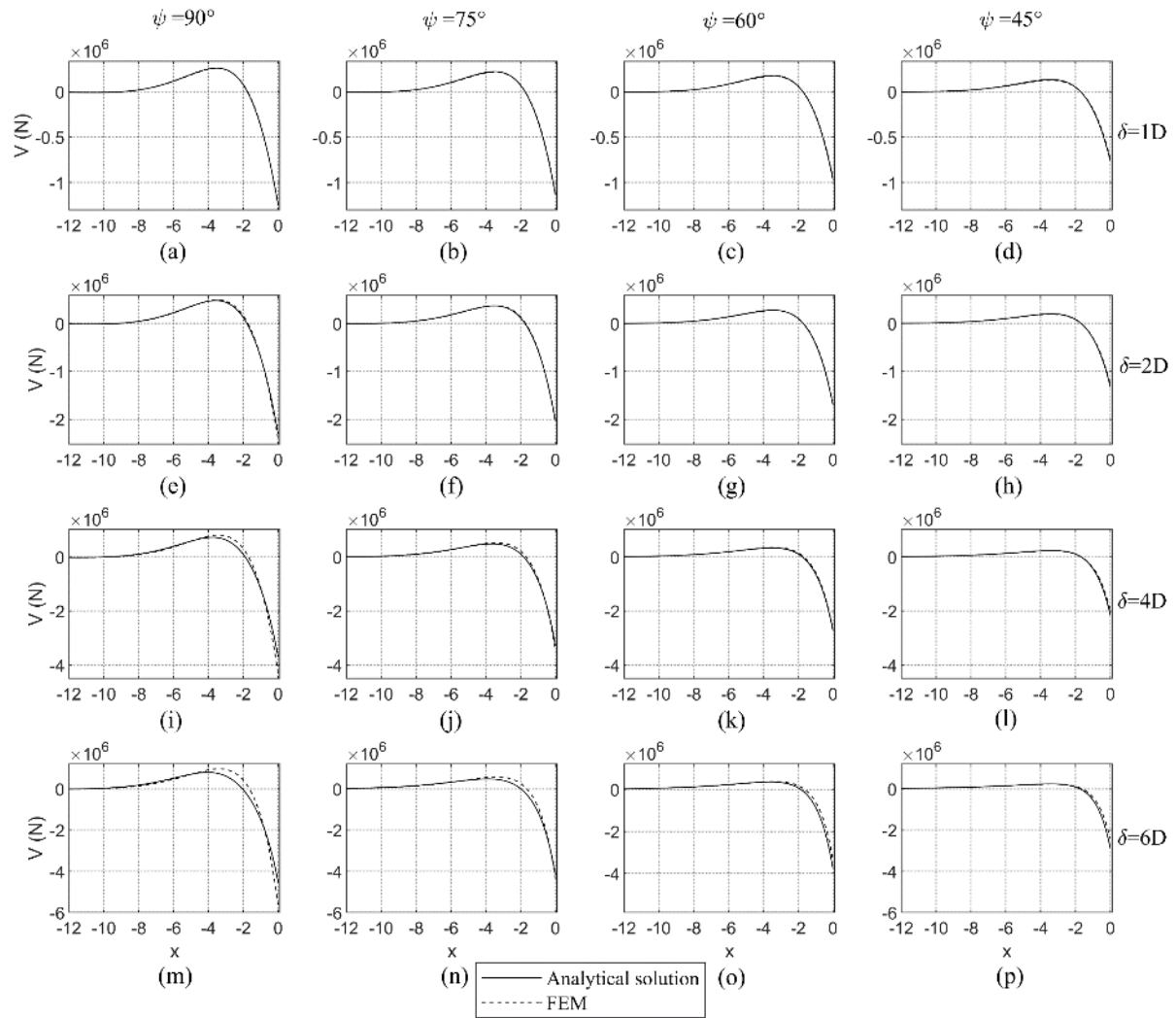


Fig. 4.13. Shear force response of buried pipeline subjected to strike-slip fault movement (analytical versus FEM results) [1].

Shear forces generated by the proposed analytical methodology have high accuracy and excellent agreement with the FE-based results (**Fig. 4.13**), especially for cases with fault displacement up to 2D and any faulting angles. A small discrepancy is observed between the analytical and FEM-based results by increasing the fault movement and decreasing the fault angle, wherein a maximum difference of 19% is observed in the case of $\delta = 6D$ and $\psi = 90^\circ$ (**Fig. 4.13m**). Shear force has a direct relation with ψ and δ and the case of $\delta = 6D$ and $\psi = 90^\circ$ has the highest shear force response among the analysis cases.

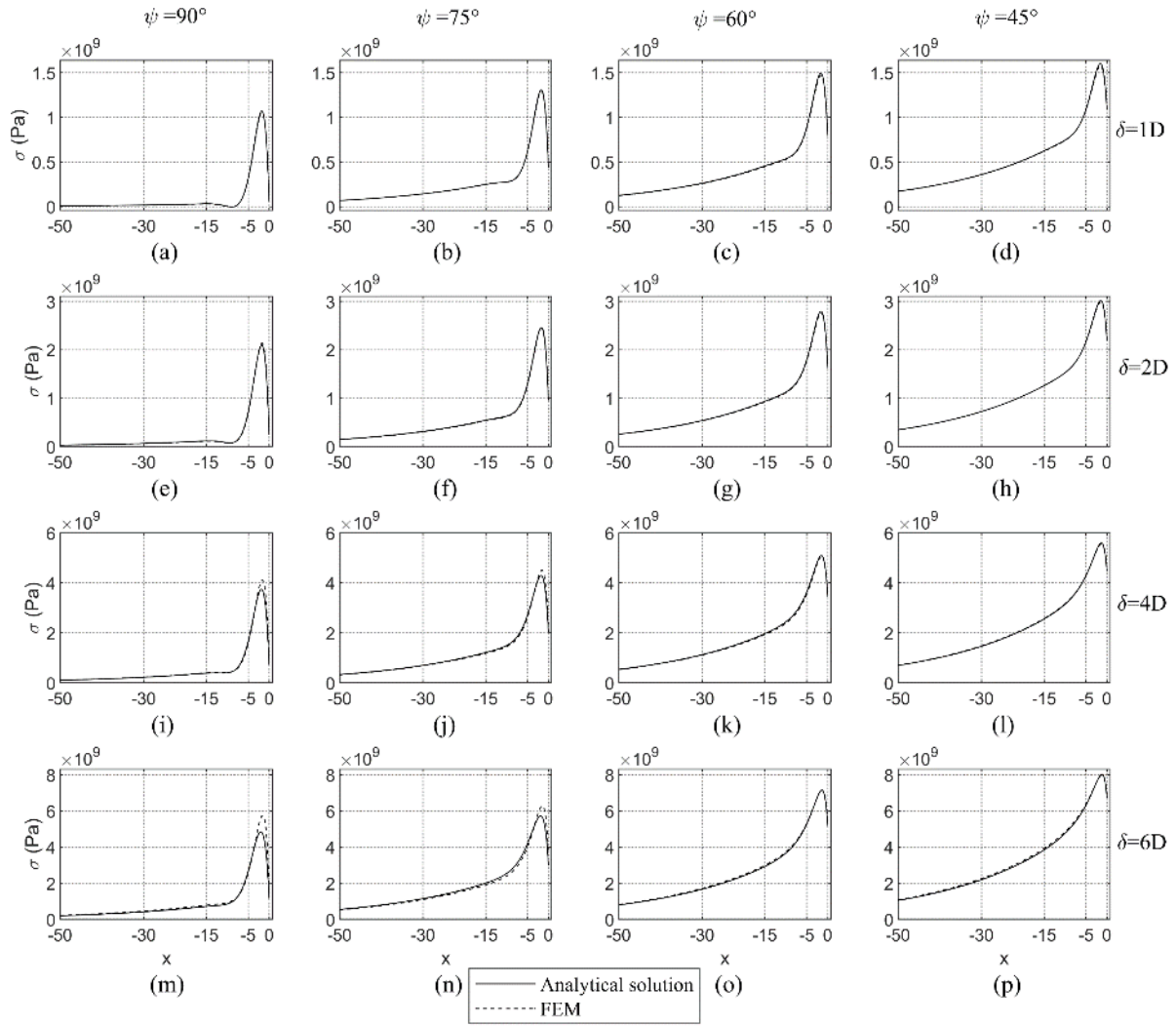


Fig. 4.14. Maximum stress (springline stress) response of buried pipeline subjected to strike-slip fault movement (analytical versus FEM results) [1].

Maximum stress (springline stress) is one of the most important engineering responses of buried pipeline in structural analysis. The stress field results of the proposed analytical methodology are highly validated with respect to the FEM-based analysis results.

Referring to **Fig. 4.14**, the maximum stress response occurs in cases with fault dislocations up to 2D and any faulting angles and in cases with 4D and 6D fault dislocation and 60° and 45° faulting angles are meticulously covered by the FEM-based analysis results. Only in the case of 6D fault movement with 90° faulting angle does the difference between analytical and FEM-derived maximum bending moment exceed 9%, reaching up to 14% (**Fig. 4.14**). Because the bending moment at the pipeline-fault crossing point is zero, the maximum stress at the intersecting point is equal to the maximum axial stress of the pipeline. The maximum stress response is generated by a combination of the maximum bending stress and axial stress. The maximum bending stress predominates at higher faulting angles and the maximum axial stress predominates at lower faulting angles. The maximum stress response of the buried pipeline is directly related to δ and reversely related to ψ with a maximum occurring in the case with $\delta =$

$6D$ and $\psi = 45^\circ$ (**Fig. 4.14p**) and minimum occurring in the case with $\delta = 1D$ and $\psi = 90^\circ$ (**Fig. 4.14a**). Because of the linearity of the materials the strain results were exactly same as stress results in shape and ratio, thus neglected to be shown.

In **Figs. 4.10–4.14**, there is a small discrepancy observed between the proposed analytical solution and FEM analysis results for cases with faulting angles close to $\psi = 90^\circ$ and $\delta \geq 4D$. This is because of very large deflection in a short distance, which occurs owing to the removal of higher-order differentials of deflection in the governing equation. However, the results accuracy is sufficient for problems related to pipelines crossing strike-slip faults. Linear assumption of soil-pipe interaction is another limitation of this study, Which authors hope future researches could apply the nonlinearity of the axial and transverse soil-pipe interaction in the governing equation. Additionally, because of the complexity, the buckling and ovalization phenomenon is not included in this study. However, the FE-based beam-spring models also can not consider the buckling and ovalization phenomenon.

The stress response obtained from the proposed analytical method in comparison with the FE analysis has the highest accuracy among other outputs which is the most important output in structural design. The analytical methodology is therefore deemed a reliable method for verification of FEM-based analysis with linear materials and preliminary design of a buried pipeline subjected to strike-slip fault movement.

4.6. Conclusions

An improved analytical method has been established for analyzing buried pipeline with linear material subjected to active strike-slip faults. This theory is a substantial development based on the theory of beam-on-elastic-foundation by applying axial force terms with further improvements to the existing analytical approaches [3–6], [16–20] and includes:

1. The axial soil-pipe interaction and axial force terms of the pipeline are applied inside the governing equation. Axial forces are calculated by the governing equation with no need for external calculations, which increases the analysis accuracy.
2. The geometrical nonlinearity term for calculation of the large deformation effects is calculated and applied inside the governing equation.
3. The new governing equation and improved calculation procedure are advantageous because it decreases the number of assumptions made in previous studies.
4. All the analytical method results up to 2D fault movement with any faulting angle are meticulously same with FEM-based analysis results.
5. The introduced analytical methodology has extended the application area of analytical solutions by the reproduction of higher accuracy in results even for large fault

movements. (only 0.4% to 16% differences have been observed in pipeline maximum stress in comparison with numerical analysis results in large fault deformation of $6D$ and angles of 45° to 90° , respectively).

To validate the results of the proposed analytical method, we compare values with those obtained using FEM with different faulting angles and fault displacement ranges. Results obtained from the analytical methods are found to be in very good agreement with the numerical results in both qualitative and quantitative aspects for various loading cases. In summary, the proposed analytical methodology is a reliable approach for verifying FEM-based analysis with linear materials for the problem of a buried pipeline subjected to the strike-slip fault movement.

References

- [1] Talebi, F. Kiyono, J. [2020] “Introduction of the axial force terms to governing equation for buried pipeline subjected to strike-slip fault movements” *Soil Dyn Earthq Eng* ;133:106125. <https://doi.org/10.1016/j.soildyn.2020.106125>
- [2] American Lifelines Alliance—ASCE. Guidelines for the Design of Buried Steel Pipe” July 2001 (with addenda through February 2005).
- [3] Karamitros, D., Bouckovalas, G., Kouretzis, G. [2007] “Stress analysis of buried steel pipelines at strike-slip fault crossings,” *Soil Dynamics and Earthquake Engineering* 27, 200–11.
- [4] Trifonov, O. V., Cherniy, V. P. [2010] “A semi-analytical approach to a nonlinear stress–strain analysis of buried steel pipelines crossing active faults,” *Soil Dynamics and Earthquake Engineering* 30(11), 1298–308.
- [5] Karamitros, D. K., Bouckovalas, G. D., Kouretzis G. P., Gkesouli V. [2011] “An analytical method for strength verification of buried steel pipelines at normal fault crossings,” *Soil Dynamics and Earthquake Engineering* (13), 1452-1464.
- [6] Trifonov, O. V., Cherniy V. P. (2012). “Elastoplastic stress-strain analysis of buried steel pipelines subjected to fault displacements with account for service loads,” *Soil Dyn Earthq Eng* 33,54–62.
- [7] Lim, M. L., Kim, M. K., Kim, T. W., Jang, J. W. (2001). “The behavior analysis of buried pipeline considering longitudinal permanent ground deformation,” In *pipeline 2001: advances in pipelines engineering & construction* (San Diego, California), vol. 3, 107. ASCE. [https://doi.org/10.1061/40574\(2001\)3](https://doi.org/10.1061/40574(2001)3)
- [8] O’Rourke, M. J., Vikram, G., Abdoun, T. (2003). “Centrifuge modeling of buried pipelines,” In: *Proceedings of the Sixth U.S. conference and workshop on lifeline earthquake engineering*, August 10–13, 2003, Long Beach, CA. pp. 757–768.
- [9] Sakanoue, T., Yoshizaki, K. (2004). “A study on earthquake-resistant design for buried pipeline using lightweight backfill,” In: *Proceedings of the 13th world conference on earthquake engineering*, Vancouver, B.C., Canada, August 1-6, Paper No.2389.
- [10] Takada, S., Hassani, N., Fukuda, K. (2001). “A new proposal for simplified design of buried steel pipes crossing active faults,” *Earthq Eng Struct Dyn* ;30:1243–57.
- [11] Vazouras, P., Karamanos, S. A., Dakoulas, P. (2010). “Finite element analysis of buried steel pipelines under strike-slip fault displacement,” *Soil Dyn Earthq Eng* ;30:1361–76.
- [12] Vazouras, P., Karamanos, S. A., Dakoulas, P. (2012). “Mechanical behavior of buried steel pipes crossing active strike-slip fault,” *S, Soil Dyn Earthq Eng*;41:164–80.
- [13] Vazouras, P., Dakoulas, P., Karamanos, S. A. (2015). “Pipe–soil interaction and pipeline

- performance under strike–slip fault movements,” *Soil Dyn Earthq Eng* ;72:48–65.
- [14] Zhang, L., Zhao, X., Yan, X., Yang, X. (2016). “A new finite element model of buried steel pipelines crossing strike-slip faults considering equivalent boundary springs,” *Eng Struct*;123:30–44.
- [15] Demirci, H. E., Bhattacharya, S., Karamitros, D., Alexander, N. (2018) “Experimental and numerical modelling of buried pipelines crossing reverse faults,” *Soil Dyn Earthq Eng* ;114:198–214.
- [16] Newmark, N. M., Hall, W. J. [1975] “Pipeline design to resist large fault displacement,” *Proc. of the U.S. national conference on earthquake engineering, University of Michigan, Ann Arbor, Michigan*, 416–25.
- [17] Kennedy, R. P., Chow, A. M., Williamson, R. A. [1977] “Fault movement effects on buried oil pipeline,” *ASCE Transportation Engineering Journal* 103(5), 617–33.
- [18] ASCE Technical Council on Lifeline Earthquake Engineering [1984] “Differential ground movement effects on buried pipelines,” *Guidelines for the Seismic Design of Oil and Gas Pipeline Systems*.
- [19] Kennedy, R. P., Kincaid, R. H. [1983] “Fault crossing design for buried gas oil pipelines” *ASME, PVP conference 77*, 1–9.
- [20] Wang, L. R. L., Yeh, Y. A. [1983] “A refined seismic analysis and design of buried pipeline for fault movement,” *Earthquake Engineering and Structural Dynamics* 13(1), 75–96.
- [21] Talebi, F., Kiyono, J. [2018] “Force-displacement analysis of buried steel pipelines for strike-slip faulting” *Vietnam- Japan Symposium on Natural Disasters, Ho Chi Minh, Vietnam*: 90-94.
- [22] Talebi, F. Kiyono, J. [2018] “Evaluation of buried pipeline behavior subjected to strike-slip fault” *15th Japan Earthquake Engineering Symposium (JEES), Sendai, Japan*: 2619-2625.
- [23] ABAQUS/CAE 2017. Dassault Systems Simulia Corp, documentation of 2017 release.
- [24] Kierzenka, J. [1998] “Studies in the Numerical Solution of Ordinary Differential Equations” *Southern Methodist University, Book, Dallas, TX*.
- [25] Ascher, U., Mattheij, R., Russell, R. [1995] “Numerical Solution of Boundary Value Problems for Ordinary Differential Equations” *Society of industrial and Applied Mathematics, Book, Philadelphia, PA*, 327-357
- [26] Keller, H. B. [1992] “Numerical Methods for Two-Point Boundary-Value Problems” *Dover, Book, New York*.
- [27] Japan Gas Association. [2013] “Seismic Design Guideline for High-Pressure Gas

Pipeline” JGA, specified, 206-13 (in Japanese)

Chapter V:

Introduction of nonlinear governing equation and corresponding semi-analytical solution for buried pipelines at strike-slip faults crossing

5.1. General remarks

We have established a nonlinear governing equation and solution procedure to analyze buried pipeline at an active strike-slip fault crossing. The methodology includes exact nonlinear axial and transverse soil-pipe interaction terms in addition to geometrical nonlinearity terms within the governing equation. The assumption of partitioning the pipeline into four segments with four governing equations based on the soil yield threshold is removed, and a united governing equation is introduced. In comparison with existing methodologies, the proposed method has a significantly extended application range with improved accuracy and offers the advantage of including buried pipeline sliding, transverse soil spring plasticity, and large-deformation effects. The solution procedure is further improved by removing optimization steps and external calculations. The proposed methodology is verified against a verified finite element-based model with various fault displacements and angles. The results are in excellent quantitative and qualitative agreement with numerical results, even for cases of large fault movement [1].

5.2. Background

Recent developments in computing and finite element method (FEM) offer applicable solutions to the problem of buried pipelines at fault crossings [2]. FEM has been extensively used for a range of applications including evaluation of factors that influence pipe response under different PGD types, verification and refinement of analytical methods, and pipeline performance assessment with respect to performance criteria (e.g. local buckling, ovalization, tensile rupture) [3–16]. However, FEM-based analysis for the reproduction of valid results is needed to be verified by experiments or analytical methods.

The first analytical attempt in this area was based on a simplified analytical model by Newmark and Hall [17] that has been further extended [18,19]. However, these papers ignored the bending stiffness of the pipeline at the high-curvature zone, which results in an overestimation of the bending strain while increasing the axial forces and strains. The study of Kennedy et al. [18] was extended to strike-slip fault crossings with a simple development of pipeline bending stiffness by Wang and Yeh [20] who modeled transverse soil yielding conditions and partitioned the pipeline into four segments (two on both sides of the crossing fault, called the high-curvature zone) and two others further from the fault line and beside the high-curvature zone. The partitioning of the pipeline into four segments assumes that the soil yields over the entire high-curvature zone. However, in real cases, the yield of transverse soil springs across and beyond the high-curvature segments depends on the soil properties and fault movement amplitude. Moreover, the pipeline partitioning assumption causes each segment to be solved as a separate problem even with different equations, which increases the solution complexity and decreases the accuracy of the obtained results. Karamitros et al. [3] developed an analytical method for strike-slip faults that partitioned the pipeline into four segments for analysis based on beam-on-elastic-foundation and elastic beam theories, and the effects of axial

forces and the steel pipe material's non-linearity was calculated externally and separately. Karamitros et al. [3] solved some limitations of previous methods but some shortcomings remain, as summarized here. (1) The same assumptions and issues faced by Wang and Yeh regarding the pipeline partitioning into four segments for the nonlinearity of transverse soil-pipe interaction. (2) The axial force terms and axial soil-pipe interaction are not implemented inside the governing equation and its effect is calculated in an indirect, external, and simplified manner. It is evident that a lack of axial forces within the governing equation has important consequences on the overall pipeline results (e.g. deflection, bending moment, shear force, stress, strain). (3) The effects of steel pipe material nonlinearity is applied by updating the Young's modulus of the steel inside the governing equation. A pipeline during fault movement can yield in specific areas, however, they use the same updated Young's modulus for all of the pipeline elongation even in sections that do not yield. In real cases, the Young's modulus changes only in the yielded sections and may differ in different sections depending on their yield ratio. (4) The calculation of bending strain is unclear. Trifonov and Cherniy [4] extended the Karamitros et al. [3] model to normal fault crossings, removed the symmetry conditions about the intersection point, and contributed transverse displacements for estimating a pipeline's axial elongation. The axial force was included in the governing differential equations only at the high-curvature zone, and geometrically induced second-order effects were taken into account. Although the study by Trifonov and Cherniy [4] presents progress for semi-analytical pipeline models, some shortcomings also remain. (1) The axial force and geometrical nonlinearity in the governing differential equation is only conducted in the two high-curvature segments, and axial forces are assumed to be zero in the two further segments. In real cases, the axial force exists not only at the high-curvature zone but also along the pipeline elongation, which exponentially attenuates several hundred meters beyond the fault line. This assumption can drastically affect all of the pipeline results (e.g. deflection, stress, strain distributions). (2) The axial force term and geometrical nonlinearity within the governing equation at the high-curvature zone is implemented as a constant and calculated externally from another approximate solution for the entire pipeline at the high-curvature segment. In reality, the axial force of the pipeline is from friction and geometrical nonlinearity effects and is not constant, even in yielded soil. It undergoes a maximum at the crossing point with the fault line and, in most cases, does not attenuate even up to hundreds of meters beyond the fault line along either side of the pipeline. (3) The model includes shortcoming nos. 1, 2, and 3 from Karamitros et al. [3] regarding the partitioning of the pipeline into four segments and steel pipe material nonlinearity problems. These simplification assumptions introduce errors to the obtained results. Additionally, the developed solution by Trifonov et al. entails a complex system of equations, which can only be solved using optimization techniques among experts. In 2011, Karamitros et al. [5] extended their previous study to normal-slip fault crossings, which was not as complicated as that of Trifonov and Cherniy [4]. However, this solution had the same shortcomings as the results obtained in Karamitros et al. [3]. In 2012, Trifonov and Cherniy [6] presented an analytical model for the stress-strain analysis of buried steel pipelines that cross

active faults by considering the effects of operational loads (internal pressure and temperature variation) on the basis of plane strain plasticity theory. However, their study had the same shortcomings as those of Trifonov and Cherniy [4] with regards to the governing differential equation of the buried pipeline. In 2020, Talebi and Kiyono [21] (previous chapter) removed most of the previous simplification assumptions and introduced a new governing equation that includes axial force, axial soil-pipe interaction, and geometrical nonlinearity effects within the governing equation, which substantially increased the accuracy of the analytical solution for linear analysis. However, axial and transverse soil-pipe interaction nonlinearity and pipe material nonlinearity were not considered within the governing equation and the calculation of the axial force term presented some complexities.

Despite substantial advances made by previous studies in the development of analytical solutions, the nonlinearity of soil-pipe interaction has not yet been introduced within the governing equation. In previous studies, the transverse soil-pipe interaction nonlinearity was assumed by partitioning the pipeline into four segments, which does not reproduce real pipeline behavior and presents several issues. Moreover, none of the previous studies designed the axial soil-pipe interaction nonlinearity to include pipeline sliding and its effects on the geometrical nonlinearity terms inside the analytical solutions. An inappropriate definition of soil-pipe interaction in the analytical solutions can lead to an unrealistic and uneconomical design and even disaster during future earthquakes. The development of a comprehensive analytical solution that incorporates exact nonlinear axial and transverse soil-pipe interaction terms within a united governing equation is therefore urgently required.

In this study, we first derived the analytical terms of nonlinear axial soil-pipe interaction and the frictional axial force by closed-form solutions in the case of a pipeline at a 0° strike-slip fault crossing. Second, we derived and implemented the axial force made by geometrical nonlinearity effects of the pipeline under large deformation. Third, we derived the pipeline sliding length and on its basis, calculated the pipeline axial force from axial force made by soil-pipe interaction (frictional) and axial force made by geometrical nonlinearity effects. Fourth, we developed a united comprehensive governing equation for the entire pipeline elongation based on the beam-on-elastoplastic-foundation case and introduced the elastoplastic transverse soil pipe-interaction springs within the comprehensive governing differential equation. Fifth, we improved the solution procedure for the governing equation including the axial force calculation. Sixth, we verified the FEM model with results from the closed-form solutions for the case of a pipeline at a 0° strike-slip fault crossing. Finally, the analytical solution results were thoroughly validated using verified FEM models (consisting of geometrical nonlinearity and soil-pipe interaction nonlinearity with elastic pipe material) for a buried pipeline at a strike-slip fault crossing with various fault angles and dislocation amplitudes [1].

5.3. Evaluation of axial force of pipeline

On the basis of the previous study [21], the axial force of the pipeline is made of (1) frictional axial soil-pipe interaction and (2) geometrical nonlinearity effects (membrane force) owing to

large deflections at the pipeline high-curvature zone. The horizontal projection of the buried pipeline axial force on the x -axis (H) is then derived according to:

$$H = H_s + H_m \quad (5.1)$$

where H_s is horizontal projection of frictional axial force and H_m is the horizontal projection of the pipeline membrane force.

5.3.1. Frictional axial soil-pipe interaction

Previous studies have shown that axial soil-pipe interaction is related to the axial component of fault displacement and not largely affected by the transverse component of fault displacement [22, 23]:

$$\delta_x = \delta \cdot \cos\psi \quad (5.2)$$

$$\delta_y = \delta \cdot \sin\psi \quad (5.3)$$

where δ_x and δ_y are the horizontal and transverse components of the fault displacement (δ), respectively (**Fig. 5.1**), and ψ is the faulting angle.

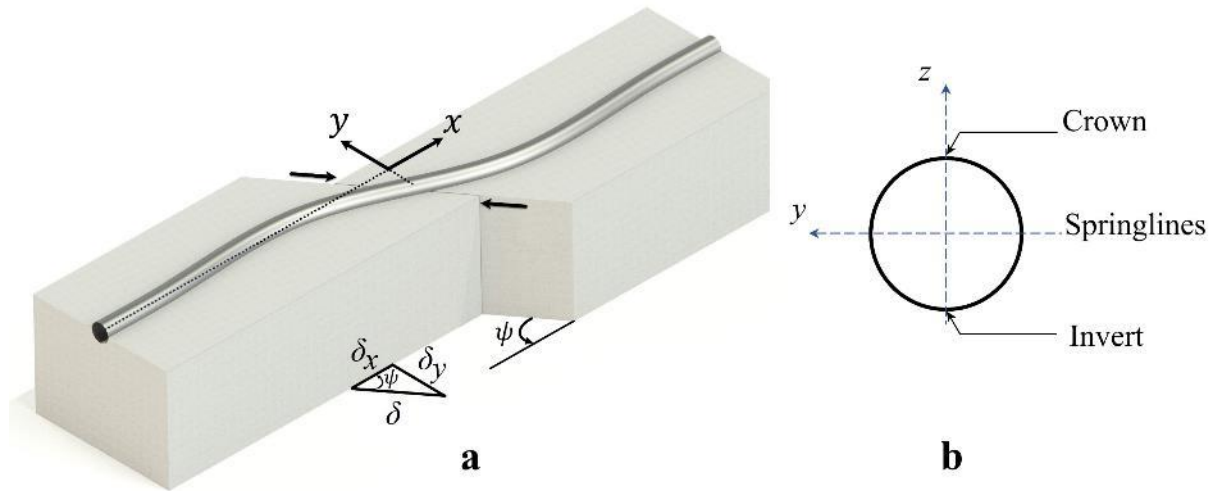


Fig. 5.1. Buried pipeline subjected to a strike-slip fault with faulting angle of (ψ). (a) 3D view [21]. (b) pipe section.

Because δ_y does not substantially affect the frictional axial soil-pipe interaction, the model of a buried pipeline subjected to a 0° strike-slip fault is analytically modeled as shown in **Fig. 5.2** to evaluate the axial soil-pipe interaction.

As shown in **Fig. 5.2b**, the pipeline slides around the fault line and rest does not. L_s is the slid pipe length and L_n is the non-slid pipe length, the latter of which is essentially infinite. The axial soil-pipe interaction is shown schematically in **Fig. 5.3**, where h_{sy} and u_y are the yielding force and yielding displacement of the axial soil spring, respectively.

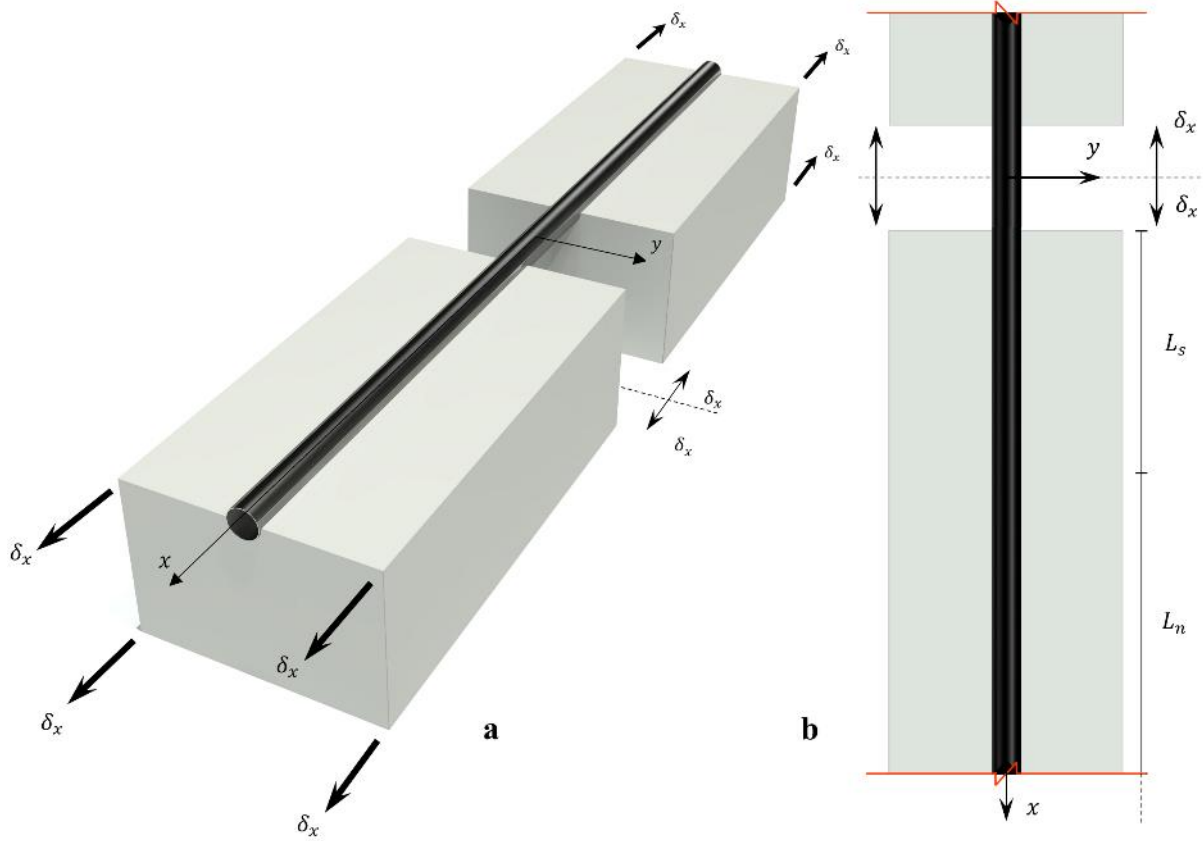


Fig. 5.2. Buried pipeline subjected to a strike-slip fault with $\psi = 0^\circ$: (a) 3D section view, (b) vertical section view.

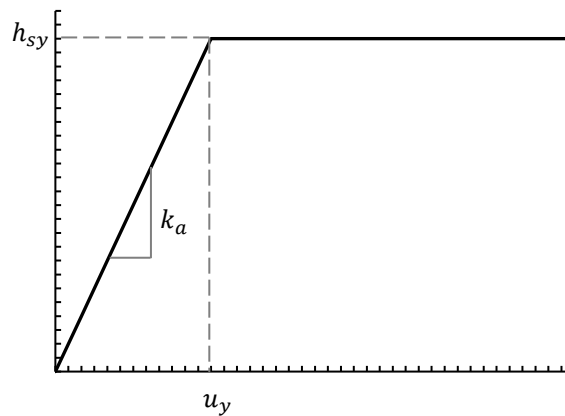


Fig. 5.3. Axial soil-pipe interaction's (axial soil spring) force-displacement curve.

5.3.1.1. Linear behavior (non-sliding)

Fig. 5.2b illustrates a segment of a buried pipeline subjected to a 0° strike-slip fault. The governing equation for one side of the fault line with no sliding behavior is derived as:

$$\frac{d^2u}{dx^2} - \lambda^2 u = 0 \quad (5.4)$$

where

$$\lambda = \sqrt{\frac{k_a}{EA}} \quad (5.5)$$

By imposing boundary conditions of $u = 0$ at $x \rightarrow \infty$ and $u = \delta_x$ at $x = 0$, Eq. (5.4) yields:

$$u = \delta_x e^{-\lambda x} \quad (5.6)$$

where u is axial soil spring displacement. From the axial displacement of the pipeline from Eq. (5.6), the axial force of the soil spring (h_s) is derived as:

$$h_s(x) = k_a \delta_x e^{-\lambda x} \quad (5.7)$$

According to Eq. (5.7) for cases where sliding starts at $x = 0$ (non-sliding case) the frictional axial force of the pipeline is given by:

$$H_s(x) = \frac{k_a \delta_x}{\lambda} e^{-\lambda x} \quad (5.8)$$

5.3.1.2. Nonlinear behavior (sliding interface)

When the fault horizontal movement is larger than the yield displacement of the axial soil-pipe interaction springs, the buried pipeline slides within the soil. This sliding occurs in a pipeline segment with a length of L_s and rest of the pipe remains under non-sliding conditions. The pipe is then divided into two segments, the segment with $x < L_s$ (sliding segment) and the rest with $x > L_s$ (non-sliding segment).

(A). Calculation of the slid segment length (L_s)

A free body diagram of the slid segment of the pipe is illustrated in **Fig. 5.4**, where H_s is the axial force of pipeline and H_{sy} is the axial force at $x = L_s$ (where soil starts to yield).

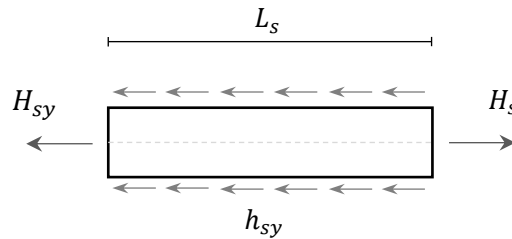


Fig. 5.4. Free body diagram of the slid segment of the pipeline.

According to Eq. (5.8) at fault intersection:

$$H_s = \frac{h_{sy}}{\lambda} \quad (5.9)$$

where h_{sy} is the yielding axial force of axial soil spring:

$$h_{sy} = k_a u_y \quad (5.10)$$

From the horizontal rigid body equilibrium for **Fig. 5.4**, the axial force of the pipe for slid segment is:

$$H_s(x) = \frac{h_{sy}}{\lambda} + h_{sy}(L_s - x) \quad (5.11)$$

Because the axial strain of the pipe is:

$$\varepsilon_a = \frac{H_s(x)}{EA} \quad (5.12)$$

Then elongation of the pipe inside the slid segment (yielded soil segment) is derived as:

$$\Delta L_p = \frac{h_{sy}}{EA} \left(\frac{L_s}{\lambda} + \frac{L_s^2}{2} \right) \quad (5.13)$$

Because displacement of the soil springs at $x = L_s$ is u_y and displacements of the soil springs and pipe are equal,

$$\Delta L_p = \delta_x - u_y \quad (5.14)$$

According to Eqs. (5.13) and (5.14), the slid length of pipeline is derived as:

$$L_s = \frac{1}{\lambda} \left(\sqrt{\frac{2\delta_x - u_y}{u_y}} - 1 \right) \quad (5.15)$$

(B). Non-slid segment $x > L_s$

For the non-sliding segment of the slid pipeline, based on Eqs. (5.6–5.8) the pipe axial displacement, axial soil springs force, and axial force of pipeline are derived as:

$$u(x) = u e^{-\lambda(x-L_s)} \quad (5.16)$$

$$h_s(x) = k_a u_y e^{-\lambda(x-L_s)} \quad (5.17)$$

$$H_s(x) = \frac{k_a u_y}{\lambda} e^{-\lambda(x-L_s)} \quad (5.18)$$

(C). Slid segment $x < L_s$

At the slid segment ($x < L_s$), all of the axial soil springs have yielded. Accounting for the equilibrium of the pipe element leads to:

$$\frac{d^2 u}{dx^2} - \lambda^2 u_y = 0 \quad (5.19)$$

Using boundary conditions of $u = u_y$ for $x = L_s$ and $u = \delta_x$ for $x = 0$, Eq. (5.4), and L_s

from Eq. (5.15), the axial displacement of pipeline and soil are derived as:

$$u(x) = \frac{\lambda u_y}{2EA} x^2 + \left(\frac{2(u_y - \delta_x) - \lambda^2 u_y L_s^2}{2L_s} \right) x + \delta_x \quad (5.20)$$

According to Eq. (5.20), it can be shown that the axial force of the pipeline at the slid segment is:

$$H_s(x) = k_a u_y (L_s - x) + \frac{k_a u_y}{\lambda} \quad (5.21)$$

(D). *Nonlinear fractional behavior of pipeline*

Based on the pipeline nonlinear frictional behavior in the previous sections and $w_x(x) = u(x)$, the axial displacement of the pipeline and soil springs are:

$$\begin{cases} u(x) = \frac{\lambda^2 u_y}{2} x^2 + \left(\frac{2(u_y - \delta_x) - \lambda^2 u_y L_s^2}{2L_s} \right) x + \delta_x & x \leq L_s, L_s > 0 \\ u(x) = u_y e^{-\lambda(x-L_s)} & x > L_s, L_s > 0 \\ u(x) = u_y e^{-\lambda x} & L_s = 0 \end{cases} \quad (5.22)$$

The axial force of the soil springs is:

$$\begin{cases} h_s(x) = k_a u_y & x < L_s \\ h_s(x) = k_a u_y e^{-\lambda(x-L_s)} & x > L_s \\ h_s(x) = k_a \delta_x e^{-\lambda x} & L_s = 0 \end{cases} \quad (5.23)$$

And, the axial frictional force of pipeline is derived as:

$$\begin{cases} H_s(x) = k_a u_y (L_s - x) + \frac{k_a u_y}{\lambda} & x \leq L_s, L_s > 0 \\ H_s(x) = \frac{k_a u_y}{\lambda} e^{-\lambda(x-L_s)} & x > L_s, L_s > 0 \\ H_s(x) = \frac{\delta_x u_y}{\lambda} e^{-\lambda x} & L_s = 0 \end{cases} \quad (5.24)$$

5.3.2. *Axial force owing to geometrical nonlinearity (membrane force)*

In the problem of a buried pipeline at a fault crossing (**Fig. 5.1**), a tensile axial force appears in the pipe cross-section owing to extensive deflection of the pipeline in the high-curvature zone around the fault-pipe crossing. The axial strain of the pipeline owing to this large deflection (membrane strain) at point x is derived as:

$$\varepsilon_m(x) = \sqrt{1 + \left(\frac{\partial w}{\partial x} \right)^2} - 1 \quad (5.25)$$

where w is the deflection in the y -direction of the pipeline.

The calculation of the membrane force is improved in comparison with the previous study [21] and applied to the entire pipeline length. Following Eq. (5.25), the pipeline membrane force at the fault-pipe crossing ($x = 0$) is:

$$H_{mMax} = \frac{2EA}{L_N} \int_0^{\infty} \left(\sqrt{1 + \varphi^2(0)} - 1 \right) dx \quad (5.26)$$

where L_N is the length that the axial force of the pipeline attenuates and φ is pipeline rotation:

$$\varphi(x) = \frac{\partial w}{\partial x} \quad (5.27)$$

The horizontal projection of the pipeline membrane force on the x -axis is:

$$H_m(x) = \begin{cases} H_{mMax} \cdot \cos\varphi & x \leq L_s \\ H_{mMax} \cdot \cos\varphi \cdot e^{-\lambda(x-L_s)} & x > L_s \end{cases} \quad (5.28)$$

Based on Eqs. (5.1) and (5.24), in case of a pipeline with $\psi = 90^\circ$ at strike-slip fault crossing, because δ_x is zero, almost there is no frictional axial force in pipeline and the axial force of the pipeline is caused only by membrane forces owing to deflection. In this case ($\psi = 90^\circ$), the calculation of L_s must be based on the membrane force. Based on Eqs. (5.15) and (5.24), in general, the sliding length is derived as:

$$\begin{cases} L_s = \frac{1}{\lambda} \left(\sqrt{\frac{2\delta_x - u_y}{u_y}} - 1 \right) & \delta_x > u_y, \psi \neq 90^\circ \\ L_s = 0 & \delta_x < u_y, \psi \neq 90^\circ \\ L_s = \frac{H_{mMax} \cdot \cos\varphi(0)}{k_a u_y} & \psi = 90^\circ \end{cases} \quad (5.29)$$

Based on Eqs. (5.1), (5.24), and (5.28) the projection of the total pipeline axial force onto the x -axis (H) is derived as:

$$\begin{cases} H(x) = k_a u_y (L_s - x) + \frac{k_a u_y}{\lambda} + H_{mMax} \cdot \cos\varphi & x \leq L_s, L_s > 0 \\ H(x) = \frac{k_a u_y}{\lambda} e^{-\lambda(x-L_s)} + H_{mMax} \cdot \cos\varphi \cdot e^{-\lambda(x-L_s)} & x > L_s, L_s > 0 \\ H(x) = \frac{\delta_x u_y}{\lambda} e^{-\lambda x} + H_{mMax} \cdot \cos\varphi \cdot e^{-\lambda x} & L_s = 0 \end{cases} \quad (5.30)$$

5.4. Transverse soil-pipe interaction nonlinearity

As described in the introduction, previous studies introduced the transverse spring yield by partitioning of the pipeline into four segments, which this simplification assumption presents several problems. Moreover, for simplicity, the transverse soil-pipe interaction springs behavior in the design codes and previous studies were introduced as elastic perfectly plastic [2–6]. However, these springs have elastoplastic behavior [24]. In this study, the nonlinearity

of the springs is introduced as a bilinear elastoplastic spring (**Fig. 5.5**).

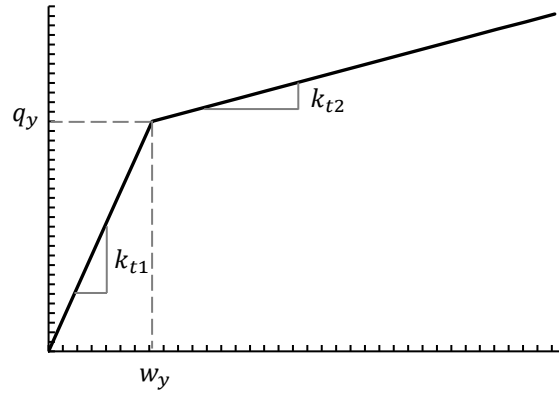


Fig. 5.5. Transverse elastoplastic soil pipe-interaction curve

To implement the nonlinearity of the transverse soil-pipe interaction springs in the governing equation, we extend the theory of beam-on-elastic-foundation to the theory of beam-on-elastoplastic-foundation. The reaction forces of the transverse soil springs are introduced as:

$$q(x) = \begin{cases} k_{t1}w & w \leq w_y \\ k_{t2}w + (k_{t1} - k_{t2})w_y & w > w_y \end{cases} \quad (5.31)$$

where k_{t1} is transverse soil spring elastic stiffness and k_{t2} is transverse soil spring plastic stiffness.

5.5. Pipeline model

The proposed methodology solves the problem of a buried pipeline crossing a strike-slip fault including the geometrical nonlinearity effects with nonlinear elastic perfectly plastic axial soil springs and elastoplastic transverse soil-pipe interaction springs. In this analytical method, the axial and transverse soil-pipe interactions and geometrical nonlinearity terms are properly implemented in the comprehensive governing equation. Moreover, the optimization steps in the previous study [21], including development of the membrane force calculation, are removed and the solution procedure is more simplified.

5.5.1. Solution algorithm

As illustrated in **Fig. 5.6**, a buried pipeline subjected to strike-slip fault movement is a symmetric problem. For sake of simplicity, only pipeline on the left side of the fault-line (segment OC) is evaluated in the analytical model and the results can be extended to the other side. The solution of the analytical model is presented in four steps:

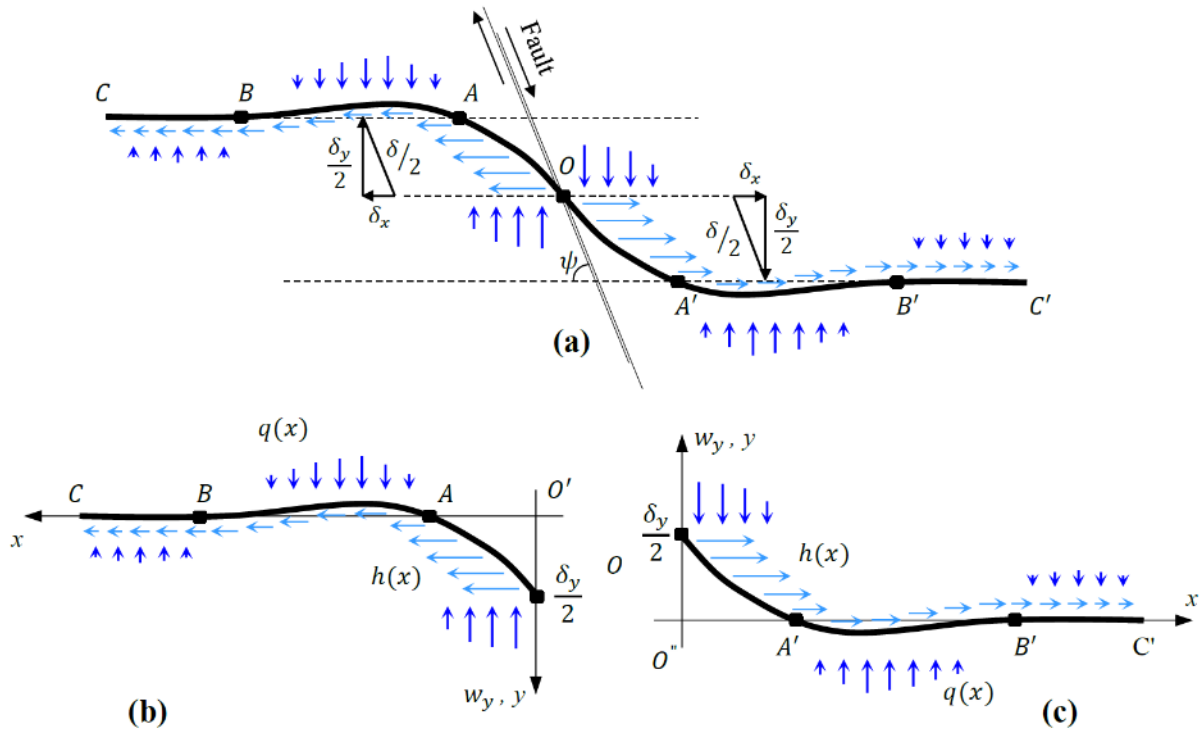


Fig. 5.6. Coordinate system and pipeline partitioning for the analytical solution.

5.5.1.1. Step 1

The bending moment of the pipeline is:

$$M = -EI \frac{\partial^2 y}{\partial x^2} \quad (5.32)$$

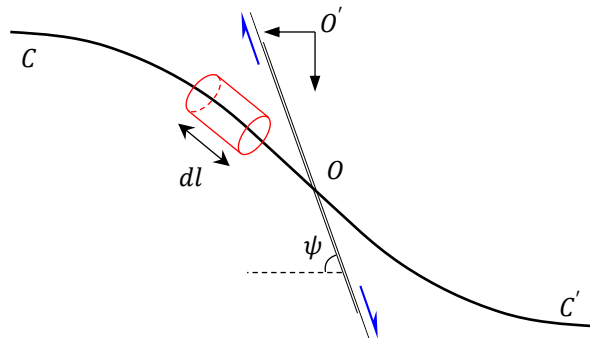


Fig. 5.7. Deformed pipeline element subjected to strike-slip fault movement.

Based on the derived nonlinear axial forces of the buried pipeline from section 2 (Eq. (5.30)), nonlinear transverse reaction forces from section 3 (Eq. (5.31)), Eq. (5.32), the coordinate system for segment OC (**Fig. 5.6**), and equilibrium for a given pipe element (**Fig. 5.7**), the comprehensive governing differential equilibrium equation for OC segment is:

$$EI \frac{\partial^4 w}{\partial x^4} - \left[\begin{array}{l} \left(k_a u_y (L_s - x) + \frac{k_a u_y}{\lambda} + H_{mMax} \cdot \cos\varphi \right. \\ \left. \frac{k_a u_y}{\lambda} e^{-\lambda(x-L_s)} + H_{mMax} \cdot \cos\varphi \cdot e^{-\lambda(x-L_s)} \right. \\ \left. \frac{\delta_x u_y}{\lambda} e^{-\lambda x} + H_{mMax} \cdot \cos\varphi \cdot e^{-\lambda x} \right. \\ \left. L_s = 0 \right] \frac{\partial^2 w}{\partial x^2} \\ + \left(\begin{array}{l} \left(k_a u_y \right. \\ \left. k_a u_y e^{-\lambda(x-L_s)} + \lambda H_{mMax} \cdot \cos\varphi \cdot e^{-\lambda(x-L_s)} \right. \\ \left. k_a \delta_x e^{-\lambda x} + \lambda H_{mMax} \cdot \cos\varphi \cdot e^{-\lambda x} \right. \\ \left. L_s = 0 \right) \frac{dw}{dx} \\ + \frac{1}{\cos(\varphi)} \begin{cases} k_{t1} w & w \leq w_y \\ k_{t2} w + (k_{t1} - k_{t2}) w_y & w > w_y \end{cases} = 0 \end{array} \right) \quad (5.33)$$

where x is distance from point O along the pipeline axis (**Figs. 5.6** and **5.7**), E is the elastic Young's modulus of the pipeline material, w is the transverse deflection, and I is moment of inertia of the pipeline cross-section. The boundary conditions at $x = 0$ are $w \rightarrow \delta_y/2$, $\partial^2 w/\partial x^2 \rightarrow 0$, and at $x \rightarrow \infty$, they are $w \rightarrow 0$, $\partial w_y/\partial x \rightarrow 0$.

Eq. (5.33) is the comprehensive governing differential equilibrium equation for the problem of a buried pipeline subjected to strike-slip faulting. This is a boundary value problem, which is a nonlinear 4th order ordinary differential equation.

The closed-form solution of this complex governing equation is cumbersome and after some attempts, it was found that there is no analytical solution. The differential equation of Eq. (5.33) is therefore solved numerically by the collocation method and Simpson's method [25–27].

The value of H_{mMax} (based on Eq. (5.26)), which refers to geometrical nonlinearity effects, is not available in step 1, because L_N and $\varphi(x)$ are unknown in the solution initiation. Therefore, in step 1, it has assumed that $H_{mMax} = 0$ and the analysis is performed on the basis of the introduced boundary conditions. From the solution of the differential equilibrium Eq. (5.33) in step 1, the deflection of pipeline (w) is acquired for the case of no nonlinear geometrical effects, and $\varphi(x)$ and L_N are calculated from Eqs. (5.23) and (5.34). H_{mMax} is calculated for the case of step 1 by Eq. (5.26). Moreover, if $\psi = 90^\circ$, L_s is calculated from Eq. (5.29).

5.5.1.2. Step 2

Through substituting the acquired H_{mMax} (and L_s for the case $\psi = 90^\circ$) from step 1 into Eq. (5.33) and reanalyzing, a new value of H_{mMax} is calculated by the same procedure for step 2. The value of H_{mMax} calculated in step 2 includes the geometrical nonlinearity effects and can be substituted into governing Eq. (5.33).

5.5.1.3. Step 3

The calculated H_{mMax} (and L_s for the case $\psi = 90^\circ$) based on step 2 is substituted into the governing equation, and Eq. (5.33) is solved. The H_{mMax} value should be calculated for step 3

and compared with H_{mMax} determined in step 2. If they are almost same, the procedure is completed. If not, the procedure for step 3 must be repeated. In general, H_{mMax} values of all of the cases investigated here converge by this step.

5.5.1.4. Step 4

After acquiring the converged analysis and final $w(x)$, the remaining pipeline responses can be extracted on the basis of the pipeline's deflection response. The converged analysis is the final solution and the pipeline responses can be computed from the obtained $w(x)$ from the last step. The bending moment of the pipeline is as Eq. (5.32) and the axial force of the pipeline is:

$$\begin{cases} N(x) = (\cos \varphi + \varphi \sin \varphi) \cdot \left[k_a u_y (L_s - x) + \frac{k_a u_y}{\lambda} + H_{mMax} \cdot \cos \varphi \right] + EI \frac{\partial^3 w}{\partial x^3} \sin \varphi & x \leq L_s, L_s > 0 \\ N(x) = (\cos \varphi + \varphi \sin \varphi) \cdot \left[\frac{k_a u_y}{\lambda} e^{-\lambda(x-L_s)} + H_{mMax} \cdot \cos \varphi \cdot e^{-\lambda(x-L_s)} \right] + EI \frac{\partial^3 w}{\partial x^3} \sin \varphi & x > L_s, L_s > 0 \\ N(x) = (\cos \varphi + \varphi \sin \varphi) \cdot \left[\frac{k_a \delta_x}{\lambda} e^{-\lambda x} + H_{mMax} \cdot \cos \varphi \cdot e^{-\lambda x} \right] + EI \frac{\partial^3 w}{\partial x^3} \sin \varphi & L_s = 0 \end{cases} \quad (5.34)$$

The shear force of the pipeline is given by:

$$\begin{cases} V(x) = (\sin \varphi - \varphi \cos \varphi) \cdot \left[k_a u_y (L_s - x) + \frac{k_a u_y}{\lambda} + H_{mMax} \cdot \cos \varphi \right] - EI \frac{\partial^3 w}{\partial x^3} \cos \varphi & x \leq L_s, L_s > 0 \\ V(x) = (\sin \varphi - \varphi \cos \varphi) \cdot \left[\frac{k_a u_y}{\lambda} e^{-\lambda(x-L_s)} + H_{mMax} \cdot \cos \varphi \cdot e^{-\lambda(x-L_s)} \right] - EI \frac{\partial^3 w}{\partial x^3} \cos \varphi & x > L_s, L_s > 0 \\ V(x) = (\sin \varphi - \varphi \cos \varphi) \cdot \left[\frac{k_a \delta_x}{\lambda} e^{-\lambda x} + H_{mMax} \cdot \cos \varphi \cdot e^{-\lambda x} \right] - EI \frac{\partial^3 w}{\partial x^3} \cos \varphi & L_s = 0 \end{cases} \quad (5.35)$$

By obtaining all of the pipeline responses, the axial stress, axial strain on the springline and invert (**Fig. 5.1b**), bending stress, and bending strain on the pipeline springlines (**Fig. 5.1b**) are respectively given as:

$$\sigma_a(x) = \frac{N}{A} \quad (5.36)$$

$$\varepsilon_a(x) = \frac{N}{EA} \quad (5.37)$$

$$\sigma_b(x) = \frac{M \cdot (D - t)}{2I} \quad (5.38)$$

$$\varepsilon_b(x) = \frac{M \cdot (D - t)}{2EI} \quad (5.39)$$

where σ_a and ε_a are axial stress and strain of the pipeline at crown/invert, respectively, and σ_b and ε_b are the bending stress and strain of the pipeline at the springlines. The maximum and minimum (maximum tensile/compression) elastic stress and strain of the pipeline cross-section on springlines (**Fig. 5.1b**) are respectively:

$$\sigma_{sp(max/min)}(x) = \frac{N}{A} \pm \frac{M \cdot (D - t)}{2I} \quad (5.40)$$

$$\varepsilon_{sp(max/min)}(x) = \frac{\sigma_{sp(max/min)}}{E} \quad (5.41)$$

The maximum shear stress and shear strain of the pile cross-section occurs on the crown/invert points (**Fig. 5.1b**) of the pipeline, which is:

$$\tau_{max} = \frac{VQ_{max}}{It} \quad (5.42)$$

$$\gamma_{max} = \frac{\tau_{max}}{G} \quad (5.43)$$

where Q_{max} is first moment of inertia, t is pipe cross-section thickness, and I is second moment of inertia. The maximum/minimum principal stress of pipe at the crown/invert point is given as:

$$\sigma_{cr(max/min)}(x) = \frac{\sigma_a}{2} \pm \sqrt{\left(\frac{\sigma_a}{2}\right)^2 + \tau_{max}^2} \quad (5.44)$$

5.6. Finite element model description and verification

We created an FEM-based model for the problem of buried pipeline at a strike-slip fault crossing subjected to various faulting angles with nonlinear soil. FEM-based analyses were implemented in Abaqus 2017 [28]. For the analysis cases, we model a 16" steel pipeline with an external diameter of 0.4064 m, thickness of 0.0071 m without internal pressure, and a total length of 3 km. The material is SS400 steel with an elastic Young's modulus of 200 GPa and Poisson's ratio of 0.3. The pipeline is assumed to be buried under 1 m of medium-density sand with a unit weight of 1800 kg/m³ and internal frictional angle of 35°. The soil-pipe interaction springs properties are calculated on the basis of the ALA-ASCE guidelines for the design of buried pipe [2], as in **Table 5.1** and **Fig. 5.8**. In ALA-ASCE, for simplicity, the transverse horizontal soil-pipe interaction is considered elastic perfectly plastic, however, in experimental studies, its behavior is considered elastoplastic [24]. Therefore, we add k_{t2} to have an elastoplastic soil model. In this model, the pipe material is elastic and the soil-pipe interactions

Table 5.1. Soil-pipe interaction properties.

	Elastic stiffness k_1 (kN/m/m)	Plastic stiffness k_2 (kN/m/m)	Yielding force (kN/m)	Yielding displacement (mm)
Axial direction (k_a)	2662.27	0	6.66	2.50
Transverse horizontal direction (k_t)	4461.69	134	80.52	18.05
Vertical upward direction (k_{v_u})	1590.91	0	14.32	9
Vertical downward (k_{v_d})	8848.16	0	310.46	36.58

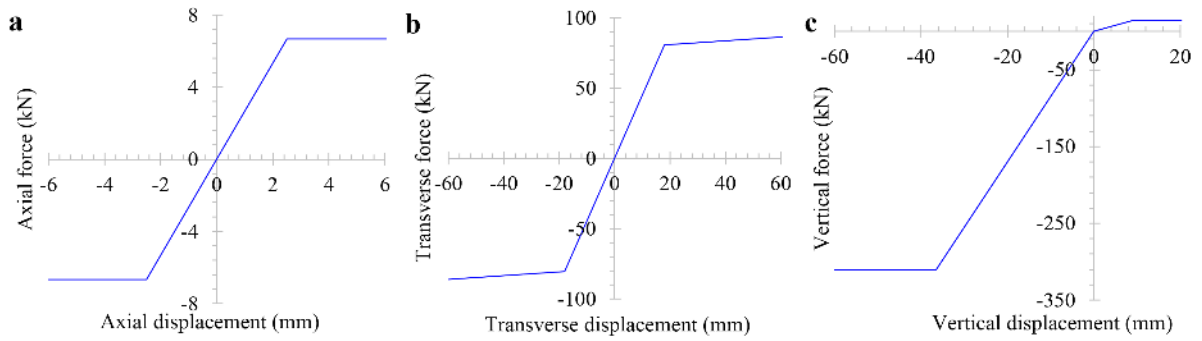


Fig. 5.8. Force-displacement curves of the soil-pipe interaction springs.

are completely nonlinear.

In the creation of an FEM-based model for modeling pipeline, we used a B32 Timoshenko beam element on the basis of shear flexible beam theory, which provides useful results for transverse shear deformation and large axial strain. The soil-pipe interaction spring elements are modeled by connector CONN3D2 elements oriented in three orthogonal directions (schematically shown in **Fig. 5.9**). Two rigid beams are then made as boundary condition input points of the RB3D2 rigid-beam element. The element size after sensitivity analysis is determined. The pipeline is gradually discretized from fine at the fault zone to slightly bigger mesh sizes at further distances (0.0125 to 1 m) symmetric to the fault line. A segment of the FE model is illustrated in **Fig. 5.10**.

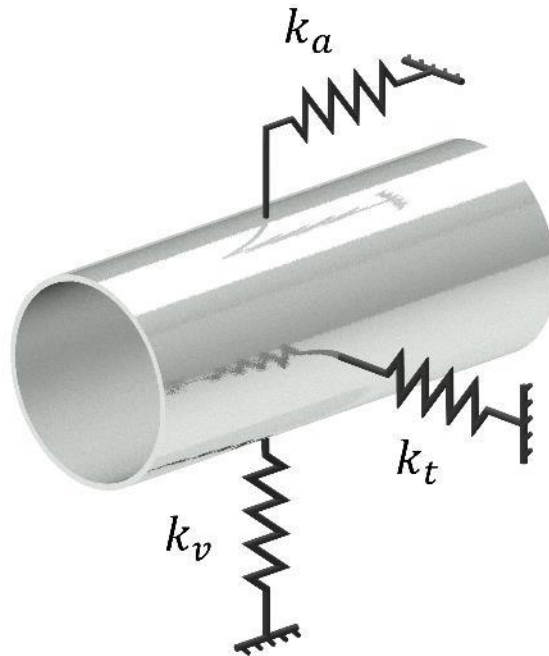


Fig. 5.9. Soil-pipe interaction spring adjustment.

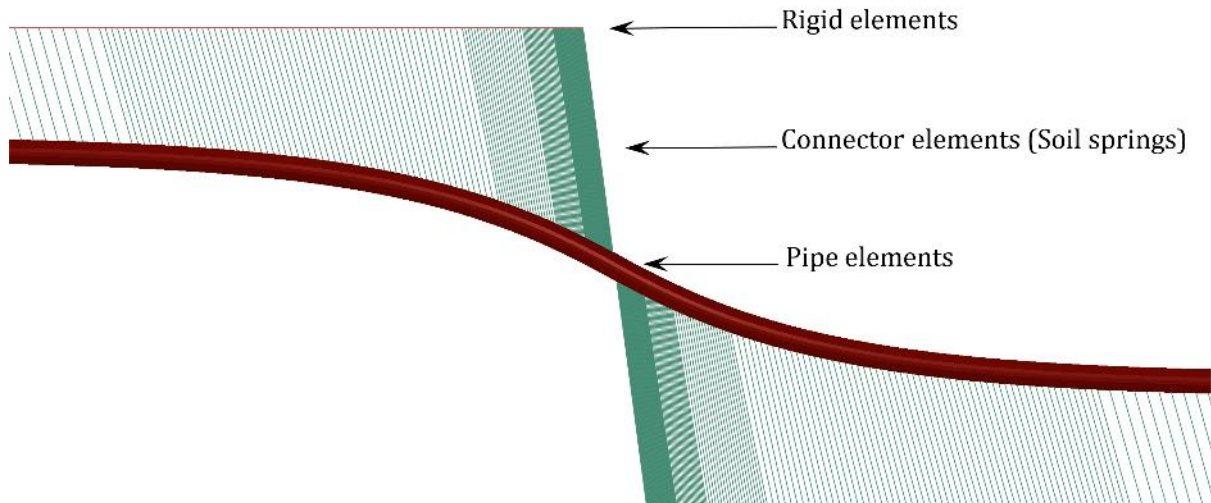


Fig. 5.10. Part of the finite element model and attached soil-pipe interaction springs.

Because the problem of a buried pipeline subjected to fault movement is a large deformation problem, we implemented the *NIgeom* option in Abaqus to have the geometric nonlinearity effects in the simulations. The boundary conditions of the fault displacement components of the analysis cases are specified to the rigid beams, which are connected to the ends of soil springs (**Fig. 5.10**).

5.6.1. Verification of the finite element model

The problem of a buried pipeline subjected to a 0° strike-slip fault movement including nonlinear soil-pipe interaction (sliding) is solved in a closed-form solution in section 2. To validate the introduced FE model in section 5, the results of this FEM for the case of ($\psi = 0^\circ$)

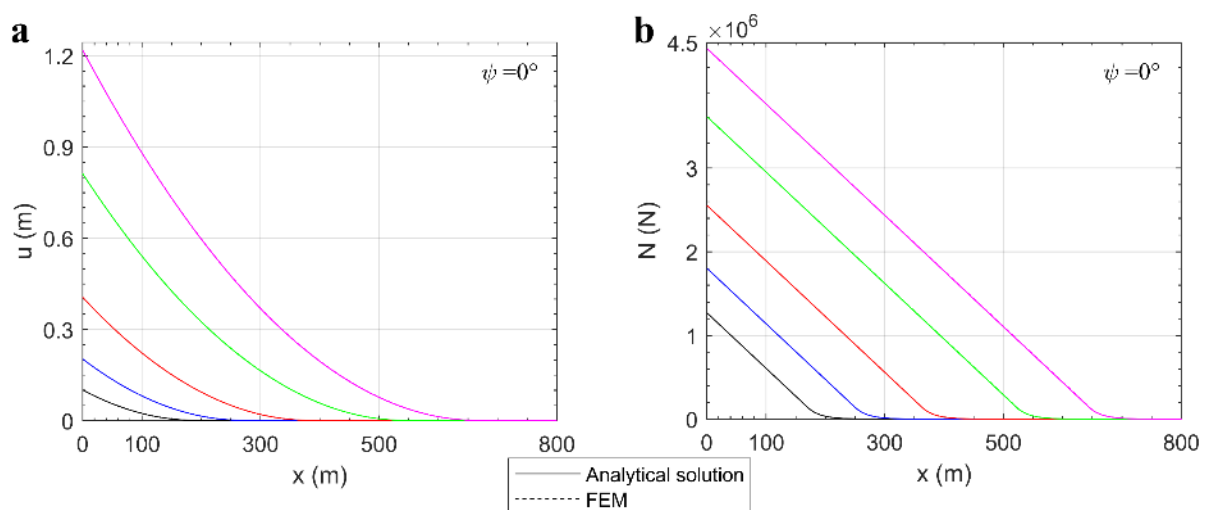


Fig. 5.11. Response of a buried pipeline at a 0° strike-slip fault crossing, FEM (dashed curves) versus closed-form solution (solid curves). Analysis cases with fault movements of $0.5D$, $1D$, $2D$, $4D$, and $6D$ are shown in black, blue, red, green, and magenta, respectively: **(a)** Axial displacement distribution of the pipeline. **(b)** Axial force distribution of the pipeline.

are compared with results of the closed-form solution.

FEM axial displacement and axial force responses of the pipeline for the case of $\psi = 0^\circ$ is compared with the closed-form Eqs. (5.22) and (5.24) for fault movements of 0.5D–6D as shown in **Fig. 5.11**, where D is the pipe external diameter. In **Fig. 5.11**, closed-form analytical solution results are plotted in solid lines and FEM results are in dashed lines. And results of the analysis cases with fault movement of 0.5D, 1D, 2D, 4D, and 6D are respectively in black, blue, red, green, and magenta lines. Owing to the symmetry of the problem, all of the responses are provided for only one side of the fault line.

Fig. 5.11 shows that results of Eqs. (5.22) and (5.24) meticulously cover the FEM model results. The FEM-based model is therefore highly verified by the closed-form analytical solution even in cases of very large fault dislocations (e.g., 4D and 6D cases).

5.7. Validation of proposed analytical methodology versus FEM

In this section, we extend the verified FEM model of the buried pipeline at a 0° strike-slip fault crossing from section 5 to other faulting angles. The results of the proposed analytical methodology from section 4 are verified against validated FEM analyses for the identical cases. Numerical and analytical results are obtained for the 16-in buried pipeline that crosses a strike-slip fault at different angles and fault displacement amplitudes, considering the typical geometric and mechanical properties presented in section 5 with a 3-km pipe length. Both the FEM models and analytical solutions include the geometrical nonlinearity effects with nonlinear elastic perfectly plastic axial soil springs and elastoplastic transverse soil-pipe interaction springs.

Figs. 5.12–5.17 illustrate the deflection, axial force, bending moment, shear force, maximum stress on the springline, and maximum stress on the crown/invert responses of the buried pipeline subjected to strike-slip fault movement. For a comprehensive evaluation of the proposed method, analyses are implemented for faulting angles of 90° to 45° and fault movement (δ) of 0.5D to 6D. The analytical results are plotted as solid lines and the FEM results are plotted as dashed lines. And results of the analysis cases with fault movement of 0.5D, 1D, 2D, 4D, and 6D are plotted respectively in black, blue, red, green, and magenta lines same as those for **Fig. 5.11**. Cases with fault movements of 4D and 6D are proposed to evaluate the analytical method results under very large deformation. Each figure is shown with four sub-figures **a** to **d** that respectively represent the results of cases with $\psi = 90^\circ$, 75° , 60° , and 45° . Owing to the symmetry of the problem, all responses in **Figs. 5.12–5.17** are provided only on one side of the fault line and the coordinate system is based on **Fig. 5.6b**.

The deflection responses of the proposed analytical method in **Fig. 5.12** are in excellent agreement with the FEM-based analysis. The FEM-based deflection results for all cases including the very large fault movement cases (4D and 6D) and all of the faulting angles are meticulously covered by the analytical results. **Fig. 5.12** shows that the deflection response attenuation length does not change substantially with faulting angle (ψ) and shows a direct

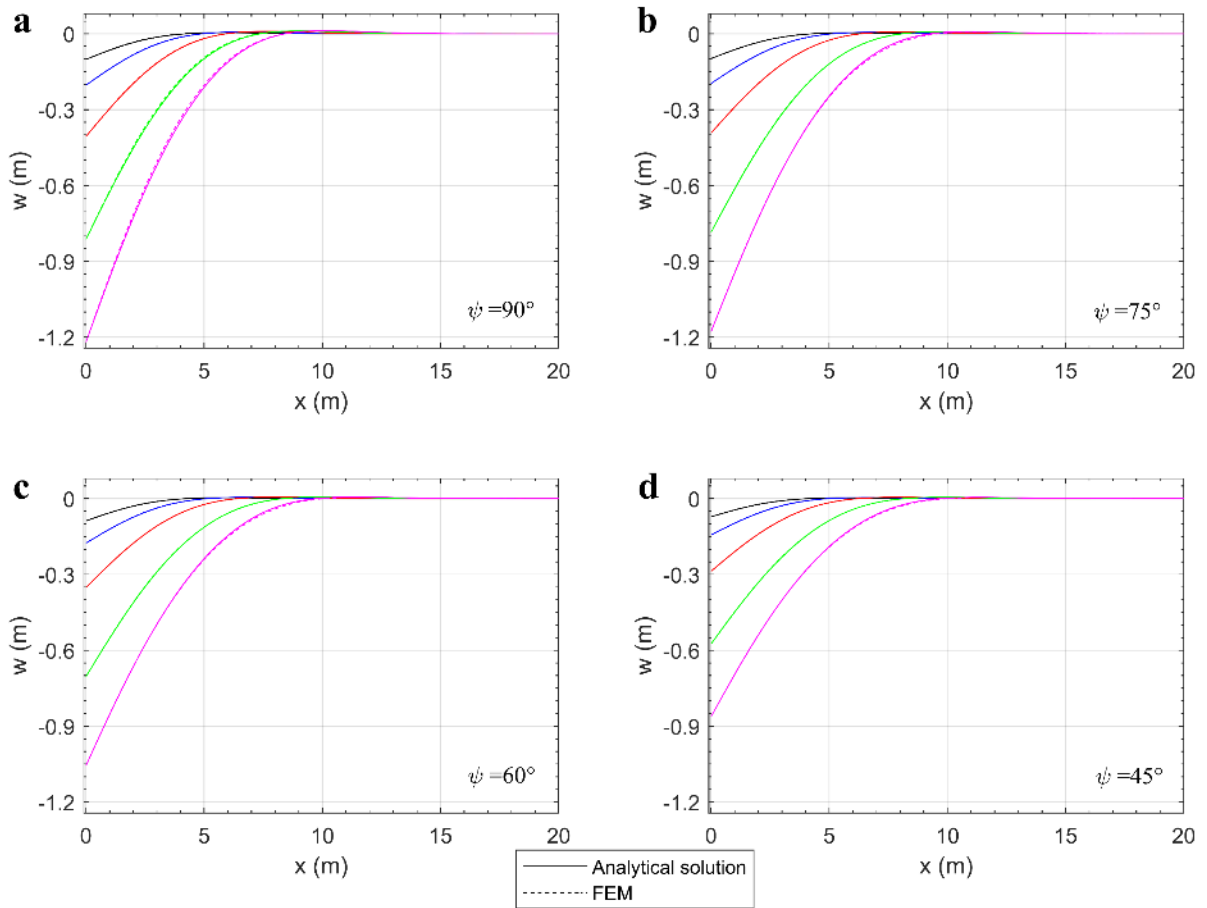


Fig. 5.12. Transverse deflection response of a buried pipeline subjected to strike-slip fault movement (analytical versus FEM results) for $\delta = 0.5D-6D$ and $\psi = 90^\circ-45^\circ$. Curve and color representations are the same as in **Fig. 5.11**.

relationship with fault movement (δ) amplitude.

The analytical axial force response in all cases of δ and ψ except for $\psi = 90^\circ$ are in excellent agreement with the FEM-based analysis results (**Fig. 5.13**). A discrepancy is observed between the analytical and FEM results at fault intersection, in cases of $\psi = 90^\circ$ (**Fig. 5.13a**) for which the difference between the analytical and FEM results for cases 0.5D to 6D is 53%, 11%, 4%, and 4%, respectively. However, in the rest of the cases including those with very large deformation, this difference is less than 6%, and in cases with $\delta \leq 2D$, the difference is less than 1%. The bending moment predominates the stress results for cases with $\psi = 90^\circ$ (**Figs. 5.14, 5.16**), which shows that the mentioned difference in the axial force response of the 90° cases is negligible in the stress and strain results. The analytical axial force response of the buried pipeline (**Fig. 5.13**) is consistent with the FEM results for the remaining cases. The results show that N increases with decreasing ψ and increasing δ , and the highest axial force occurs in the case of a pipeline with $\delta = 6D$ and $\psi = 45^\circ$ (**Fig. 5.13c**). Moreover, a relationship is observed between N and δ_x , such that a doubling of δ for 1D to 6D and any ψ results in an increase of the axial force response of the pipeline by a factor of 1.5.

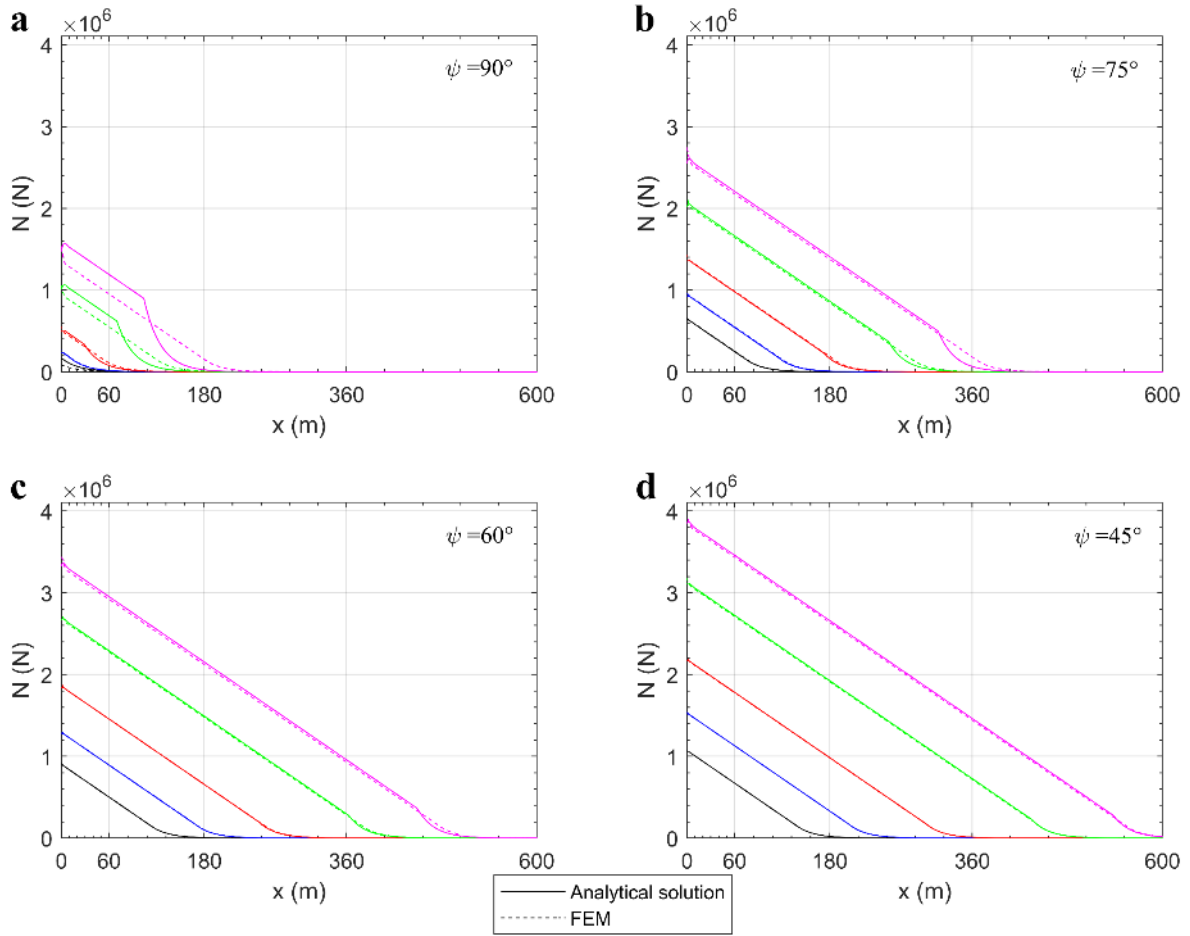


Fig. 5.13. Axial force distribution of buried pipeline subjected to strike-slip fault movement (analytical versus FEM results) for $\delta = 0.5D-6D$ and $\psi = 90^\circ-45^\circ$. Curve and color representations are the same as in **Fig. 5.11**.

The analytical bending moment distribution is consistent with the FEM-based results not only quantitatively but also in the shape of the curves with a nearly identical location of the maximum bending moment obtained from both approaches (**Fig. 5.14**). The difference between the analytical bending moment and FEM is less than 1% for cases of $\delta \leq 2D$ and all ψ , less than 3% for $\delta \leq 4D$ and all ψ , and less than 0.6% for cases with $\psi = 90^\circ$ and all δ . **Fig. 5.14** shows that the pipeline bending moment substantially increases with increasing ψ and δ , with the highest bending moment observed for the case of $6D$ fault movement and a faulting angle of 90° (**Fig. 5.14a**).

The analytical pipeline shear force distribution is also in very good agreement with the FEM-based results (**Fig. 5.15**), especially for cases with $\delta \leq 4D$. A discrepancy is observed in the case of $\delta = 6D$ with a maximum difference of 18% observed when $\psi = 75^\circ$ (**Fig. 5.15b**). The pipeline shear force demonstrates a direct relationship with ψ and δ with the highest and lowest shear force response obtained from the cases of $\delta = 6D$ and $\psi = 90^\circ$ and $\delta = 0.5D$ and $\psi = 45^\circ$, respectively.

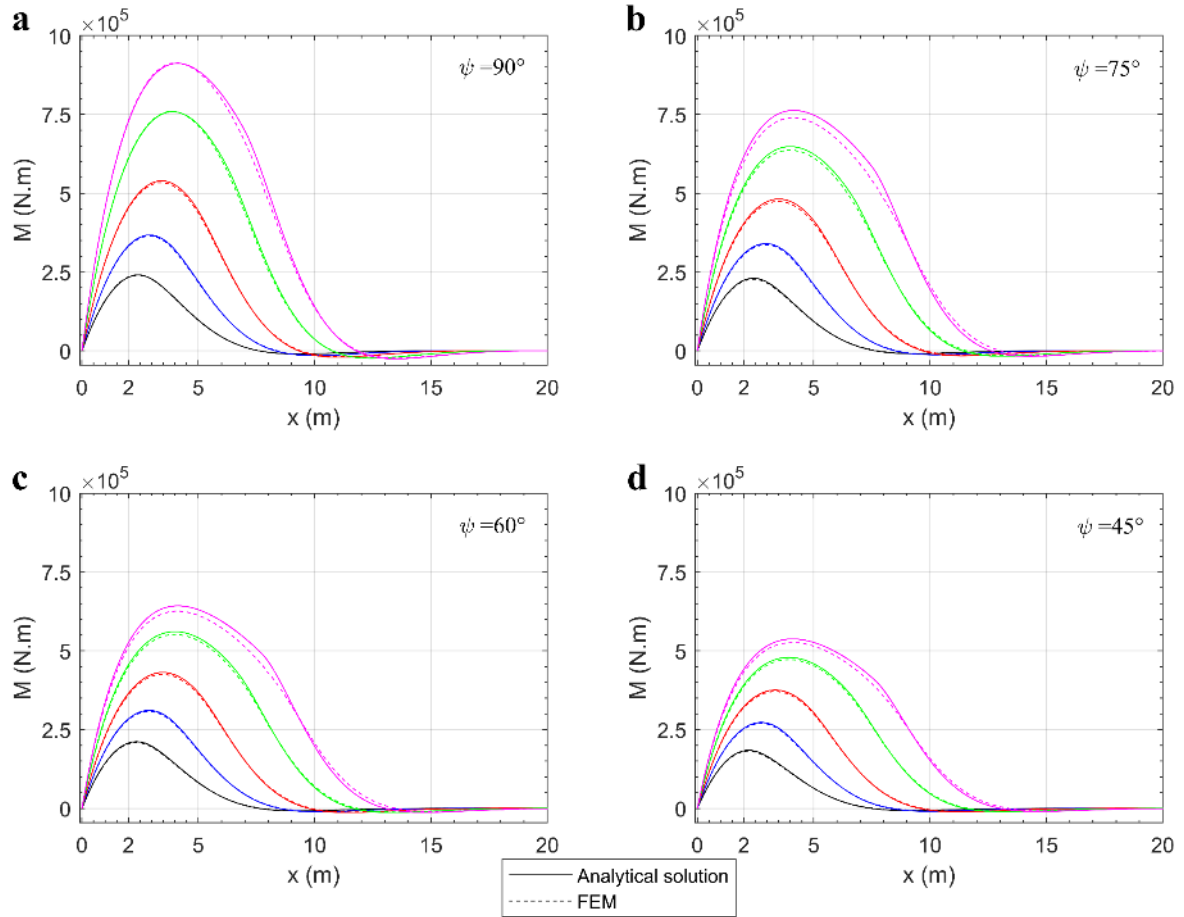


Fig. 5.14. Bending moment distribution of buried pipeline subjected to strike-slip fault movement (analytical versus FEM results) for $\delta = 0.5D-6D$ and $\psi = 90^\circ-45^\circ$. Curve and color representations are the same as in **Fig. 5.11**.

The maximum stress (on springline) represents the highest stress points on the pipe section and is one of the most important engineering terms for structural design of buried pipeline. **Fig. 5.16** shows that the springline maximum stress distribution determined from the analytical method is in excellent agreement with the FEM-based results for all cases not only in quantity but also in the shape of the curves. The analytical maximum stress distribution in cases with $\delta \leq 2D$ are practically identical to the FEM-based analysis results with a mismatch of less than 1%. The discrepancy between the maximum springline stress results obtained from the proposed analytical methodology and FEM analyses for large deformation cases $\delta = 4D$ and $6D$ are less than 1.3% and 2.5%, respectively. This therefore demonstrates the high accuracy of the analytical method for engineering purposes. Moreover, because the analytical stress results are equal or slightly higher than FEM results in all cases, these small discrepancies are conservative with regards to the safety factor. At the pipeline-fault crossing point ($x = 0$), the bending moment is zero. The springline stress of the pipeline, $\sigma_{sp(max/min)}$, at this point are equal to the maximum axial stress of the pipeline, σ_a . The highest maximum axial stress occurs in the case of $\delta = 6D$ and $\psi = 45^\circ$ (**Fig. 5.16d**) and the lowest occurs when $\delta = 0.5D$ and $\psi = 90^\circ$ (**Fig. 5.16a**). This shows that σ_a has a direct relationship with ψ and δ . However, σ_b has

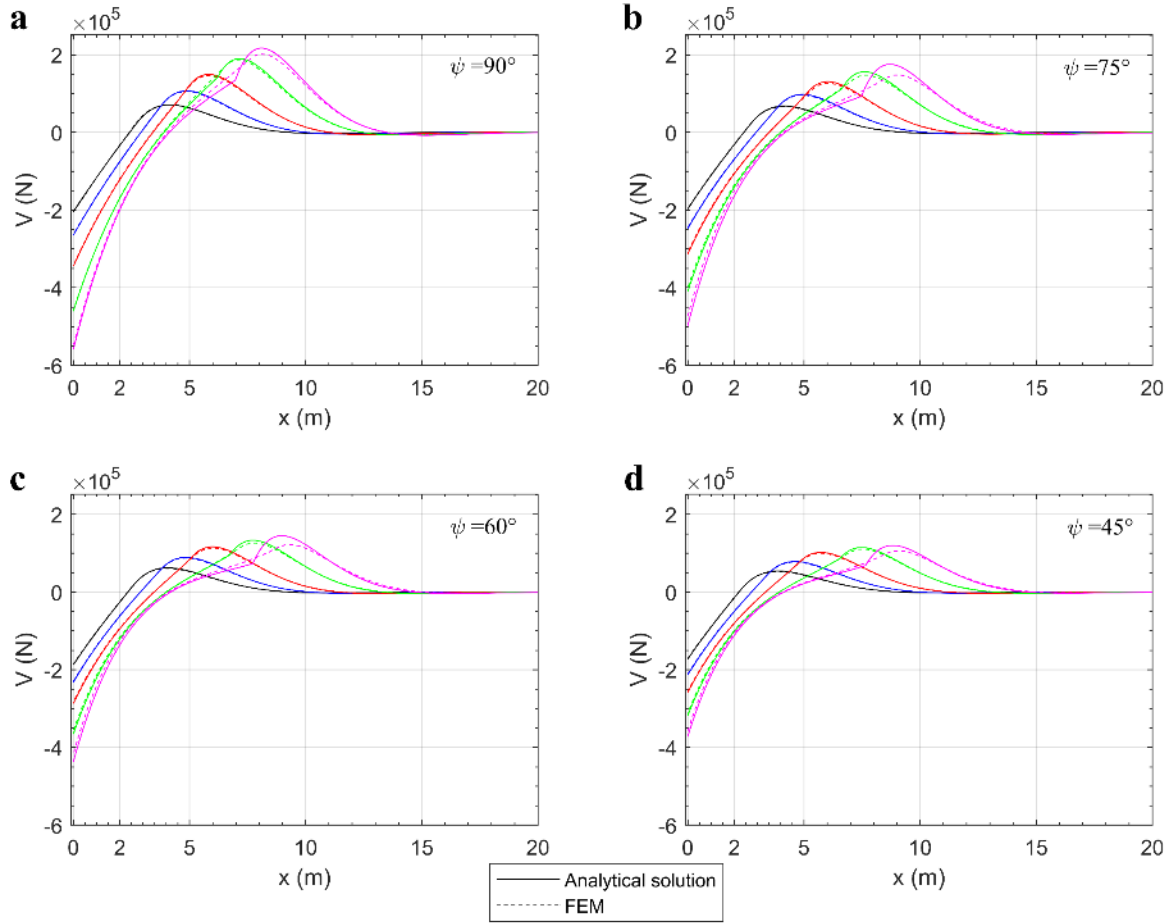


Fig. 5.15. Shear force response of buried pipeline subjected to strike-slip fault movement (analytical versus FEM results) for $\delta = 0.5D-6D$ and $\psi = 90^\circ-45^\circ$. Curve and color representations are the same as in **Fig. 5.11**.

an inverse relationship with ψ and direct relationship with δ , with a maximum in the case with $\delta = 6D$ and $\psi = 90^\circ$ (**Fig. 5.16a**).

The maximum σ_b predominates in cases of higher ψ , whereas the maximum σ_a predominates in cases of lower ψ . In large deformation cases ($\delta \geq 4D$), the peak $\sigma_{sp(max)}$ is directly related to δ and ψ with a maximum occurring in the case with $\delta = 6D$ and $\psi = 90^\circ$ (**Fig. 5.16a**) and minimum in the case of $\delta = 0.5D$ and $\psi = 45^\circ$ (**Fig. 5.16d**). However, in the remaining cases ($\delta \leq 2D$), the maximum $\sigma_{sp(max)}$ is observed from highest to lowest in cases with $\psi = 60^\circ, 75^\circ, 45^\circ$, and 90° . The yield stress of SS400 steel material is $\sigma_y = 400$ MPa, and its limitation is shown as a cyan dash-dot line in **Fig. 5.16**. Owing to the combination of high σ_a and σ_b in cases of $\psi = 60^\circ$ and 75° , the peak $\sigma_{sp(max)}$ reaches the plastic zone earlier in these cases. In $\psi = 90^\circ$ and $\delta > 0.5D$ cases, because the springline stress $\sigma_{sp(max)}$ exceeds the yielding stress in a concentrated length of pipeline (owing to high σ_b) and the axial tensile stress at pipe cross-section is low, a high trend creates a hinge point and generates local buckling damage on the pipeline, which begins from the springline at the maximum bending moment point on pipeline.

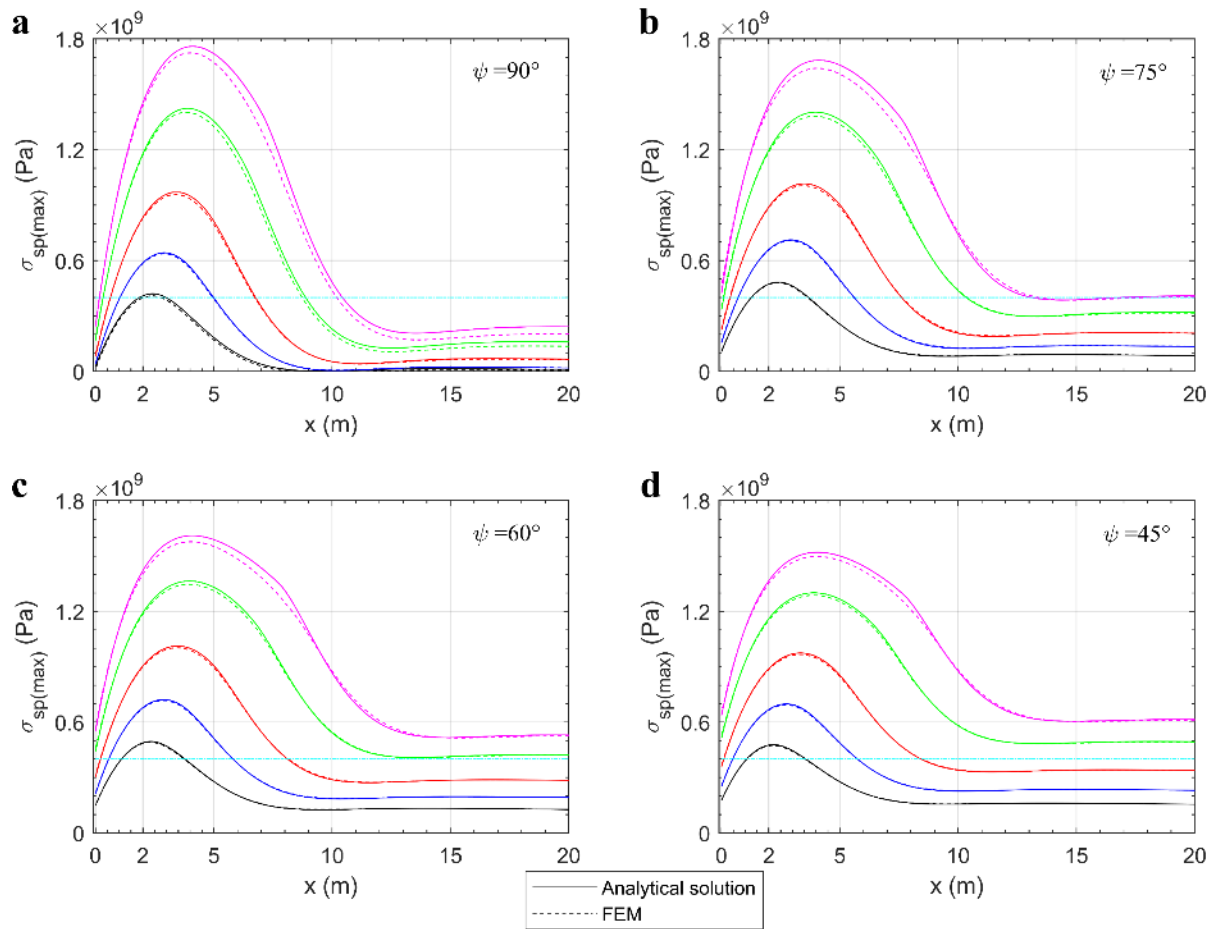


Fig. 5.16. Maximum stress distribution (on springlines) of buried pipeline at a strike-slip fault crossing (analytical versus FEM results) for $\delta = 0.5D-6D$ and $\psi = 90^\circ-45^\circ$. Curve and color representations are the same as in **Fig. 5.11**.

The maximum axial stress and maximum shear stress of the pipe section occur on crown/invert points of the pipeline. **Fig. 5.17** shows the distribution of the maximum principal stress $\sigma_{cr(max)}$ of pipe at the crown/invert point, which is made by the combination of τ_{max} and σ_a (Eq. (5.44)) with a maximum at $x = 0$. The obtained analytical $\sigma_{cr(max)}$ response is also in excellent agreement with the FEM-based results. The pipeline at zones where $\sigma_{cr(max)} \geq \sigma_y$ is highly vulnerable to ovalization and tensile crack damage. **Fig. 5.17** shows that this damage is directly related to δ and has an inverse relationship with ψ . Based on the **Fig. 5.17**, the highest damage vulnerability happens in cases with $\psi = 45^\circ$, which $\sigma_{cr(max)}$ exceeds σ_y in cases $\delta \geq 2D$. Moreover, vulnerability begins even in cases of $\psi = 90^\circ$ under very severe deformation conditions ($\delta = 6D$). And, it is in a good agreement with experimental studies. Owing to the elastic assumption of the steel material, the strain results are the same as the stress results with regards to the shape and ratio (not shown).

A limitation of the proposed methodology is the linear assumption of the pipe material in the governing equation. While past studies also did not consider the pipe material nonlinearity correctly. Authors hope future studies could apply it into the introduced governing equation.

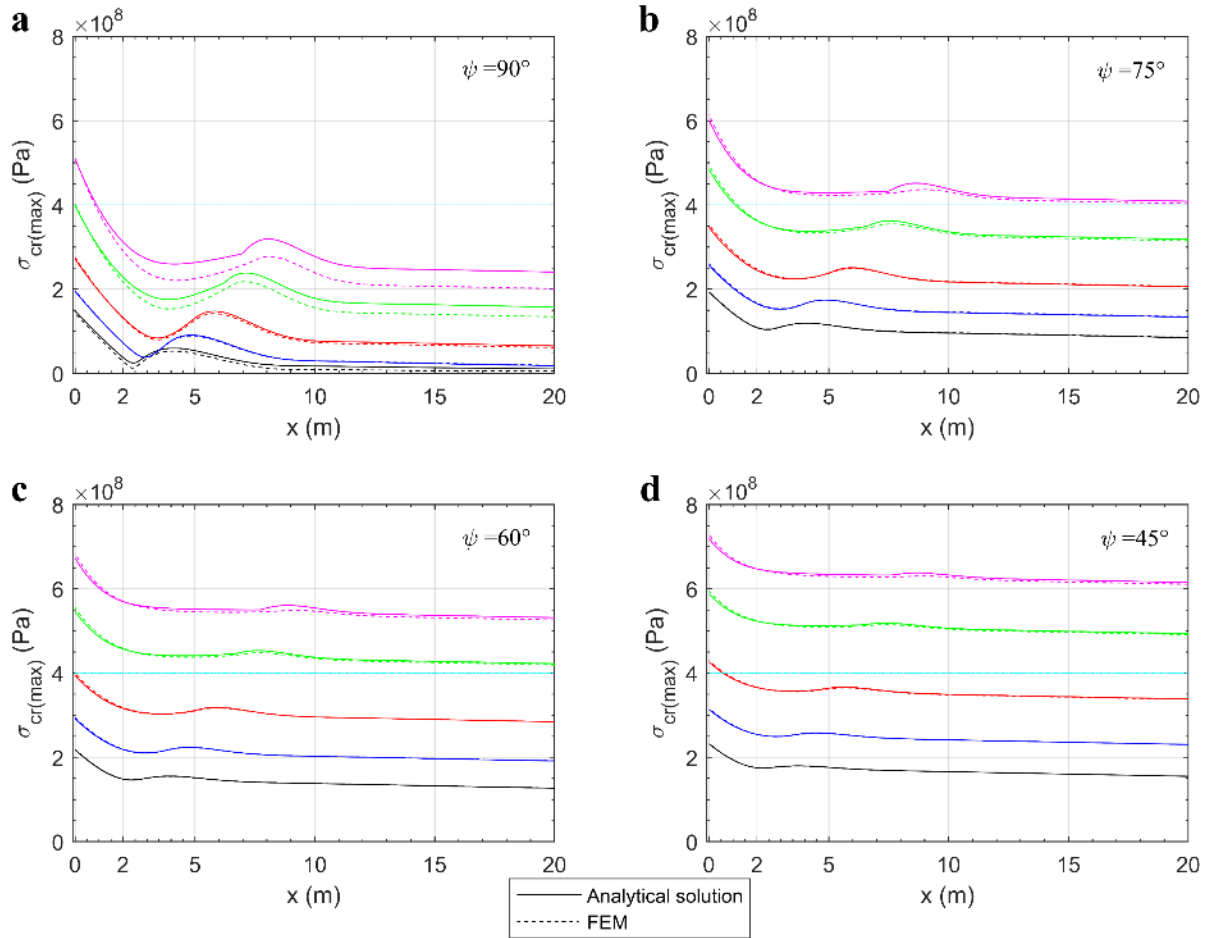


Fig. 5.17. Maximum stress distribution (on crown/invert) of buried pipeline at a strike-slip fault crossing (analytical versus FEM results) for $\delta = 0.5D-6D$ and $\psi = 90^\circ-45^\circ$. Curve and color representations are the same as in **Fig. 5.11**.

The results of the proposed nonlinear analytical methodology are in an excellent agreement both qualitatively and quantitatively with the verified FEM results, which verifies its accuracy, and in most cases, the graphs obtained from both methods are identical. The analytical stress response of the pipeline is the most important term for the engineering design of pipeline and shows very high accuracy compared with the verified FEM results. Furthermore, the small discrepancies in analytical methodology results are all in the direction of higher safety factors. The analytical methodology is therefore reliable for verifying the FEM-based analysis and design of a buried pipeline subjected to strike-slip fault movement.

5.8. Conclusions

An improved analytical method is established for analyzing buried pipeline with nonlinear (elastic perfectly plastic in axial and elastoplastic in transverse directions) soil-pipe interaction and elastic pipe material subjected to active strike-slip faults, and its results are verified with high consistency with FEM results. This methodology presents a substantial development based on the theory of beam-on-elastic-foundation by introducing nonlinear axial force and nonlinear transverse soil reaction terms. This study has further improved the existing analytical

approaches [3–6], [17–21] including:

1. In this study, we have removed the assumption to partition the pipeline into four segments based on the soil yield threshold. We introduce a united nonlinear governing equation that includes exact nonlinear axial and nonlinear transverse soil-pipe interaction terms.
2. The nonlinear axial and nonlinear transverse soil-pipe interaction are introduced within the governing equation. Axial forces are calculated by the governing equation, which significantly improves the results by removing the simplification assumptions and external calculations.
3. The geometrical nonlinearity term for calculation of large deformation effects is improved and applied within the governing equation.
4. The accuracy is significantly improved, for all of the cases, including the cases of a 90° faulting angle compared with previous studies. The solution procedure is further improved by removing the optimization steps, which increases the result accuracy and simplifies the solution procedure.
5. The introduced analytical methodology extends the application field of the analytical solutions by providing higher accuracy reproduction of results even under large fault movements. The discrepancy between the introduced methodology and FEM in cases of large deformation ($\delta \geq 4D$) are less than 2.5% in the maximum stress of pipeline. All of the small discrepancies are within the conservative direction with regards to the safety factor.
6. We propose the $\sigma_{cr(max)}$ response as a criterion for evaluating pipeline ovalization damage.
7. The proposed nonlinear analytical results are in excellent agreement with verified FEM results in both qualitative and quantitative aspects for various faulting angles (ψ) and fault dislocations (δ). The verified methodology is therefore deemed reliable for verifying FEM-based analysis and design of buried pipeline subjected to strike-slip fault movement.

References

- [1] Talebi, F. Kiyono, J. [2020] “Introduction of nonlinear governing equation and corresponding semi-analytical solution for buried pipelines at strike-slip faults crossing” *Soil Dyn Earthq Eng*; (under review).
- [2] American Lifelines Alliance—ASCE. Guidelines for the Design of Buried Steel Pipe” July 2001 (with addenda through February 2005).
- [3] Karamitros, D., Bouckovalas, G., Kouretzis, G. [2007] “Stress analysis of buried steel pipelines at strike-slip fault crossings,” *Soil Dynamics and Earthquake Engineering* 27, 200–11.
- [4] Trifonov, O. V., Cherniy, V. P. [2010] “A semi-analytical approach to a nonlinear stress–strain analysis of buried steel pipelines crossing active faults,” *Soil Dynamics and Earthquake Engineering* 30(11), 1298–308.
- [5] Karamitros, D. K., Bouckovalas, G. D., Kouretzis G. P., Gkesouli V. [2011] “An analytical method for strength verification of buried steel pipelines at normal fault crossings,” *Soil Dynamics and Earthquake Engineering* (13), 1452-1464.
- [6] Trifonov, O. V., Cherniy V. P. (2012). “Elastoplastic stress-strain analysis of buried steel pipelines subjected to fault displacements with account for service loads,” *Soil Dyn Earthq Eng* 33,54–62.
- [7] Lim, M. L., Kim, M. K., Kim, T. W., Jang, J. W. (2001). “The behavior analysis of buried pipeline considering longitudinal permanent ground deformation,” In *pipeline 2001: advances in pipelines engineering & construction* (San Diego, California), vol. 3, 107. ASCE. [https://doi.org/10.1061/40574\(2001\)3](https://doi.org/10.1061/40574(2001)3)
- [8] O’Rourke, M. J., Vikram, G., Abdoun, T. (2003). “Centrifuge modeling of buried pipelines,” In: *Proceedings of the Sixth U.S. conference and workshop on lifeline earthquake engineering*, August 10–13, 2003, Long Beach, CA. pp. 757–768.
- [9] Sakanoue, T., Yoshizaki, K. (2004). “A study on earthquake-resistant design for buried pipeline using lightweight backfill,” In: *Proceedings of the 13th world conference on earthquake engineering*, Vancouver, B.C., Canada, August 1-6, Paper No.2389.
- [10] Takada, S., Hassani, N., Fukuda, K. (2001). “A new proposal for simplified design of buried steel pipes crossing active faults,” *Earthq Eng Struct Dyn* ;30:1243–57.
- [11] Vazouras, P., Karamanos, S. A., Dakoulas, P. (2010). “Finite element analysis of buried steel pipelines under strike-slip fault displacement,” *Soil Dyn Earthq Eng* ;30:1361–76.
- [12] Vazouras, P., Karamanos, S. A., Dakoulas, P. (2012). “Mechanical behavior of buried steel pipes crossing active strike-slip fault,” *S, Soil Dyn Earthq Eng*;41:164–80.
- [13] Vazouras, P., Dakoulas, P., Karamanos, S. A. (2015). “Pipe–soil interaction and pipeline

- performance under strike–slip fault movements,” *Soil Dyn Earthq Eng* ;72:48–65.
- [14] Zhang, L., Zhao, X., Yan, X., Yang, X. (2016). “A new finite element model of buried steel pipelines crossing strike-slip faults considering equivalent boundary springs,” *Eng Struct*;123:30–44.
- [15] Liu, X., Zhang, H., Li, M., Xia, M., Zheng, W., Wu, K., Han, Y. (2016). “Effects of steel properties on the local buckling response of high strength pipelines subjected to reverse faulting,” *J Nat Gas Sci Eng* ;33:378–87.
- [16] Demirci, H. E., Bhattacharya, S., Karamitros, D., Alexander, N. (2018) “Experimental and numerical modelling of buried pipelines crossing reverse faults,” *Soil Dyn Earthq Eng* ;114:198–214.
- [17] Newmark, N. M., Hall, W. J. [1975] “Pipeline design to resist large fault displacement,” *Proc. of the U.S. national conference on earthquake engineering, University of Michigan, Ann Arbor, Michigan, 416–25.*
- [18] Kennedy, R. P., Chow, A. M., Williamson, R. A. [1977] “Fault movement effects on buried oil pipeline,” *ASCE Transportation Engineering Journal* 103(5), 617–33.
- [19] Kennedy, R. P., Kincaid, R. H. [1983] “Fault crossing design for buried gas oil pipelines” *ASME, PVP conference 77, 1–9.*
- [20] Wang, L. R. L., Yeh, Y. A. [1983] “A refined seismic analysis and design of buried pipeline for fault movement,” *Earthquake Engineering and Structural Dynamics* 13(1), 75–96.
- [21] Talebi, F. Kiyono, J. [2020] “Introduction of the axial force terms to governing equation for buried pipeline subjected to strike-slip fault movements” *Soil Dyn Earthq Eng* ;133:106125. <https://doi.org/10.1016/j.soildyn.2020.106125>
- [22] Talebi, F., Kiyono, J. [2018] “Force-displacement analysis of buried steel pipelines for strike-slip faulting” *Vietnam- Japan Symposium on Natural Disasters, Ho Chi Minh, Vietnam: 90-94.*
- [23] Talebi, F. Kiyono, J. [2018] “Evaluation of buried pipeline behavior subjected to strike-slip fault” *15th Japan Earthquake Engineering Symposium (JEES), Sendai, Japan: 2619-2625.*
- [24] Erami, M. H., Miyajima, M., Kaneko. Sh., Toshima, T., Kishi, Sh. “Pipe–soil interaction for segmented buried pipelines subjected to dip faults” *Earthquake Engineering Structural Dynamics* 44:403-417.
- [25] Kierzenka, J. [1998] “Studies in the Numerical Solution of Ordinary Differential Equations” *Southern Methodist University, Book, Dallas, TX.*
- [26] Ascher, U., Mattheij, R., Russell, R. [1995] “Numerical Solution of Boundary Value Problems for Ordinary Differential Equations” *Society of industrial and Applied*

Mathematics, Book, Philadelphia, PA, 327-357

[27] Keller, H. B. [1992] “Numerical Methods for Two-Point Boundary-Value Problems”
Dover, Book, New York.

[28] ABAQUS/CAE 2017. Dassault Systems Simulia Corp, documentation of 2017 release.

Nomenclature

A	Pipe cross-section area	u	Axial displacement of the axial pipeline and soil spring
D	Pipe cross-section diameter	u_y	Yielding displacement of the axial soil spring
d_y	Yielding displacement of the axial soil springs	V	Shear force of the pipeline
E	Young's modulus of the pipeline	w	Pipeline deflection in the y -direction
G	Shear modulus of the pipeline	w_x	Pipeline displacement in the x -direction
H	Total pipeline axial force on the x -axis	w_y	Yielding deflection of the transverse soil springs
H_m	Horizontal projection of pipe membrane force on the x -axis	x	Position on the x -axis
H_{mMax}	Horizontal projection of pipe membrane force at the fault-line	y	Position on the y -axis
H_s	Horizontal projection of the pipe frictional axial force	δ	Total fault displacement
h_s	Axial force of the axial soil spring	δ_x	Horizontal component of the fault displacement on the x -axis
h_{sy}	Yielding force of the axial soil spring	δ_y	Transverse components of the fault displacement on the y -axis
I	Second moment of inertia of the pipeline	ψ	Faulting angle
k_a	Axial soil spring elastic stiffness	φ	Pipeline rotation
k_{t1}	Transverse soil spring elastic stiffness	λ	Coefficient defined in Eq. (5.5)
k_{t2}	Transverse soil spring plastic stiffness	τ_{max}	Maximum shear stress of the pipeline section
k_{v_d}	Vertical downward spring elastic stiffness	σ_a	Axial stress of the pipeline
k_{v_u}	Vertical upward spring elastic stiffness	σ_b	Maximum bending stress of the pipeline on the springlines
L_s	Slid pipe length	$\sigma_{sp(max)}$	Maximum stress of the pipeline on the springlines (tensile)
L_n	Non-slid pipe length	$\sigma_{sp(min)}$	Minimum stress of the pipeline on the springlines
L_N	Axial force dissipation length	$\sigma_{cr(max)}$	Maximum stress of the pipeline on the crown/invert points (tensile)
ΔL_p	Elongation of the pipe inside the slid-segment (yielded soil segment)	$\sigma_{cr(min)}$	Maximum stress of the pipeline on the crown/invert points (tensile)
N	Axial force of the pipeline	$\varepsilon_{sp(max)}$	Maximum strain of the pipeline on the springlines
Q_{max}	First moment of inertia of the pipeline	$\varepsilon_{sp(min)}$	Minimum strain of the pipeline on the springlines
q	Reaction force of the transverse soil springs	ε_m	Membrane strain of the pipeline
r	Pipeline outer radius	γ_{max}	Maximum shear strain of the pipeline section
t	Pipeline cross-section thickness		

Chapter VI:

Evaluation of FEM modeling approaches and buried pipeline's performance at fault crossing

6.1. General remarks

This chapter mainly has focused on the analysis approaches of the buried pipeline subjected to the strike-slip fault movement during strong ground deformation. There have been 2 main modeling approaches for the problem of buried pipeline subjected to the fault movement. In the first approach, soil-pipe interaction has been modeled by soil spring elements and their characteristics which is the most popular in design codes and in the second approach soil-pipe interaction is modeled by 3D solid soil elements and its contact characteristics with the pipeline which is more complex in the aspect of analyzing and mainly is used for research purposes. This study desired to evaluate the performance of the buried steel pipeline by both spring and solid elements and compare the force-displacement and stress-strain field responses of the buried pipeline for these finite element method-based modeling approaches. Since the problem of buried pipeline subjected to fault movement is a large deformation problem, pipeline material nonlinearity, soil-pipe interaction nonlinearity, and geometrical nonlinearity effects have been applied to the finite-element based analysis [1].

6.2. Background

Nowadays, by improvement of processors and finite element method (FEM), FEM-based analysis is applicable solutions for the problem of the buried pipeline crossing active fault. FEM has been recently used for verification of analytical solutions and evaluation of the buried pipeline performance for assessment of criteria such as local buckling, ovalization and tensile damages [2-14]. There exist several FEM-based pieces of research, with different modeling approaches. In 2015, Vazouras et al. modeled a hybrid (shell and solid elements beside equivalent springs) pipeline buried in solid soil, by adding the analytically extracted equivalent axial springs of soil and pipeline, they shortened the size of needed FEM model with the same accuracy of the full FEM model [12]. Liu et al., modeled buried pipeline at reverse fault crossing using FE commercial code ABAQUS which pipe was modeled as shell elements and soil-pipe interaction was modeled as non-linear soil springs. They modeled pipe as shell elements and soil-pipe interaction was modeled as non-linear soil springs. besides, they had an investigation on buckling of buried pipeline influenced by yield strength and strain hardening parameters [15]. Demirci et al. studied the behavior of a continuous buried pipeline subjected to reverse fault motion by a new experimental centrifuge modeling of pipeline crossing reverse fault. Which used 3D FEM analyses besides for more details. A review of the FEM-based researches in the literature shows that for modeling of pipe various modeling approaches including beam, shell, hybrid (beam+shell), new hybrid (spring+shell) and soil continuum-shell model are used to evaluate pipeline performance against earthquake fault movement.

Simulation of the buried pipeline and surrounding soil respectively by shell elements and solid elements for a 3D FEM-based analysis is the most detailed approach for modeling the pipeline at fault crossing problem. which can produce the most realistic performance of buried pipeline including the local buckling, ovalization, and tensile damages. Because of the

modeling complexity, this method mostly is used for research purposes which in this study we call it 3D-solid modeling approach. It is common to use the beam element for modeling of pipe and spring elements for modeling of soil-pipe interactions for design and even research purposes which is simpler than the 3D-solid modeling approach and in this study, we call it beam modeling approach. Both over mentioned FEM models include the geometrical nonlinearity effects and material nonlinearity effects.

In this study, it is intended to have a FEM-based investigation on the performance of buried pipeline at strike-slip fault crossing through 3D-solid and beam modeling approaches. Firstly, force-displacement curvatures of equivariant soil springs in axial, transverse and vertical directions are extracted through the FEM-based 3D-solid model soil box. Secondly, response of buried pipeline modeled by 3D-solid approach is compared versus beam approach to evaluate the capability range of the FEM modeling approaches to understand the performance of pipeline for through both modeling approaches and compare the damage related parameters.

6.3. Axial and transverse soil springs

To study the axial and transverse soil pipe interaction two 3D FEM models have been created. The first model is an axial pipe pull-out test of the pipeline for extracting the of the axial soil-pipe interaction force-displacement curve. And the Second model is a transverse pipe sliding test to extract the transverse soil-pipe interaction force-displacement curve.

Both of the analysis results are obtained for an X65 steel 36" pipeline with an outer diameter of $D=0.914\text{m}$, thickness $t=0.0095\text{m}$ Young's Modulus of $E=21\text{Tpa}$, Poisson's ratio of $\nu = 0.3$ and density of 7850 kg/m^3 . the young's module for pipe material has been assumed 100 times stiffer than X65 steel to decrease the pipeline deformation effect on soil-pipe interaction evaluation. The pipeline is assumed to be buried in undrained clay. The soil has density of 2000 kg/m^3 , Young's Modulus of $E_s = 25\text{ MPa}$, Poisson's ratio of $\nu_s = 0.5$, cohesion of $c = 50\text{ kPa}$, friction angle of $\phi = 0^\circ$. Same with real cases, it has assumed that the buried pipeline has sounded by a thin layer of sand. Thus, frictional soil-pipe interaction has been employed. The soil box is modeled in multi-purpose finite element program ABAQUS [16] in dimensions of $20\text{ m} \times 10\text{ m} \times 5\text{ m}$.

Soil material is defined as an elastic-perfectly plastic Mohr-coulomb constitutive model. Pipe elements are 4-node shell S4R element type and soil elements are 8-node linear brick, reduced integration with hourglass control C3D8R element type. Geometrical nonlinearity effect has been taken into account for all the analyses by Nlgeom method, which is conducted by finite element program of ABAQUS.

6.3.1. 3D FEM analyses results

6.3.1.1. Axial pull-out test analyses

To evaluate the axial soil pipe interaction, three 3D FEM cases for axial pull-out tests has

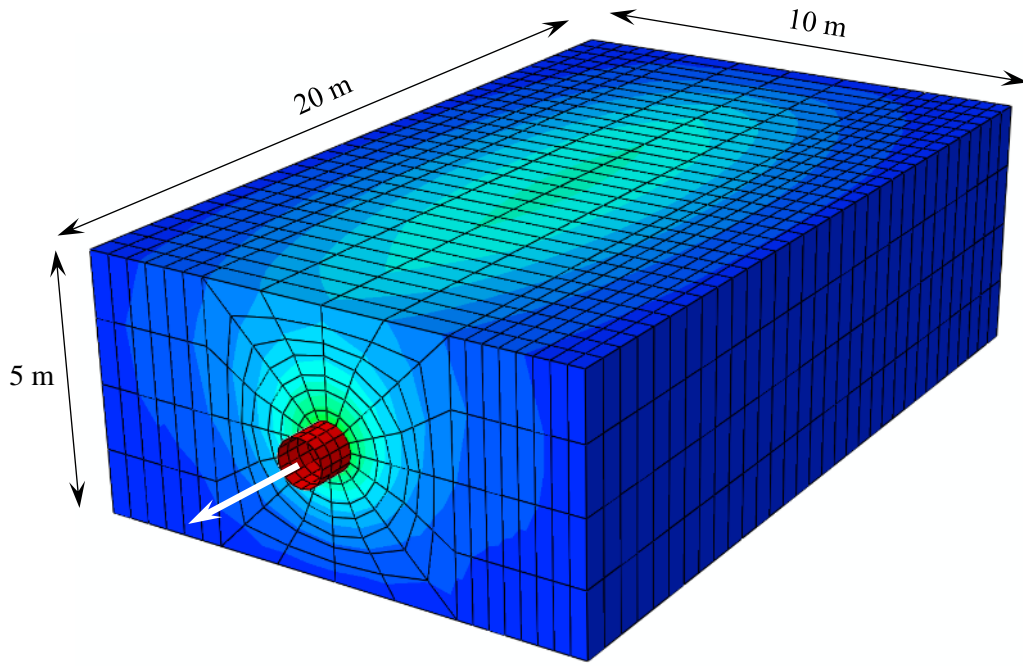


Fig. 6.1. Axial pull-out test model of buried pipeline (displacement contours) [1].

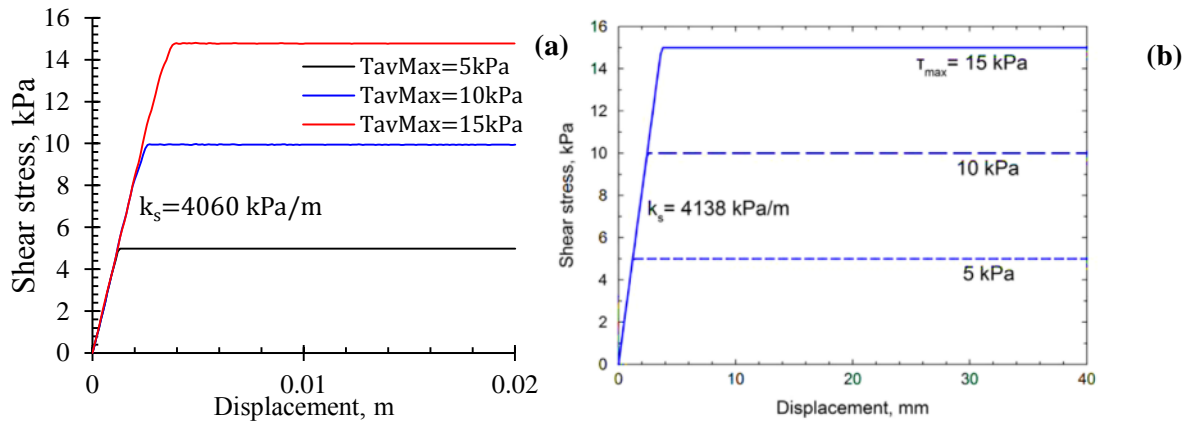


Fig. 6.2. stress–strain relationship at the pipe–soil interface for friction coefficients of 0.2, 0.3 and 0.4: (a) this study, (b) Vazouras et al. (2015) [12].

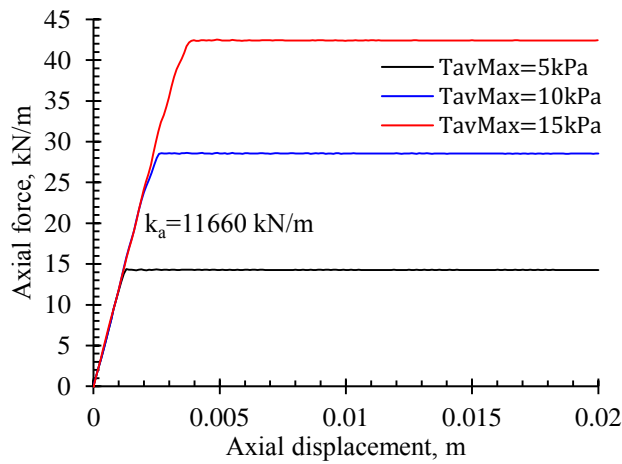


Fig. 6.3. Axial soil pipe interaction force–displacement relationship at the pipe–soil interface for friction coefficients of 0.2, 0.3 and 0.4 [1].

6.3.1.2. Transverse sliding test analyses

After verification of the soil-pipe contact results for axial soil-pipe interaction, FEM model is extended to the transverse sliding test for reproduction of the transverse soil-pipe interaction curve. Displacement contours for the transverse sliding test model is illustrated in **Fig. 6.4**. From **Fig. 6.5**, the transverse soil-pipe interaction curves for cases with friction coefficients of 0.2, 0.3 and 0.4 in elastic range are almost same and have almost equal stiffness. And The variation of transverse soil-pipe interaction curves for mentioned cases is not so much. By little difference, the case with 0.4 friction coefficient case has the highest transverse force and 0.2 case has the lowest. However, transverse soil-pipe interaction curves for all the cases are almost same.

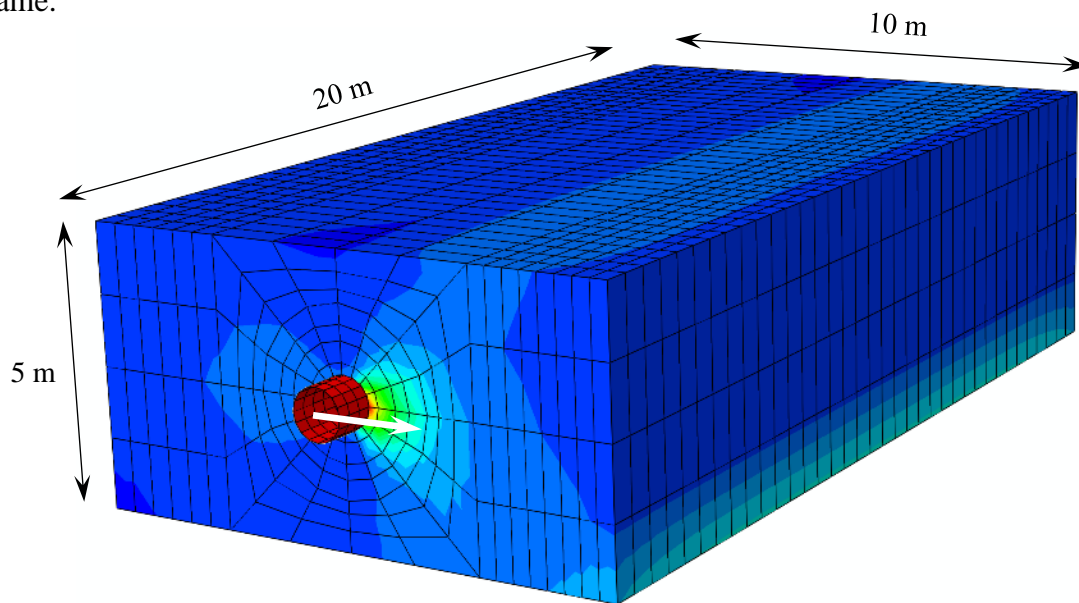


Fig. 6.4. Transverse sliding test model of buried pipeline (displacement contours) [1].

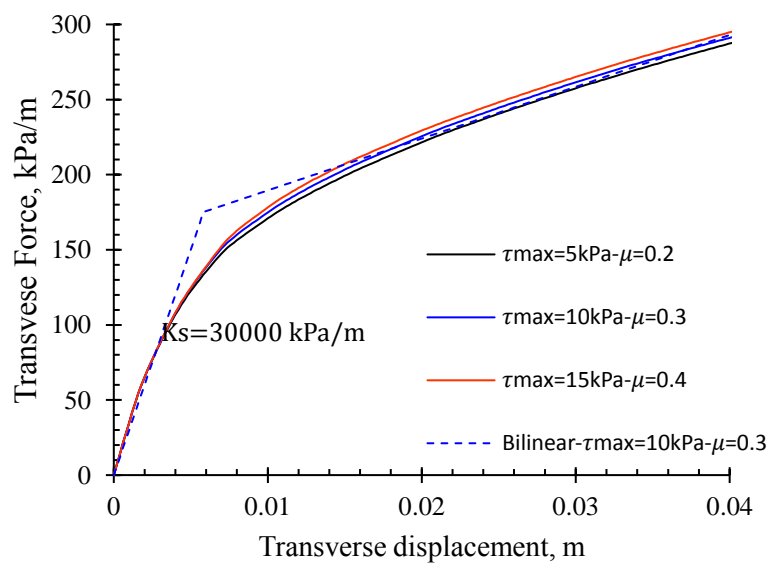


Fig. 6.5. Transverse soil-pipe interactions force displacement relationship for friction coefficients of 0.2, 0.3 and 0.4 [1].

6.4. Modeling of buried pipeline at strike-slip fault crossing

To study on the FEM modeling approaches effect for problem of buried pipeline at crossing with strike-slip fault, same case has been modeled by 3D-solid and beam modeling approaches. Both of the analysis results are obtained for an X65 steel 36” pipeline with outer diameter of $D=0.914\text{m}$, thickness $t=0.0095\text{m}$ Young’s Modulus of $E=210\text{Gpa}$, Poisson’s ratio of $\nu = 0.3$ and density of 7850 kg/m^3 . The pipeline steel is of the API5L-X65 type, the properties listed in **Table 6.1**. Pipeline’s steel material plasticity is modeled based on the Ramberg-Osgood in Eq. (6.1) (**Fig. 6.6**).

$$\varepsilon = \frac{\sigma}{E_i} \left[1 + \left(\frac{a}{r+1} \right) \left(\frac{|\sigma|}{\sigma_y} \right)^r \right] \quad (6.1)$$

The FEM analyses are performed using an equivalent Ramberg–Osgood stress–strain curve as the properties listed in **Table 6.2**. The pipeline is assumed to be buried in undrained clay. The soil has density of 2000 kg/m^3 , Young’s Modulus of $E_s = 25 \text{ MPa}$, Poisson’s ratio of $\nu_s = 0.5$, cohesion of $c = 50 \text{ kPa}$, friction angle of $\phi = 0^\circ$. Same with real cases, it has assumed that the buried pipeline has sounded by a thin layer of sand. Thus, frictional soil-pipe interaction has been anticipated. In this model Buried pipeline is subjected to a 60° strike-slip fault movement.

Table 6.1. API5L-X65 steel material of pipeline [1].

Young modulus (E)	210 GPa
Yielding stress (σ_y)	490 MPa
Yielding strain (ε_y)	0.233%
Failure stress (σ_f)	531MPa
Failure strain (ε_f)	4.0%
Poisson’s ratio (ν)	0.3

Table 6.2. Parameters of Ramberg-Osgood stress-strain for steel API5L-X65 [1].

Initial Young’s modulus (E)	210 GPa
Yielding stress	490 MPa
a	38.31
r	31.51

For the 3D-solid model, soil box is modeled in multi-purpose finite element program ABAQUS in dimensions of $60 \text{ m} \times 10 \text{ m} \times 5 \text{ m}$ as illustrated in **Fig. 6.7**. Soil material is defined as elastic-perfectly plastic Mohr-coulomb constitutive model. Pipe elements are 4-node shell S4R element type and soil elements are 8-node linear brick, reduced integration with hourglass

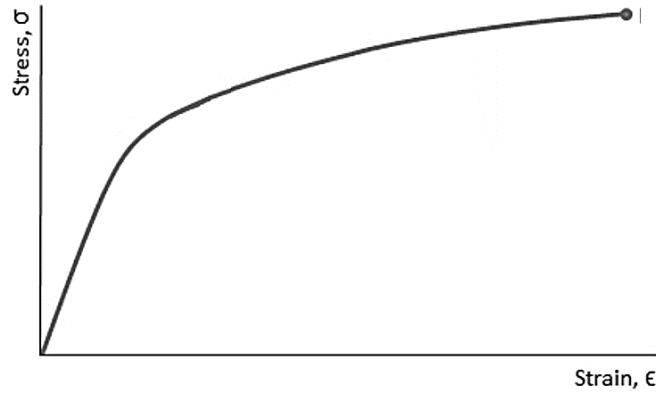


Fig. 6.6. Ramberg-Osgood steel model.

control C3D8R element type. Friction coefficient of 0.3 is assumed for contact modeling, which is equivalent with the demonstrated soil to $T_{avMax} = 10\text{kpa}$ soil at previous section. The Geometrical nonlinearity effect has been taken into account for all the analyses by Nlgeom method, which is conducted by finite element program of ABAQUS. The fault movements and boundary conditions all are applied to the soil box's faces.

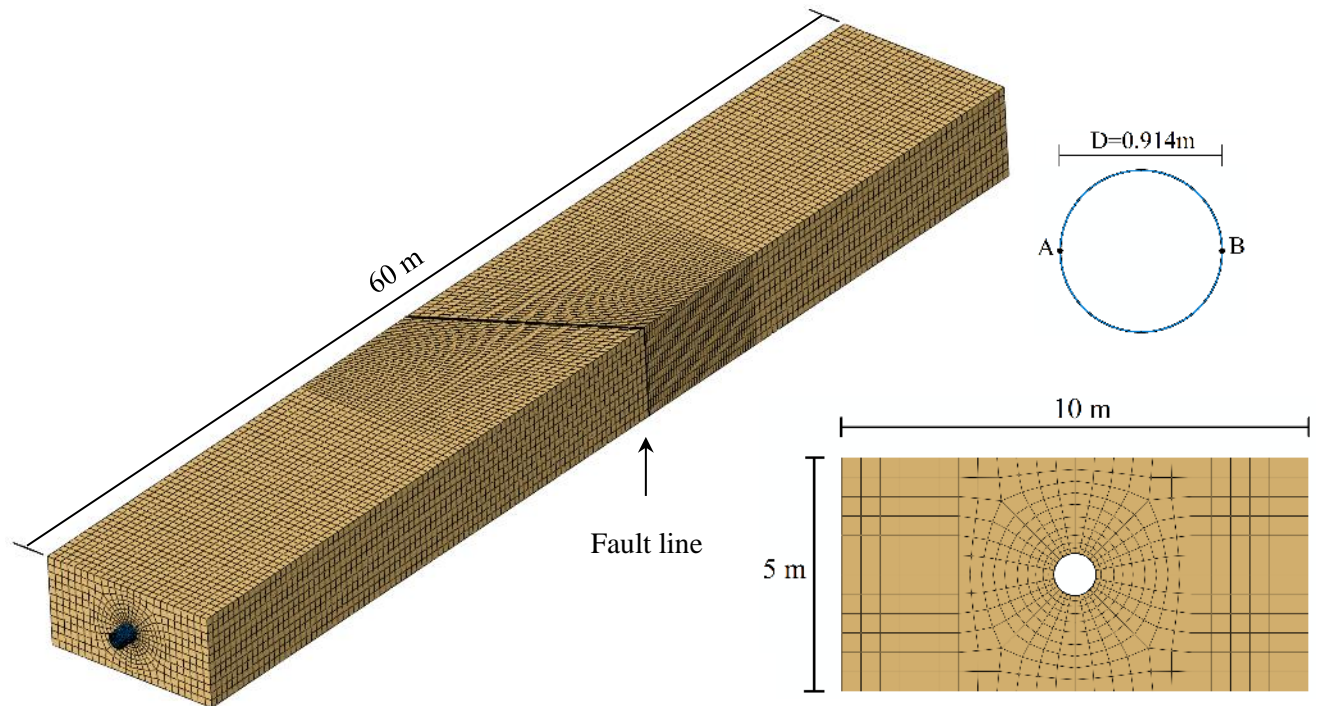


Fig. 6.7. 3D-solid model for buried steel pipeline subjected to 60° strike-slip fault movement. Points A and B are springlines of the pipe.

For beam model, all the properties are same as the 3D-solid model. A 60 m pipeline made of API5L-X65 steel material is modeled through Abaqus (**Fig. 6.8**). For pipe elements in beam model B31 elements, for rigid bodies RB3D2 elements and for soil CONN3D2 elements are used. Soil-pipe interaction in beam model is modeled through, equivalent nonlinear soil springs in axial, transverse (horizontal) and vertical directions extracted from FEM simulations of

section 2 for case of 0.3 friction coefficient and $\tau_{max} = 10\text{kPa}$, which are shown in **Fig. 6.9**. The fault displacement components are applied to the ends of the rigid elements at the end of the soil spring elements and the pipeline is free to move on axial direction in both ends. The geometrical nonlinearity effect also same as the 3D-soild model has been taken into account for all the analyses by the Nlgeom method.

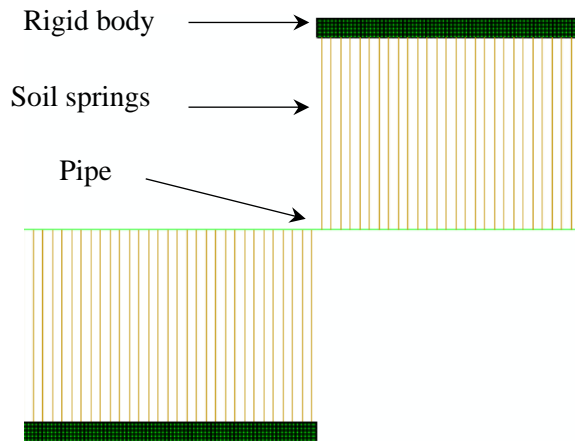


Fig. 6.8. A part of beam model for buried steel pipeline subjected to 60° strike-slip fault movement with length of 60 m [1].

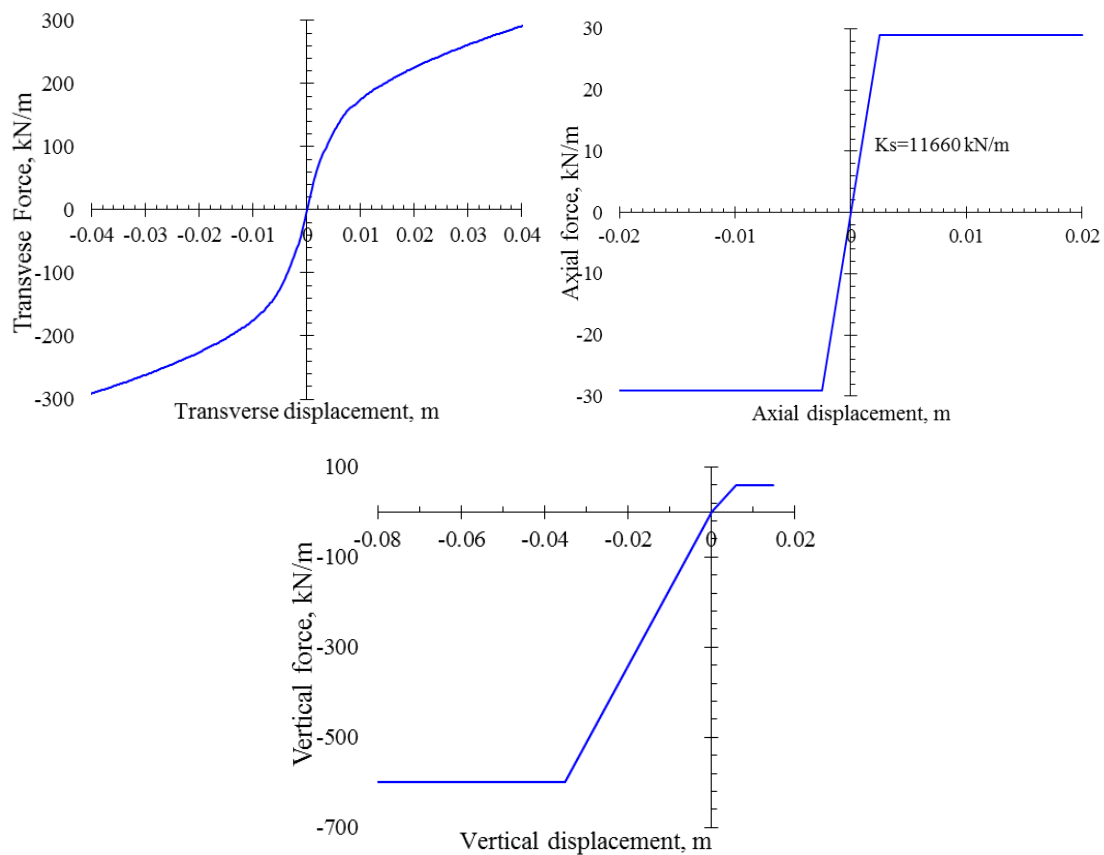


Fig. 6.9. Equivalent nonlinear soil springs for beam model [1].

6.5. Results and discussion

Performance of buried pipeline at 60° strike-slip fault crossing has been evaluated through FEM based beam and 3D-solid models' analysis. Regarding **Fig. 6.10**, transverse displacement behavior of buried pipeline for 3D- solid and beam models are in good agreement. However, around fault zone, there is a gap between 3Dsolid and beam model and high curvature zone for the 3D-solid model is shorter and it shows that in the 3D-solid model, soil stiffness at fault crossing zone has got locally increased. The reason for this local stiffening of soil is the confinement of soil which appeared due to the Faultline movement at fault crossing zone.

Fig. 6.11 shows the mises stress outputs of 3D-solid buried pipeline deformation and it's buckling for each of fault movement cases. Additionally, because of buckling of the pipeline at 3D-solid model, transverse displacement of pipeline at further parts than fault line is less than beam model results.

Stress and strain outputs are shown for left and right springlines (A and B points at **Fig. 6.7**) for the pipeline at one side of fault due to symmetry of the problem. The left springline side is in tensile and the right springline side is in compression owing to the bending of pipeline. As shown in **Figs 6.12–6.15**, the distance between maximum tensile/compression stress and strain of buried pipeline and Faultline for the case of 3D-solid model is shorter than beam model. This is again because of the shortening of the high curvature zone due to the local stiffening of soil at 3D-solid model.

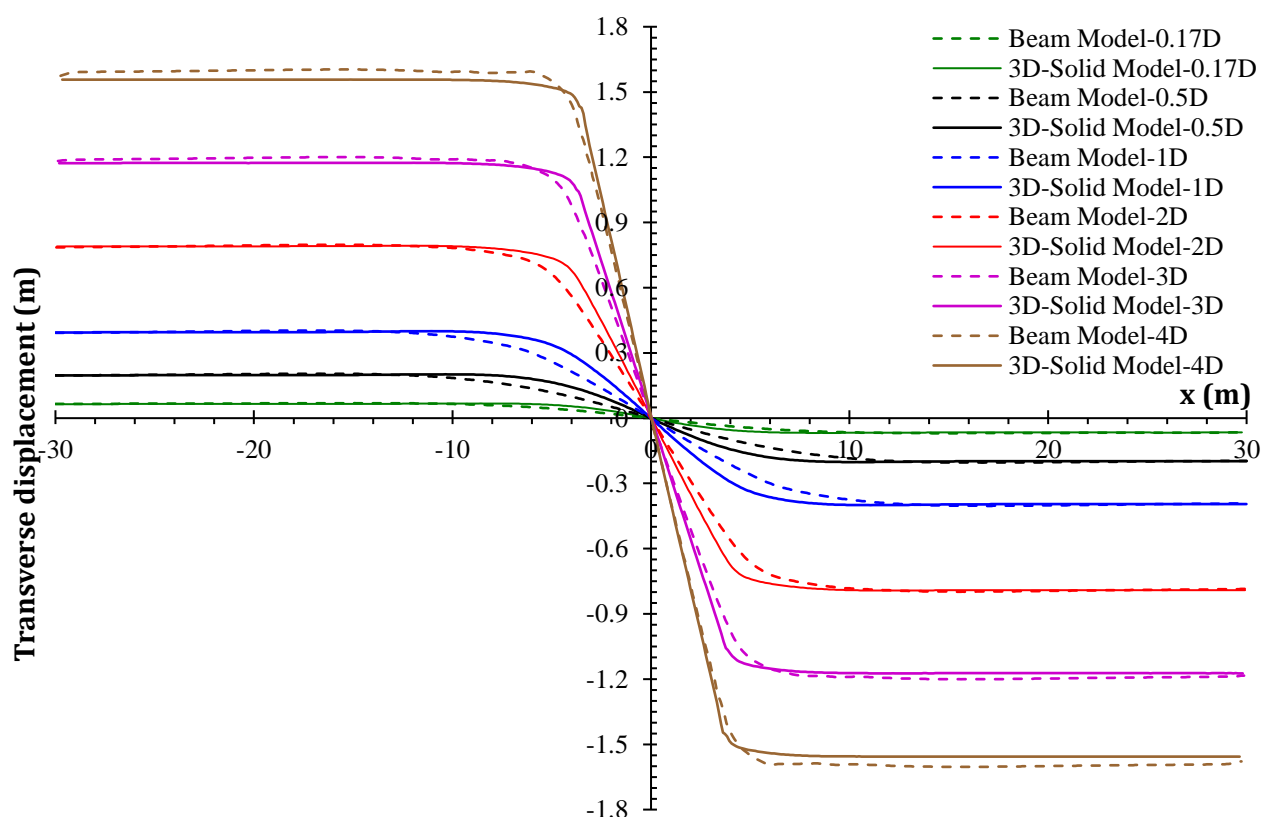


Fig. 6.10. Transverse displacement of pipeline 3D-solid model versus Beam model at strike-slip fault crossing on neutral axis of pipe section [1].

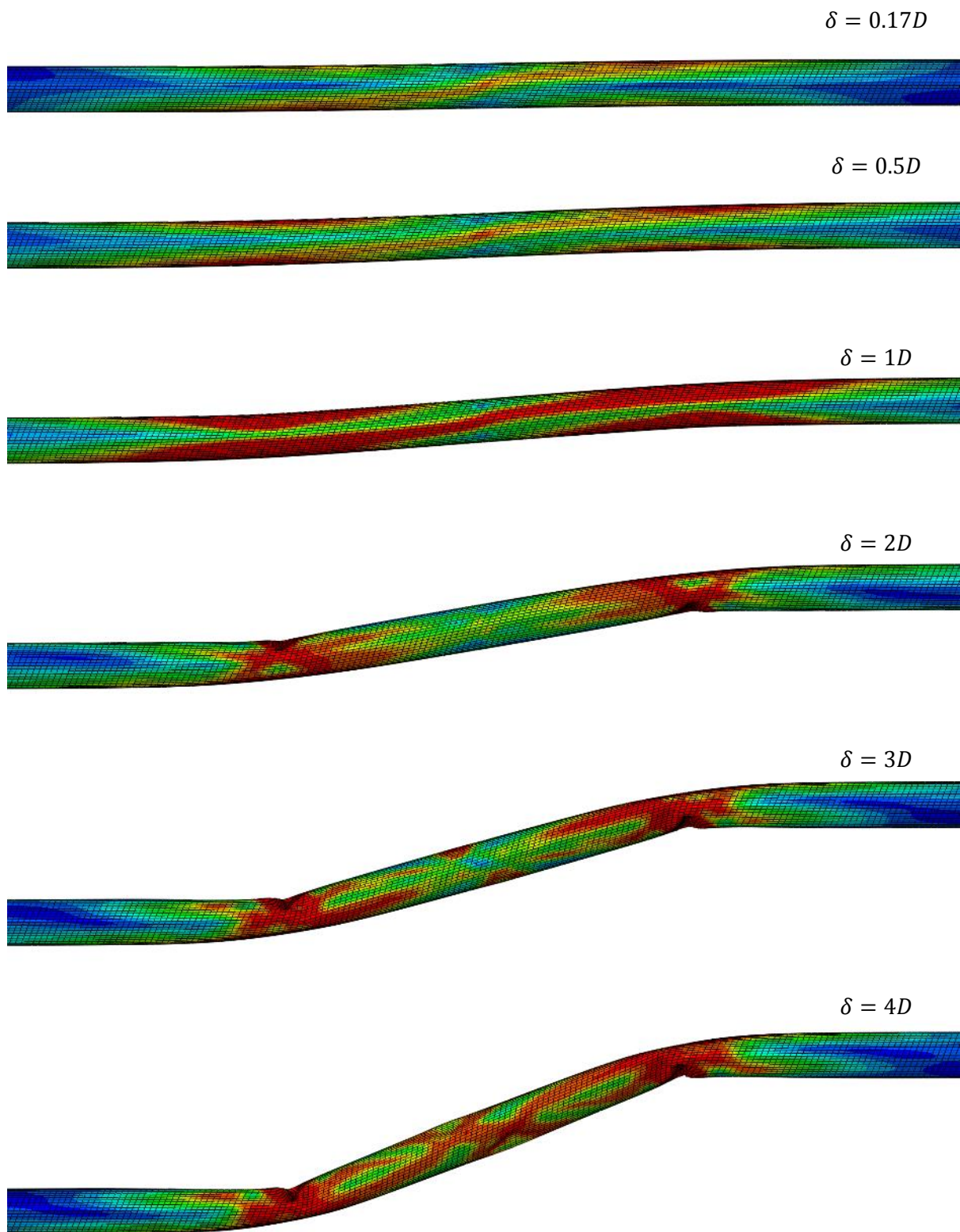


Fig. 6.11. Mises stress and buckling status of buried pipeline at 60° strike-slip fault crossing with $0.17D$, $0.5D$, $1D$, $2D$, $3D$ and $4D$ fault movements [1].

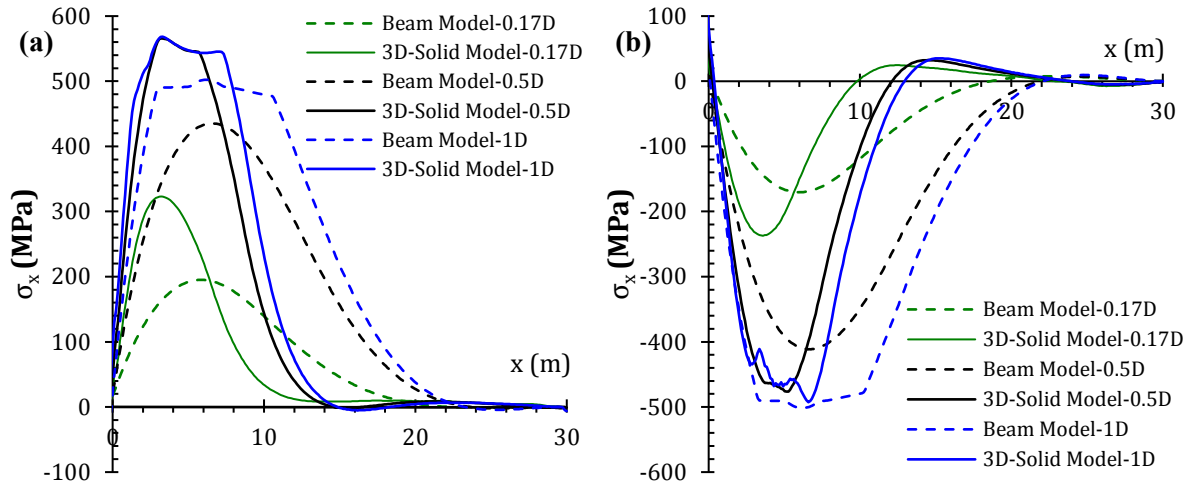


Fig. 6.12. Maximum longitudinal stresses of buried pipeline subjected to 60° strike-slip fault 0.17D to 1D movement, 3D-solid model versus Beam model: (a) Left springline (b) Right springline [1].

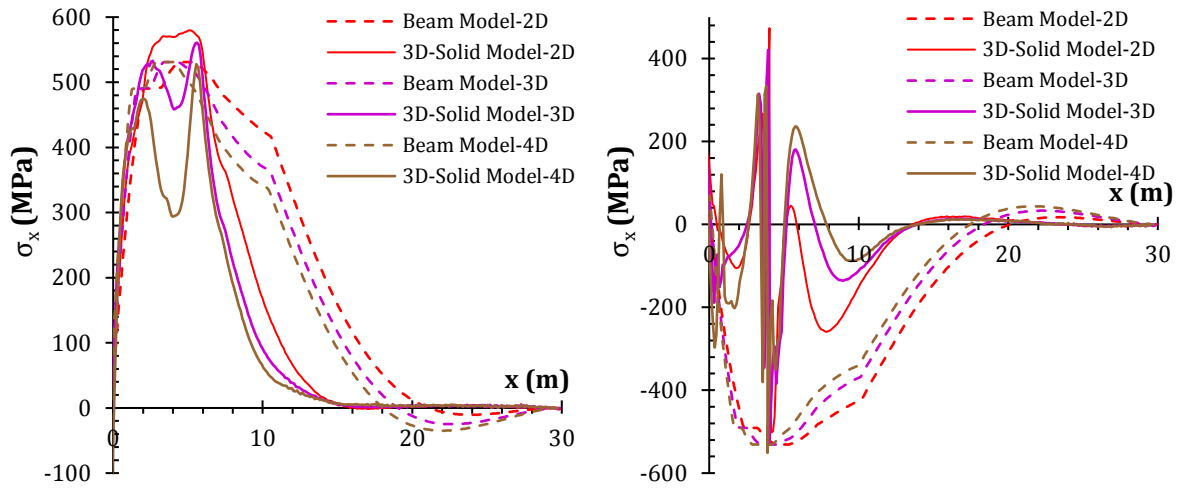


Fig. 6.13. Maximum longitudinal stresses of buried pipeline subjected to 60° strike-slip fault 2D to 4D movement, 3D-solid model versus Beam model: (a) Left springline (b) Right springline [1].

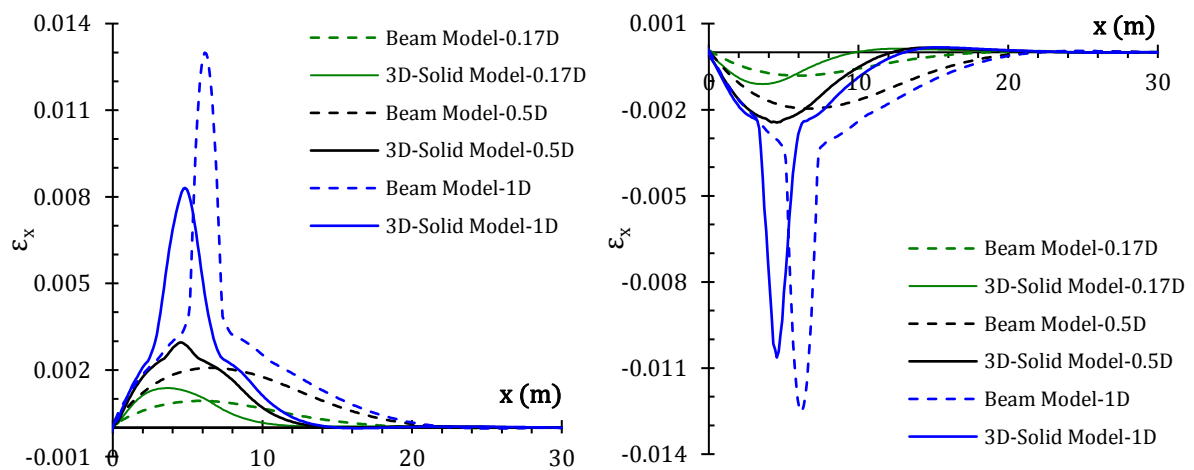


Fig. 6.14. Maximum longitudinal strain of buried pipeline subjected to 60° strike-slip fault 0.17D to 1D movement, 3D-solid model versus Beam model: (a) Left springline (b) Right springline [1].

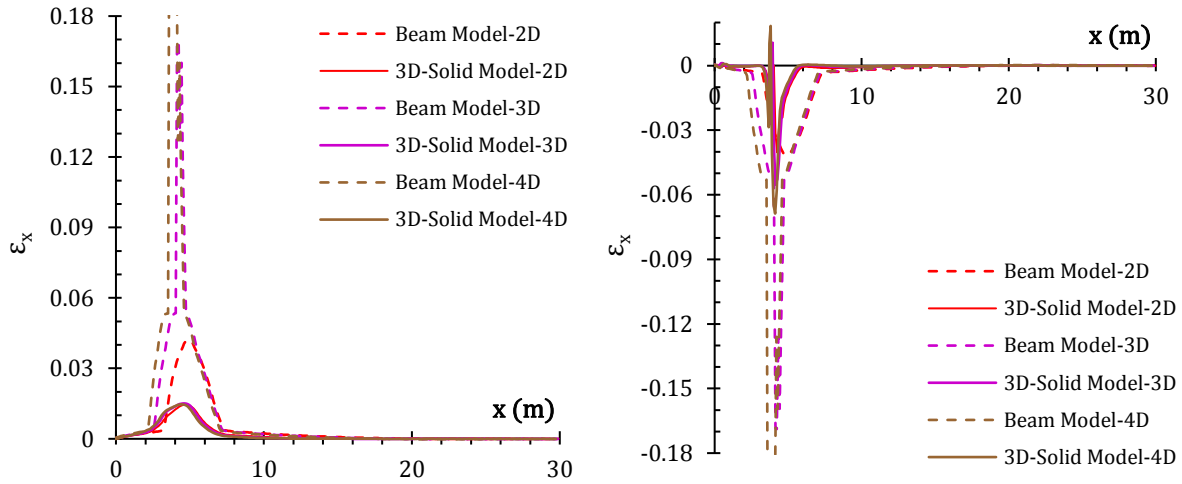


Fig. 6.15. Maximum longitudinal strain of buried pipeline subjected to 60° strike-slip fault 2D to 4D movement, 3D-solid model versus Beam model: **(a)** Left springline **(b)** Right springline [1].

Because of local stiffening of soil material around the fault zone at the 3D-solid model, pipeline experiences higher stresses at elastic zone and maximum stress of pipeline reach yielding stress earlier than beam model. After yielding of the pipeline at local buckling zones cases with deformation over 2D, because of buckling of pipeline, stress response of pipeline is decreasing at local buckling zones and are chaotic. Strain and stress responses of buried pipeline before appearing of local buckling in the 3D-solid model, are similar to the beam model. However, in 3D-solid model after buckling, stress and strain responses are lower than beam model and tensile strain response in cases over 2D fault movement (with local buckling) do not change by increasing of fault movement; though the compression strains are increasing and are very chaotic (because of local buckling).

Indeed, in beam models, in cases over 2D fault movement, strain responses are significantly high and can represent a damaged pipeline possibility correspondingly.

6.6. Conclusions

In this study, 6 cases of buried pipeline subjected to 60° strike-slip fault have been evaluated through beam and 3D-solid modeling approaches. Finally, it has been found that:

- 1- In the 3D-solid model, due to the confinement effect of fault movement on soil around fault zone, soil stiffness increases locally around fault zone.
- 2- High curvature zone for pipeline modeled with 3D-solid approach is shorter than beam approach, because of local stiffening of soil at 3D-solid model.
- 3- Stress and strain responses of buried pipeline before occurrence of local buckling in 3D-Solid model, are higher than beam model.
- 4- After occurrence of local buckling in the 3D-solid model, pipeline strain on springline in beam model drastically increases, which can represent pipeline is damaged.
- 5- In The 3D-solid model damages to pipeline can be observed and in case of beam model strain responses of pipeline can be a good criterion about damage evaluation of the pipeline.
- 6- Creating of the 3D-solid model is much complex than the beam model and it is easy to make mistake in modeling for an amateur analyst, besides modeling and analyzing take much more

time and cost. However, it can reproduce much detailed results and cover all phenomenon.

References

- [1] Talebi, F. Kiyono, J. [2020] “Evaluation of modeling approaches for buried pipeline subjected to strike-slip fault movements” 17th World Conference on Earthquake Engineering, Sendai Japan.
- [2] Karamitros, D., Bouckovalas, G., Kouretzis, G. (2007). “Stress analysis of buried steel pipelines at strike-slip fault crossings,” *Soil Dynamics and Earthquake Engineering* 27, 200–11.
- [3] Trifonov, O. V., Cherniy, V. P. (2010). “A semi-analytical approach to a nonlinear stress–strain analysis of buried steel pipelines crossing active faults,” *Soil Dynamics and Earthquake Engineering* 30(11), 1298–308.
- [4] Karamitros, D. K., Bouckovalas, G. D., Kouretzis G. P., Gkesouli V. (2011). “An analytical method for strength verification of buried steel pipelines at normal fault crossings,” *Soil Dynamics and Earthquake Engineering* (13), 1452-1464.
- [5] Trifonov, O. V., Cherniy V. P. (2012). “Elastoplastic stress-strain analysis of buried steel pipelines subjected to fault displacements with account for service loads,” *Soil Dyn Earthq Eng* 33,54–62.
- [6] Lim, M. L., Kim, M. K., Kim, T. W., Jang, J. W. (2001). “The behavior analysis of buried pipeline considering longitudinal permanent ground deformation,” In *pipeline 2001: advances in pipelines engineering & construction* (San Diego, California), vol. 3, 107. ASCE. [https://doi.org/10.1061/40574\(2001\)3](https://doi.org/10.1061/40574(2001)3)
- [7] O’Rourke, M. J., Vikram, G., Abdoun, T. (2003). “Centrifuge modeling of buried pipelines,” In: *Proceedings of the Sixth U.S. conference and workshop on lifeline earthquake engineering*, August 10–13, 2003, Long Beach, CA. pp. 757–768.
- [8] Sakanoue, T., Yoshizaki, K. (2004). “A study on earthquake-resistant design for buried pipeline using lightweight backfill,” In: *Proceedings of the 13th world conference on earthquake engineering*, Vancouver, B.C., Canada, August 1-6, Paper No.2389.
- [9] Takada, S., Hassani, N., Fukuda, K. (2001). “A new proposal for simplified design of buried steel pipes crossing active faults,” *Earthq Eng Struct Dyn* ;30:1243–57.
- [10] Vazouras, P., Karamanos, S. A., Dakoulas, P. (2010). “Finite element analysis of buried steel pipelines under strike-slip fault displacement,” *Soil Dyn Earthq Eng* ;30:1361–76.
- [11] Vazouras, P., Karamanos, S. A., Dakoulas, P. (2012). “Mechanical behavior of buried steel pipes crossing active strike-slip fault,” *S, Soil Dyn Earthq Eng*;41:164–80.
- [12] Vazouras, P., Dakoulas, P., Karamanos, S. A. (2015). “Pipe–soil interaction and pipeline performance under strike–slip fault movements,” *Soil Dyn Earthq Eng* ;72:48–65.
- [13] Zhang, L., Zhao, X., Yan, X., Yang, X. (2016). “A new finite element model of buried

steel pipelines crossing strike-slip faults considering equivalent boundary springs,” *Eng Struct*;123:30–44.

[14] Demirci, H. E., Bhattacharya, S., Karamitros, D., Alexander, N. (2018) “Experimental and numerical modelling of buried pipelines crossing reverse faults,” *Soil Dyn Earthq Eng* ;114:198–214.

[15] Liu, X., Zhang, H., Li, M., Xia, M., Zheng, W., Wu, K., Han, Y. (2016). “Effects of steel properties on the local buckling response of high strength pipelines subjected to reverse faulting,” *J Nat Gas Sci Eng* ;33:378–87.

[16] ABAQUS/CAE 2017. Dassault Systems Simulia Corp, documentation of 2017 release.

Chapter VII:

Full-scale experiments on buried HDPE pipelines subjected to strike- slip Faults movements

7.1. General remarks

In this chapter, two full-scale experiments are carried out for two 63mm buried HDPE pipeline at a 90° strike-slip fault crossing. Experiments are designated for performance evaluation of the SEKISUI CHEMICAL CO's HDPE pipes subjected to the strike-slip fault movements. Experiments are implemented for 2 cases of loose and dense sands, which based on its results, two 3D nonlinear FEM models are calibrated to evaluate soil-pipe interaction forces beside the HDPE pipeline performance more detailly at strike-slip fault crossing. Moreover, the influence of important variables on the buried HDPE pipeline at 90° strike-slip is studied to improve the seismic design guidelines of buried HDPE pipelines.

7.2. Background

Nowadays, FEM-based analysis offers applicable solutions to the problem of pipelines that cross faults [1]. Recently FEM has been used for the verification and refinement of analytical methods, evaluation of factors influencing pipe response under different types of PGD, and assessment of pipeline performance criteria (e.g., local buckling, ovalization, tensile rupture) [2-14].

Yoshizaki et al. [15] using a large split-box at Cornell University did an experimental study on the effects of PGD caused by pure strike-slip fault movement on buried steel pipelines with elbows, and calibrated FE models for further studies. Palmer et al. [16] described a large-scale testing facility at Cornell University and its working principles. O'Rourke and Bonneau [17] then carried out large-scale tests to evaluate the effects of 60° strike-slip fault movement on high-density polyethylene (HDPE) pipelines and performance evaluation of steel gas pipelines with 90° elbows. Lin et al. [18] performed small-scale tests to analyze the performance of buried pipelines under strike-slip faults. The centrifuge-based approach was first proposed by O'Rourke et al. [18, 19] to model ground faulting effects on buried pipelines and several centrifuge tests have been performed to investigate the response of buried HDPE pipeline subjected to faulting movements [20-25].

Several studies [20–25] have done by centrifuge test to study the effect of various parameters on the performance of HDPE pipelines at earthquake fault crossing. They were accomplished at Rensselaer Polytechnic Institute (RPI) accompanied by several large-scale experiments at NEES facility at Cornell University on buried HDPE pipes. More detailed explanations about experiments are available in the NEESR-SG final report [26]. Rofooei et al. [27] performed a full-scale experiment on a steel pipe under reverse faulting of 0.6 m with a dip angle of 61° and calibrated a three-dimensional FE model using the experimental results. Recently, Demirci et al. [28] studied the behavior of a continuous buried pipeline subjected to reverse fault motion and proposed experimental centrifuge model for reverse faults in addition to a calibrated three-dimensional FE model.

Several experimental studies have been carried out on the behavior of buried pipelines subjected to strike-slip fault movements. However, more experimental research is needed to

investigate the performance of buried HDPE pipelines and their complex soil–pipe interaction at strike-slip fault crossing. There is a need to investigate the performance of the HDPE pipeline buried in special soil types subjected to earthquake fault movements to improve seismic design guidelines of the HDPE pipelines and validate the FE models that are usually created for parametric studies and predicting the buried pipeline performance under seismically-induced PGD.

In this study, two full-scale experiments on HDPE pipelines of the SEKISUI company buried in the noncompacted sand and compacted sand of the Yura river subjected to 90° strike-slip fault with various movement up to $10D$ is accomplished (D is diameter of pipe). Soil properties are extracted through two laboratory triaxial tests and two in site “Lateral Load Test” (LLT) for compacted and non-compacted sand of the Yura river. HDPE pipe material properties are also extracted based on the experiment results for used pipelines [29]. Additionally, Two FE models are created and calibrated using the experimental results. FEM based results are compared with the experimental results for the problem of buried HDPE pipeline subjected to 90° strike-slip fault movement. This study conducted to investigate the performance of buried HDPE pipeline, its damage criteria, and soil-pipe interaction more detailly.

7.3. Split-box size estimation

The full-scale laboratory testing of buried pipelines subjected to strike-slip faulting should allow for field conditions to be closely accounted for. However, it should be noted that simplifying some of the field conditions for laboratory testing is inevitable. A length of buried pipeline which carries forces and moment under strike-faulting is in some cases even up to hundreds of meters in each side [30], however, it is not practical to have a laboratory model with hundreds of meters length of split-box and buried pipeline within. During full-scale laboratory testing, the buried pipeline’s length is limited, and we must neglect further distances from the fault line. Although this pipe length limitation should not carry out randomly. At least three inflection points of pipe transverse deflection at each side of the fault must be inside the split-box to neglect the pipe length limiting effect on the pipe flexural behavior. However, because of the pipe length limitation, missing a part of axial forces along the pipeline is inevitable. For this reason, we have created several nonlinear beam-spring FEM analyses with 2 km length to estimate the appropriate needed split-box length.

7.3.1. FEM analyses for split-box size estimation

We created a FEM-based model for the problem of buried pipelines subjected to a 90° strike-slip fault with nonlinear soil and nonlinear HDPE pipe material. FEM-based analyses were implemented in Abaqus 2017 [31]. For the analysis cases, we model an HDPE pipeline with an external diameter of 0.063 m, the thickness of 0.0058 m without internal pressure, and a total length of 2 km. The pipe material is HDPE with an elastic Young’s modulus of 1 GPa and

Poisson's ratio of 0.46. The pipeline is assumed to be buried under 0.6 m with a unit weight of 1720 kg/m^3 and an internal frictional angle of 36° . Properties of the soil-pipe interaction springs (**Table 7.1**) are calculated based on Hasegawa and Kiyono [32] experiment and seismic design guidelines for a high-pressure gas pipeline in Japan [33].

Table 7.1. Estimated nonlinear soil-pipe interaction springs properties [33].

	Yielding force (kN/m)	Yielding displacement (mm)
Axial direction (k_a)	0.267	2.6
Transverse horizontal direction (k_t)	2.036	9.9

In the creation of a FEM-based model for modeling pipeline, we used a B32 Timoshenko beam element on the basis of shear flexible beam theory, which provides useful results for transverse shear deformation and large axial strain. The soil-pipe interaction spring elements are modeled by connector CONN3D2 elements oriented in three orthogonal directions (schematically shown in **Fig. 7.1**). Two rigid beams are then made as boundary condition input points of the RB3D2 rigid-beam element. The element size after sensitivity analysis is determined. The pipeline is gradually discretized from fine at the fault zone to slightly bigger mesh sizes at further distances (0.0125 to 1 m) symmetric to the fault line. A segment of the FE model is illustrated in **Fig. 7.2**.

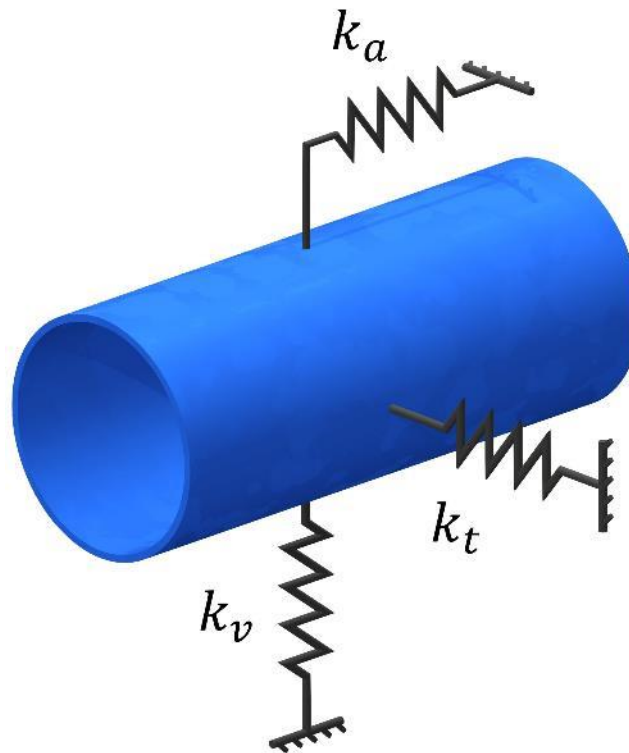


Fig. 7.1. Soil-pipe interaction springs adjustment.

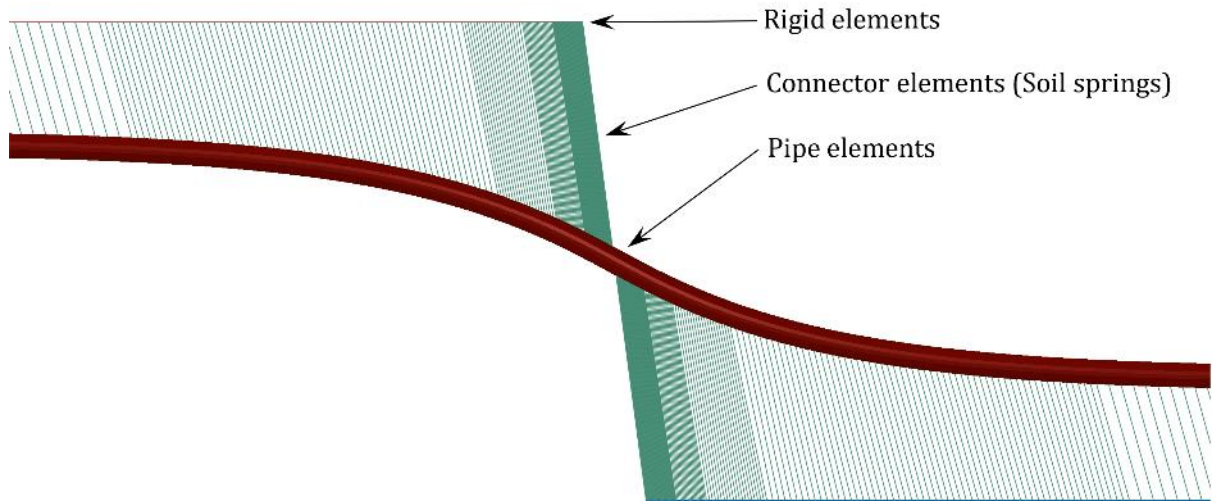


Fig. 7.2. Part of the finite element model and attached soil-pipe interaction springs [30].

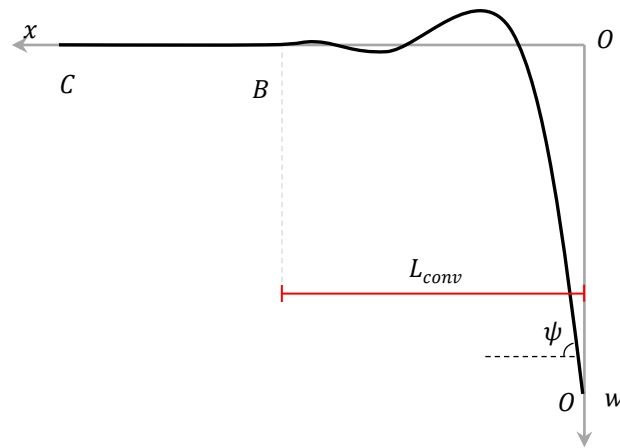


Fig. 7.3. L_{conv} length of the pipeline based on deflection $w(x)$ [30].

In **Fig. 7.3**, L_{conv} is the length of the pipeline between the fault line (point O) and point B where the deflection of the pipeline is almost attenuated [30]. According to FEM analyses, split-box length is estimated to have at least L_{conv} at each side of the fault as **Table 7.2**.

Table 7.2. The FEM analysis cases detail and the FEM analysis results.

Case No.	D* (mm)	Faulting angle φ	Fault Displacement (mm)	Estimated split-box length (m)
1	63	90°	2D = 126	4.3
2	63	90°	4D = 252	4.7
3	63	90°	5D = 315	4.7
4	63	90°	10D = 630	4.9

* : Outer Diameter

According to the **Table 7.2** in **Table 7.3** and **Fig. 7.4**, split-box dimensions are estimated for case of 10D fault dislocation.

Table 7.3. Split-box estimated

	L	W	H
<i>Estimated length (FEM)</i>		$\geq 15D$	$\geq 12D$
<i>Split-box dimensions</i>	5m	1.2m	0.9 m

D pipe's outer diameter =0.063m

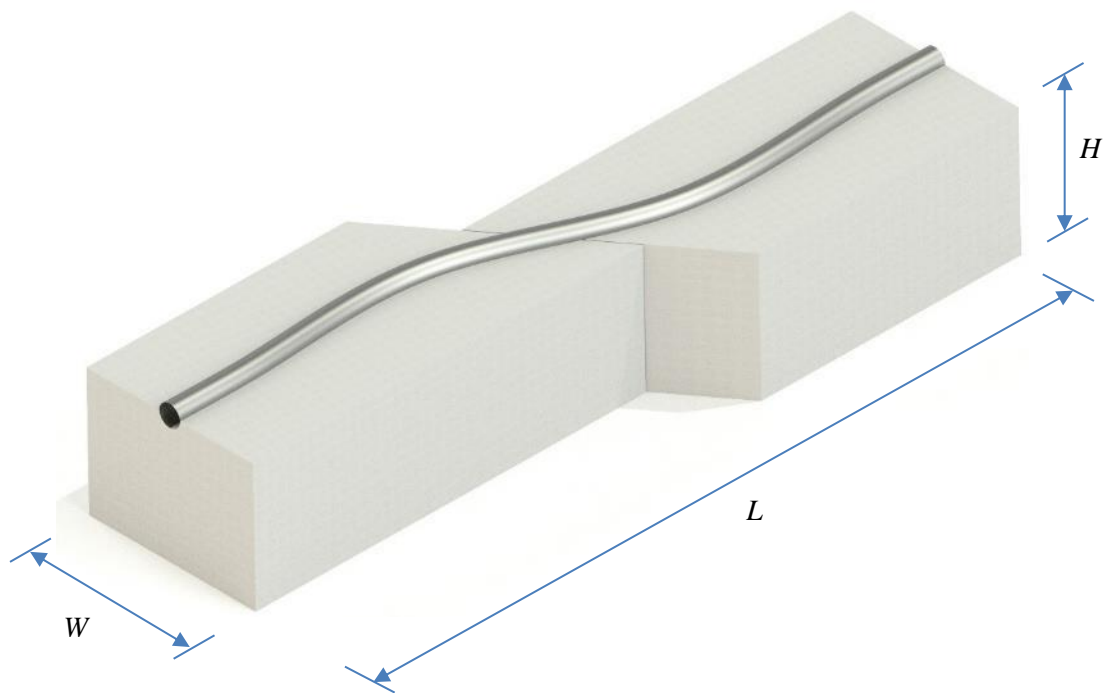


Fig. 7.4. Test box schematic partitions

7.4. Experimental study

7.4.1. Experimental setup

A large split-box is built for studying the behavior of buried HDPE pipelines subjected to strike-slip faulting (**Fig. 7.5**). The split-box is designed to test two 6 m-long steel pipes with roller end supports. Pipe ends at each side of the split-box are closed to translate in vertical and transverse directions, but they are free to slide along pipe normal direction and rotational degrees of freedom all are free. The approximate dimensions of inside the split-box are $5 \times 1.2 \times 0.9$ m (length-width-height) with a faulting angle of 90° . The HDPE pipeline is buried under 60cm sand (pipe's top crown). The strike-slip fault plane is at the center of the split-box, dividing the box into two moving boxes. During the experiments, each of the moving boxes is displaced up to 31.5 cm along the fault plane, which in total is $10D = 63$ cm fault dislocation, as shown in **Fig. 7.5b**. The floor of the test basin is polished steel plates with 1cm thickness to facilitate split-box sliding during the faulting. The configuration of the test basin can be reasonably modified to meet alternative test configurations.

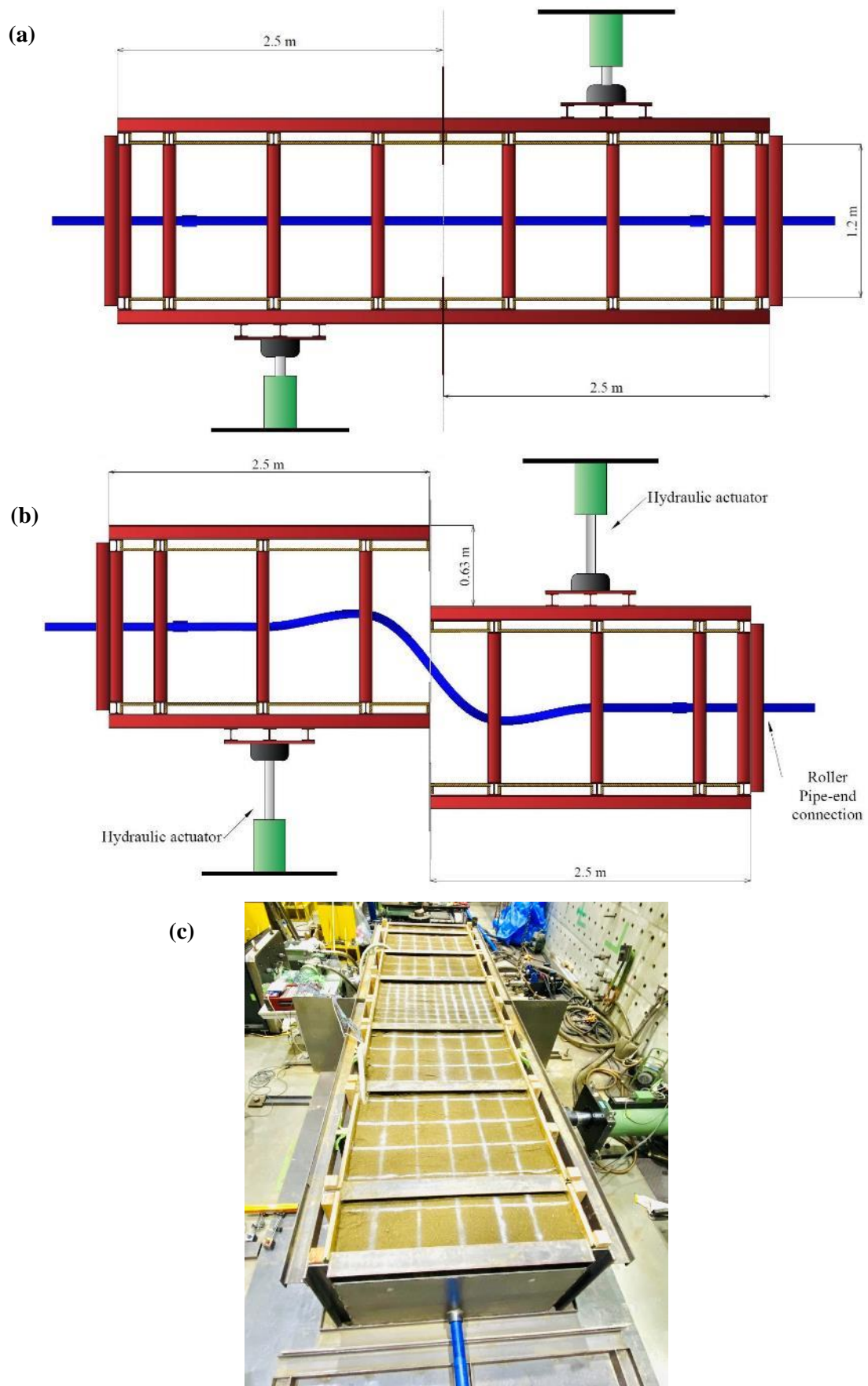


Fig. 7.5. The split-box test basin for 90° strike-slip faulting: (a) sketch before faulting, (b) sketch after 10D faulting, (c) photograph of the experiment split-box.

The split-box framing is composed of W-shape steel sections with 24mm oriented strand board (OSB) panels as sheathing and steel plate as decking and Faultline covering. Each part of the split-box, when filled with sand, will weight approximately 4650kg and 3800kg in compacted (dense sand) and non-compacted sand (loose sand) cases. Four rails, two at the fault-interface as plates and two on the external frames were used to guide the moving part of the split-box, as it is shown in **Fig. 7.5**. Two hydraulic actuators in the tests are synchronized to have the same transverse displacement. The external frames were considered to improve the stability of the moving part. Two hydraulic actuators are placed at opposite sides of the split-box and are configured, aligned with the fault line. During the faulting test, both actuators were moving simultaneously.

7.4.2. Experiment material

The soil used in these experiments is well-graded sand (SW) from the Yura river in Kyoto, which commonly used as backfill, with a water content of about 13.4%. This sand is used for filling the split-box in compacted and non-compacted cases which in this paper, they are called loose sand and dense sand cases, relatively. The grain size distribution of the sand in this study is shown in **Fig. 7.6**, and details are presented in **Table 7.4**. Dense and loose sand's nonlinear properties are determined based on two triaxial shear consolidated drained tests, as shown in **Fig. 7.7** and its results are detailed in **Fig. 7.8** and **Table 7.4**. Two lateral load test (LLT) is done inside the split-box in 60 cm depth (same with pipe level) before doing the faulting test (see **Fig. 7.9**) to determine the elastic modulus of the loose and dense sand cases (see **Table 7.4**). HDPE pipelines in the experiments are Eslo hyper JW pipes of the Sekisui company, manufactured according to PE100. HDPE material's elastic Young's modulus is 1000 MPa, Poisson's ratio is 0.46, and its stress-strain curve is extracted from tensile test and compression test, which are shown in **Fig. 7.10**.

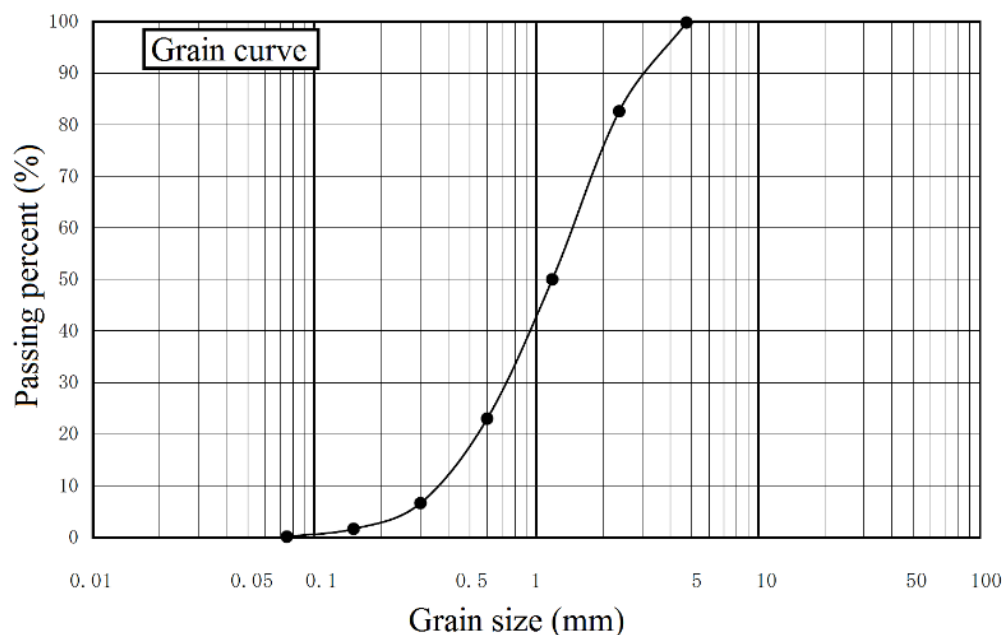


Fig. 7.6. Loose and dense sand grain size distribution.



Fig. 7.7. Triaxial shear test (CD) photograph.

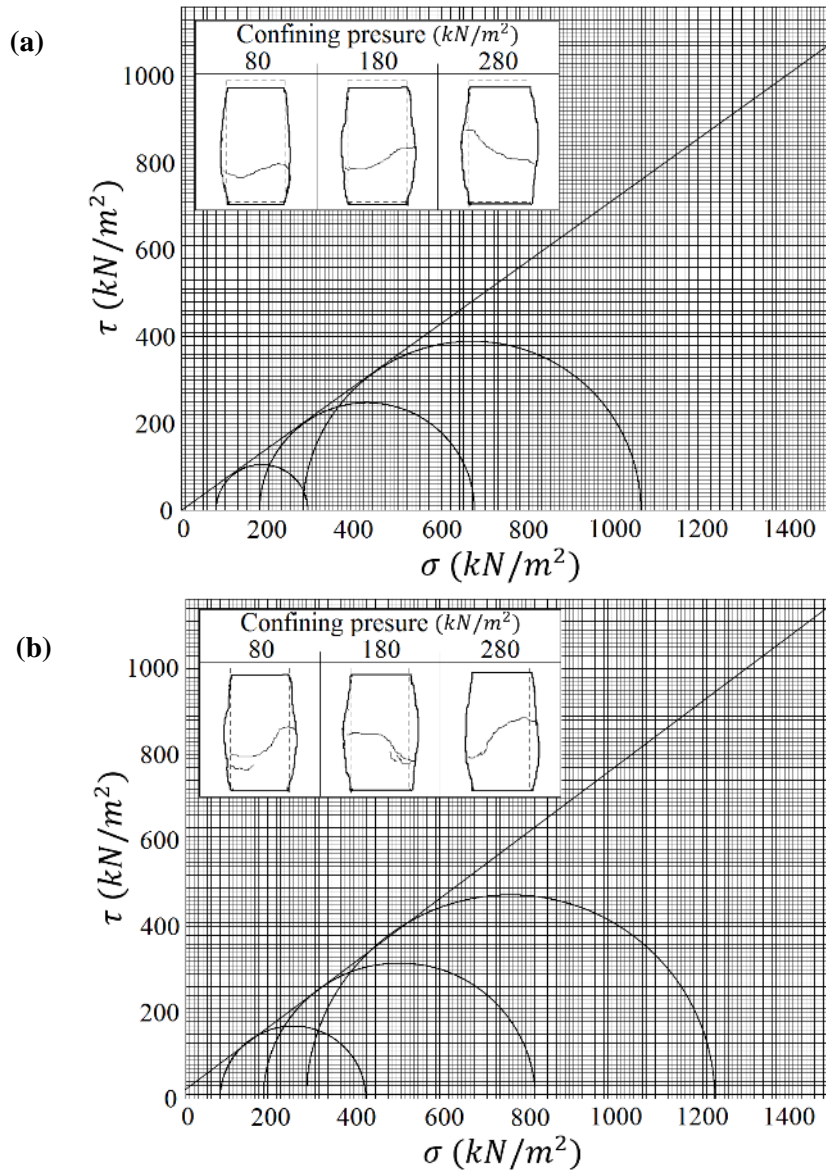


Fig. 7.8. Triaxial shear consolidated drained test results: (a) Loose sand ($D_r = 75\%$), (b) Dense sand ($D_r = 95\%$).



Fig. 7.9. Lateral load test (LLT) inside the split-box, before faulting.

Table 7.4. Loose and dense properties based on aggregate test, triaxial CD testes and LLT.

	Loose sand	Dense sand
Specific gravity G_s (kg/m^3)	2687	2787
Wet density γ_t (kg/m^3)	1527	1853
Dry density γ_d (kg/m^3)	1347	1634
Water content ratio w_n (%)	12.5-13.5	12.5-13.5
Optimum water content ratio w_{opt} (%)	13.8	13.8
Average particle size D_{50} (mm)	1.18	1.18
Elastic modulus E_s (Mpa)	0.102	4.717
Ground reaction coefficient k_m (kN/m^3)	1888	90663
Friction angle φ	35.7°	36.9°
Cohesion C_d (kN/m^2)	0.0	22.2

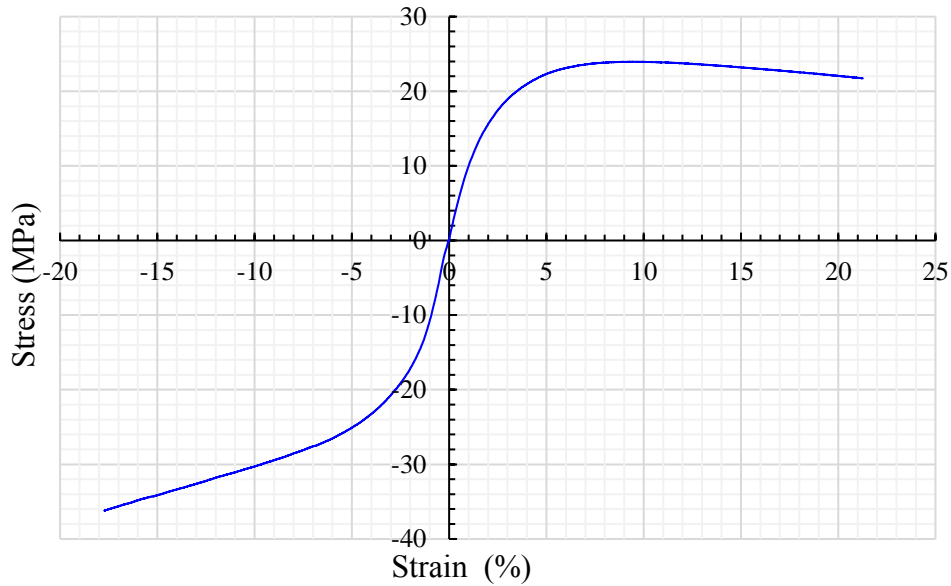


Fig. 7.10. HDPE pipe material stress-strain curve extracted from tensile/compression tests.

7.4.3. Instrumentation

To monitor the behavior of the buried pipeline during faulting experiment, each of the pipelines is equipped with 40 strain gauges on the springlines (see **Fig. 7.11**) of pipes and 9 strain gauges on the crown of pipes in 20 stations to measure the strains in the longitudinal direction during the faulting. The strain gauges used in this study are YEFLA-5 post-yield strain gauges made by Tokyo Measuring Instruments Laboratory Co. Ltd which are applicable to the measurement of large strain up to 10 to 15%. The strain gauges are attached to the HDPE pipe using CNY adhesive, produced by the same company. 2 displacement transducers at sides of each the moving parts of the split-box parallel to the Faultline are instrumented to measure the split-box lateral movements (strike-slip fault movement). Used displacement transducers (SPD-300D/NJ-NP) and data logger (YDS-530) in this study are also made by Tokyo

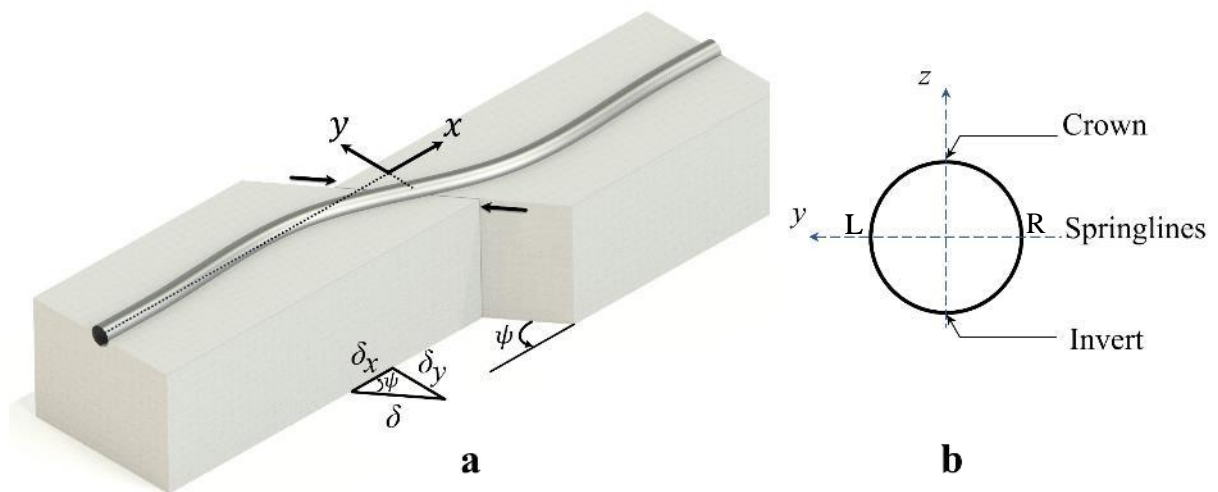


Fig. 7.11. Buried pipeline subjected to a strike-slip fault with faulting angle of (ψ). **(a)** Schematically 3D view [30], **(b)** Pipe section.

Measuring Instruments also made by Tokyo Measuring Instruments Laboratory Co. Ltd. For higher accuracy strain gauges are also attached to the pipe crown at 9 stations along the pipeline.

7.4.4. Experiment model

Split-box designed and built with steel frames have an approximately rigid behavior during the faulting. The experiment of the HDPE buried pipeline subjected to a strike-slip fault in a 90° crossing is shown schematically in **Figs. 7.5a** and **7.5b**. The experiment is done for two cases of HDPE pipeline buried in loose and dense sand. After instrumenting the strain gauges on the HDPE pipes (see **Fig. 7.12**) and instrumenting the displacement transducers on the moving parts of the split-box, a pipe is put inside the split-box and the split-box filled with sand using cranes and soil packs. The loose sand case has very low compaction and dense soil case is compacted well. Approximately 6 m^3 of soil is placed in three lifts, approximately, each 300 mm thick, and is compacted using a vibrator tamping rammer. Finally, the soil surface was prepared by levelling and painting gridlines as shown in **Fig. 7.13**. In **Fig. 7.13** dashed and continuous lines represent the pipeline and fault trace, respectively. The experiment is a displacement-controlled test, where the moving parts of the split-box are displaced using two actuators at each side of the pipeline up to a final displacement of $10D = 0.63 \text{ m}$. The burial depths for both tests were kept similar to their field installations depths (0.6 m from the pipe crown). **Table 7.5** explains the details of the two full-scale experiments, which are designed to study the behavior of HDPE buried pipelines at 90° strike-slip fault crossing with special attention to the influence of soil stiffness. Both tests have no internal pressure inside the pipeline during the faulting.



Fig. 7.12. Setup of the sensors.

Additionally, in both tests, each HDPE pipeline has two joints at both sides of the pipeline at 0.5 m offset from the end of split-box, as shown schematically in Fig. 7.5(a).

Table 7.5. Details of the experiment cases.

Test no.	Soil type	D (m)	t(m)	H(m)	H/D	Faulting angle	Fault dislocation (m)
1	Loose sand	0.063	0.0058	0.6	9.52	90°	10D = 0.63
2	Dense sand	0.063	0.0058	0.6	9.52	90°	10D = 0.63

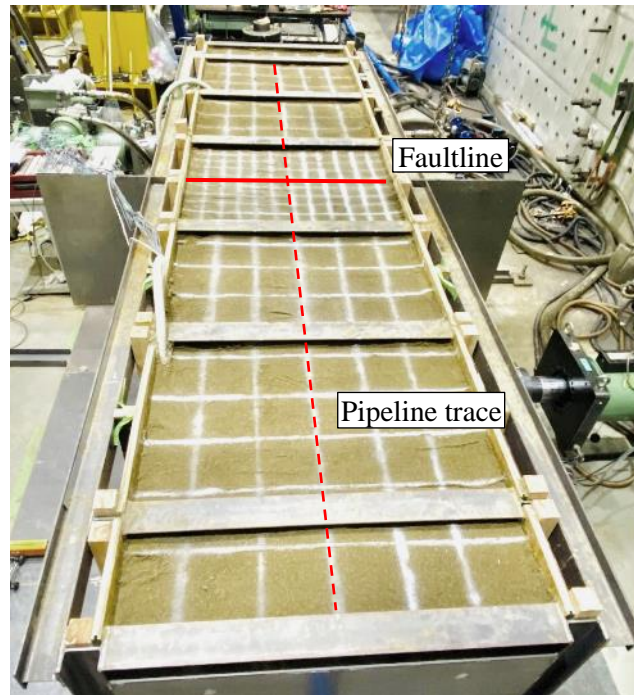


Fig. 7.13. Faultline and soil surface gridlines in experiment, fine and coarse grids size are 0.1 m and 0.2 m, respectively.

7.5. Experiment results

Two experiments result detailly monitored during the faulting experiments. And results are presented below.

7.5.1. Deformation results

7.5.1.1. Soil deformations

Cracks on soil surface observed mainly around the fault during both experiments. The cracks and soil failure plane on the fault line reached the soil surface in early stages after 0.12 m and 0.04 m fault movement in loose and dense soil tests, respectively. And then major cracks started to grow exactly on fault plane and around the fault zone in the range of 1 m in loose and dense sand cases, respectively. However, in loose sand case, some cracks in further distances observed but the reason of these cracks is settlement of loose sand because of pipe movement. It should be noted that the openings of the cracks for the dense sand case were wider due to the

larger soil–pipe interaction forces and larger frictional forces in the fault plane. An uplift expansion of soil around the fault plane observed in both tests, which its level in case of loose and dense soil was almost 20mm and 55mm, respectively. And maximum observed settlement of soil in loose and dense sand cases were 120 mm and 3 mm, respectively. The soil surface deformation for both tests at $10D = 0.63$ m movement is shown in **Fig. 7.14**.

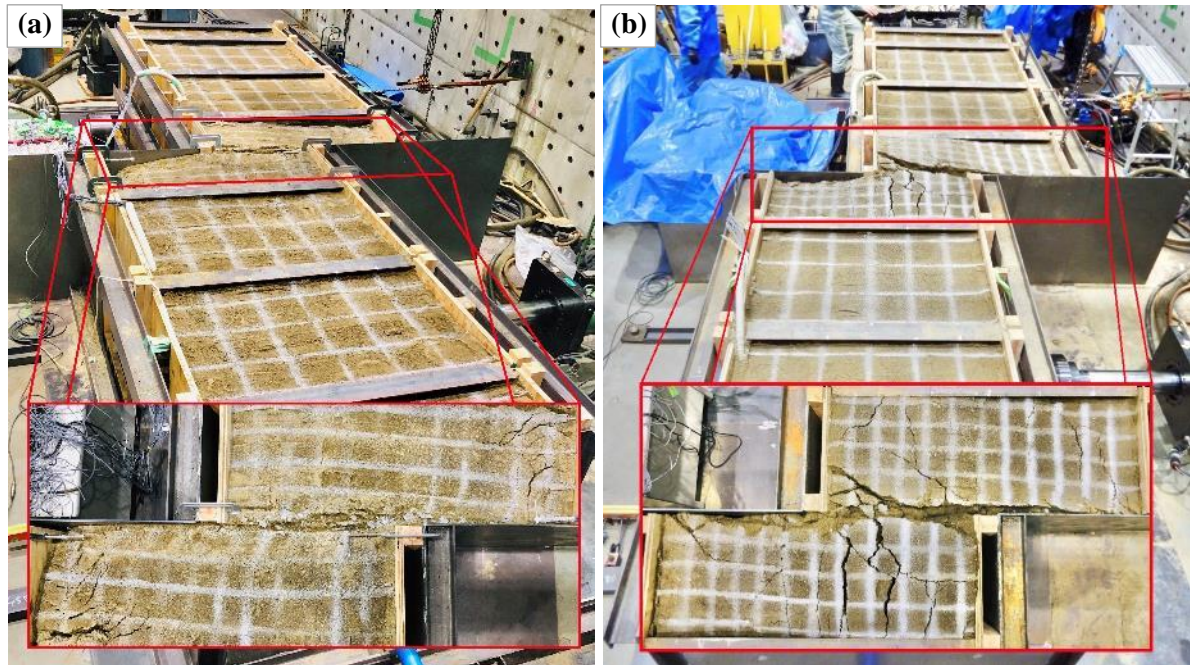


Fig. 7.14. Surface deformation at $10D = 0.63$ m strike-slip fault movement: (a) case 1 (loose soil), (b) case 2 (dense soil).

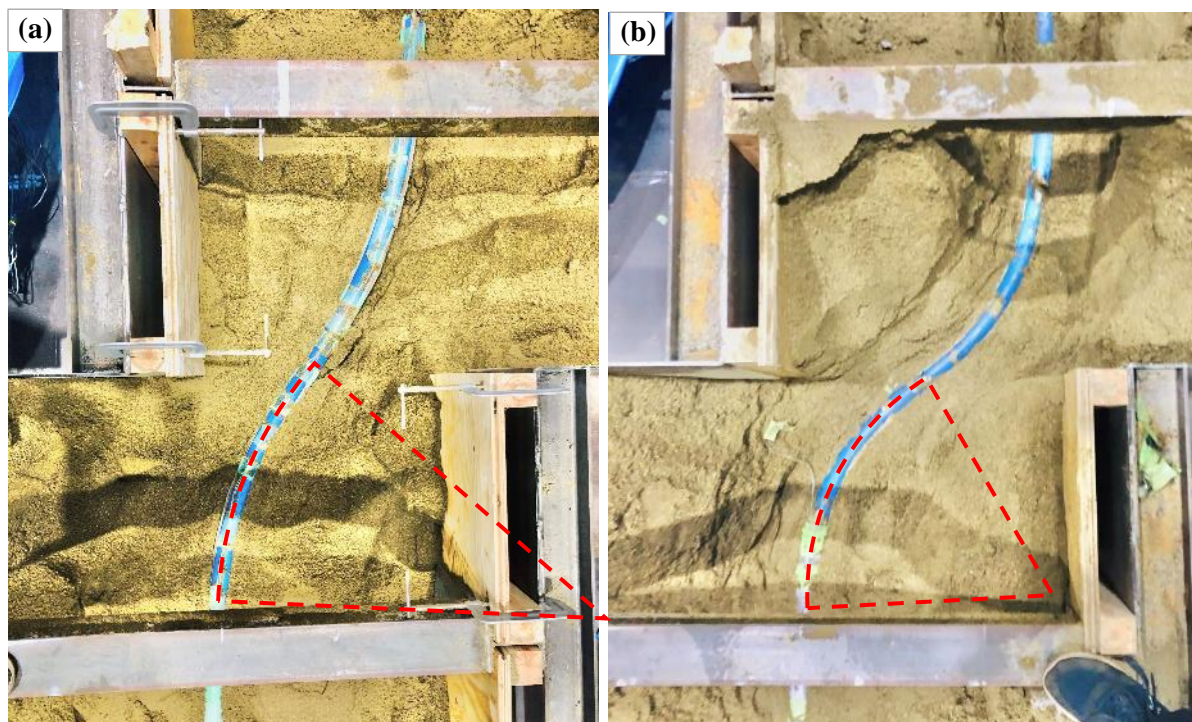


Fig. 7.15. HDPE pipe deformation at $10D = 0.63$ m strike-slip fault movement: (a) case 1 (loose sand), (b) case 2 (dense sand).

7.5.1.2. Pipe deformations

HDPE pipelines in both tests have an S-shape deformation. According to **Fig. 7.15**, HDPE pipes are not buckled up to the 10D fault movement. Although, in the case of dense soil, partial ovalization is observed at the high curvature zone, which at fault crossing, pipe's diameter has a 4 mm decreasing on springline direction and 2 mm increasing on pipe crown direction. The high curvature zone in case of loose sand is longer than dense soil case, and accordingly, in dense sand case, the pipe bends more sharply, and hence have higher curvature (see **Fig. 7.15**). In another word, as much as the soil is stiffer, pipe curvature is higher, and the high curvature zone is shorter.

After finishing the faulting test, the sand over the pipe in a V-shape form is removed and

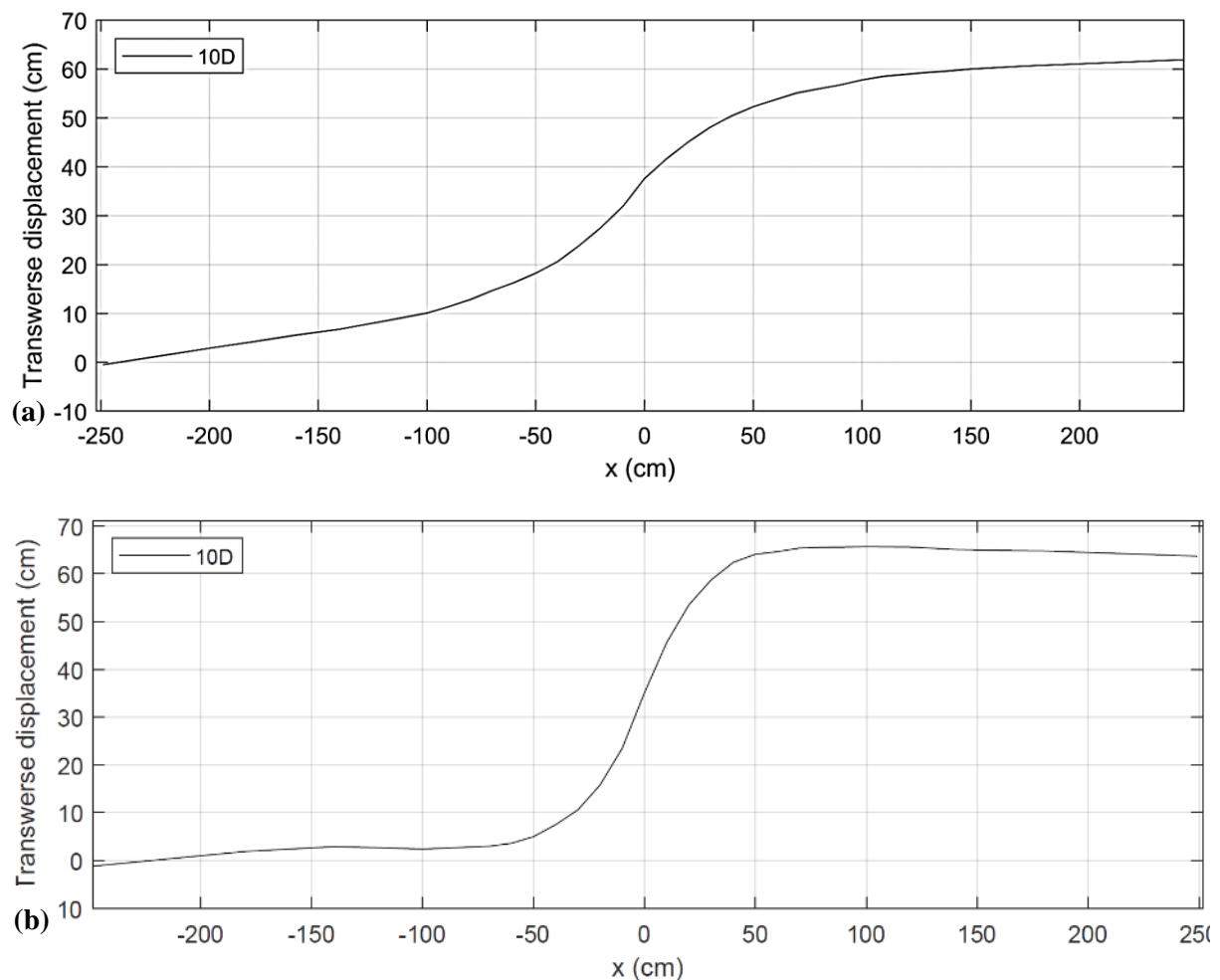


Fig. 7.16. HDPE pipelines deflection at $10D = 0.63\text{ m}$ fault movement: (a) Loose sand case, (b) Dense sand case.

the HDPE pipelines deflection at the final stage (10D fault movement) is measured, which its results are presented in **Fig. 7.16**. Regarding **Fig. 7.14** and **7.15**, it is evident that the high curvature zone length of the pipeline in dense sand case (test 2) is much shorter than the loose sand case. At 10D fault movement, in test 2 (dense sand case), 8 and 10 cm axial sliding of pipeline in each side of the split-box is observed.

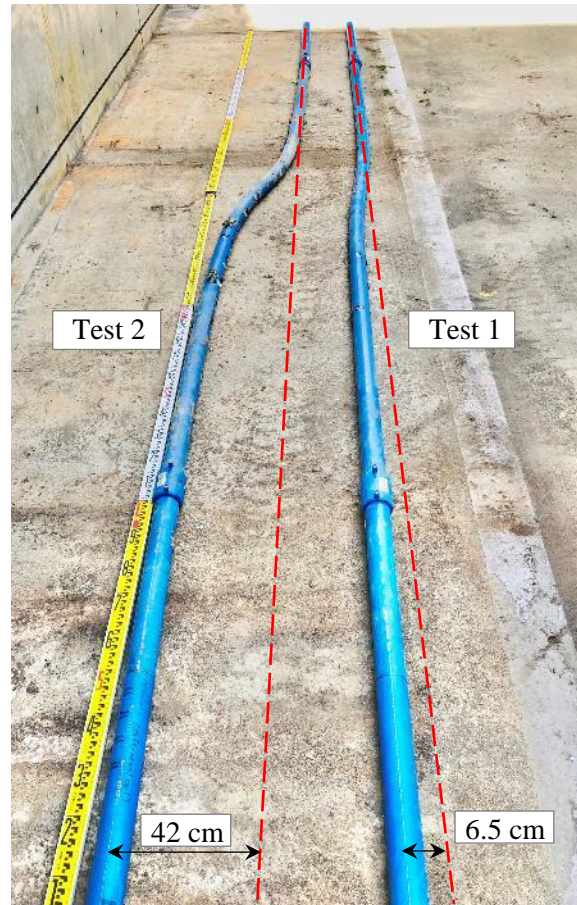


Fig. 7.17. Residual deformation of the pipeline after faulting experiments.

After completely removing the sand from the split-box, both HDPE pipes had residual strains and deformations which remain after removing the faulting load. As shown in **Fig. 7.17**, total residual deflections of the pipelines at both ends are 6.5 cm and 42 cm in loose sand and dense sand cases, respectively. Which represents that HDPE pipe buried in dense soil, due to the higher soil-pipe interaction forces experienced much higher plastic strains.

7.5.2. Strain results

Buried HDPE pipelines are monitored using strain gauges during the two faulting experiments. However, some unexpected failures happened in strain mainly, in very large fault movements of 8D and 10D at the dense sand case. We deem these failures mainly happen because of reaching strain gauge ultimate strain, using vibrator tamping rammer for compaction of the sand, and some human errors in laboratory testing procedure.

Strain gauges results are discrete results along the HDPE pipeline. To have a continued strain result along the pipeline, we did cubic interpolation analyses on the strain gauges results and approximately predicted the strain of the pipeline between two strain gauges. In **Figs 7.18–7.22**, black nodes and continuous lines represent the strain gauges results and interpolated strains between two strain gauges, respectively.

7.5.2.1. Longitudinal strain on the pipe springlines

Fig.18 and **Fig.19** show the monitored and predicted longitudinal springlines strains along the HDPE buried in loose sand and dense sand with different levels of strike-slip fault movement (2D –10D), respectively. where D, is pipe outer diameter. The strain distribution follows a similar trend in both the experiments. However, in the dense sand experiment (test 2), the HDPE pipeline experienced higher plastic strains and after the 8D fault movement, some of the strain gauges are failed. In loose sand case (test 1), maximum strains appeared in ± 30 cm from the fault plane. however, the HDPE pipeline didn't experience a high level of plastic strains and did not reach the HDPE material's ultimate stress. In the case of dense sand (test 2) after 2D fault movement, HDPE pipe at some parts of high curvature zone experiences plastic strains, and up to 10D fault movement pipe in all the high curvature zone has plastic strains.

As we know, the bending stress is much higher than axial and shear stresses in a buried pipeline subjected to a 90° strike-slip fault movement. Therefore, in this problem, maximum stress/strain happens on the springlines of the pipeline [34]. In this study, maximum

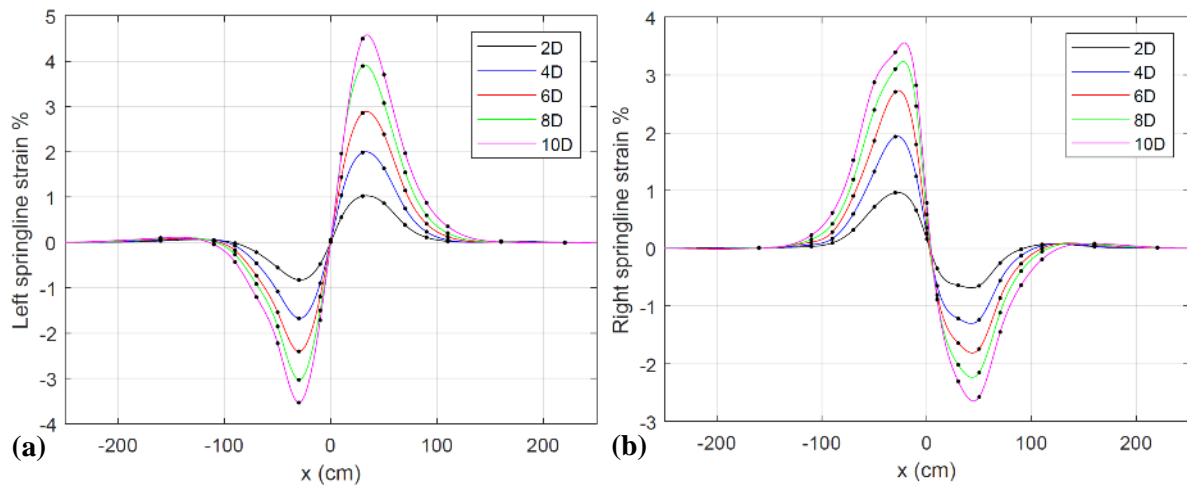


Fig. 7.18. longitudinal strain on springlines of the HDPE pipeline buried in loose sand (test 1) at 2D–10D fault movements: (a) Right side (b) Left side.

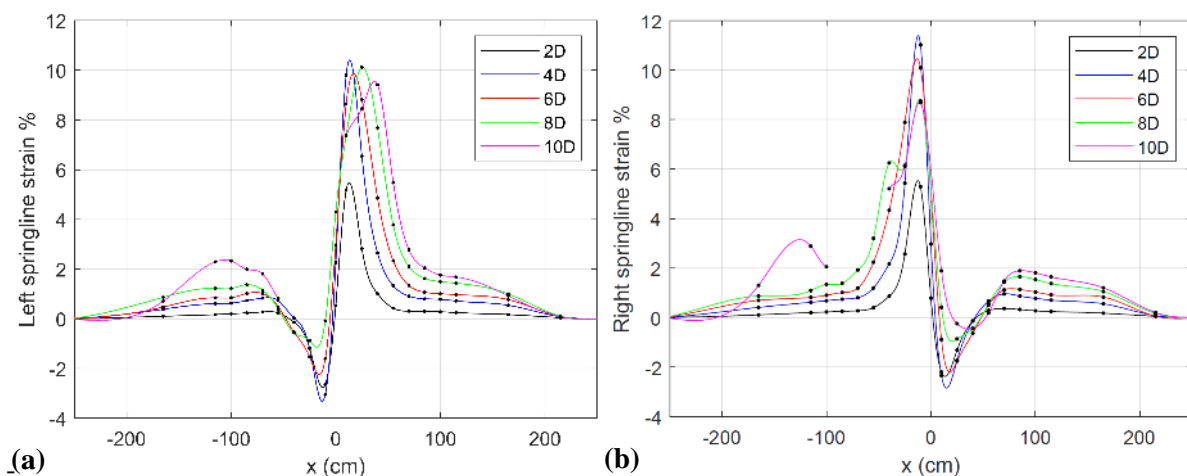


Fig. 7.19. Longitudinal strain on springlines of the HDPE pipeline buried in dense sand (test 2) at 2D–10D fault movements: (a) Right side, (b) Left side.

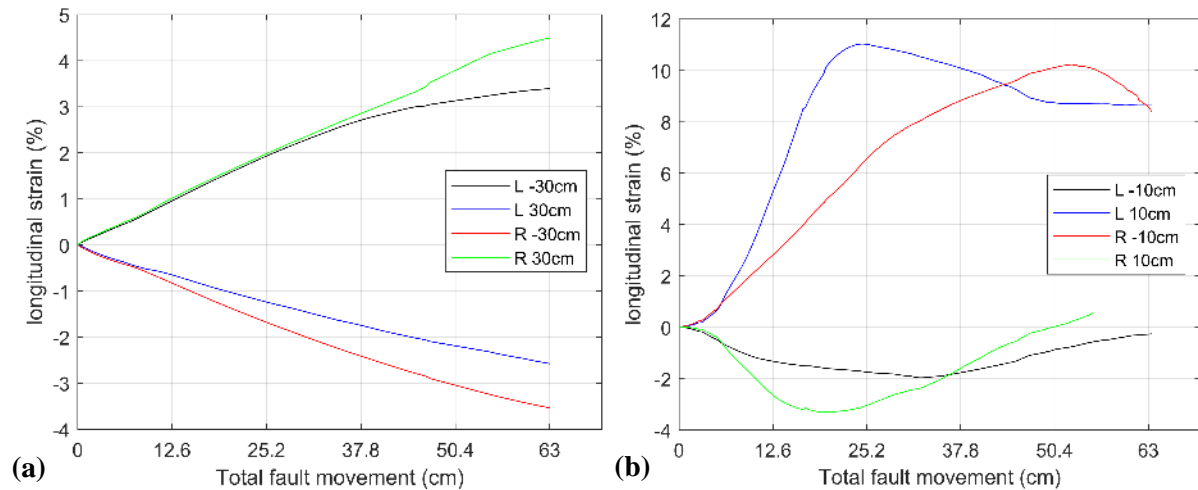


Fig. 7.20. Peak longitudinal strain growth on pipe springlines: **(a)** loose sand case (test 1) at ± 30 cm from fault plane, **(b)** Dense sand case (test 2) at ± 10 cm from fault plane.

longitudinal strains of HDPE pipe on springlines observed at ± 30 cm and ± 10 cm strain gauges from Faultline in loose sand (test 1) and dense sand (test 2) cases, respectively. Maximum recorded longitudinal tensile strains of buried HDPE pipeline by strain gauges are 4.5% and 11% in test 1 and test 2, respectively. And maximum recorded longitudinal compression strains of the pipe by strain gauges are 3.5% and 3.3% in test-1 and test 2, respectively. Which strain growth of strain path at maximum points during the fault movements for both experiments are shown in **Fig. 7.20**. Regarding **Fig. 7.10**, HDPE pipe material reaches its ultimate stress at around 9.5% strain, and after this strain, bearing stress of material won't increase and even gradually decreases up to the failure of the material. **Fig. 7.20b** in R 10cm strain gauge (left side strain gauge in 10 cm distance from Faultline), shows that strain of HDPE pipeline at around 4D fault movement after reaching 11% gradually decreases. Hence after yielding and passing the ultimate stress of HDPE material, by increasing the plastic strains the flexural stiffness of pipeline decreases in this cross-section. Since the prominent stress/strain in this experiment is the bending stress/strain, by decreasing the flexural stiffness of pipeline, stress and strain in this section decreases. Because of higher flexural stiffness in adjacent sections, maximum bending moment moves to the adjacent sections in pipe both ends directions. Accordingly, stress and strain of pipe in these cross-sections gradually increase up to reaching the ultimate stress of the HDPE, and after that same phenomenon happens. For better understanding, in **Fig. 7.19a**, maximum strains from 4D to 10D gradually moves from L 10 cm strain gauge to the around L 40 cm strain gauges, and the maximum strains are decreasing because of decreasing the flexural stiffness at these cross-sections.

7.5.2.2. Axial and bending strain

In the problem of buried pipeline in strike-slip faulting crossing, the pipe is subjected to bending moment, axial force, and shear force which the bending moment in 90° faulting is predominant force. On the springlines of the buried pipeline during the faulting, almost there is no shear stress/strain. Therefore, longitudinal strains on springlines are a combination of

axial and bending strains. **Fig. 7.21** and **Fig. 7.22** showing axial strain and bending strain of the HDPE pipe along the pipeline in test 1 and test 2. The axial strain of pipeline, in dense sand case (test 2), is much higher than loose sand (test 1), which is because of higher soil-pipe interaction forces in stiffer sand. As mentioned in the previous section, and also based on **Fig. 7.21**, HDPE pipeline in test 1 almost has not experienced plastic strains. Which the peak axial strain, peak tensile bending strain, and peak compression bending strain of HDPE pipe in test 1 are 1.1%, 3.5%, and 3.4%, respectively. In test 2, HDPE pipeline experienced higher soil-pipe interaction forces, and consequently, higher axial and bending strains in the plastic range that the peak axial strain, peak tensile bending strain, and peak compression bending strain of HDPE pipeline are 4.6%, 7%, and 6.2%, respectively, as shown in **Fig. 7.22**.

Regarding **Fig. 7.21a** in test 1, in position -30 cm result of axial strain is weird, and it seems left strain gauge in position -30 cm is not adjusted perfectly and has a little eccentricity from pipe springline direction. However, other positions have valid results.

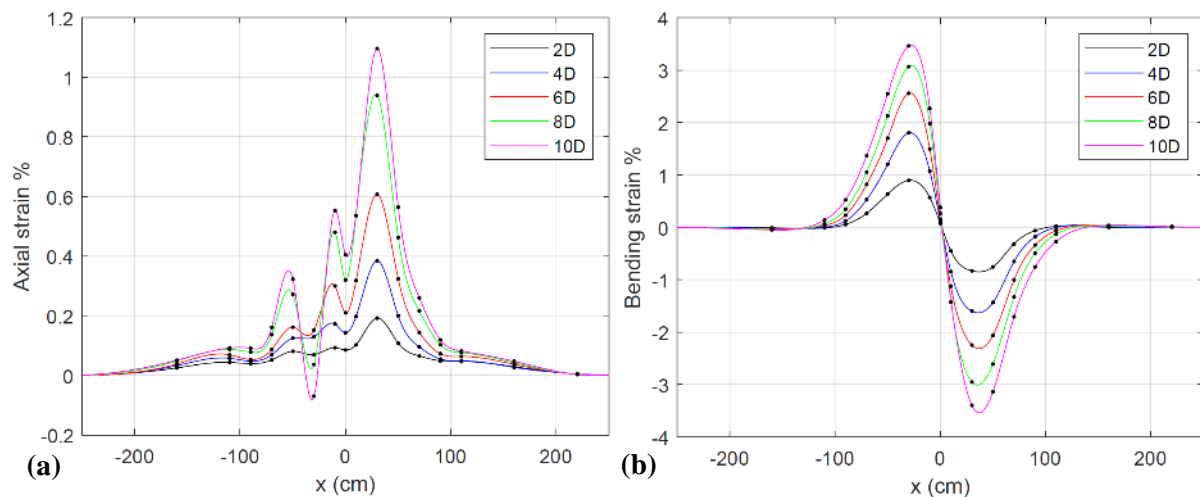


Fig. 7.21. Strain distribution of the HDPE pipeline buried in loose sand (test 1) at 2D–10D fault movements: (a) Axial strains, (b) Maximum bending strains.

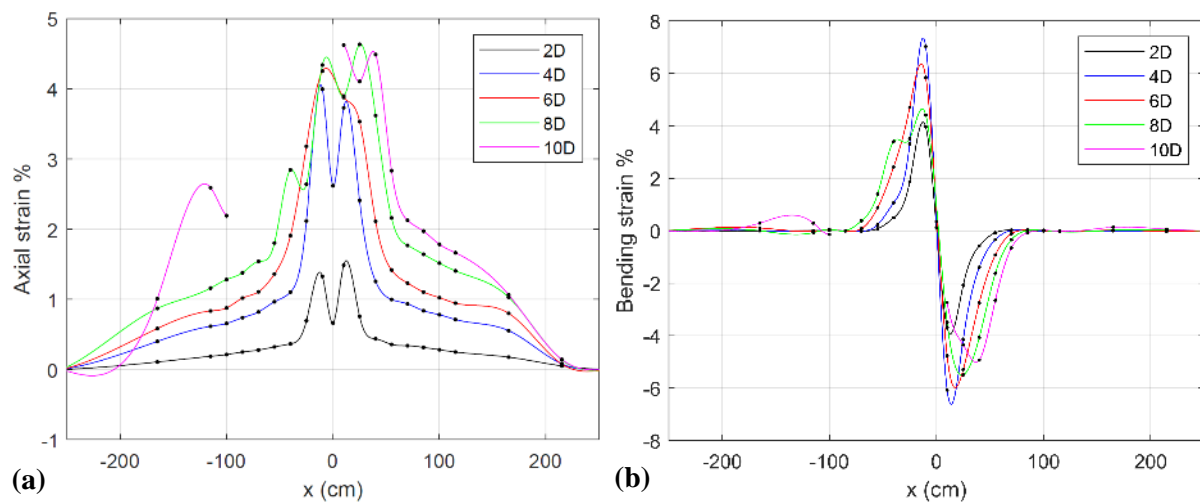


Fig. 7.22. Strain distribution of the HDPE pipeline buried in dense sand (test 2) at 2D–10D fault movements: (a) Axial strains, (b) Maximum bending strains.

Based on the results of **Fig. 7.21** and **Fig. 7.22**, axial strains and bending strains (on springline) of the HDPE pipeline increase by increasing the fault movement up to a limit that longitudinal strain on springline reaches around strain corresponding to the ultimate stress of HDPE and has large plastic strains. After that by increasing the fault movement, peak axial strain increase rate drastically decreases and then remains almost same and by further fault movements, a longer length of pipeline reach to peak strain range, and in bending strains after reaching that ultimate stress limit because of flexural stiffness drop in peak bending strain cross-section, by increasing the fault movement peak bending stress/strain drops and gradually moves to further cross-sections from the fault plane. This procedure continues up to a fault movement that damage appears on the pipeline (e.g. local buckling, wrinkling, and ovalization).

7.5.3. Local buckling and ovalization

In past experimental studies on steel buried pipeline at fault crossing [35], several equations are proposed for critical stress/strain of pipeline at local buckling limit, which all unanimously show an inverse relationship between D/t and pipe critical strain at buckling moment. However, there is no exact equation only for HDPE pipelines. In this study, D/t is 11.9, which is a low number and made pipe hard to buckle. Gresnigt [36] in 1986 proposed an empirical equation for the critical buckling strain of pipeline (Eq. (7.1)), including the pipe internal pressure effect, which used in the 2001 ALA pipeline guideline [37] and 2005 ALA water pipeline guideline [38].

$$\varepsilon_{cr-ALA} = 0.5 \frac{t}{D} - 0.0025 + 3000 \left[\frac{(P_i - P_e) \cdot D}{2tE_s} \right]^2 \quad (7.1)$$

where P_i is the internal pressure, assumed to be larger than the external pressure P_e and E_s is secant modulus of elasticity.

In 1995, Zimmerman et al. [39] compared test data and various empirical curves for the onset of wrinkling. According to this comparison, the empirical equation by Stephens et al. [40] was judged to be the more appropriate lower bound limitation to have higher safety factor:

$$\varepsilon_{cr-Steph} = 2.42 \left(\frac{t}{D} \right)^{1.59} \quad (7.2)$$

In our study, ε_{cr-ALA} and $\varepsilon_{cr-Steph}$ are 4.4% and 5.5%, respectively. Observed peak longitudinal compression stress of HDPE pipeline buried in loose sand (test 1) and dense sand (test 2) are 3.5% and 3.3% respectively which are lower than ε_{cr-ALA} and $\varepsilon_{cr-Steph}$, And no buckling damage observed in test 1 and test 2 up to 10D fault movements.

The factor of ovality is defined in Eq. (7.3) to represent the degree of distortion of the pipe cross-section. In Eq. (7.3) f_o is factor of ovality, D_{min} and D_{max} are minimum and maximum diameters of the pipe cross-section after ovalization, respectively.

$$f_o = \frac{D_{max} - D_{min}}{D} \quad (7.3)$$

In case of loose sand (test 1), almost there is no ovaliation on the HDPE pipe cross-section, and f_o is almost zero. However, in dense sand (test 2), HDPE pipe cross-section at 10D movement has ovalized, and f_o is 0.1.

7.6. 3D nonlinear FEM simulations

We created two three-dimensional (3D), nonlinear finite element models, for two tests of buried HDPE pipelines subjected to 90° strike-slip movement (models are shown in Table 7.5), beside a 3D nonlinear FE model for buried HDPE pipeline push-in test, all the FEM models include the soil and pipe materials' nonlinearity and geometrical nonlinearity effects. FEM-based analyses are implemented in Abaqus 2017 [41].

In this section, our final goal is to calibrate and verify 3D FE models for buried HDPE



Fig. 7.23. Push-in experiment for 63 mm HDPE pipeline buried in dense sand (95% compacted sand) by Nishikawa 2017 [42].

pipelines subjected to 90° strike-slip fault movement versus full-scale experiments. We calibrated FE models, to study soil-pipe interaction and HDPE buried pipeline performance at strike-slip fault crossing. Since soil-pipe interaction (contact properties) of these models are so complex, firstly, we created an FE model of Nishikawa et al. [42] push-in test for the HDPE pipeline with identical soil properties, pipe size, and buried depth with dense sand (test 2) and calibrated the soil-pipe interaction of FE model based on this experiment. Secondly, we extended the calibrated FE model to our full-scale loose and dense sand tests, and finally verified the results of FE models against test 1 and test 2 experiments.

7.6.1. Calibration of soil-pipe interaction

In 2016 Nishikawa et al., conducted push-in tests on buried HDPE pipelines to extract HDPE pipeline's axial soil-pipe interaction curve, see **Fig. 7.23**. In one of their push-in tests, experiment conditions are identical to our test 1 (dense sand) experiment. In this test, HDPE pipeline's outer diameter is 0.063, pipe thickness is 0.0058 m, with an internal water pressure of 0.5 Mpa, pipe material is same (**Fig. 7.10**) and the pipe is buried in 0.6 m within the same dense sand with almost similar compaction ratio (Table 7.4). In this model, for the creation of the FEM-based model of pipeline and soil, we used continuum C3D8R elements with 8-node linear brick, reduced integration, and hourglass control. Elements geometry is distributed in

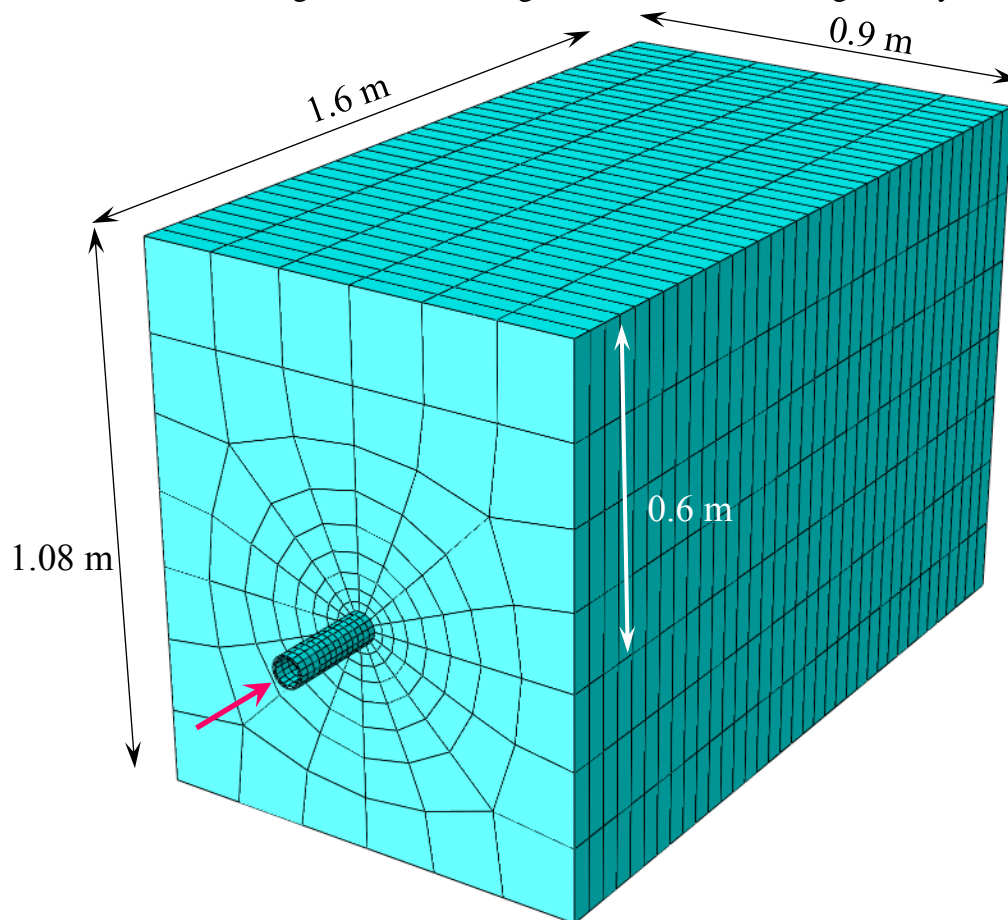


Fig. 7.24. 3D FEM model geometry and meshing of push-in test.

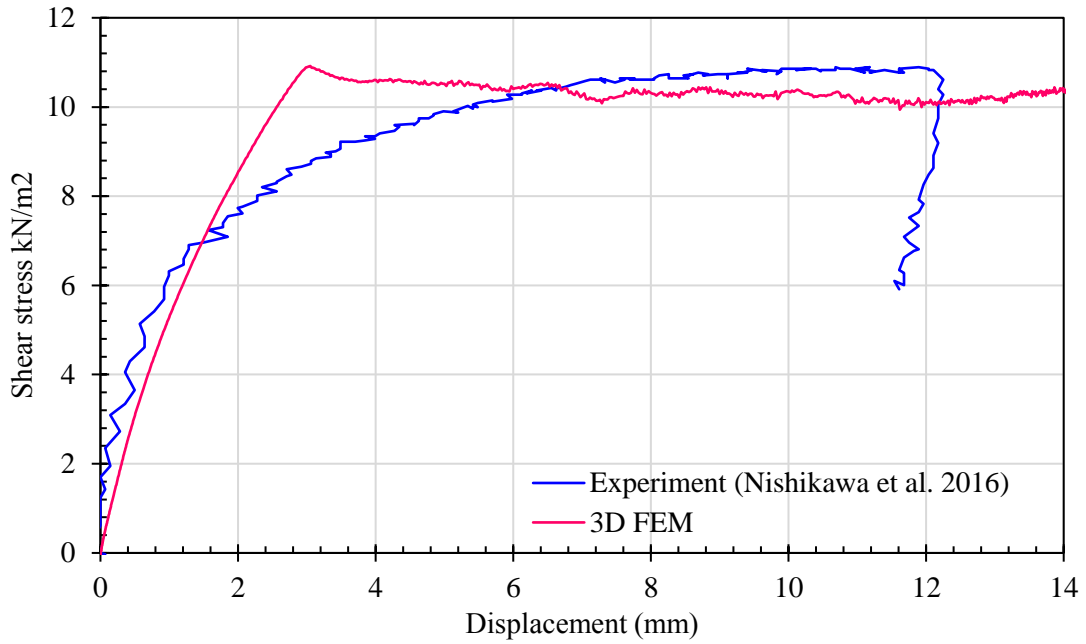


Fig. 7.25. Shear stress–displacement curvature of the soil-pipe interaction interface for our FE model in comparison with full-scale push-in test of Nishikawa et al. [42].

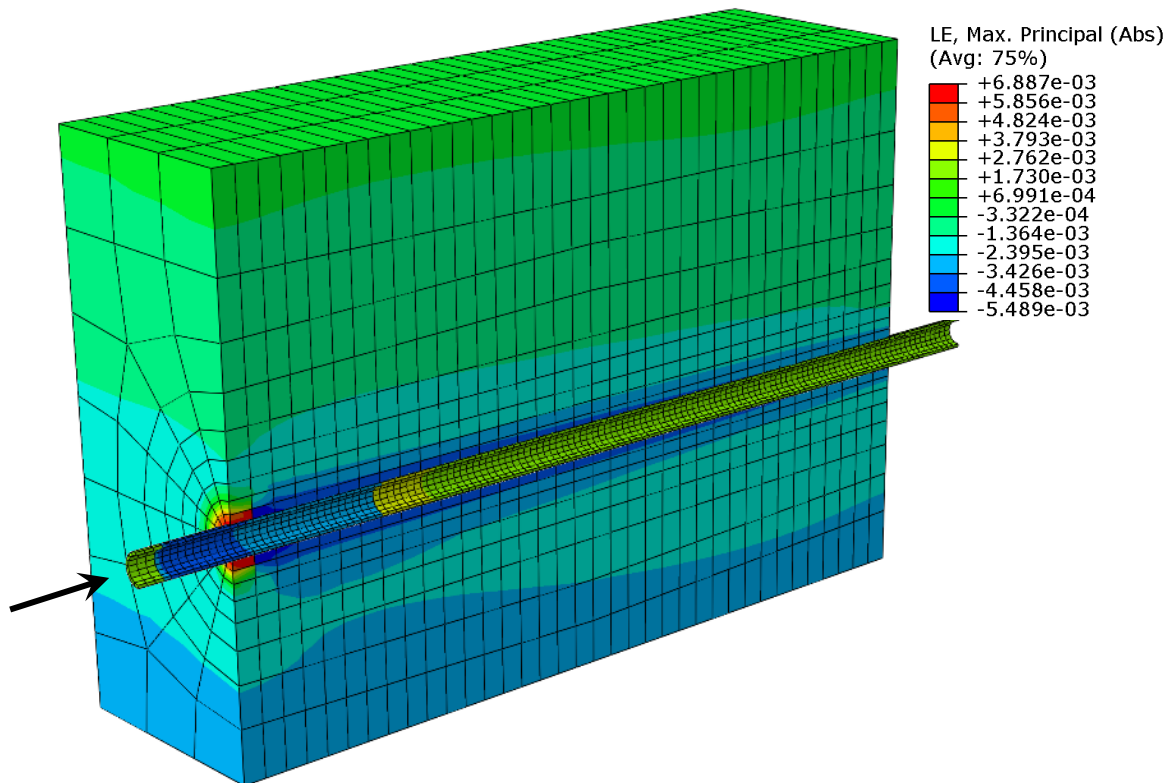


Fig. 7.26. Fe-based maximum principal strain distribution of push-in test at 1.5 cm push.

good quality and elements size after sensitivity analysis, is determined.

In the 3D FE model of the push-in test, soil-box is modeled in dimensions of $1.6 \text{ m} \times 1.08 \text{ m} \times 0.9 \text{ m}$, and pipe is 2 m as illustrated in **Fig. 7.24**. After several attempts, soil-pipe interaction interface of the 3D FE model was calibrated against Nishikawa et al. experimental

study. The pipe is pushed inwards at the near end, whereas the far end remains free. **Fig. 26** plots, shear stress–displacement relationship at dense sand and HDPE pipe interface during the push-in test. And based on **Fig. 7.25**, soil-pipe interaction of the FEM model is verified versus experimental results for the identical case of the HDPE pipeline buried in 0.6 m dense sand. **Fig. 7.26** plots the maximum principal strain distribution for a 15 mm pipe push.

7.6.2. 3D nonlinear FE models versus full-scale experiments for HDPE pipelines at fault crossing

3D FEM models are created exactly in the same dimensions and boundary conditions with full-scale faulting experiments. For the analysis cases, we modeled HDPE pipelines with an external diameter of 0.063 m, a thickness of 0.0058 m without internal pressure, and a total length of 6 m. The material of HDPE is modeled based on the experiment-based nonlinear stress-strain curve shown in **Fig. 7.10**, which its elastic Young's modulus is 1000 MPa, and Poisson's ratio is 0.46. The pipeline is buried under 0.6 m of loose/dense sands with properties shown in **Table 7.4**. The split-box length is 5 m, and its detailed size is shown in **Fig. 7.27**. Soil material is defined as an elastic-perfectly plastic Mohr-coulomb constitutive model based on properties in **Table 7.4**. The geometrical nonlinearity effect has been taken into account for all the analyses by the Nlgeom method.

In the creation of FEM models for modeling pipe and sand, we used continuum C3D8R elements with 8-node linear brick, reduced integration, and hourglass control. The elements

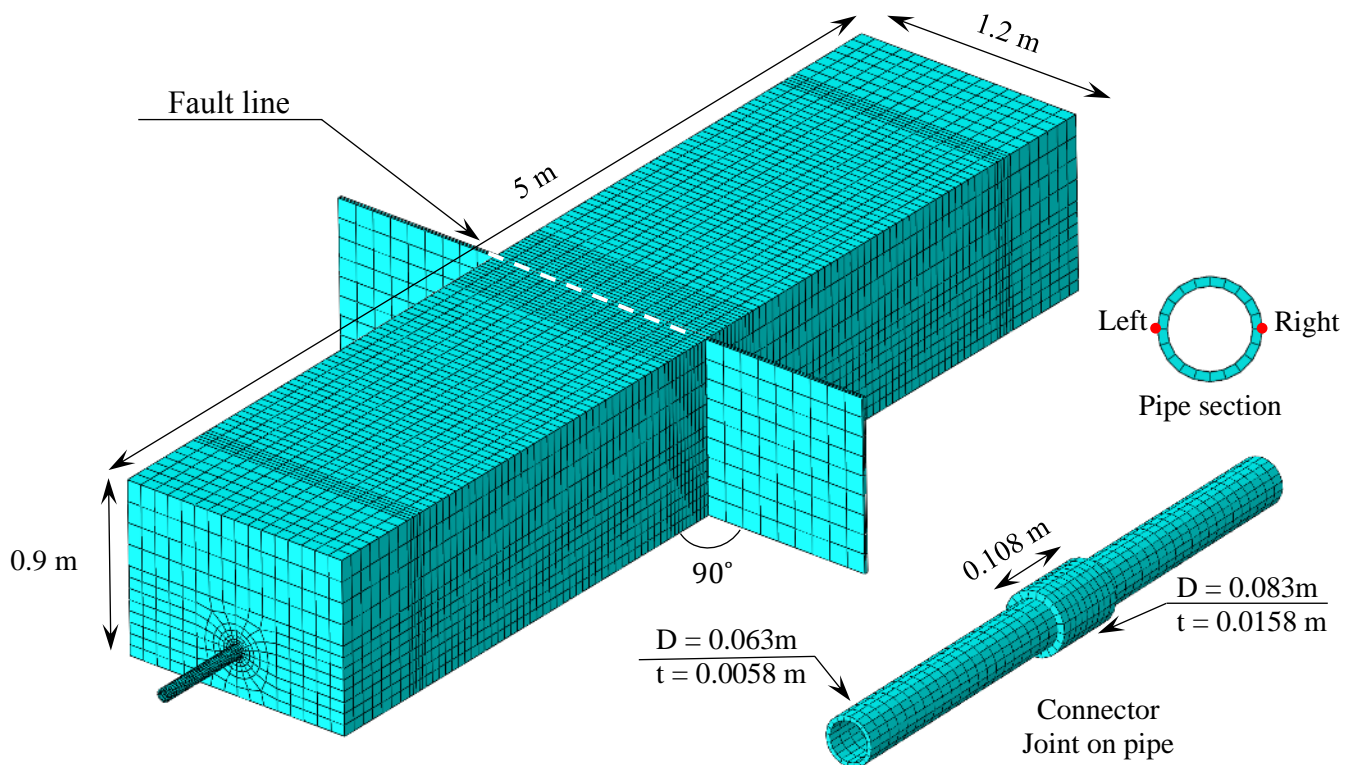


Fig. 7.27. 3D FE model for buried HDPE pipeline subjected to 90° strike-slip fault movement, Left and Right points are springlines of the pipe section.

size is determined after sensitivity analyses. The pipeline and soil are gradually discretized from fine at the fault zone to slightly bigger mesh sizes at further distances symmetric to the fault line except having finer mesh around the joints. All the boundary conditions are applied to the split-box surfaces similarly to our experiments.

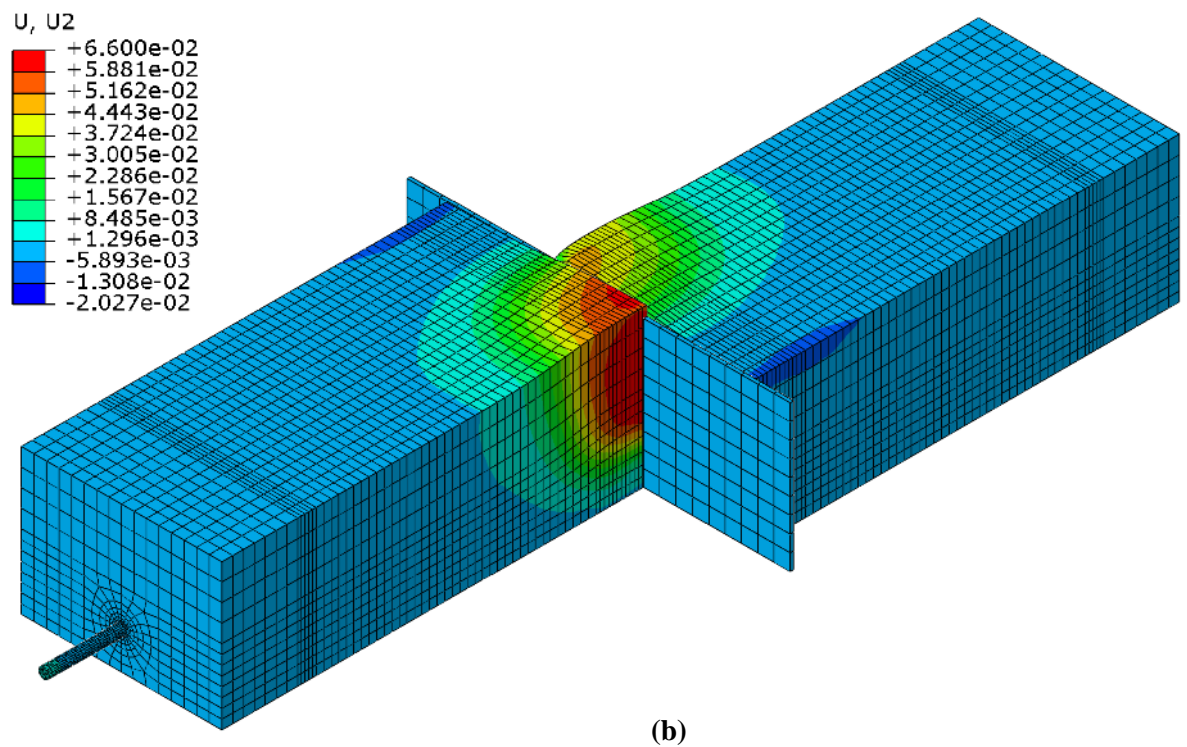
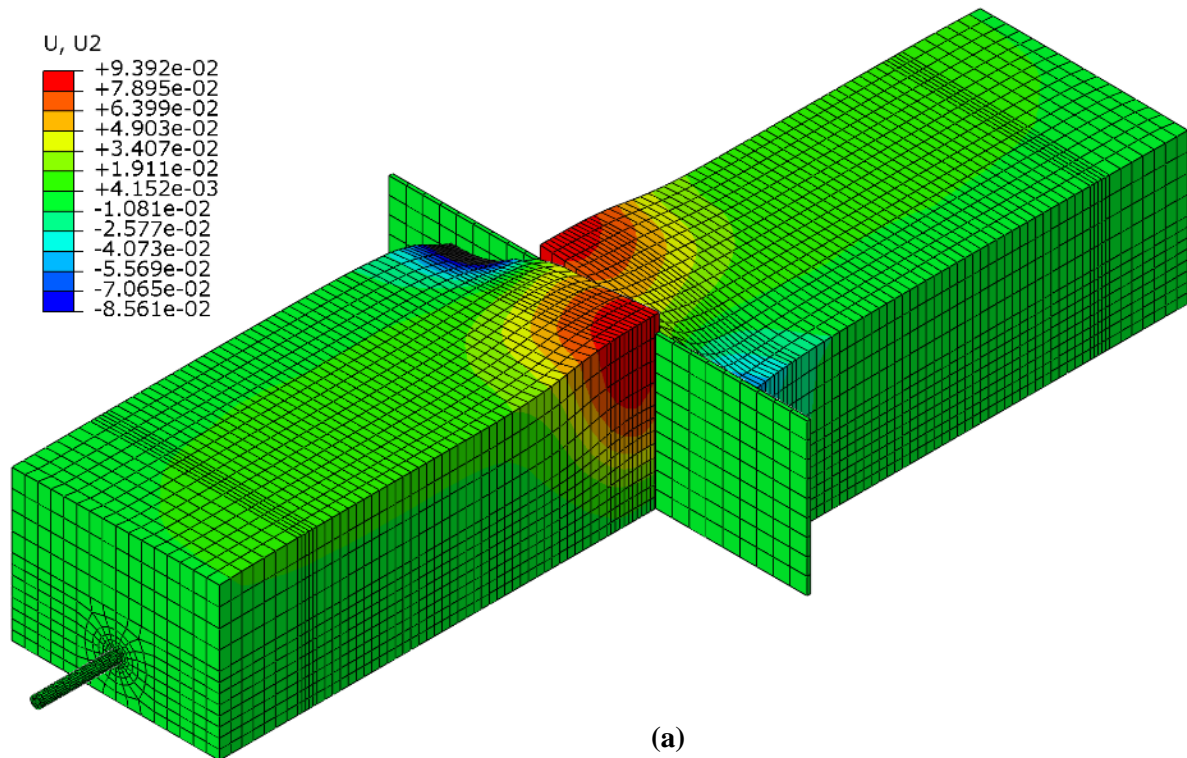


Fig. 7.28. Vertical deformation distribution at 10D movement of 90° strike-slip fault, (a) test 1, (b) test 2.

We extended verified contact properties of the FE model of push-in test to 3D-FE models of the buried pipeline at strike-fault crossing tests (test 1 and test 2). In a similar manner with experiments, in FE models, 90° strike-slip fault moved up to 10D = 0.63 m, where D is the outer diameter of pipe.

7.6.2.1. Soil deformation

Vertical deformation of the soil in the loose and dense sand cases at 10D fault movement is plotted in **Fig. 7.28**. And soil deformation of FE models in both tests is in good agreement with experiments.

7.6.2.2. HDPE pipe strain

Strain outputs of the HDPE pipeline on Left and right springlines (see **Fig. 7.27**) for the FEM analyses of test 1 (loose sand) and test 2 (dense sand) are shown versus strain gauges

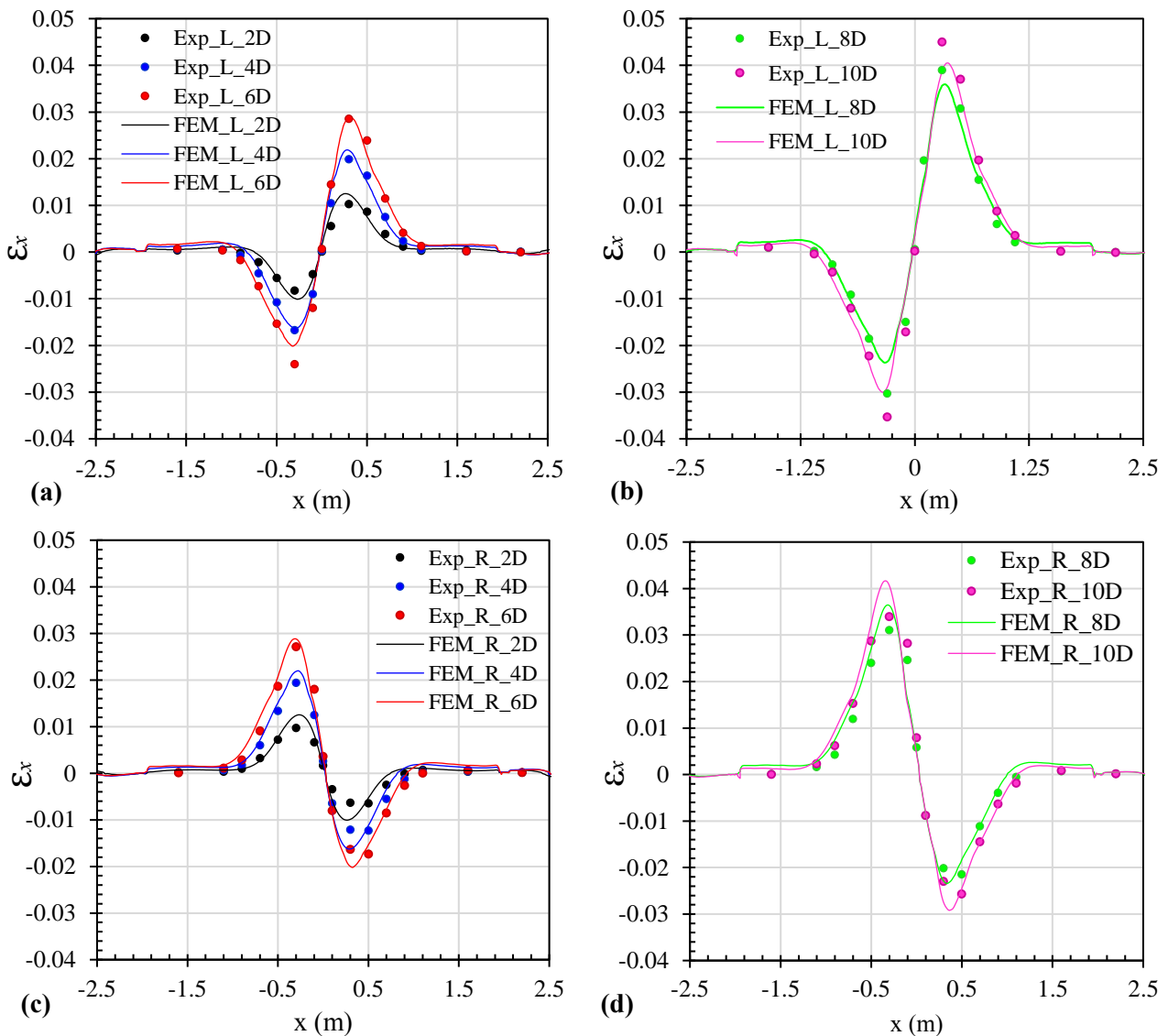


Fig. 7.29. Longitudinal strain distribution of HDPE pipeline buried in loose sand subjected to 90° strike-slip fault with 2D to 10D movement for FEM versus experiment (test 1): **(a,b)** Left springline, **(c,d)** Right springline.

results of the full-scale faulting tests in **Figs. 7.29–30**. In **Figs. 7.29–30**, Exp abbreviation indicates experimental results (strain gauges results), L and R indicate results on left and right springline of the pipeline section, respectively. Regarding **Figs. 7.29–30**, FE models' results for pipe longitudinal strain distribution in test 1 and test 2, show good agreement with experimental outputs in quality and quantities. The maximum strain locations and strain curve distributions of FE models, even in very nonlinear stages of pipe material are in good agreement with the experiments. In the dense sand case at large fault movements (over 6D), because of large soil-pipe interaction forces around fault plane and maximum bending points, some of the strain gauges exceed their allowable strain limits and failed. As shown in **Fig. 7.30 b,d**, at the same fault movements in the same locations with the failed strain gauges, FE models experienced very large strains, which shows FE models' nonlinear behavior is in a good

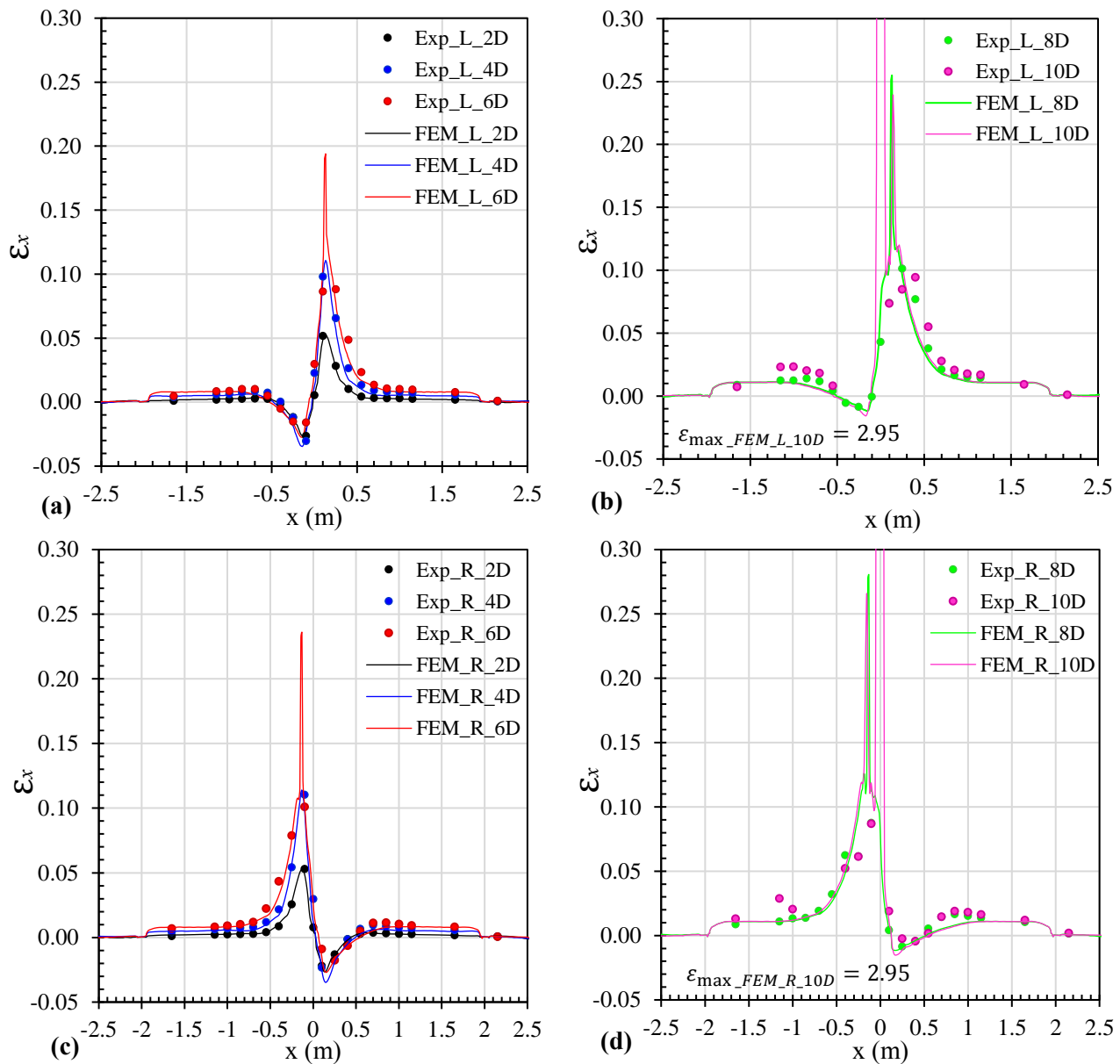


Fig. 7.30. Longitudinal strain distribution of HDPE pipeline buried in dense sand subjected to 90° strike-slip fault with 2D to 10D movement for FEM versus experiment (test 2): **(a,b)** Left springline, **(c,d)** Right springline.

argument with full-scale experiments, and FE models results are highly validated. Regarding FEM results, in test 2 for 4D fault movement at maximum bending strain locations on pipe springlines, pipe tensile strain starts to exceed HDPE material's ultimate strain (9.5%), and highly plastic strains appear on the pipe at these locations (see Fig. 7.30). By increasing the fault movement from 4D to 10D, gradually maximum strain on these points increases, and damage length (highly plastic zone) increases from 3 cm to 23 cm around the maximum tensile bending strains. In FEM in similar behavior with the experiment (see Figs. 7.19, 20 and 30), maximum strain location gradually moves from 10 cm to 15 cm on x-axis by increasing the fault movement and locally yielding of HDPE pipe material.

In test 2 (dens sand) at 10D fault movements, FE model shows a very large strain on springlines of the HDPE pipe at the crossing point with fault plane (longitudinal strain is 2.9), which during the experiment strain gauges of this location were failed at 8D fault movement. This very large strain has appeared in 10D fault movement because of the yielding of the pipe material on crown and invert points due to large axial and shear forces. Which stiffness of pipe material in invert and crown at $x = 0$ drastically has decreased and gradually, stress on the pipe section is absorbed to stiffer parts (springlines), and then all the pipe cross-section in fault plane experienced very large plastic strain. Therefore, around the fault plane at 10D fault movement, longitudinal strain on springlines at pipe cross-section instantaneously increased and ovalization damage has been observed.

In both test-1 and test-2 experiments, HDPE joints are located on ± 2 m from fault plane on

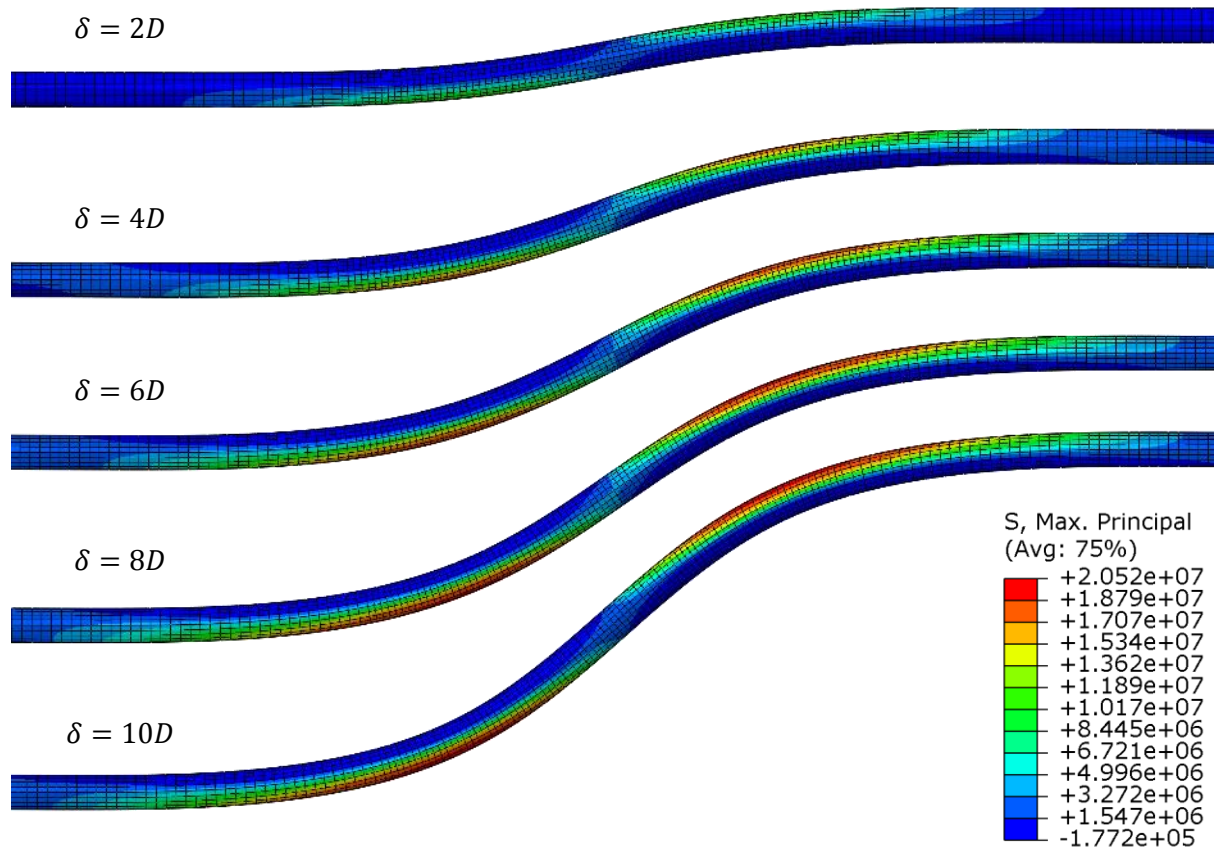


Fig. 7.31. Maximum principal stress distribution of HDPE pipeline buried in loose sand at 90° strike-slip fault crossing (test 1) for 2D, 4D, 6D, 8D and 10D fault movements (unit: Pa).

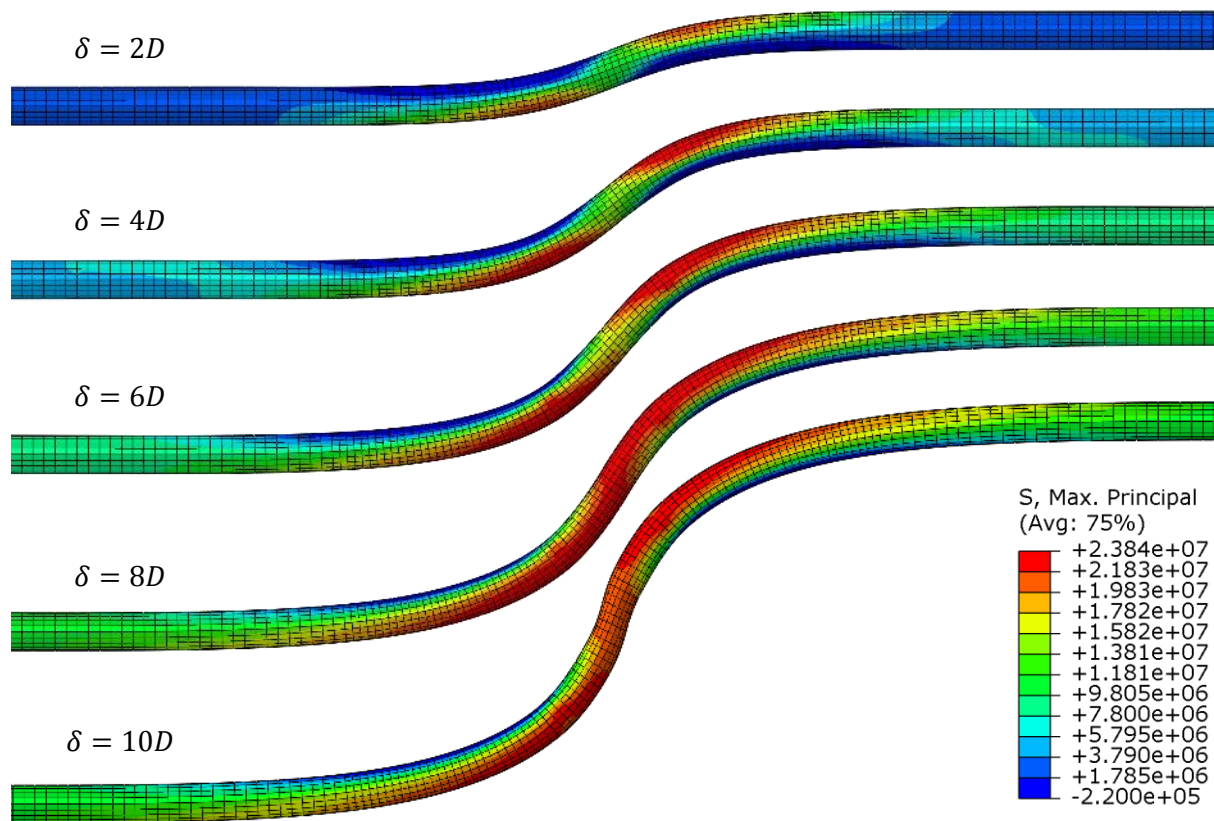


Fig. 7.32. Maximum principal stress distribution of HDPE pipeline buried in dense sand at 90° strike-slip fault crossing (test 2) for 2D, 4D, 6D, 8D and 10D fault movements (unit: Pa).

the buried HDPE pipelines. Figs. 7.29–30 show a large change in strain results of the pipe at the location of HDPE joints, which is because of a significant increase in axial soil-pipe interaction on joints. HDPE Joints because of their larger diameter in comparison with the pipe have larger frictional area and consequently larger frictional soil-pipe interaction forces. Besides, due to the compaction of the soil around joints during sliding of pipe within the soil, a bearing force appears on the perpendicular surfaces to the pipe normal axis (x-axis) at fault-side on the joints. These two forces increase the soil-pipe interaction force significantly around joints, therefore, it is crucial to have the locally increasing effect of joints on soil-pipe interaction in analyzing for the problem of buried pipeline subjected to fault movement, especially for beam-spring models.

7.6.2.3. Stress on HDPE pipe

Regarding stress- strain curve of HDPE material in **Fig. 7.10**, pipe material after around 14 MPa is in the plastic zone, and after stress around 23.8 Mpa exceed the ultimate stress and experiences large plastic deformations. In test 1, because of lower soil-pipe interaction forces from loose sand, the HDPE pipeline didn't experience large plastic stress/strains, and pipe didn't meet the ultimate stress during the faulting up to the large movement of 10D (see **Fig. 7.31**). In test 1, after 4D fault movement, HDPE pipe at maximum bending points (on springlines), started to experience plastic stresses and this zone's length increased gradually up to 10D movement, however, Pipe didn't exceed its ultimate stress, and almost there was no

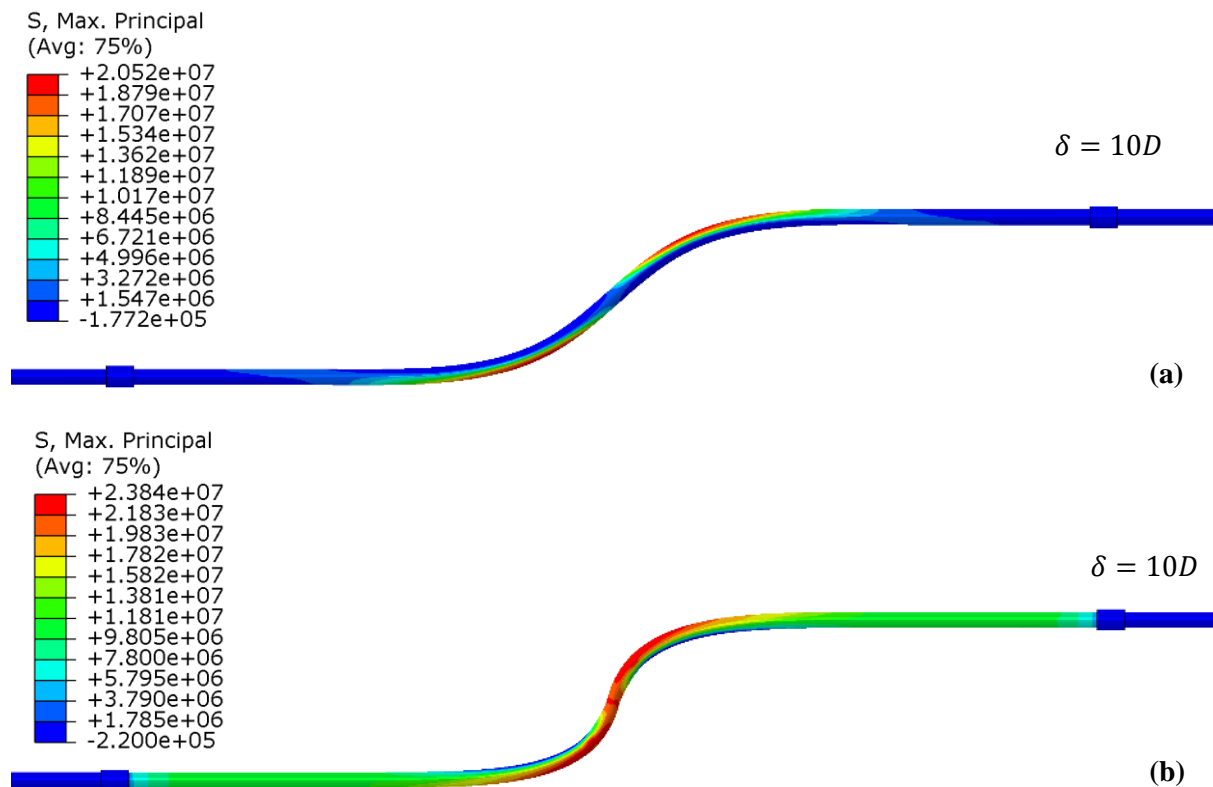


Fig. 7.33. Maximum principal stress distribution of HDPE pipeline buried in Dense sand at 90° strike-slip fault crossing with 10D fault movements: (a) Loose sand case, (b) Dense sand case.

damage on the pipeline. In test 2, because of very large soil-pipe interaction forces in dense sand, HDPE pipe from very early stages of the faulting experienced plastic stress/strain at maximum bending stress locations on pipe springlines (see **Fig. 7.32**). Maximum principal stresses on these zones gradually increased up to 10D fault movements and exceeded the ultimate stress of HDPE material after around 4D fault movements. In test 2, because high soil-pipe interaction forces and consequently very large axial and shear forces at pipe cross-section on the fault plane, after around 8D fault movements, principal stress on the crown and invert points of the pipe section exceeded ultimate stress/strain and pipe starts to experience ovalization damage, which at 10D fault movement ovalization at fault crossing is in a critical range.

Fig. 7.33, plots the maximum principal stress of test 1 and test 2 for all the pipeline at 10D fault movement. In **Fig. 7.33b**, pipe segment between joints experience much higher stress in comparison with further parts, and it shows axial soil-pipe interaction on joints is significantly higher than the normal pipe, and even it has decreased sliding of the pipe with an anchor behavior within the soil. Evidently, it has a large effect on pipe performance during the faulting. Therefore, it is essential to consider the effect of joints on the analyzing and designing of the buried pipelines at fault crossing problems, otherwise because of joints interaction pipe will experience higher soil-pipe interaction force and even damages during the earthquakes.

We clearly observed ovalization damage has a direct relationship with principal stress on the crown/invert of pipe cross-section. Based on verified FE analyses (see **Fig. 7.32**), ovalization

damage on pipe cross-section at fault plane ($x = 0$) started after principal stress/strain of crown/invert points exceeded ultimate stress/strain of the HDPE pipe material. Most of the existing design guidelines [35,37,38] introduced a maximum longitudinal strain limit for controlling the ovalization damage to the pipeline, which is a general idea and is not economic for all cases. Therefore, for having a reliable and economic seismic design for buried pipeline against ovalization damage, it is essential to control the maximum principal stress/strain of the pipe on the crown/invert less than the ultimate stress/strain of the pipe material.

7.6.2.4. Local buckling and ovalization (FEM)

Since in FE models, pipes are modeled by continuum C3D8R elements, local buckling and ovalization can be captured during the strike-slip faulting. In a similar behavior with experiment results (in section 7.5.3), FE models for test 1 and test 2 didn't experience buckling during faulting up to 10D fault movement.

HDPE pipelines are initially manufactured with minimal ovality of less than 3%. Acceptance criteria ovality of an HDPE pipe during the service in ASTM F2160 [43] is 7-10%, and acceptance criteria of pipelines ovality in CSA Z662-11 defaults to 5% [44].

Regarding verified FEM, ovality factor (f_o) on critical cross-sections of test 1 and test 2 at 10D fault movement are calculated based on Eq. (7.3) and shown in Eq. (7.4) and (7.5), respectively (see **Fig. 7.34**).

$$f_{o-FEM-test\ 1} = \frac{0.064 - 0.062}{6.3} = 3\% \quad (7.4)$$

$$f_{o-FEM-test\ 2} = \frac{6.1 - 5.13}{6.3} = 15\% \quad (7.5)$$

Critical ovalization cross-section in the loose sand case appeared in maximum bending moment location which it's ovality in a similar manner with experiment is low ($f_{o-FEM} = 0.03$) and it is in the acceptable range. Critical ovalization cross-section of HDPE pipe in the dense sand case is observed on the fault plane location, which it's ovality in a similar way with experiment ($f_{o-Exp} = 0.1$) is high ($f_{o-FEM} = 0.15$) and exceeded acceptance ovality criteria.

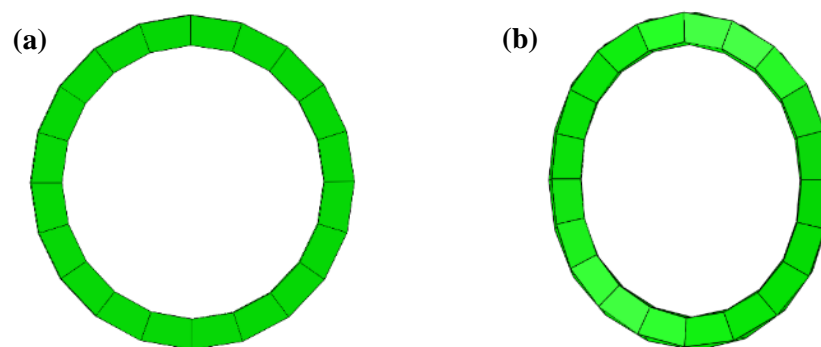
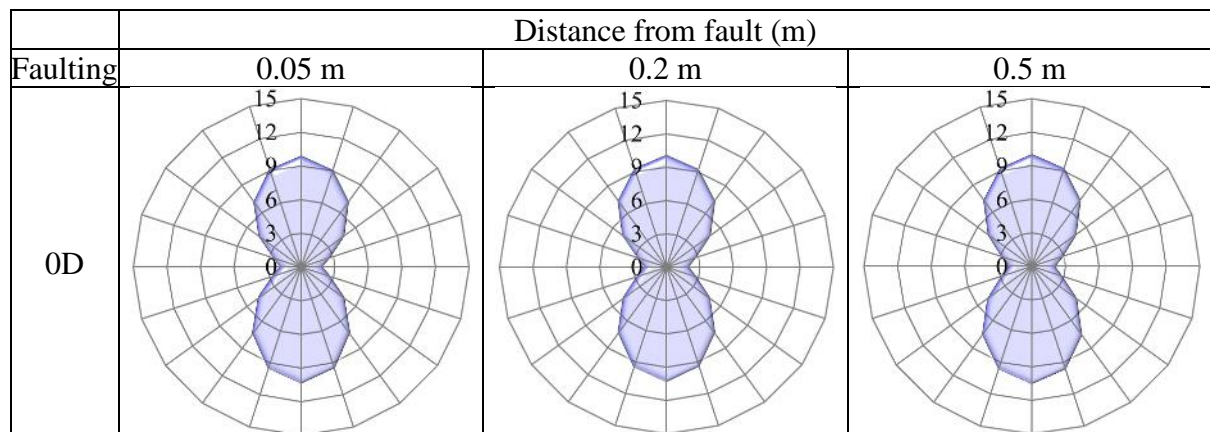


Fig. 7.34. Critical ovalized pipe cross-section at 10D movement: (a) test 1 (loose sand), (b) test 2 (dense sand).

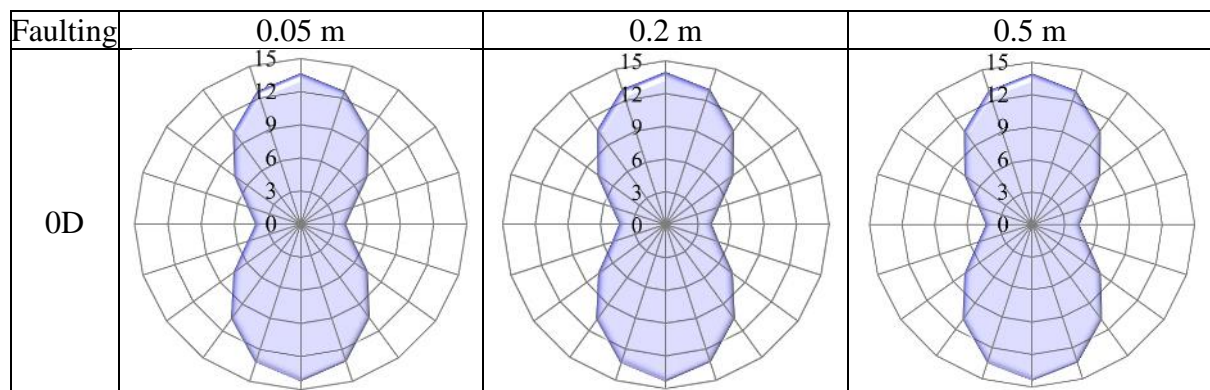
7.6.2.5. Soil pressure on HDPE pipe

After accurate verification of FE models in capturing the real behavior of the HDPE pipes during strike-slip faulting, FE models are used to extract soil-pipe interaction forces. These soil-pipe interaction forces are extracted based on pressure on the contact between soil and pipe. Because maximum soil-pipe interaction force takes place around fault plane and after a distance, they are so low, we have tracked these forces at sections 0.05 m, 0.2 m, and 0.5 m from fault plane and due to the symmetry of the problem we just show one side of the fault plane. In **Fig. 7.35**, we plotted the soil pressure distribution around the pipe perimeter under the gravity load for two cases of test 1 and test 2. Soil pressure on the crown and invert of HDPE pipe is maximum and it is minimum on the springlines. Fig. 7.35 shows, soil pressure distribution along the pipe on cross-sections with different distances from the fault plane are equal, which shows FE models' boundary conditions assumed correctly. In test 2, because of higher soil density pipe experienced higher soil pressure during the gravity loading.

Fig. 7.37. and **Fig. 7.38** show the FE-based pressure distribution around the HDPE pipe perimeter at different locations from the fault plane and at different fault movements of 2D, 4D, 8D, and 10D for test 1 and test 2. **Figs. 7.37** and **7.38** demonstrate pressure on the springline of the compression side of the pipe has a direct relation with fault movement, and this pressure around the fault plane is maximum and along the pipeline and away from the fault



(a)



(b)

Fig. 7.35. Pressure distributions on buried HDPE pipe perimeter under gravity load (unit: kPa): (a) Test 1, (b) Test 2.

plane decreases drastically. Major part of this soil pressure on pipe perimeter is distributed within the high curved length of the pipeline. Moreover, we observed, there is a positive correlation between soil stiffness and soil-pipe interaction pressure on the pipe perimeter. Wherein HDPE pipe in loose sand (test 1) and dense sand (test 2), experienced maximum soil pressure of 200 kPa and 1100 kPa, respectively. pipe experienced remarkable pressure on the tensile side springline around fault plane, because of frictional forces on the fault plane in large fault movements and the large rotation of pipe axis due to very large deformation of the pipe, especially in the stiffer sand case.

we used extracted pressure distribution from **Figs. 7.37–7.38**, to calculate lateral soil-pipe interaction force during faulting in test 1 and test 2. Ha et al [45] introduced Eq. (7.6) for to extraction of lateral soil-pipe interaction force along HDPE pipes, wherein we adopted the same methodology in this paper. The lateral force per unit length of the HDPE pipe (P_h) is derived by taking horizontal component of the pressure and friction and integrating them on the perimeter of pipe (see **Fig. 7.36**).

$$P_h = \int_0^{2\pi} Rp(\theta)\cos\theta d\theta + \int_0^{2\pi} \mu Rp(\theta)\sin\theta d\theta \quad (7.6)$$

Where R is pipe radius, θ is the angle defining the position of a differential segment of the pipe on its perimeter, and μ is the coefficient of friction between pipe and soil contact.

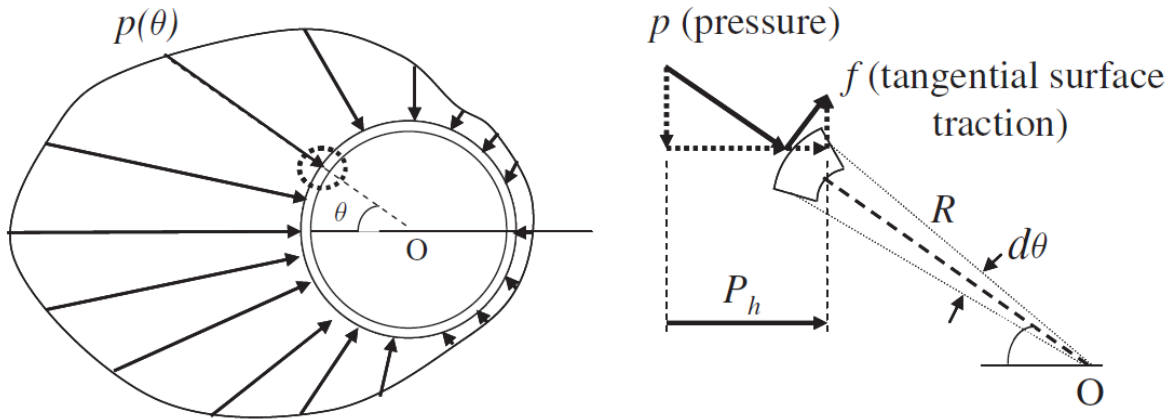


Fig. 7.36. Sketch of the assumptions and soil pressure distribution in integrating lateral soil-pipe interaction force calculation [45].

Based on American Lifeline Alliance [37,38], The maximum lateral soil force per unit length of pipe (P_u) is as Eq. (7.7)

$$P_u = N_{ch}cD + N_{qh}\gamma HD \quad (7.7)$$

Where N_{ch} and N_{qh} are horizontal bearing capacity factors for cohesive soil and sand, H is buried depth of springline of pipe, and D is pipe outer diameter. For our experiment in test 1, N_{ch} , N_{qh} are equal to 9 and 19.5, respectively, and $P_u = 10.9 \text{ kN/m}$. For test 2, N_{ch} , N_{qh} are equal to 9 and 21, respectively, and $P_u = 14.2 \text{ kN/m}$.

Fig. 7.39 shows FE-based lateral soil-pipe interaction force distribution along the pipe at

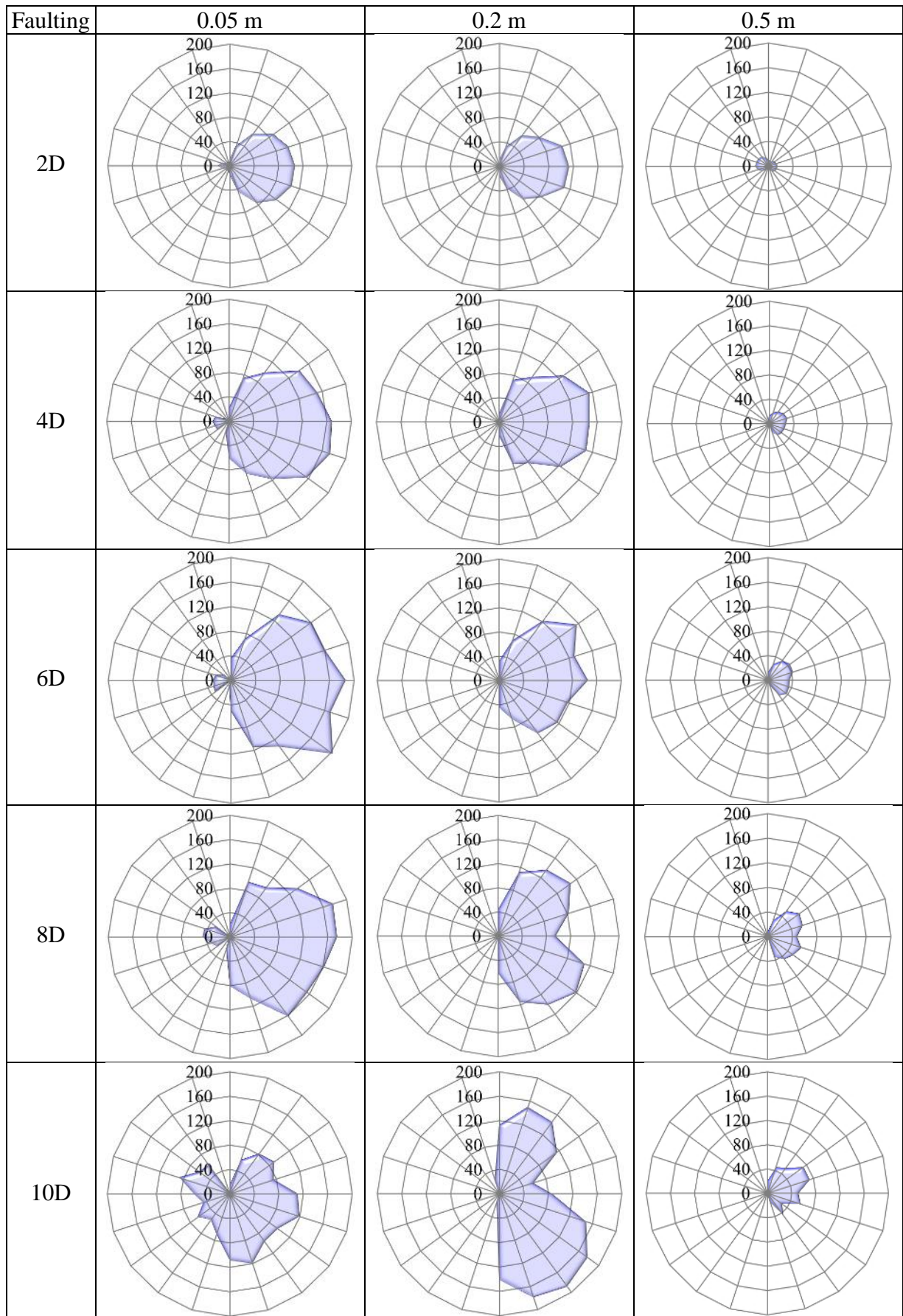


Fig. 7.37. Pressure distributions on HDPE pipe perimeter buried in loose sand during faulting (test 1) (unit: kPa).

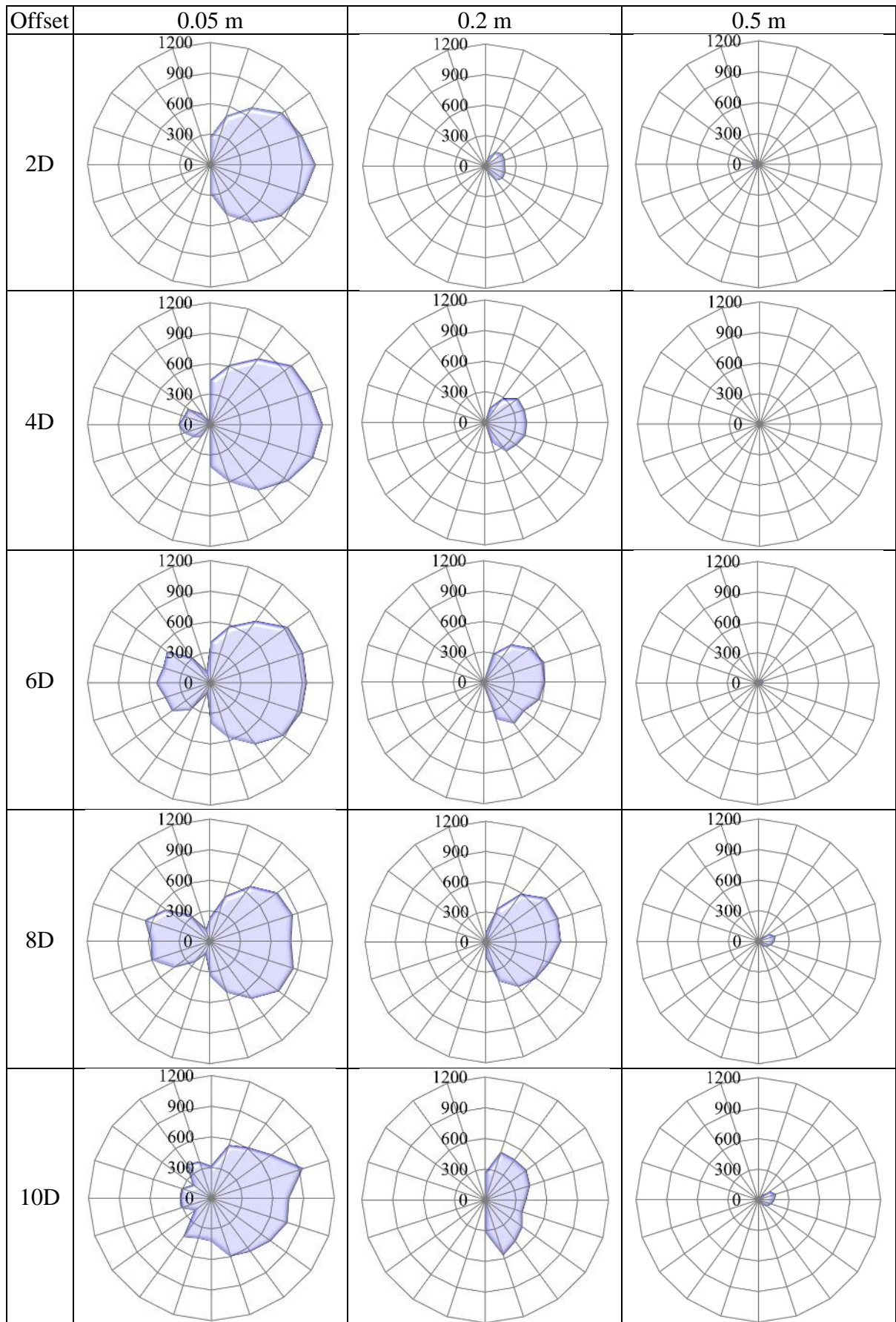


Fig. 7.38. Pressure distributions on HDPE pipe perimeter buried in dense sand during faulting (test 2) (unit: kPa).

selected locations on pipe high curvature length for different fault movements and compares them to the suggested ultimate values by ALA [38]. HDPE pipe buried in dense sand because of stiffer soil experienced much higher (almost 5-fold) lateral soil-pipe interaction force in comparison with the loose sand case.

In both tests, we observed a negative correlation between lateral soil-pipe interaction force and distance from fault in the elastic range of the soil. At 5 cm from fault plane, after yielding of soil in test 1 at 8D and test 2 at 2D, lateral soil-pipe interaction force significantly dropped by increasing of fault movement (see **Fig. 7.38**). Maximum lateral soil-pipe interaction force for test 1 and test 2 are observed at 5 cm distance from the fault plane at 6D fault movement and 2D fault movement, respectively.

Fig. 7.39 shows the maximum lateral force for the loose sand case is less than the suggested value of ALA [38], while the maximum lateral force of the HDPE pipe buried in dense sand is 3.8-fold of ALA suggested value. Lateral soil force value for loose sand is in good agreement with ALA suggested value, however, ALA's suggested value for dense sand (compacted sand) is much lower than the verified FEM results and is not in the valid range. Evidently, ALA 2005 [38] guideline has not considered the effect of the soil compaction on the ultimate lateral soil-pipe interaction force calculation.

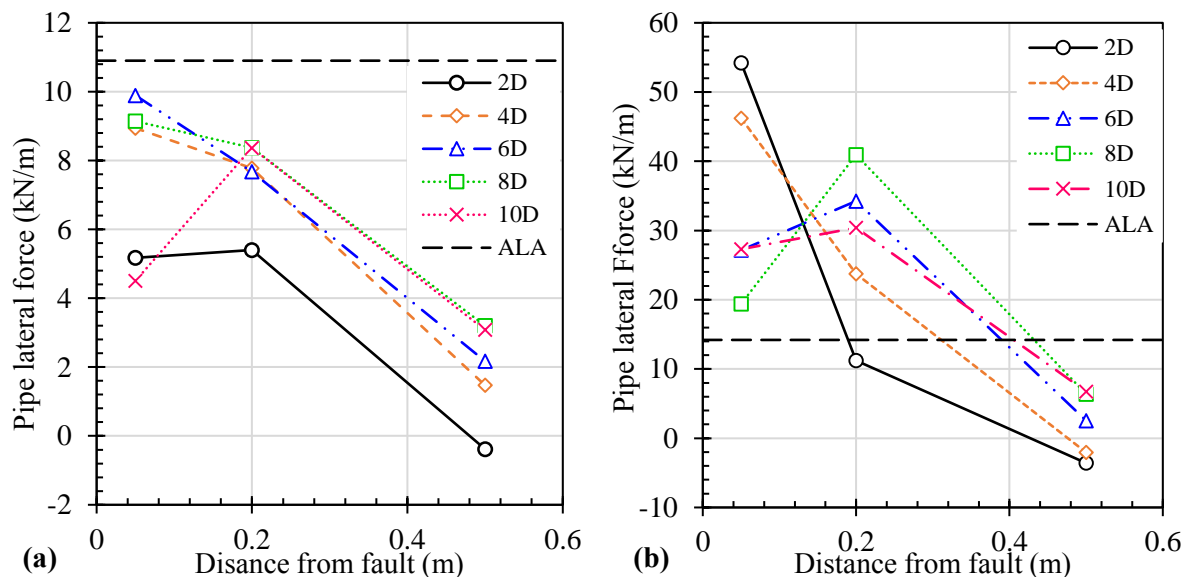


Fig. 7.39. Lateral soil-pipe interaction force at different strike-slip fault movements for: (a) test 1 (loose sand), (b) test 2 (dense sand).

7.6.2.6. Bearing force of soil on HDPE joints

As mentioned earlier, based on verified FEM analysis results, we observed soil-pipe interaction forces on the HDPE pipe joints are larger than HDPE pipe because of larger frictional forces and existing of bearing forces from soil on the fault-side corner of HDPE joints. This additional bearing force on HDPE joints makes joints behave as an anchor within the soil. We observed a positive correlation between bearing force on the joint corner and its longitudinal sliding. Fig. 7.40 shows, bearing force on one corner (fault-side) of one of HDPE

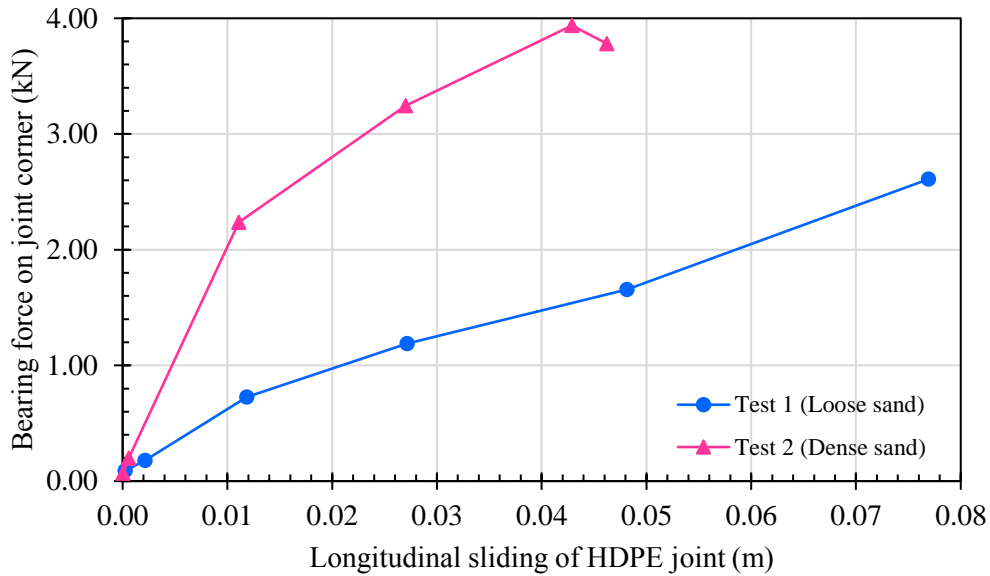


Fig. 7.40. Longitudinal bearing soil force on corner of HDPE joint of HDPE pipes.

joints against its longitudinal sliding within the loose and dense sand. Each of the nodes in **Fig. 7.40** represents joint status at 1D, 2D, 4D, 8D, and 10D fault movements, respectively. **Fig 7.40** shows, HDPE joint buried in dense sand experienced higher bearing force and lower longitudinal sliding in comparison with the loose sand case. The slope of bearing force-sliding displacement curve of the HDPE joint in both tests changes after around 1 cm sliding (yields) and at around bearing force of 4 kN reaches to the ultimate force in dense sand case. Corner of HDPE joints experienced maximum longitudinal bearing force at 8D fault movement (4kN) and at 10D fault movement (2.6 kN) in test 1 and test 2, respectively. This bearing force on each joint can make remarkable axial force in the pipeline at critical cross-section on the fault plane. Therefore, it is essential to have the effect of bearing force and additional frictional force of the HDPE joint in the analysis of buried HDPE pipelines at fault crossing.

7.7. Conclusions

In this study, to evaluate the performance of HDPE pipelines at fault crossings, two full-scale experiments for 63mm HDPE pipeline buried in loose sand and dense sand subjected to strike-slip fault at a 90° crossing are carried out. Besides, two 3D nonlinear FE models created for identical problems, and these two models are calibrated based on experiment results. Accomplished conclusions of this study are as below:

1. Because from early stages of the faulting in fault plane of strike-slip fault, soil fails up to the surface and large cracks along the fault plane appear, It is more realistic in FEM analyses, to model the soil parts of each side of the fault plane (each of split-box sides) as a separated part (not connected soil parts).
2. An uplift expansion of soil around the fault plane observed in both tests, which its level in case of loose and dense soil was almost 20mm and 55mm, respectively. Additionally,

in loose sand case, a subsidence observed around the high curvature zone of the pipeline at the split-box sides.

3. As soil is stiffer, the curvature of the HDPE pipe is higher, and the high curvature zone is shorter.
4. Peak axial strains and peak bending strains (on springline) of the HDPE pipeline increase by increasing the fault movement up to a limit that longitudinal strain on springline reaches around strain corresponding to the ultimate stress of HDPE and has large plastic strains. After that by increasing the fault movement, peak axial strain increase rate drastically decreases and then remains almost same and by further fault movements, a longer length of pipeline reach to peak strain range, and in bending strains after reaching that ultimate stress limit because of flexural stiffness drop in peak bending strain cross-section, by increasing the fault movement peak bending stress/strain drops and gradually moves to further cross-sections from the fault plane. This procedure continues up to a fault movement that damage appears on the pipeline (e.g. local buckling, wrinkling, and ovalization).
5. HDPE buried in stiffer soil experiences higher axial and bending stress/strain at strike-slip fault crossing problem.
6. Axial strains of HDPE pipelines buried in dense sand is not negligible, even in case of a 90° crossing with strike-slip fault movement.
7. As we know, buried pipelines subjected to a strike-slip fault at 90° crossings are highly vulnerable for local buckling damages. However, during tests 1 and 2, which HDPE pipelines were subjected to very large fault movements (up to 10D), they show high flexibility and good performance during the faulting, and no local buckling damage appeared on the buried HDPE pipelines.
8. HDPE pipelines with lower diameters have a larger (D/t) ratio which increases the critical buckling strain and increases the safety of pipe against buckling damages. However, for large size HDPE pipelines, there is a need for further investigations.
9. HDPE pipe in case of buried in dense sand at 10D strike-slip fault movement, experienced early stages of the ovalization, and factor of ovality is 0.1.
10. During the full-scale test 2 experiment, peak tensile longitudinal strain, peak compression

longitudinal strain, peak axial strain, and bending strain of HDPE pipeline buried in dense sand are 11%, -3.3%, -7%, and 4.6%, respectively.

11. Soil-pipe interaction forces on the HDPE pipe joints are larger than the HDPE pipe because of larger frictional forces and bearing forces from soil on the joints. Therefore, it is crucial to have a locally increasing effect of soil-pipe interaction at joints in analyzing the problem of buried pipeline subjected to fault movement especially on beam spring models.
12. ALA 2005 [38] guideline has not considered effect of the soil compaction on the ultimate soil-pipe interaction forces. And its suggested values for dense sand case is much lower than verified FEM results.
13. Ovalization damage has a direct relationship with principal stress/strain on the crown/invert of pipe cross-section. For having a reliable and economic seismic design for buried pipeline against ovalization damage, it is essential to control the maximum principal stress/strain of the pipe on the crown/invert less than the ultimate stress/strain of the pipe material.
14. lateral soil-pipe interaction force and soil pressure on pipe perimeter have a negative correlation with distance from fault in elastic range of the soil, and after yielding of soil around fault plane they drop in that zone.

References

- [1] American Lifelines Alliance—ASCE. Guidelines for the Design of Buried Steel Pipe” July 2001 (with addenda through February 2005).
- [2] Karamitros, D., Bouckovalas, G., Kouretzis, G. [2007] “Stress analysis of buried steel pipelines at strike-slip fault crossings,” *Soil Dynamics and Earthquake Engineering* 27, 200–11.
- [3] Trifonov, O. V., Cherniy, V. P. [2010] “A semi-analytical approach to a nonlinear stress–strain analysis of buried steel pipelines crossing active faults,” *Soil Dynamics and Earthquake Engineering* 30(11), 1298–308.
- [4] Karamitros, D. K., Bouckovalas, G. D., Kouretzis G. P., Gkesouli V. [2011] “An analytical method for strength verification of buried steel pipelines at normal fault crossings,” *Soil Dynamics and Earthquake Engineering* (13), 1452-1464.
- [5] Trifonov, O. V., Cherniy V. P. (2012). “Elastoplastic stress-strain analysis of buried steel pipelines subjected to fault displacements with account for service loads,” *Soil Dyn Earthq Eng* 33,54–62.
- [6] Lim, M. L., Kim, M. K., Kim, T. W., Jang, J. W. (2001). “The behavior analysis of buried pipeline considering longitudinal permanent ground deformation,” In *pipeline 2001: advances in pipelines engineering & construction* (San Diego, California), vol. 3, 107. ASCE. [https://doi.org/10.1061/40574\(2001\)3](https://doi.org/10.1061/40574(2001)3)
- [7] O’Rourke, M. J., Vikram, G., Abdoun, T. (2003). “Centrifuge modeling of buried pipelines,” In: *Proceedings of the Sixth U.S. conference and workshop on lifeline earthquake engineering*, August 10–13, 2003, Long Beach, CA. pp. 757–768.
- [8] Sakanoue, T., Yoshizaki, K. (2004). “A study on earthquake-resistant design for buried pipeline using lightweight backfill,” In: *Proceedings of the 13th world conference on earthquake engineering*, Vancouver, B.C., Canada, August 1-6, Paper No.2389.
- [9] Takada, S., Hassani, N., Fukuda, K. (2001). “A new proposal for simplified design of buried steel pipes crossing active faults,” *Earthq Eng Struct Dyn* ;30:1243–57.
- [10] Vazouras, P., Karamanos, S. A., Dakoulas, P. (2010). “Finite element analysis of buried steel pipelines under strike-slip fault displacement,” *Soil Dyn Earthq Eng* ;30:1361–76.
- [11] Vazouras, P., Karamanos, S. A., Dakoulas, P. (2012). “Mechanical behavior of buried steel pipes crossing active strike-slip fault,” *S, Soil Dyn Earthq Eng*;41:164–80.
- [12] Vazouras, P., Dakoulas, P., Karamanos, S. A. (2015). “Pipe–soil interaction and pipeline performance under strike–slip fault movements,” *Soil Dyn Earthq Eng* ;72:48–65.
- [13] Zhang, L., Zhao, X., Yan, X., Yang, X. (2016). “A new finite element model of buried steel pipelines crossing strike-slip faults considering equivalent boundary springs,” *Eng*

Struct;123:30–44.

- [14] Demirci, H. E., Bhattacharya, S., Karamitros, D., Alexander, N. (2018) “Experimental and numerical modelling of buried pipelines crossing reverse faults,” *Soil Dyn Earthq Eng* ;114:198–214.
- [15] Yoshizaki K, O’Rourke TD, Hamada M. Large scale experiments of buried steel pipelines with elbows subjected to permanent ground deformation. *J Struct Mech Earthq Eng* 2003;20(1):1s–11s.
- [16] Palmer, M. C., O’Rourke, T. D., Stewart, H. E., O’Rourke, M. J., Symans, M. (2006) “Large displacement soil-structure interaction test facility for lifelines” In: Proceedings of the 8th US national conference commemorating the 1906 San Fransisco earthquake, EERI, San Fransisco.
- [17] O’Rourke, T. D., Bonneau, A. (2007) “Lifeline performance under extreme loading during earthquakes,” In: Pitilakis KD, editor. *Earthquake Geotechnical Engineering*. Dordrecht, Netherlands: Springer; 407–32.
- [18] Lin, T. J., Liu, G. Y., Chung, L. L., Chou, C.H., Huang, C. W. (2012) “Verification of Numerical Modeling in Buried Pipelines under Large Fault Movements by Small-Scale Experiments,” In: Proceedings of the 15WCEE, 9, 6685–6693.
- [19] O’Rourke, M. J., Gadicherla, V., Abdoun, T. (2005) “Centrifuge modeling of PGD response of buried pipe,” *Earthq Eng Eng Vib* ;4:69–73.
- [20] Ha, D., Abdoun, T. H., O’Rourke, M. J., Symans, M. D., O’Rourke, T. D., Palmer, M. C., Stewart, H. E. (2008) “Buried high-density polyethylene pipelines subjected to normal and strike-slip faulting — a centrifuge investigation,” *Can Geot J* ;45: 1733–1742.
- [21] Ha, D., Abdoun, T. H., O’Rourke, M. J., Symans, M. D., O’Rourke, T. D., Palmer, M. C., Stewart, H. E. (2008) “Centrifuge modeling of earthquake effects on buried high-density polyethylene (HDPE) pipelines crossing fault zones,” *ASCE J Geotech Geoenviron Eng* ;134(10):1501–15.
- [22] Abdoun T. H., Ha, D., O’Rourke, M. J., Symans M. D., O’Rourke T. D., Palmer M.C., Stewart HE. (2009) “Factors influencing the behavior of buried pipelines subjected to earthquake faulting” *Soil Dyn Earthq Eng* ;29:415–27.
- [23] Xie, X., Symans, M. D., O’Rourke, M. J., Abdoun, T. H., O’Rourke, T. D., Palmer, M. C., Stewart, H. E. (2011) “Numerical modelling of buried HDPE pipelines subjected to strike-slip faulting” *J Earthq Eng* ;15(8):1273–96.
- [24] Ha, D., Abdoun, T. H., O’Rourke M. J., Symans. M. D., O’Rourke. T. D., Palmer. M. C., Stewart, H.E. (2010) “Earthquake faulting effects on buried pipelines – case history and centrifuge study”. *J Earthq Eng* ;14(5):646–69.
- [25] Xie, X., Symans, M. D., O’Rourke, M. J., Abdoun, T. H., O’Rourke, T. D., Palmer M. C.,

- Stewart H. E. (2013) “Numerical modeling of buried HDPE pipelines subjected to normal faulting: a case study”. *Earthq Spectra* ;29(2):609–32.
- [26] NEESR-SG Final Report (2008) Prepared by Cornell University, Rensselaer Polytechnic Institute and Sciencenter Discovery Center; 47 p.
- [27] Jalali H. H., Rofooei F. R., Attari, N. K. A., Samadian, M. (2016) “Experimental and finite element study of the reverse faulting effects on buried continuous steel gas pipelines” *Soil Dyn Earthq Eng*;86:1–14
- [28] Demirci, H. E., Bhattacharya, S., Karamitros, D., Alexander, N. (2018) “Experimental and numerical modelling of buried pipelines crossing reverse faults,” *Soil Dyn Earthq Eng* ;114:198–214.
- [29] Committee for seismic performance evaluation of polyethylene pipes for water networks. (2018) “Guideline for seismic design of water polyethylene pipes” PLITEC, pp.38–39. (in Japanese)
- [30] Talebi, F. Kiyono, J. (2020) “Introduction of the axial force terms to governing equation for buried pipeline subjected to strike-slip fault movements” *Soil Dyn Earthq Eng* ;133:106125. <https://doi.org/10.1016/j.soildyn.2020.106125>
- [31] ABAQUS/CAE 2017. Dassault Systems Simulia Corp, documentation of 2017 release.
- [32] HASEGAWA N, KIYONO J, (2016) study of the plastic hinge position of buried steel pipe on fault displacement. *Journal of JSCE*, Vo. 72, pp. 161-166 (in Japanese)
- [33] Japan Gas Association. (2013) “Seismic Design Guideline for High-Pressure Gas Pipeline” JGA, specified, 206-13 (in Japanese).
- [34] Talebi, F., Kiyono, J., (2020) “Seismic response of buried pipeline to strong ground motion of strike-slip fault” *Landslides 5*- Springer.
- [35] O’Rourke M.J. and Liu X. (2012) “Seismic design of buried and offshore pipelines” Monograph MCEER-12-MN04, Multidisciplinary Center for Earthquake Engineering Research, MCEER.
- [36] Gresnigt, A.M., (1986), “Plastic Design of Buried Steel Pipelines in Settlement Areas,” *HERON*, Vol. 31, No. 4.
- [37] American Lifeline Alliance (ALA), (2001), “Guidelines for the Design of Buried Steel Pipe,” FEMA, 75p.
- [38] American Lifeline Alliance (ALA), (2005), “Design Guidelines for Seismic Resistant Water Pipeline Installations,” FEMA, 255p.
- [39] Zimmerman, T.J., Stephens, M.J., DeGreer, D.D., and Chen Q., (1995) “Compressive Strain Limits for Buried Pipelines,” *Proceedings of the 1995 Offshore Mechanics and Arctic Engineering Conference*, ASME, Vol. V, pp. 365-379.

- [40] Stephens, D.R., Olson, R.J., and Rosenfeld, M.J., (1991), “Pipeline Monitoring – Limit State Criteria,” Battelle Memorial Laboratory, AGA NG-18 Report No. 188.
- [41] ABAQUS/CAE 2017. Dassault Systems Simulia Corp, documentation of 2017 release.
- [42] Nishikawa, G., Shiohama, Y., Suzuki, Y., Onuma, H., Kiyono, J., (2016), “Evaluation of seismic performance on polyethylene pipe during an earthquake” Journal of Japan Society of Civil Engineers Ser A1 (Structural Engineering & Earthquake Engineering (SE/EE)), 72(4):424-433. DOI: 10.2208/jscejsee.72.I_424 (in Japanese)
- [43] ASTM F2160-01, (2001), “Standard Specification for Solid Wall High Density Polyethylene (HDPE) Conduit Based on Controlled Outside Diameter (OD)”, ASTM International, West Conshohocken, PA, . DOI: 10.1520/F2160-01
- [44] Canadian Standards Association Standard Z662-11 (CSA Z662-11), (2011) , “Oil and Gas Pipeline Systems”.
- [45] Ha, D., Abdoun, T. H., O’Rourke, M. J., Symans, M. D., O’Rourke, T. D., Palmer, M. C., Stewart, H. E. (2010) “Earthquake faulting effects on buried pipelines – case history and centrifuge study” J Earthq Eng ;14(5):646–69.

Chapter VIII:

Concluding Remarks

8.1. General remarks and summary

In this study, we investigated the problem of buried pipelines at faults crossing from a comprehensive point of view, including earthquake site investigation, analytical stability analysis, numerical FE based analysis, and full-scale experimental studies.

8.1.1. Damage evaluation during 2017 Sarpole-Zahab earthquake

We did a site investigation to evaluate damage to the lifeline systems during 2017 Sarpole-Zahab Earthquake and reported it as a JSCE disaster report. This site investigation demonstrates that the damage to the pipelines caused by the fault crossings did not only result in high economical loss, but also led to environmental problems in the damaged area. Therefore, the behavior of the pipeline at the fault crossings is an important engineering problem, and the resulting damage must be controlled through appropriate design based on knowledge about the responses of the pipe at crossing zones with faults [1].

8.1.2. Finite element-based study

In numerical FE-based study section of this research, we investigated problem of buried pipeline at fault crossing with two orientations: (1) performance evaluation of buried pipeline and detecting relations between the effective parameters on soil-pipe interaction using beam-spring FE models. (2) evaluation of the numerical modeling approaches and improvement of the FE based modeling approaches beside deeper understanding of the pipe behavior using 3D nonlinear FEM analysis.

In first part, performance of buried pipeline at strike-slip fault crossing is investigated using FEM analysis. Firstly, since in previous researches axial soil-pipe interaction has been roughly simplified [1–8] there was a demand on derivation of soil-pipe interaction terms for analytical solution methods even in elastic range, beside evaluation of the importance of axial force and axial soil-pipe interaction on this problem. Firstly, we concentrated on effect of axial soil-pipe interaction and axial force of pipeline on pipeline performance to derive effective parameters on axial soil-pipe interaction terms and new boundary conditions for development of future analytical studies [2]. And secondly, performance of buried pipelines crossing strike-slip fault with nonlinear pipe material and nonlinear soil-pipe interaction is investigated by FEM-based simulations. To investigate deeply the steel pipeline material nonlinearity effect on different cases by comparing plastic steel pipeline material cases with elastic ones [3].

In second part, we focused on the analysis approaches of the buried pipeline subjected to the strike-slip fault movement during strong ground deformation. a comparative study is conducted between the 3D solid and shell nonlinear FEM modeling approach and 3D nonlinear beam-spring modeling approaches and their application ranges, for the problem of buried pipelines at strike-slip faults crossing. Additionally, the performance and damage criteria are evaluated through 3D nonlinear FEM analysis. All the analyses have the nonlinear soil material, nonlinear pipe material, nonlinear interface properties, and geometrical nonlinearity effects [4].

8.1.3. Analytical studies

Present study targets the development of reliable, accurate and robust analytical stability analysis method for problem of buried pipelines subjected to earthquake fault movements. Despite substantial advances made by previous studies in the development of analytical solutions for a pipeline with regard to fault-crossing problems, axial soil-pipe interaction and axial forces owing to geometrical nonlinearity have not been appropriately applied in analytical solutions even in linear ranges. The abovementioned approximations are performed because the exact term of the axial soil-pipe interaction in the related differential equations has not thus far been considered. The main term that explains the effect of the crossing angle between the pipeline and fault in analytical analysis is the axial soil-pipe interaction. Therefore, implementation of an improper axial soil-pipe interaction term affects the buried pipeline's performance, especially in oblique fault crossings. Accordingly, there existed a need for developing a comprehensive analytical solution that incorporates the exact axial soil-pipe interaction term. Moreover, the nonlinearity of soil-pipe interaction has not been introduced within the governing equations. In previous studies, the transverse soil-pipe interaction nonlinearity was assumed by partitioning the pipeline into four segments, which does not reproduce real pipeline behavior and presents several issues. Moreover, none of the previous studies designed the axial soil-pipe interaction nonlinearity to include pipeline sliding and its effects on the geometrical nonlinearity terms inside the analytical solutions. An inappropriate definition of soil-pipe interaction in the analytical solutions can lead to an unrealistic and uneconomical design and even disaster during future earthquakes. The development of a comprehensive analytical solution that incorporates exact nonlinear axial and transverse soil-pipe interaction terms within a united governing equation is therefore urgently required.

In this study, firstly we established an improved governing equation to analyze buried pipeline as a linear material subjected to active strike-slip faults. This approach includes geometrical nonlinearity effects and exact axial force terms of the pipeline inside governing equation, and requires no additional external calculations, which significantly increases application range and accuracy even in the case of large deformation. The proposed methodology is verified against finite element-based results with various faulting angles and displacement ranges [5].

Secondly, we have established a nonlinear governing equation and solution procedure to analyze buried pipeline at an active strike-slip fault crossing. The methodology includes exact nonlinear axial and transverse soil-pipe interaction terms in addition to geometrical nonlinearity terms within the governing equation. The assumption of partitioning the pipeline into four segments with four governing equations based on the soil yield threshold is removed, and a united governing equation is introduced. In comparison with existing methodologies, the proposed method has a significantly extended application range with improved accuracy and offers the advantage of including buried pipeline sliding, transverse soil spring plasticity, and large-deformation effects. The solution procedure is further improved by removing

optimization steps and external calculations. The proposed methodology is verified against a verified finite element-based model with various fault displacements and angles. The results are in excellent quantitative and qualitative agreement with numerical results, even for cases of large fault movement.

8.1.4. Full-scale experimental study

In experimental study section, two full-scale experiments are carried out for buried HDPE pipeline at a 90° strike-slip fault crossing. Experiments are designated for performance evaluation of the SEKISUI CHEMICAL CO's HDPE pipes subjected to a strike-slip fault movement. Experiments are implemented for 2 cases of loose and dense sands. Based on experimental results, two 3D nonlinear FEM models are calibrated to evaluate the HDPE pipeline performance more detailly at strike-slip fault crossing. Moreover, influence of important variables on the buried HDPE pipeline at 90° strike-slip are studied.

8.2. Summary of the results

8.2.1. 2017 Sarpole-Zahab earthquake site investigation conclusions

1. In the 2017 Sarpole-Zahab earthquake, more than 500 cases of damages were reported for the main water pipelines, while more than 300 cases were reported for the main wastewater pipelines. These damages caused the contamination of the Sarpole-Zahab water resources for more than one week.
2. Damage to pipeline network is observed even in large polyethylene pipelines with the diameter of 600mm.

8.2.2. Finite element-based study's conclusions

The most important conclusions drawn from this study are as follows:

1. There exists a direct relationship between the axial soil-pipe interaction and axial component of fault movement (δ_x).
2. Changes in axial soil-pipe interaction of the buried pipeline crossing the strike-slip fault has substantial effect on the pipeline's force-displacement and stress field responses. The axial soil-pipe interaction exerted a decreasing effect on the shear force, bending moment, and compression stress responses and a radically increasing effect on the axial force and tensile stress responses of the buried pipeline. Because the axial soil-pipe interaction is very effective in the analytical solutions results, the implementation of an appropriate axial soil-pipe interaction in the analytical solutions is very important.
3. The adequate axial soil-pipe interaction term has high complexity and a comprehensive

analytical method is lacking. Based on conclusion 2, to ensure the simplicity and accuracy of the results, it is recommended to use the existing analytical solution as a validation method for the verification of the FE model only in the case of a buried pipeline crossing a 90° strike-slip fault in the elastic range.

4. The effect of the axial soil-pipe interaction on the buried pipeline crossing the strike-slip faults was negligible and had approximately no effect on the pipeline buried in loose soil responses subjected to the 90° strike-slip fault displacements.
5. L_c has a direct relationship with φ and a reverse relationship with kt . Additionally, there exists a relationship between φ and the axial soil-pipe interaction. Therefore, in the analytical solutions for calculating L_c , it is important to consider the axial soil-pipe interaction. However, in previous analytical studies, this important point was not adequately considered.
6. L_{conv} is almost independent of the axial soil-pipe interaction and φ . It has an inverse relationship with k_t and direct relationship with EI . Therefore, it is strongly recommended to use L_{conv} instead of L_c in the analytical calculations.
7. Owing to the appearance of the membrane force and the large deformation of the pipeline in the curved zone, a slight reverse axial displacement was observed in the curved zone. This displacement was zero at the intersection point and its rate was maximum at the intersection point of the fault and pipeline. Additionally, its rate gradually approached zero up to the point $x=L_{conv}$. Moreover, by increasing the soil stiffness, the tendency of the pipeline to reverse the displacement in the curved zone of the pipe slightly increased.
8. By decreasing the Faulting angle φ and increasing the soil stiffness, the axial forces of the pipeline substantially increased. Moreover, there existed a strong relationship between the axial force of the pipeline and the axial soil-pipe interaction, whereas in the cases without axial soil-pipe interaction, the axial force was approximately equal to zero.
9. Based on the FEM analysis for same scenarios with different soils and Eq. 9, approximately there is a strong relationship between the ratio of soils shear wave velocity and the ratio of stress, bending moment and axial force responses of the buried pipeline crossing the strike-slip fault as below.

$$\frac{\sigma_{max(i)}}{\sigma_{max(j)}} \approx \frac{M_{max(i)}}{M_{max(j)}} \approx \frac{N_{(i)}}{N_{(j)}} \approx \sqrt{\frac{k_{(i)}}{k_{(j)}}} \approx \frac{V_{s(i)}}{V_{s(j)}} \quad (3.21)$$

By changing the soil stiffness, the changes of the axial force, shear force response, bending moment response, and stress field responses of the buried pipeline crossing the strike-slip fault were approximately equal to the changes of the shear wave velocity in the soils (Eq. (3.21) has reliable results only in elastic zone of soil-pipe interaction and pipe material).

10. In the case with a 90° faulting angle, the bending moment response was predominantly in the stress field, while in the cases with smaller angles of φ (Oblique), the axial tensile force response gradually became the predominant response in the stress field of the buried pipeline. Therefore, in the case of a pipeline crossing a 90° strike-slip fault, buckling phenomena were the predominant damage case in the pipeline. Additionally, by decreasing the faulting angle (e.g., 60° and 45°), the predominant damage case is the tensile yielding of the pipeline.
11. Increasing of faulting angle (ψ) has a significant decreasing effect on the bending moment, shear force and maximum compression stress responses of the pipeline. however, it has a drastically increasing effect on the axial force and axial stress responses of the pipeline.
12. Cases with higher faulting angle experience larger yielded zone on the tensile part of the pipeline cross-section.
13. Yielding of the pipeline has a decreasing effect on the bending stiffness of the pipeline and it causes the shortening of curved zone length (L_{conv}) of the pipeline.
14. Yielding of pipeline doesn't have a remarkable effect on the axial force and axial stress responses of the pipeline, However, it has a very significant effect on the bending moment, shear force and bending stress response of the pipeline.

8.2.3. Analytical study's conclusions

An improved analytical method is introduced for analyzing buried pipeline with nonlinear (elastic perfectly plastic in axial and elastoplastic in transverse directions) soil-pipe interaction and elastic pipe material subjected to active strike-slip faults, and its results are verified with high consistency with FEM results. This methodology presents a substantial development based on the theory of beam-on-elastic-foundation by introducing nonlinear axial force and nonlinear transverse soil reaction terms. This study has further improved the existing analytical approaches [6–12] including:

1. The axial soil-pipe interaction and axial force terms of the pipeline are applied inside the governing equation. Axial forces are calculated by the governing equation with no need

for external calculations, which increases the analysis accuracy. And removed related number of assumptions made in previous studies.

2. The axial soil-pipe interaction and axial force terms of the pipeline are applied inside the governing equation. Axial forces are calculated by the governing equation with no need for external calculations, which increases the analysis accuracy. And removed related number of assumptions made in previous studies.
3. In this study, we have removed the assumption to partition the pipeline into four segments based on the soil yield threshold. We introduce a united nonlinear governing equation that includes exact nonlinear axial and nonlinear transverse soil-pipe interaction terms.
4. The geometrical nonlinearity term for calculation of the large deformation effects is calculated and applied inside the governing equation.
5. The nonlinear axial and nonlinear transverse soil-pipe interaction are introduced within the governing equation. Axial forces are calculated by the governing equation, which significantly improves the results by removing the simplification assumptions and external calculations.
6. The accuracy is significantly improved, for all of the cases, including the cases of a 90° faulting angle compared with previous studies. The solution procedure is further improved by removing the optimization steps, which increases the result accuracy and simplifies the solution procedure.
7. The introduced analytical methodology extends the application field of the analytical solutions by providing higher accuracy reproduction of results even under large fault movements. The discrepancy between the introduced methodology and FEM in cases of large deformation ($\delta \geq 4D$) are less than 2.5% in the maximum stress of pipeline. All of the small discrepancies are within the conservative direction with regards to the safety factor.
8. We proposed the $\sigma_{cr(max)}$ response as the reason and a criterion for pipeline ovalizing damage.

$$\sigma_{cr(max/min)}(x) = \frac{\sigma_a}{2} \pm \sqrt{\left(\frac{\sigma_a}{2}\right)^2 + \tau_{max}^2} \quad (5.44)$$

9. The proposed nonlinear analytical results are in excellent agreement with verified FEM

results in both qualitative and quantitative aspects for various faulting angles (ψ) and fault dislocations (δ). The verified methodology is therefore deemed reliable for verifying FEM-based analysis and design of buried pipeline subjected to strike-slip fault movement.

8.2.4. Full-scale experimental study's conclusions

Accomplished conclusions of two full-scale experiments and calibrated 3D nonlinear FE models for 63mm HDPE pipeline buried in loose sand and dense sand subjected to a strike-slip fault at a 90° crossing are as below:

1. Because from early stages of the faulting in fault plane of strike-slip fault, soil fails up to the surface and large cracks along the fault plane appear, It is more realistic in FEM analyses, to model the soil parts of each side of the fault plane (each of split-box sides) as a separated part (not connected soil parts).
2. Uplift expansion of sand around the fault plane observed in dense sand tests, and in loose sand case, subsidence observed around the high curvature zone of the pipeline.
3. As soil is stiffer, the curvature of the HDPE pipe is higher, and the high curvature zone is shorter.
4. Peak axial strains and peak bending strains (on springline) of the HDPE pipeline increase by increasing the fault movement up to a limit that longitudinal strain on springline reaches around strain corresponding to the ultimate stress of HDPE and has large plastic strains. After that by increasing the fault movement, peak axial strain increase rate drastically decreases and then remains almost same and by further fault movements, a longer length of pipeline reach to peak strain range, and in bending strains after reaching that ultimate stress limit because of flexural stiffness drop in peak bending strain cross-section, by increasing the fault movement peak bending stress/strain drops and gradually moves to further cross-sections from the fault plane. This procedure continues up to a fault movement that damage appears on the pipeline (e.g. local buckling, wrinkling, and ovalization).
5. HDPE buried in stiffer soil experiences higher axial and bending stress/strain at strike-slip fault crossing problem.
6. Axial strains of HDPE pipelines buried in dense sand is not negligible, even in case of a 90° crossing with strike-slip fault movement.

7. As we know, buried pipelines subjected to a strike-slip fault at 90° crossings are highly vulnerable for local buckling damages. However, during tests 1 and 2, which HDPE pipelines were subjected to very large fault movements (up to 10D), they show high flexibility and good performance during the faulting, and no local buckling damage appeared on the buried HDPE pipelines.
8. HDPE pipelines with lower diameters have a larger (D/t) ratio which increases the critical buckling strain and increases the safety of pipe against buckling damages. However, for large size HDPE pipelines, there is a need for further investigations.
9. Soil-pipe interaction forces on the HDPE pipe joints are larger than the HDPE pipe because of larger frictional forces and bearing forces from soil on the joints. Therefore, it is crucial to have a locally increasing effect of soil-pipe interaction at joints in analyzing the problem of buried pipeline subjected to fault movement especially on beam spring models.
10. ALA 2005 [38] guideline has not considered effect of the soil compaction on the ultimate soil-pipe interaction forces. And its suggested values for dense sand case is much lower than verified FEM results.
11. Ovalization damage has a direct relationship with principal stress/strain on the crown/invert of pipe cross-section. For having a reliable and economic seismic design for buried pipeline against ovalization damage, it is essential to control the maximum principal stress/strain of the pipe on the crown/invert less than the ultimate stress/strain of the pipe material.

8.3. Future studies

In this dissertation, we developed two analytical methodologies for stability analysis of buried pipeline at fault crossing, including the longitudinal and lateral soil-pipe interactions. Still, there is a need to include the pipe material nonlinearity effect inside the governing equation. The author suggests including the pipe material nonlinearity in the governing equation in future analytical studies. Additionally, studying the damage criteria of buried pipelines for various cases by FEM to improve the design guidelines of the pipelines is suggested.

References

- [1] Miyajima, M., Fallahi, A., Ikemoto, T., Samaei, M., Karimzadeh, S., Setiawan, H., Talebi, F., Karashi J. (2018) “Site Investigation of the Sarpole-Zahab Earthquake, Mw 7.3 in SW Iran of November 12, 2017” JSCE J. Disaster FactSheets 2018, FS2018-E-0002. Available online: http://committees.jsce.or.jp/disaster/system/files/FS2018-E0002_0.pdf
- [2] Talebi, F., Kiyono, J., (2020) “Seismic response of buried pipeline to strong ground motion of strike-slip fault” *Landslides 5*- Springer.
- [3] Talebi, F. Kiyono, J. (2019) “Steel pipeline nonlinearity effect on the force-displacement analysis of buried pipelines crossing strike-slip fault” International Conference in Commemoration of 20th Anniversary of the 1999 Chi-Chi Earthquake, Taipei, Taiwan, Sep 2019;
- [4] Talebi, F. Kiyono, J. (2020) “Evaluation of modeling approaches for buried pipeline subjected to strike-slip fault movements” 17th World Conference on Earthquake Engineering, Sendai Japan.
- [5] Talebi, F. Kiyono, J. [2020] “Introduction of the axial force terms to governing equation for buried pipeline subjected to strike-slip fault movements” *Soil Dyn Earthq Eng* ;133:106125. <https://doi.org/10.1016/j.soildyn.2020.106125>.
- [6] Karamitros, D., Bouckovalas, G., Kouretzis, G. [2007] “Stress analysis of buried steel pipelines at strike-slip fault crossings,” *Soil Dynamics and Earthquake Engineering* 27, 200–11.
- [7] Trifonov, O. V., Cherniy, V. P. [2010] “A semi-analytical approach to a nonlinear stress-strain analysis of buried steel pipelines crossing active faults,” *Soil Dynamics and Earthquake Engineering* 30(11), 1298–308.
- [8] Karamitros, D. K., Bouckovalas, G. D., Kouretzis G. P., Gkesouli V. [2011] “An analytical method for strength verification of buried steel pipelines at normal fault crossings,” *Soil Dynamics and Earthquake Engineering* (13), 1452-1464.
- [9] Trifonov, O. V., Cherniy V. P. (2012). “Elastoplastic stress-strain analysis of buried steel pipelines subjected to fault displacements with account for service loads,” *Soil Dyn Earthq Eng* 33,54–62.
- [10] Newmark, N. M., Hall, W. J. [1975] “Pipeline design to resist large fault displacement,” *Proc. of the U.S. national conference on earthquake engineering*, University of Michigan, Ann Arbor, Michigan, 416–25.
- [11] Kennedy, R. P., Chow, A. M., Williamson, R. A. [1977] “Fault movement effects on buried oil pipeline,” *ASCE Transportation Engineering Journal* 103(5), 617–33.
- [12] Kennedy, R. P., Kincaid, R. H. [1983] “Fault crossing design for buried gas oil pipelines” *ASME, PVP conference* 77, 1–9.

- [12] Wang, L. R. L., Yeh, Y. A. [1983] “A refined seismic analysis and design of buried pipeline for fault movement,” *Earthquake Engineering and Structural Dynamics* 13(1), 75–96.